

Unraveling Novel Roles in the Mitochondrial DNA Interactome: Functional Insights into the Pyruvate Dehydrogenase Complex and Yme2

NUPUR SHARMA



DISSERTATION

For the award of the doctoral degree in natural sciences
“Doctor rerum naturalium” (Dr. rer. nat.)
at the Faculty of Biology
at Ludwig-Maximilians-Universität, München

München 2025

Diese Dissertation wurde angefertigt
unter Leitung von **Prof. Dr. Christof Osman**
im Bereich Zell- und Entwicklungsbiologie
der Fakultät für Biologie
an der Ludwig-Maximilians-Universität, München

Erstgutachter/in: Prof. Dr. Christof Osman

Zweitgutachter/in: Prof. Dr. Dejana Mokranjac

Tag der Abgabe: 03.02.2025

Tag der mündlichen Prüfung: 15.05.2025

Eigenständigkeitserklärung

Hiermit versichere ich an Eidesstatt, dass die vorliegende schriftliche Dissertation / Masterarbeit / Bachelorarbeit / Zulassungsarbeit mit dem Titel

Unraveling Novel Roles in the Mitochondrial DNA Interactome: Functional Insights into the Pyruvate Dehydrogenase Complex and Yme2

von mir selbstständig verfasst wurde und dass keine anderen als die angegebenen Quellen und Hilfsmittel benutzt wurden. Die Stellen der Arbeit, die anderen Werken dem Wortlaut oder dem Sinne nach entnommen sind, wurden in jedem Fall unter Angabe der Quellen (einschließlich des World Wide Web und anderer elektronischer Text- und Datensammlungen) kenntlich gemacht. Weiterhin wurden alle Teile der Arbeit, die mit Hilfe von Werkzeugen der künstlichen Intelligenz de novo generiert wurden, durch Fußnote/Anmerkung an den entsprechenden Stellen kenntlich gemacht und die verwendeten Werkzeuge der künstlichen Intelligenz gelistet. Die genutzten Prompts befinden sich im Anhang. Diese Erklärung gilt für alle in der Arbeit enthaltenen Texte, Graphiken, Zeichnungen, Kartenskizzen und bildliche Darstellungen.

Munich, 27.05.2025

(Ort / Datum)

NUPUR SHARMA

(Vor und Nachname in Druckbuchstaben)

NUPUR SHARMA

(Unterschrift)

Affidavit

Herewith I certify under oath that I wrote the accompanying Dissertation / MSc thesis / BSc thesis / Admission thesis myself.

Unraveling Novel Roles in the Mitochondrial DNA Interactome: Functional Insights into the Pyruvate Dehydrogenase Complex and Yme2

In the thesis no other sources and aids have been used than those indicated. The passages of the thesis that are taken in wording or meaning from other sources have been marked with an indication of the sources (including the World Wide Web and other electronic text and data collections). Furthermore, all parts of the thesis that were de novo generated with the help of artificial intelligence tools were identified by footnotes/annotations at the appropriate places and the artificial intelligence tools used were listed. The prompts used were listed in the appendix. This statement applies to all text, graphics, drawings, sketch maps, and pictorial representations contained in the Work.

Munich, 27.05.2025

(Location/date)

NUPUR SHARMA

(First and last name in block letters)

NUPUR SHARMA

(Signature)

Erklärung **Declaration**

Hiermit erkläre ich, *
Hereby I declare

dass die Dissertation nicht ganz oder in wesentlichen Teilen einer anderen
Prüfungskommission vorgelegt worden ist.
*that this work, complete or in parts, has not yet been submitted to another
examination institution*

dass ich mich anderweitig einer Doktorprüfung ohne Erfolg **nicht**
unterzogen habe.
*that I did **not** undergo another doctoral examination without success*

dass ich mich mit Erfolg der Doktorprüfung im Hauptfach
that I successfully completed a doctoral examination in the main subject

und in den Nebenfächern
and in the minor subjects

bei der Fakultät für _____
at the faculty of

der
at

(Hochschule/University)

unterzogen habe.

dass ich ohne Erfolg versucht habe, eine Dissertation einzureichen oder mich
der Doktorprüfung zu unterziehen.
that I submitted a thesis or did undergo a doctoral examination without success

Munich, 27.05.2025
Ort, Datum/place, date

NUPUR SHARMA
Unterschrift/signature

*) Nichtzutreffendes streichen/
delete where not applicable

ACKNOWLEDGEMENTS

My doctoral journey has been an incredible adventure, filled with moments of excitement and confidence, as well as profound personal and professional growth. It has shaped and refined me in ways I never anticipated, and I am grateful to have experienced every moment of it.

I want to express my deepest gratitude to my supervisor, **Prof. Dr. Christof Osman**, for granting me the opportunity to pursue my doctoral studies in his lab and for shaping this journey with his exceptional guidance, unwavering support, and inspiration. **Christof**, you steered my time in the lab with the friendliest attitude, extremely engaging brainstorming sessions, and unparalleled approachability, making this experience truly rewarding. Your expertise and mentorship has been crucial in helping me overcome challenges and achieve this milestone. Your ease of conversation and ‘door always open’ policy provided me with a safe space to broadcast both my cheerful squeaks when experiments succeeded and my tearful leaks when they didn’t. I admire your childlike excitement about science and your ability to instil it in all of us. Plus, I am truly fortunate to have a mentor who not only shares my sense of humour but elevates it, making our time in and out of the lab even more enjoyable. Here’s to reserving a permanent spot at your annual summer BBQs and forever striving to be the ultimate Pictionary team!

I want to extend my gratitude to all the Osman Lab members, **Felix, Johannes, Ria, Nadja, Mengqiao, Ilaria, Simon Fish, Chris, Simon as well as all students, including Sebastian, Kati, Veronika, Romina, Sam, Rebecca, Amelie, Jasmin, Paul, Nikolai, Christos, Julia, Anna and Svenja**. The wonderful time I had in the lab would not be possible without you. Your presence in the lab made research stimulating and fun, and conversations interesting and juicy. I have nothing but respect and care for each one of you. The environment that we created, is something that I will forever cherish in my life. My PDH team, **Felix and Johannes**, I had the most fun collaborating on the PDH project with you boys. Aside from everyone’s utmost support (and countless cakes), I gained some of my closest friendships in the lab. **Nadja**, I am very thankful to you for always being there for any and every conversation we have had. Your positive insights and maturity really helped me sail through tough times. **Ria**, sharing every little experience with you and discussing it inside out was not just comforting and refreshing, but an honour that I am lucky to have felt. **Johannes**, our matching humour levels and hustle mode, made work feel like an absolutely delightful game. On a personal front, thanks for the brotherly care and affection

Acknowledgements

(and the innumerable Christmas cookies) I always got from you. **Basti**, your short presence in the lab was enough for us to realise how well we vibed. Times with you were probably one of the most fun times I had in and outside the lab. And last but not least, **Felix**, my only constant since day one in the lab, I only can be grateful that our paths crossed. Whether it was in the back lab during Covid (with Kati) or in the front lab (with Basti or Johannes), I will continue to cherish each and every moment we had because it was just BEYOND FUN. You have seen it all- my laughter, my frustration, my absurdities, my drama, and you have amplified it to another dimension. Thanks for spilling the tea with me over coffee all these years, and being my go-to person and male counterpart in lab and in life.

To all the members of **Mokranjac lab**, I want to extend my warm gratitude for the lab meetings and the constant feedback I received during my PhD. **Dejana**, you definitely were my proxy supervisor in this journey, thanks for the guidance and the extremely worthwhile conversations, both scientific and non-scientific. Your input is highly valued by me. **Marcel, Shalini, Nils and Soraya**- I have received support in every way possible from you guys, and I highly appreciate it. You really made me feel very welcome, especially when I snuck into Mokranjac lab events, whether it was for coffee downstairs, or car rides or restaurant outings. **Shalini and Marcel**- thanks for additionally being wonderful friends along the way! I am also thankful to everyone else in the **Cell Bio department**, for all the kitchen conversations, the Cellbio symposia, the BBQs, the Christmas parties, and the wonderful time and food we shared along the way. It really did feel like a big, happy family.

A special thanks to my **TAC Committee members**, Christof, Dejana and Kai as well as the **Mitoclub** attendees, who have given valuable feedback throughout the years, and with whom I have had intellectually stimulating and enriching discussions about science. I highly appreciate the input from each one of you on my projects. My gratitude also goes to **PD Dr. Serena Schwenkert**, for conducting all the Mass Spectrometry analysis for my project, as well as to **Dr. Peter Thorsness, Prof. Dr. Chris Meisinger** and **Prof. Dr. Dejana Mokranjac** for provision of a variety of antibodies for my project.

Heartfelt gratitude also goes from my side to **LSM Graduate school** as well as the **LSM Student Council** for making the past few years so memorable with the countless events and gatherings that we attended. I met amazing people along the way, some of whom will remain close friends. A special mention goes to **Korbi** and **Nadine**, who were extremely fun-loving co-ordinators and with whom I have had the comfort of talking about anything and everything for hours. Each of you had an encouraging and positively boosting presence in my journey.

I additionally thank the members of my **doctoral committee- Prof. Dr. Christof Osman, Prof. Dr. Dejana Mokranjac, PD Dr. Serena Schwenkert, Prof. Dr. Thomas Nägele, Prof. Dr. Laura Busse and Prof. Dr. Herwig Stibor**, for their insightful review of my thesis.

On a personal note, I would like to thank my family for their unconditional love and support. To my mom, **Dr. Seema Sharma**, this dissertation is as much the product of your hard work as it is mine. Your relentless love, sacrifices, and belief in me have been the foundation of my journey. You have been my greatest source of strength and inspiration in life, and I am eternally grateful for your immeasurable care, affection and your uniquely positive (and ever-inspiring) outlook on life. To my little sister, **Harshita**, your support and encouragement and ability to bring lightness in the most stressful moments have meant a lot to me. To my partner and best friend, **Avi**, I commend you for your extraordinary patience and resilience throughout my journey, and thank you for the endless understanding and love you continue to give me. I am incredibly fortunate to share this journey with someone who knows and values me as deeply as you do. Achieving this milestone would have not been possible without the balance and encouragement that you provided. I also thank **Nuns and Mans**, who have always had a warm and loving presence in my life. Your love, care and larger-than-life attitude means the world to me, and I am forever grateful that you have been my pillars of strength throughout this journey. To **Ursula**, my ‘German mother’, I thank you for the beautiful home you created for me in a new country and the utmost affection you gave me. Your wisdom and positivity will forever inspire me.

Throughout this journey, I have been blessed to meet incredible people, some of whom have become cherished friends who hold a special place in my heart today. To my best friend **Ginte**, you are my home away from home, and it was an ethereal experience to navigate every step of this journey together, including the writing process. There is no one else I could imagine sharing this unforgettable adventure with. I am deeply grateful for the loving and grounding presence you bring, and the happiness you provide in my life. In you, I have gained not only a best friend but a companion for life. A heartfelt thank you to all my friends for being my source of light during the challenging moments. Your encouragement, laughter, and steadfast presence have made all the difference, and I am deeply grateful to have each one of you by my side.

While each of the individuals mentioned has made a unique contribution to this journey, **I dedicate my PhD and this dissertation to my mother**. She has been my greatest cheerleader and has made the most unimaginable sacrifices to help me reach this point. Mumma, I love you and I will forever strive to make you proud!

ABSTRACT

Mitochondria are dynamic organelles crucial for eukaryotic life, renowned for their role in energy generation via oxidative phosphorylation. At the heart of their functionality, lies the mitochondrial DNA (mtDNA), which encodes key components of the electron transport chain, while the rest are encoded by the nuclear genome, reflecting their dual genetic origin.

The mtDNA is organized into a large nucleoprotein complex known as the mitochondrial nucleoid, that is, in turn, a part of a larger, highly-ordered expressosome-like assembly called the MIOREX complex. The MIOREX complex houses the nucleoid, along with a variety of factors involved in mitochondrial gene expression, genome organization, protein biogenesis and the mitoribosome. Although recent efforts have significantly elucidated the components and mechanisms of MIOREX complexes, the complete MIOREX interactome remains elusive, with many of its protein partners and associated molecular mechanisms yet to be identified.

This study attempts to characterize two such candidates, which have been previously identified to be present in the mtDNA interactome, and aims at studying their interaction with the mitochondrial genome. The first candidate is the pyruvate dehydrogenase complex (PDHc), that is well-known for its conserved role in glucose metabolism. The findings in this research reveal an additional role for the PDHc in promoting mitochondrial health, by contributing to mtDNA maintenance and associating with the gene expression machinery, which is independent of the traditional metabolic function of the PDHc, and involves interactions with mitochondrial RNA. Moreover, the precise molecular interactions of this complex have been elucidated through biochemical analyses, providing valuable insights into its identity as a bifunctional enzyme.

The second candidate, Yme2, an inner mitochondrial membrane protein, has been previously implicated in mitochondrial protein biogenesis, albeit its mechanism of action remains unclear. Through a combination of bioinformatics and mutagenesis approaches, this research identifies that Yme2 contains an RNA recognition motif (RRM) as well as a AAA+ domain. Moreover, the results demonstrate that *YME2* engages in genetic interactions with *MDM38*, *MBA1*, and *OXA1*, as well as biochemical interactions with mitochondrial nucleoid-associated proteins, thereby linking Yme2 to the mitochondrial protein biogenesis machinery. Collectively, by examining the interaction dynamics of PDHc and conducting mutational characterization of Yme2, I aim to contribute new perspectives to the field of the mtDNA interactome, thereby advancing research in this domain.

ZUSAMMENFASSUNG

Mitochondrien sind dynamische Organellen, die für das eukaryontische Leben von entscheidender Bedeutung sind und für ihre Rolle bei der Energieerzeugung durch oxidative Phosphorylierung bekannt sind. Das Herzstück ihrer Funktionalität ist die mitochondriale DNA (mtDNA), die für Schlüsselkomponenten der Elektronentransportkette kodiert, während der Rest vom Kerngenom kodiert wird, was ihren doppelten genetischen Ursprung widerspiegelt.

Die mtDNA ist in einem großen Nukleoproteinkomplex organisiert, der als mitochondriales Nukleoid bekannt ist. Dieser wiederum ist Teil einer größeren, hochgradig geordneten expressosomenähnlichen Anordnung, die als MIOREX-Komplex bezeichnet wird. Der MIOREX-Komplex beherbergt die Nukleoide zusammen mit einer Vielzahl von Faktoren, die an der mitochondrialen Genexpression, Genomorganisation, Proteinbiogenese und dem Mitoribosom beteiligt sind. Obwohl die Komponenten und Mechanismen der MIOREX-Komplexe in jüngster Zeit deutlich aufgeklärt wurden, ist das vollständige MIOREX-Interaktom nach wie vor schwer zu fassen, da viele seiner Proteinpartner und die damit verbundenen molekularen Mechanismen noch nicht identifiziert wurden.

In dieser Studie wird versucht, zwei solcher Kandidaten zu charakterisieren, die zuvor im mtDNA-Interaktom identifiziert worden sind, und ihre Interaktion mit dem mitochondrialen Genom zu untersuchen. Der erste Kandidat ist der Pyruvatdehydrogenase-Komplex (PDHc), der für seine konservierte Rolle im Glukosestoffwechsel bekannt ist. Die Ergebnisse dieser Forschung zeigen eine zusätzliche Rolle des PDHc bei der Förderung der mitochondrialen Gesundheit, indem er zur Aufrechterhaltung der mtDNA beiträgt und mit der Genexpressionsmaschinerie assoziiert ist, was unabhängig von der traditionellen Stoffwechselfunktion des PDHc ist und Interaktionen mit der mitochondrialen RNA beinhaltet. Darüber hinaus wurden die genauen molekularen Interaktionen dieses Komplexes durch biochemische Analysen aufgeklärt, was wertvolle Einblicke in seine Identität als bifunktionales Enzym liefert.

Der zweite Kandidat, Yme2, ein inneres mitochondriales Membranprotein, wurde bereits früher mit der mitochondrialen Proteinbiogenese in Verbindung gebracht, obwohl sein Wirkmechanismus noch unklar ist. Durch eine Kombination von Bioinformatik- und Mutagenese-Ansätzen wird in dieser Forschungsarbeit festgestellt, dass Yme2 ein RNA-Erkennungsmotiv (RRM) sowie eine AAA+-Domäne

enthält. Darüber hinaus zeigen die Ergebnisse, dass *YME2* genetische Interaktionen mit *MDM38*, *MBA1* und *OXA1* sowie biochemische Interaktionen mit mitochondrialen Nukleoid-assoziierten Proteinen eingeht, wodurch Yme2 mit der mitochondrialen Proteinbiogenese-Maschinerie in Verbindung gebracht wird. Durch die Untersuchung der Interaktionsdynamik von PDHc und die Durchführung der Mutationscharakterisierung von Yme2 möchte ich neue Perspektiven auf dem Gebiet des mtDNA-Interaktoms eröffnen und damit die Forschung in diesem Bereich voranbringen.

Contents

Acknowledgements	ix
Abstract	xiii
Zusammenfassung	xv
Contents	xvii
List of Figures	xx
List of Abbreviations	xxi
1 Introduction	1
1.1 Mitochondria	1
1.1.1 The Mitochondrial Ultrastructure	2
1.1.2 The Mitochondrial Nucleoid	3
1.2 Metabolic Remodelling and Regulation of mtDNA	4
1.3 Mitochondrial Translation and Protein Biogenesis	6
1.3.1 The Mitoribosome	6
1.3.2 The Mitochondrial Protein Biogenesis Machinery	7
1.3.3 Factors Contributing To Mitochondrial Gene Expression	8
1.4 Energy Generation by Mitochondria	8
1.4.1 Glycolysis and TCA cycle	8
1.4.2 Oxidative Phosphorylation	9
1.5 Mitochondrial Protein Quality control	10
1.5.1 The role of AAA+ proteins in mitochondrial quality control	11
1.5.2 The domain architecture of AAA+ proteins allows ATP binding and hydrolysis	12
1.6 <i>Saccharomyces cerevisiae</i> as the Model Organism	13
1.7 The mtNucleoid-binding candidates characterized in this study	14
1.7.1 The Pyruvate Dehydrogenase Complex	14

1.7.2	Yme2	18
2	Aim of this Study	21
3	Results	23
3.1	The Pyruvate Dehydrogenase Complex (PDHc)	23
3.1.1	PDHc subunits contribute to overall mitochondrial health and integrity	24
3.1.2	PDHc functions in mtDNA maintenance	26
3.1.3	The role of PDHc in mtDNA maintenance is uncoupled from its metabolic function	27
3.1.4	Association of PDHc with the mitochondrial gene expression machinery	31
3.1.5	PDHc subunits interact with mitochondrial RNA	34
3.2	Yme2 as a mtNucleoid interacting protein	38
3.2.1	<i>YME2</i> exhibits a negative genetic interaction with members of the mitochondrial protein biogenesis machinery	38
3.2.2	The putative C-terminal Walker motifs are crucial for the function of Yme2	40
3.2.3	Yme2 exists as a multimeric complex	44
3.2.4	<i>In-vitro</i> purification of the Yme2 Walker domains	47
3.2.5	The putative N-terminal RNA binding domain is important for Yme2 function	48
3.2.6	An additional N-terminal domain of Yme2 with features similar to the putative RRM2 domain	51
3.2.7	Mass Spectrometry analysis of the Yme2 interactome reveals presence of mtNucleoid proteins	55
4	Discussion	57
4.1	The Pyruvate Dehydrogenase Complex (PDHc)	58
4.1.1	Accessory Role of PDHc in Maintaining Mitochondrial Health	58
4.1.2	PDHc Associates with the Mitochondrial Gene Expression Machinery	60
4.1.3	Concluding Remarks	62
4.2	Yme2	64
4.2.1	The Characterization of Yme2 as a Potential AAA+ Protein Featuring RRM Domains	64
4.2.2	The mtNucleoid Association of Yme2	66
4.2.3	The Proposed Working Model for the Putative Function of Yme2	66
4.2.4	Concluding Remarks	68

5 Outlook	71
6 Materials and Methods	73
6.1 Materials	73
6.2 Methods	73
6.2.1 Strain generation and cloning	73
6.2.2 Molecular and Cell Biology methods	74
6.2.3 Biochemical methods	77
6.2.4 Microscopy and Image Processing	87
6.2.5 <i>In-silico</i> analysis of the Yme2 sequence	88
A Supplementary Figures	89
B Supplementary Tables	101
B.1 Chemicals and Reagents	101
B.2 Growth Media Composition	104
B.3 Buffer Composition	105
B.4 Antibodies	107
B.5 Yeast Strains	108
B.6 List of Plasmids	118
B.7 Mass Spectrometry data from Lat1 Co-immunoprecipitation	121
B.8 Mass Spectrometry data from Proximity Labelling Assay	128
B.9 Mass Spectrometry data from Myc tag Co-immunoprecipitation	137
C Curriculum vitae	143
D Publications	145

List of Figures

1	The Mitochondrial ultrastructure	3
2	Components of the MIOREX complex	7
3	The Energy Generation Pathway in Yeast	10
4	The structure of PDHc along with its enzymatic reaction	16
5	PDHc Subunits affect mitochondrial health	25
6	The metabolic role of PDHc is uncoupled from its function in mtNucleoid maintenance	30
7	The interacting partners of PDHc	34
8	PDHc associates with mitochondrial RNA	37
9	Genetic interactions of Yme2 with mitochondrial protein biogenesis machinery	39
10	Putative structure and motif architecture of Yme2	41
11	Architectural layout of the Walker A and B motifs of Yme2	42
12	Yme2 is a multimeric protein	46
13	Structural organization of RRM2 domain of Yme2	49
14	Domain architecture of RRM1 domain of Yme2	53
15	Yme2 interactome has mtNucleoid-related proteins	55
16	The proposed working model for the function of Yme2	67

List of Abbreviations

AAA+	ATPases Associated with diverse cellular Activities
ABC	Ammonium Bicarbonate
ACN	Acetonitrile
ATP	Adenosine Triphosphate
BN-PAGE	Blue Native PolyAcrylamide Gel Electrophoresis
Co-IP	Co-Immunoprecipitation
DTT	Dithiothreitol
EtBr	Ethidium Bromide
ETC	Electron Transport Chain
FA	Formic Acid
Floaty-TurboID	Mitochondrial matrix-targeted freely-floating TurboID
GO	Gene Ontology
HMG	High-Mobility Group
IMM	Inner Mitochondrial Membrane
IMS	Inter-Membrane Space
IAA	Iodoacetamide
LFQ	Label Free Quantification
LSU	Large Subunit
MIOREX	Mitochondrial Organization of Gene Expression
MPC	Mitochondrial Pyruvate Carrier
MS	Mass Spectrometry
mtDNA	Mitochondrial DNA
mtNucleoid	Mitochondrial Nucleoid

List of Abbreviations

mtRNA	Mitochondrial RNA
OMM	Outer Mitochondrial Membrane
OXPPOS	Oxidative Phosphorylation
PAGE	PolyAcrylamide Gel Electrophoresis
PDC	Pyruvate Decarboxylase
PDHc	Pyruvate Dehydrogenase Complex
P-loop	Phosphate Loop
qPCR	Quantitative PCR
RRM	RNA Recognition Motif
RT	Room Temperature
SDS	Sodium Dodecyl Sulphate
SSU	Small Subunit
TCA	Tricarboxylic Acid Cycle
TIM	Translocases of Inner Membrane
TOM	Translocases of Outer Membrane
WT	Wildtype

1 Introduction

1.1 Mitochondria

The fitness of every cell, of every organism, relies on its ability to efficiently uptake and assimilate the nutrients available in its environment, in a manner that contributes to its meaningful subsistence. In order to sustain this existence, eukaryotic cells harbor multitude of dedicated organelles that not only individually perform specific functions in a so-called division of labor, but work together to integrate those functions in life-sustaining harmony. One of the most important and fundamental functions in the cells is the generation of energy in the form of ATP, that further fuels virtually every other process that occurs within the cells. A crucial role in energy generation by the eukaryotic cells is played by dynamic, membrane-bound structures known as mitochondria.

Mitochondria are highly adaptable, tubular networks that extend throughout the cell and have a crucial function in cellular metabolism. Popularly regarded as the ‘powerhouse’ or the ‘energy factories’ of the cell, the role of mitochondria in the cells reaches far beyond bioenergetics. Not only do they carryout ATP production by housing the respiratory chain complexes, they serve as sites for iron-sulfur cluster biogenesis, fatty acid oxidation, calcium homeostasis, and generation of precursors for macromolecules like lipids, proteins, DNA and RNA (McBride et al., 2006; Spinelli and Haigis, 2018; Stehling et al., 2014; Suomalainen and Nunnari, 2024). As the functions performed by mitochondria are absolutely vital for the cell, defects within the mitochondria can manifest as aging and life-threatening conditions like muscular and neurodegenerative diseases, myopathies, metabolic disorders and cancer (Bratic and Larsson, 2013; Nunnari and Suomalainen, 2012; Vyas et al., 2016).

The origin of mitochondria is thought to have occurred due to an endosymbiotic event, as proposed by Lynn Margulis in 1967. The Endosymbiosis Theory, as it is called, is regarded as the best explanation for the origin of mitochondria, their structural and functional complexity, as well as the mitochondrial genome. The endosymbiotic theory posits that mitochondria are direct descendants of a prokaryotic precursor that highly resembles the modern-day alpha-proteobacteria, *Rickettsia* (Andersson et al., 1998; Gray, 1989; Gray, 2014; Sagan, 1967). It is important to note that the bacterially-derived mitochondrial genome has undergone significant reductive evolution, marked by extensive gene loss and multiple rounds of endosymbiotic gene transfer events to the nucleus (Andersson et al., 1998; Gray, 2015). This major turnover has diminished the alpha-proteobacterial fraction of mitochondrial proteome to a mere 10-20% (Gabaldón and Huynen, 2007; Gray,

2015). The majority of the mitochondrial proteome is believed to have arisen from either diverse prokaryotic or archaeal ancestors, or specifically due to eukaryotic divergence (Butenko et al., 2024; Karlberg et al., 2000; Kurland and Andersson, 2000). This has led to a variety in size and number of encoded genes among mitochondrial genomes of different eukaryotes.

1.1.1 The Mitochondrial Ultrastructure

The remnants of the evolution of mitochondria from their bacterial ancestor are apparent in their ultrastructure. Mitochondria are surrounded by two membranes, which divide the organelle into four sub-compartments: the Outer Mitochondrial Membrane (OMM), the Inter-Membrane Space (IMS), the Inter-Membrane Space (IMS), the Inter-Membrane Space (IMS), and the matrix (fig. 1a). This compartmentalization is instrumental for mitochondria to perform their functions in generation of energy, and maintenance of redox homeostasis (Iovine et al., 2021; Spinelli and Haigis, 2018). The IMM is further divided into the inner boundary membrane, which is in proximity of the OMM, and cristae, which are the lamellar or tubular invaginations of the IMM into the interior of the organelle (Frey and Mannella, 2000; Mannella, 2006). The inner boundary membrane and cristae meet at limited number of discrete sites known as cristae junctions (Frey et al., 2002). Cristae are highly dynamic protrusions of the IMM which house the respiratory chain complexes that are required for oxidative phosphorylation (Cogliati et al., 2016; Gilkerson et al., 2003). Furthermore, the large surface area provided by cristae allows for large amount of chemical reactions to occur, making the IMM one of the most protein-rich membranes known (Becker et al., 2009). Apart from the presence of two membranes, another feature of mitochondria that is a relic of their bacterial progenitor is the presence of their own, albeit, small genome, and protein synthesis factories called the mitoribosomes (discussed in detail in section 1.3.1).

Even though the mitochondrial genome is small, the mitochondrial proteome consists of about 1000 proteins in *S. cerevisiae* (1500 in humans), which are important for their role in ATP production, metabolism, apoptosis, and mitochondrial quality control (Reinders et al., 2006; Sickmann et al., 2003). 99% of these proteins are nuclear-encoded and synthesized by cytosolic ribosomes, and then further imported into mitochondria via a sophisticated network of membrane-embedded multi-protein translocases (Hansen and Herrmann, 2019; Rehling et al., 2004). The Translocases of Outer Membrane (TOM) and Translocases of Inter-Membrane (TIM) complexes are intricate machineries that sort the incoming proteins into their destined compartments within mitochondria (Neupert, 2015; Wiedemann and Pfanner, 2017). 1% of the mitochondrial proteome, however, is encoded by the mitochondrial DNA (mtDNA) and synthesized by the dedicated ribosomes present

in the mitochondria (Hällberg and Larsson, 2014; Larsson, 2010). Even though the mtDNA codes for a small fraction of mitochondrial proteins, these proteins form the core of the respiratory chain complexes and are required for oxidative phosphorylation (fig. 1b). Therefore, the presence of the mtDNA is imperative for cell survival and fitness in most eukaryotes (with yeast as an exception, as it can perform fermentation to produce energy in the absence of mtDNA). The absence or mutations of mtDNA can lead to deleterious consequences in the cell and can result in various disorders in humans (Habbane et al., 2021; Taylor and Turnbull, 2005; Tuppen et al., 2010).

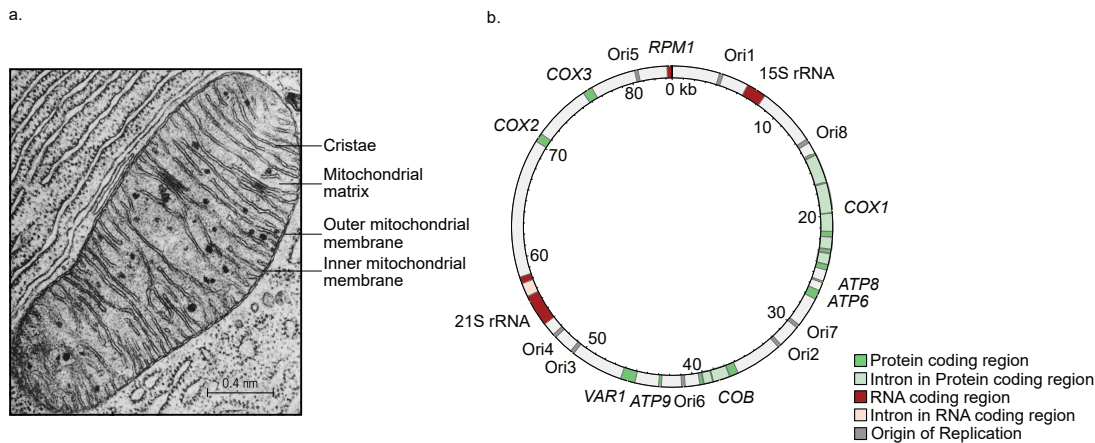


Figure 1: **The Mitochondrial Ultrastructure.** (a) Transmission electron microscopy image of the longitudinal section of mitochondria from pancreas of the bat, *Myotis lucifugus*. Image adapted and modified from Kieth Porter, 2011. (b) A schematic showing the mtDNA map in yeast, *S. cerevisiae*. The different segments are color coded as shown. The figure was adapted and modified from Osman et al., 2015.

1.1.2 The Mitochondrial Nucleoid

The mtDNA is an extranuclear, circular molecule present in the mitochondrial matrix, that has been subject to extensive reductive evolution and divergence since it arose from its bacterial ancestor (Lane and Martin, 2010; Lang et al., 1999). In yeast, the mtDNA is about 80kb in size and encodes for seven essential subunits of the respiratory chain (13 in humans), one mitoribosomal protein Var1, two RNA subunits of mitoribosome (21S rRNA and 15S rRNA), 24 tRNAs and the RNA subunit of RNase P (fig. 1b). The seven protein-coding genes that make up the electron transport chain complexes, namely, Cytochrome B, Cox1, Cox2, Cox3, Atp6, Atp8, Atp9, form the essential cores of their respective assembled complexes,

making them indispensable to the respiratory function of mitochondria (Turk et al., 2013).

Every cell harbours multiple (20-40 in *S.cerevisiae*; 500-100,000 in humans) copies of mtDNA which are organized into highly ordered nucleoprotein complexes called mitochondrial nucleoids (mtNucleoid), with each nucleoid containing mostly a single molecule of mtDNA (X. Chen et al., 1995; Göke et al., 2020; Kukat et al., 2011; Lipinski et al., 2010; Williamson, 2002). The mtNucleoids are distributed throughout the mitochondrial network in a semi-regular manner, which spatially links the mtDNA copies to their gene products, by creating a so-called ‘Sphere of Influence’ (Busch et al., 2014; Jakubke et al., 2021; Osman et al., 2015). Furthermore, mtNucleoids have been observed to be anchored to the IMM via a number of different tethers that anchor the mtNucleoid via the mitoribosome (Itoh et al., 2021; Kehrein et al., 2015; Möller-Hergt et al., 2018; Ott et al., 2006).

Within the mtNucleoid, the mtDNA molecules in yeast are packaged by Abf2, a high mobility-group (HMG) box protein that has the ability to bend the mtDNA, but contrary to its mammalian homolog TFAM, does not additionally act as a transcription factor (Brewer et al., 2003; Friddle et al., 2004; Kaufman et al., 2007; Kukat et al., 2015; Newman et al., 1996; Shi et al., 2012). Apart from acting as an mtDNA packaging factor, Abf2 can also maintain and influence mtDNA copy number (Bonekamp et al., 2021; Ekstrand et al., 2004; Zelenaya-Troitskaya et al., 1998). Furthermore, in addition to mtDNA and Abf2, mtNucleoids also contain proteins required for replication, expression as well as maintenance of mtDNA (Gerhold et al., 2015; He et al., 2012). This means that the complicated assembly of mtNucleoids could spatially link all steps of mitochondrial gene expression, namely transcription, translation as well as insertion into the IMM via presumably facilitating transport of mitochondrial RNAs (mtRNAs), which has been already proposed (Jourdain et al., 2016; Kehrein et al., 2015; Singh et al., 2020). However, knowledge about the mobility of mtRNAs within the mtNucleoid still remains elusive.

1.2 Metabolic Remodelling and Regulation of mtDNA

In a study where mass spectrometry was performed on *in organello* formaldehyde-crosslinked mitochondria, several unanticipated proteins were identified cross-linked to the mtDNA (Kaufman et al., 2000). These included proteins like Hsp60 (a chaperonin), Aco1 (aconitase, a TCA cycle enzyme), subunits of pyruvate dehydrogenase complex (Pda1, Pdb1, Lpd1), α -ketoglutarate dehydrogenase complex

(Kgd2 and Lpd1), and Ilv5 (component of branched chain amino acid synthesis pathway), among others (X. J. Chen et al., 2005; Kaufman et al., 2000). This subset of identified proteins in complex with mtDNA was rather surprising, as their main functions were metabolism-related and they had little to do with mtDNA in general. Upon further research, a few of these proteins (Ilv5, Aco1, Hsp60, Kgd2) were then classified as ‘bifunctional proteins’ (X. J. Chen et al., 2007; Kaufman et al., 2000; Kaufman et al., 2007; Zelenaya-Troitskaya et al., 1995). The bifunctional proteins, as the name suggests, have a ‘moonlighting’ function in mtDNA maintenance, inheritance and stability apart from their already described roles in metabolism.

As aforementioned, the yeast HMG box protein Abf2, packages mtDNA within a nucleoprotein-yielding structure called the mtNucleoid and contributes to its stability, especially when cells are grown on fermentable media (Diffley and Stillman, 1991; Kaufman et al., 2007). It has been observed that in glucose-repressed conditions, the mtNucleoids are more tightly packed by Abf2 with an increased ratio of Abf2 to mtDNA (Brewer et al., 2003; Friddle et al., 2004; Kucej et al., 2008). In contrast, when cells are grown on non-fermentable media like glycerol, the copy number increase in mtDNA lowers the ratio of Abf2 to mtDNA, resulting in less compact packaging (Kucej et al., 2008). This means that the packaging mechanism of mtDNA is highly dynamic, and subject to remodelling upon changes in metabolic cues like presence of fermentable or non-fermentable media. Furthermore, it was observed that in mutants lacking Abf2, the mtDNA was less protected and displayed increased sensitivity to nuclease attack and oxidative stress, which also becomes true for less tightly bound mtNucleoids from cells grown on glycerol (Kucej et al., 2008; Newman et al., 1996; O’Rourke et al., 2002). In these conditions, other mtDNA-binding proteins (the bifunctional proteins, for instance) may partially overtake the roles of mtDNA protection (X. J. Chen et al., 2005, 2007; Kucej et al., 2008).

The support for the idea of partially overlapping functions of Abf2 and some bifunctional proteins in mtDNA stability comes from their recruitment to the mtNucleoids in conditions of glucose repression (Hsp60) and amino acid starvation (Ilv5) (Kaufman et al., 2003; Kucej et al., 2008; Zelenaya-Troitskaya et al., 1995). Additionally, it has been observed that Aco1 (both WT and catalytically inactive forms), when constitutively expressed, can replace the mtDNA packaging function of Abf2 to some extent, as well as potentially protect mtDNA from damage (X. J. Chen et al., 2005, 2007; Shadel, 2005). These findings provide exciting insights on how metabolic cues can remodel and regulate the stability of mtDNA.

1.3 Mitochondrial Translation and Protein Biogenesis

A small subset of the mitochondrial proteome (8 proteins in yeast, 13 in humans) is encoded for by the mtDNA, which gets translated on the mitoribosomes. The mitoribosomes almost exclusively synthesize hydrophobic membrane proteins that form the core of the respiratory chain complexes (Bieri et al., 2018). Similar to bacteria, mitochondrial protein biogenesis obeys a co-translational insertion and translocation of its encoded proteins (Gruschke et al., 2010; Ott and Herrmann, 2010). The presumable direct molecular crosstalk between transcription, translation and membrane insertion of proteins is thought to be orchestrated in large expressosome-like assemblies known as the ‘Mitochondrial Organization of Gene Expression’ (MIOREX) complexes (Kehrein et al., 2015). The MIOREX complexes are large clusters comprising mitochondrial ribosomes, along with the proteins implicated in post-transcriptional mRNA metabolism, mRNA translation and decay, effectively coupling gene expression processes from transcription to translation (Kehrein et al., 2015). The MIOREX complexes are evenly distributed throughout the mitochondrial network, where a fraction of them are present as mtNucleoid-MIOREX complexes that amalgamate the entire spectrum of mitochondrial gene expression (Bogenhagen et al., 2014; Kehrein et al., 2015; Singh et al., 2020) (fig. 2). Some important components of the MIOREX complex are summarized below.

1.3.1 The Mitoribosome

The mitoribosome represents a modified and evolved bacterial ribosome with regard to its structure and constituents. The mitoribosome (74S) has a molecular weight of 3 MDa in yeast, and comprises a 54S large subunit (LSU) of 1.9 MDa and a 37S small subunit (SSU) of 1.1 MDa. The LSU is made up of 39 proteins, along with expansion segments of mitoribosomal 21S rRNA. The SSU, on the other hand, includes 34 proteins and a 15S rRNA (Amunts et al., 2014; Desai et al., 2017; Greber and Ban, 2016; Kaushal et al., 2014). The assembly of the mitoribosome takes place in the mitochondrial matrix, wherein individual mitoribosomal proteins are imported after being synthesized in the cytosol, and the rRNA components are processed and modified after being mitochondrially-encoded (Harper et al., 2023; Kummer and Ban, 2021; Zeng et al., 2018). The fully functional mitoribosome is assembled in a stepwise and concerted manner close to the mtNucleoid (Bogenhagen et al., 2014; Kehrein et al., 2015).

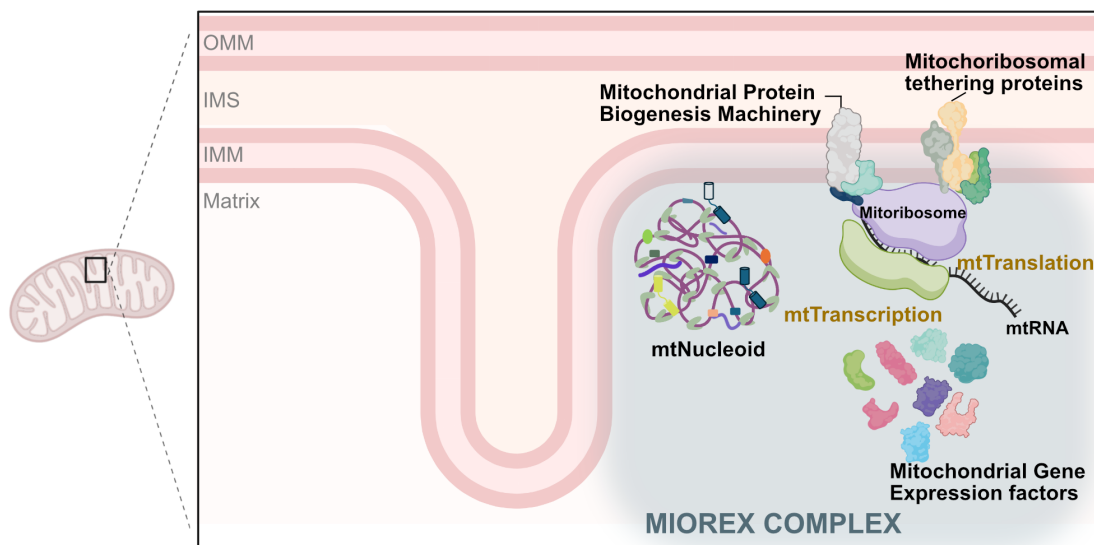


Figure 2: **A schematic showing the composition of the MIOREX complex in yeast *S. cerevisiae*.** The MIOREX complex consists of mtDNA and proteins required for mtDNA maintenance, the mitoribosome as well as factors involved in mitochondrial gene expression, mtRNA maturation, processing, stability and decay. The figure was created using BioRender.com and Affinity designer.

1.3.2 The Mitochondrial Protein Biogenesis Machinery

The mtDNA-encoded proteins are highly hydrophobic members of the OXPHOS complexes and their co-translational insertion into the IMM is mediated via the Oxa1 insertase (Gruschke et al., 2010; McDowell et al., 2021; Szyrach et al., 2003). This is achieved by the docking and extensive interaction of the mitoribosome LSU (54S) with the IMM, which additionally also reduces the probability of unproductive protein aggregates during transport (Ott et al., 2016). Oxa1 has been observed to cross-link to the peptide exit tunnel of the mitoribosome as well as the emerging nascent chains (Gruschke et al., 2010; Hell et al., 2001; Jia et al., 2003), suggesting that newly synthesized proteins might engage with the Oxa1 insertion machinery as soon as they emerge from the mitoribosome (Ott and Herrmann, 2010). However, this interaction of Oxa1 with the mitoribosome is co-ordinated with two acceptor proteins of the mitochondrial protein biogenesis machinery, Mba1 and Mdm38, which aid in anchoring the mitoribosome to the IMM (Frazier et al., 2006; Ott et al., 2006; Pfeffer et al., 2015; Preuss et al., 2001). It needs to be considered, nonetheless, that the tethering of the mitoribosome to the IMM in general is thought to be mediated by a multitude of factors (proteins like Mba1 and Mdm38, as well as a 96-nucleotide expansion segment of the 21S mitochondrial rRNA), many of which

still remain to be identified (Kehrein et al., 2015; Möller-Hergt et al., 2018; Pfeffer et al., 2015).

The receptors of the mitochondrial protein biogenesis machinery, Mdm38 and Mba1, display overlapping functions in regulating mitochondrial translation and insertion (Bauerschmitt et al., 2010). Moreover, cryoelectron tomography and subtomogram analysis of isolated yeast mitochondria have further revealed that Mba1 may additionally align the bound mitoribosome with Oxa1 via its interaction with the exit tunnel of the mitoribosome (Ott et al., 2006, 2016; Pfeffer et al., 2015). Recently, additional novel tethers (for example, Mrx15) have been discovered upon further characterizing the MIOREX complex that help to position and anchor mitoribosome either constantly or dynamically (Möller-Hergt et al., 2018). It remains exciting to further catalogue the yeast mitoribosome interactome and document how different processes are organized in this space.

1.3.3 Factors Contributing To Mitochondrial Gene Expression

In addition to the mtNucleoid, the mitoribosome and the components of the mitochondrial protein biogenesis machinery, the MIOREX complexes have accessory proteins and factors that contribute to all the processes that partake in mitochondrial gene expression (fig. 2). These include proteins involved not just in transcription and translation, but also RNA maturation, processing, stability and decay. Furthermore, MIOREX complexes also contain factors responsible for mtDNA maintenance, regulation and stability, among other proteins that exhibit a ‘bifunctional behaviour’ (X. J. Chen et al., 2005; Kehrein et al., 2015; Singh et al., 2020; Woellhaf et al., 2016). This plethora of proteins make the presence of the MIOREX complexes of paramount importance to the mitochondria, and defects in these proteins can result in drastic phenotypes and diseases in humans (Boczonadi and Horvath, 2014; F. Wang et al., 2021).

1.4 Energy Generation by Mitochondria

1.4.1 Glycolysis and TCA cycle

The conversion of energy through the production of ATP is inarguably one of the most important functions performed by mitochondria. The mechanism of glucose metabolism is a highly conserved process, which, in eukaryotes, takes place partly in the cytosol and partly in mitochondria (fig. 3). After entering the cells, glucose is first converted to pyruvate in a multi-step multi-enzymatic pathway called glycolysis

which takes place in the cytosol. The end product of glycolysis, pyruvate, then enters the mitochondria via dedicated Mitochondrial Pyruvate Carrier proteins (MPC). There are three types of carrier proteins called Mpc1, Mpc2 and Mpc3, which, along with the first enzyme of fermentation pathway, pyruvate decarboxylase (PDC), decide whether the flux of pyruvate goes towards respiration or fermentation in yeast (Bender et al., 2015; Timón-Gómez et al., 2013). Mpc1 and Mpc3 facilitate entry of pyruvate in mitochondria, which is then metabolized for generation of ATP, lipogenesis as well as synthesis of branched chain amino-acids (Bricker et al., 2012; Herzig et al., 2012).

Once pyruvate enters the mitochondria, it is destined for respiration via the Krebs cycle/TCA cycle. In order to enter the TCA cycle, pyruvate first gets converted to acetyl CoA via a multi-subunit enzyme complex called the Pyruvate Dehydrogenase Complex (PDHc) (discussed in detail in section 1.7.1). The PDHc serves as the bridging link between glycolysis and tricarboxylic acid (TCA) cycle. Acetyl-CoA then enters the multi-step TCA cycle, gets oxidized to carbon dioxide, thereby generating NADH and FADH₂ which feed electrons into the respiratory chain (or Electron Transport Chain, ETC) for oxidative phosphorylation (OXPHOS) to take place (Raimundo et al., 2011).

1.4.2 Oxidative Phosphorylation

The electrons generated via TCA cycle enter the ETC, which is composed of five multisubunit complexes from a dual genetic origin. These complexes shuttle the electrons across the IMM and couple it to proton pumping, which generates a membrane potential. The membrane potential drives the activity of the ATP synthase to generate ATP. The shuttling of electrons to generate ATP is termed as OXPHOS. The synthesized ATP, which is commonly referred to as the energy currency of the cell, in turn, fuels and energizes a plethora of chemical reactions in the cell.

The assembly of the respiratory chain complexes is a sophisticated process constituting a large number of assembly factors as well as co-ordinated expression of nuclear and mitochondrial genes (Smith et al., 2012; Song et al., 2018; Timón-Gómez et al., 2018). There are a total of five complexes: NADH dehydrogenase (complex I), succinate dehydrogenase (complex II), cytochrome bc1 complex (complex III), cytochrome c oxidase (complex IV) and the ATP synthase (complex V), which work in synergy to generate ATP. In yeast, however, the canonical complex I is replaced by three alternative NADH dehydrogenases, namely Ndi1, Nde2 and Nde3 (fig. 3) (Barros and McStay, 2020; Matus-Ortega et al., 2015; Overkamp et al., 2000; Priesnitz and Becker, 2018). Furthermore, catalytic enhancement and substrate channeling in the process of OXPHOS in the IMM is achieved by the organization

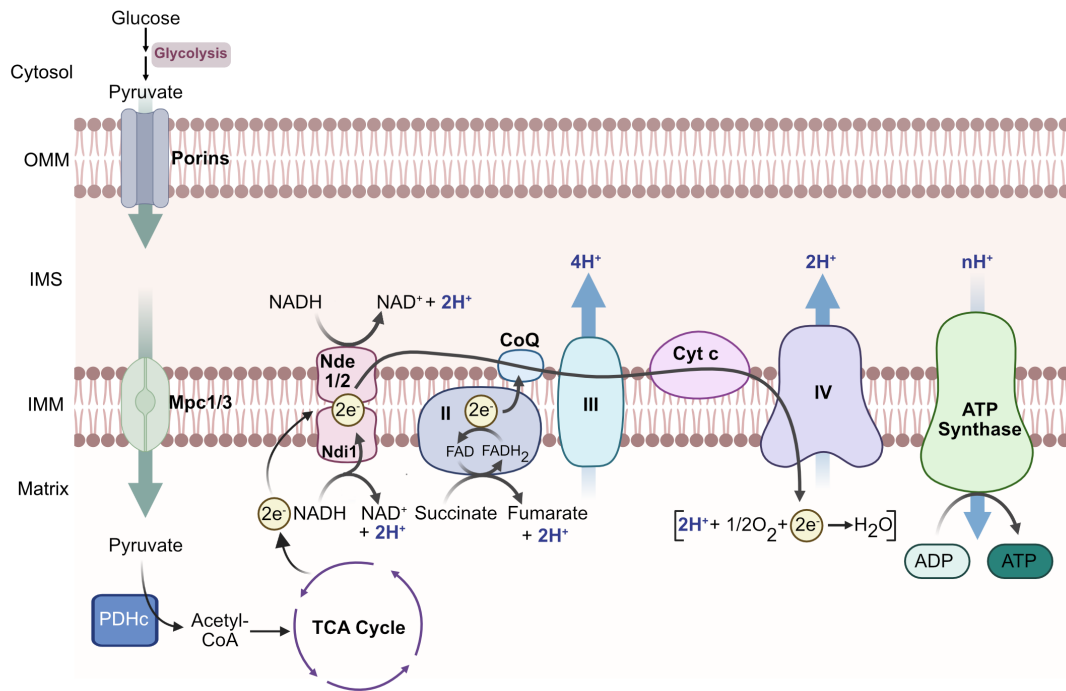


Figure 3: **A schematic showing the pathway for energy generation in yeast *S.cerevisiae*.** Glucose uptake is followed by conversion into pyruvate (Glycolysis) and entry of pyruvate into mitochondria via the Mitochondrial Pyruvate Carrier Proteins (Mpc 1/3). Pyruvate is further converted to acetyl-CoA by PDHc, where it enters the TCA cycle. The TCA cycle further contributes electrons to the electron transport chain, where they shuttle between the different complexes, which culminates into generation of energy in the form of ATP by the process of oxidative phosphorylation. The figure was created by using BioRender.com as well as Affinity designer.

of the ETC complexes into higher-order supercomplexes (Acín-Pérez et al., 2008; Rathore et al., 2019; Schägger, 2001). Defects in efficient assembly of the OXPHOS complexes has been linked to various neurodegenerative disorders and myopathies (Fernandez-Vizarra and Zeviani, 2021; Smeitink et al., 2006).

1.5 Mitochondrial Protein Quality control

The mitochondrial proteome consists of proteins encoded by both mitochondria and nucleus, of which most of the proteins are synthesized in the cytosol and are imported via a sophisticated network of translocases into their designated mitochondrial compartment (Neupert, 2015; Wiedemann and Pfanner, 2017). On the other

hand, mitochondrially-encoded proteins are sorted to their destined compartment via the mitochondrial protein biogenesis machinery, wherein Oxa1 insertase co-translationally inserts proteins into the IMM. It, however, is important that a toxic accumulation of mislocalized or superfluous proteins is prevented, for mitochondrial functions to ensue smoothly. For mitochondria to carryout respiration efficiently, there exists a tight co-ordination between the expression of both genomes in order to minimize buildup of unassembled respiratory chain subunits (Kotiadis et al., 2014; Song et al., 2021; Wiese and Bannister, 2020; Woodson and Chory, 2008). Due to the intricate process of mitochondrial biogenesis, mitochondrial proteins are particularly susceptible to faulty ETC assembly, especially under conditions of cellular stress (Böttlinger and Becker, 2012; Tatsuta, 2009). A faulty complex assembly may further lead to production of reactive oxygen species and have damaging effects on mitochondrial integrity, causing various muscular and neurodegenerative disorders in humans (Nunnari and Suomalainen, 2012). Therefore, a variety of protein quality control mechanisms exist to ensure a well-regulated environment within the mitochondria, not only by extracting and degrading defective proteins, but also by initiating mitochondrial stress responses upon encountering suboptimal conditions in the mitochondrial compartments (Song et al., 2021).

1.5.1 The role of AAA+ proteins in mitochondrial quality control

Protein quality control within mitochondria involves a multitude of different pathways that carryout surveillance of proteins during import and assembly. A variety of these mechanisms involve extraction of stalled or misfolded proteins from different compartments of mitochondria, using a mechanical pulling force by a class of ATP-dependent proteins called the AAA+ proteins (ATPases Associated with diverse cellular Activities). For example, the mitochondrial protein translocation-associated degradation (mitoTAD) pathway, that monitors the TOM translocase, removes the arrested precursor proteins from the Tom40 channel with the help of AAA+ protein Cdc48 (Mårtensson et al., 2019). Similarly, during the mitochondrial compromised protein import response (mitoCPR), a AAA+ protein of the OMM, Msp1, promotes removal of non-imported mitochondrial precursors (Basch et al., 2020; Weidberg and Amon, 2018). Moreover, in the IMM, the i-AAA and the m-AAA proteases are the two important AAA+ protein complexes that degrade faulty IMM proteins (Arlt et al., 1996; Gerdes et al., 2012; Glynn, 2017; Leonhard et al., 1996; Levytskyy et al., 2017). Other functions of proteins belonging to the AAA+ superfamily have been linked to array of cellular processes like DNA replication, membrane fusion, as well as macromolecular complex disassembly (Hanson and Whiteheart, 2005; Song et al., 2021). Mutations in these AAA+ proteins from each compartment

has been linked to various neurological disorders (Deshwal et al., 2020). Thus, the presence of AAA+ proteins in the cell is imperative to safeguard the mitochondrial proteome.

1.5.2 The domain architecture of AAA+ proteins allows ATP binding and hydrolysis

AAA+ proteins are ‘molecular machines’ that may carry out ATP-driven extraction and degradation of dysfunctional proteins (Gates and Martin, 2020; Miller and Enemark, 2016; Steele and Glynn, 2019). These proteins belong to the P-loop (Phosphate loop) superfamily of nucleoside triphosphates binding proteins, which are characterized by a very conserved domain architecture (Snider et al., 2008). Structurally, the proteins belonging to the P-loop superfamily have a distinct $\alpha\beta$ fold, that typically contains the Walker A and B motifs, which are the hallmarks of this superfamily (Miller and Enemark, 2016; Walker et al., 1982). Within the P-loop superfamily, the AAA+ proteins belong to the ASCE (Additional Strand Catalytic “E”) subdivision, wherein the strands of the core β -sheet are arranged in $\beta 5$ - $\beta 1$ - $\beta 4$ - $\beta 3$ - $\beta 2$ arrangement (Erzberger and Berger, 2006; Iyer et al., 2004; Puchades et al., 2020; Seraphim and Houry, 2020). The core β -sheet in AAA+ proteins is flanked on both sides by α helices to form a three-tier $\alpha\beta\alpha$ sandwich (Seraphim and Houry, 2020). In addition to the core, AAA+ proteins also contain a C-terminal α helical bundle, which forms a lid-like structure over the ATP-binding site (Miller and Enemark, 2016).

AAA+ proteins typically expand over 200-250 amino acids, and form homo- or hetero-oligomeric complexes, that assemble into ring like structures (Gerdes et al., 2012; Miller and Enemark, 2016; Opalińska and Jańska, 2018). AAA+ proteins possess Walker A and B motifs, which are strongly conserved ATP binding and hydrolysis motifs in these proteins (Walker et al., 1982). The Walker A motif, which has the consensus sequence of G-X(4)-GK-[TS] (X- any amino acid), forms a loop between $\beta 1$ and $\alpha 1$ called the P-loop (phosphate loop). The Walker A motif is intimately involved in ATP binding, as it co-ordinates the β and γ phosphates of the nucleotide during ATP hydrolysis. The presence of an invariant lysine aids in this function of the Walker A motif (Gates and Martin, 2020; Wendler et al., 2012). The Walker B motif, on the other hand, has a consensus sequence of hhhhDE (h- a hydrophobic amino acid), and is present in the $\beta 3$ strand. It activates a water molecule for nucleophilic attack, as well as co-ordinates magnesium ion with the help of its acidic residues, glutamate and aspartate (Hanson and Whiteheart, 2005; Wendler et al., 2012).

In addition to the Walker motifs, AAA+ proteins contain another feature called

the Second Region of Homology (SRH), located C-terminal to the Walker B motifs. The SRH comprises of two attributes, a Sensor I motif and an Arginine finger (Gates and Martin, 2020; Puchades et al., 2020). The sensor I motif acts together with the Walker B motif to orient the water molecule for nucleophilic attack on the γ phosphate of ATP, and is typically an asparagine residue, but can also be a serine, threonine or aspartate. The Arginine fingers, on the other hand, are located at the inter-subunit interface, and extend into the ATP-binding pocket of the neighbouring subunit of the AAA+ ring (Miller and Enemark, 2016; Snider et al., 2008). The Arginine finger is important for oligomerization and is the only ‘*trans-acting*’ motif in the AAA+ fold. In general, the active sites of each AAA+ domain in the oligomer are present at the interface of two adjacent subunits, where they promote efficient ATP hydrolysis and ‘translocation’ of the substrates via a central channel in the ring-like assembly (Miller and Enemark, 2016; Puchades et al., 2020).

By virtue of the aforementioned properties, the AAA+ proteins bring about mechanical unfolding of proteins not only in quality control processes like protein aggregation and precursor protein import arrest, but also act as key candidates in routine pathways like DNA replication and macromolecular complex disassembly (Hanson and Whiteheart, 2005; Opalińska and Jańska, 2018; Song et al., 2021).

1.6 *Saccharomyces cerevisiae* as the Model Organism

Mitochondrial functions are highly conserved from single-celled eukaryotes like the baker’s yeast (*Saccharomyces cerevisiae*) to higher eukaryotes like humans. Much of the current knowledge about mitochondrial function and dysfunction comes from studies using yeast. Besides providing the classical advantages of ease of genetic manipulation and biochemical handling in laboratories, yeast is an excellent model organism to study mutations that cause defects in oxidative phosphorylation and other mitochondrial processes, owing to its good fermentative capacity (Baile and Claypool, 2013; Lasserre et al., 2015).

Another major advantage for studying yeast for mitochondrial biology, due to its ability to carry out fermentation, is its tolerance to loss or mutations of mtDNA, so long as a fermentable carbon source (like glucose) is available, a feature that is named as ‘petite-positivity’. This petite-positive nature can be explained by formation of small (*petite*) colonies by respiratory-deficient yeast, when concentration of glucose in the environment is limiting. The first characterized respiratory-deficient yeast mutant revealed that respiration is regulated in yeast by the ρ (rho) factor, which

was later discovered to be a genetic element located in the mtDNA (Mounolou et al., 1966). Today, we still use the ‘ ρ ’ or ‘rho’ notation in yeast for presence of fully functional mtDNA (ρ^+ or rho^+), respiratory-insufficient mtDNA with mutations or deletions (ρ^- or rho^-), or total absence of mtDNA (ρ^0 or rho^0). Owing to this potential, several yeast species have been instrumental in studying molecular mechanisms surrounding mtDNA and its related disease manifestations at a fundamental level (Rinaldi et al., 2010; Shadel, 1999).

For the duration of this study, the yeast *Saccharomyces cerevisiae* has been employed in order to gain insights about the mutational and biochemical basis of the functions of the mitochondrial proteins that are explored in the stipulated thesis.

1.7 The mtNucleoid-binding candidates characterized in this study

The mtNucleoid has been a focus of extensive research over the past decade, yet the full scope of proteins and molecular entities within its environment remains only partially understood. Known factors within the mtNucleoid interactome are essential for its maintenance, gene expression, replication, and structural integrity, but many unknown elements persist, leaving this intricate network largely enigmatic. My research aims to delve into this interactome, applying a biochemical perspective to characterize both the established pyruvate dehydrogenase complex (PDHc) and the relatively underexplored protein Yme2, shedding light on their roles within the mtNucleoid.

1.7.1 The Pyruvate Dehydrogenase Complex

The pyruvate dehydrogenase complex (PDHc) is an evolutionarily-conserved, multi-subunit enzyme complex located in the mitochondrial matrix that links glycolysis to aerobic respiration. It catalyzes the oxidation of pyruvate (the end product of glycolysis) to form acetyl-CoA, which acts as a key substrate for TCA cycle, fueling the next step in the process of energy generation. Therefore, PDHc plays a vital role in prompting respiratory energy generation in both prokaryotes and eukaryotes. In humans, defects or deficiencies in the PDHc are linked to diseases like lactic acidosis and progressive neuromuscular degeneration (Gray, 2014; Imbard et al., 2011; K. P. Patel et al., 2012).

As PDHc acts as a gatekeeper of irreversible consumption of carbohydrates, its activity is tightly regulated in mitochondria by reversible phosphorylation by a co-ordinated activity of kinases and phosphatases (M. S. Patel and Korotchkina,

2006; Reed, 1981). The regulation by dedicated kinases and phosphatases takes place on Pda1, the E1 α subunit of the PDHc (James et al., 1995). Different organisms have different number of Pda1 phosphorylation sites (M. S. Patel and Korotchkina, 2006). In yeast, only one site has been identified so far (S313), in contrast to mammals (3 phosphorylation sites on Pda1) (Uhlinger et al., 1986). The kinases (Pkp1 and Pkp2) have a complementary activity in inactivation by phosphorylation of the PDHc. On the other hand, the phosphatases (Ppp1 and Ppp2) lead to restoration of the activity by dephosphorylation of PDHc (Gey et al., 2008; Krause-Buchholz et al., 2006). Furthermore, it was recently shown that modulation of PDHc activity can also occur due to the flexible nature of PDHc, as it can dissociate into sub-megadalton individual components in an ionic strength-dependent manner, making it a salt-labile complex (Lee et al., 2020).

Structure and Metabolic Function of PDHc

PDHc in prokaryotes and in eukaryotes is composed of multiple copies of three enzymatic centers (E1, E2 and E3), which help in catalysis of the three-step reaction of using NAD⁺ and CoA-SH to convert pyruvate to acetyl-CoA, NADH, H⁺ and CO₂ (fig. 4a). The first step of the reaction is catalyzed by the enzymatic center E1 (pyruvate dehydrogenase). The active site of E1 is bound by a cofactor TPP (thiamine pyrrophosphate), which gets transferred onto pyruvate, causing its decarboxylation to release CO₂. This is the rate-limiting step of the overall reaction and its end product, hydroxy-ethyl TPP is the substrate for the E2 (dihydrolipoyl transacetylase) enzyme center, which has an oxidised lipoyllysine group attached on a ‘swinging arm’. The hydroxyethyl group is then oxidised to acetate by E2, and further on esterified to one of the lipoyl groups of E2, resulting in reduction of the lipoyl group (-S-S-) to form two thiol (-SH) groups. The acetyl moiety attached to the lipoyl group then gets transesterified to CoA to form acetyl-CoA, which is the main end product of the overall reaction. The remaining steps of the reaction are electron transfers carried out by enzyme center E3 (dihydrolipoyl dehydrogenase) necessary to regenerate the oxidized lipoyl group of E2 for the next round of catalysis. In the last step, E3 promotes transfer of two hydrogen atoms from E2 lipoyl groups to its prosthetic group, FAD, generating FADH₂. The FADH₂, in the final step, transfers a hydride ion to NAD⁺, forming NADH. With this reaction, the entire complex is ready for the next round of catalysis and oxidation of pyruvate to acetyl-CoA (DL Nelson, AL Lehninger, MM Cox, 2008; Harris et al., 2002).

The PDHc is one of the largest known protein complexes to mankind, with peculiar and rarely seen structural features. The exact subunit composition of the fully assembled PDHc is variable among species, but the common architectural principle

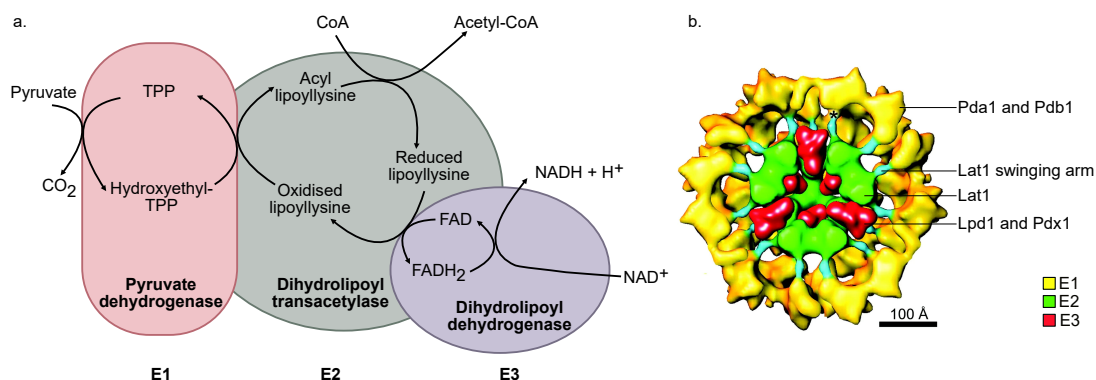


Figure 4: **The structure of PDHc along with its enzymatic reaction.** (a) A schematic showing the reaction catalyzed by the PDHc, depicting the three enzymatic centers as different colors. (b) The cut-away model of the fully assembled eukaryotic PDHc on its 3-fold axis (3D reconstructed using the deduced bovine kidney PDHc atomic structure). The colors depict the three enzymatic centers: E1, E2 and E3. The figure was adapted from Zhou, McCarthy, et al., 2001.

of the complex is conserved. The complex features an oligomeric E2 core, which serves as the structural scaffold, with multiple copies of E3 arranged at its periphery and E1 forming the outermost shell (M. S. Patel et al., 2014). Within the assembled complex, efficient shuttling of the reaction intermediates between the enzyme centers E1, E2 and E3 is carried out via the C-terminal ‘swinging arm’ domain of E2 core, which exists as long, flexible linkers that establish the physical link between the three enzymatic centers (Reed, 1974; Škerlová et al., 2021). In addition to making the complex structure highly dynamic, the E2 core also acts as a scaffold on which the pentagonal dodecahedron structure of the enzyme is built, resulting in the formation of a ‘breathing core’. The breathability confers thermally-driven structural flexibility to the PDHc (Gu et al., 2003; Zhou, Liao, et al., 2001; Zhou, McCarthy, et al., 2001).

The molecular mass of the fully assembled complex can range from 1.5 MDa in prokaryotes to around 10 MDa in eukaryotes. Unlike bacteria, eukaryotic PDHc is constituted by five subunits: E1 α (Pda1), E1 β (Pdb1), E2 (Lat1), E3 (Lpd1) and E3-binding protein or E3BP (Pdx1). In general, there are multiple models on how these subunits are arranged into the pentagonal dodecahedron structure of eukaryotic PDHc (fig. 4b) (Stoops et al., 1992, 1997; Zdanowicz et al., 2024; Zhou, Liao, et al., 2001; Zhou, McCarthy, et al., 2001). According to the ‘addition model’, 20 E2 trimers are arranged at the 20 vertices of the pentagonal dodecahedron, forming the core, with 12 E3 and E3BP molecules at the 12 faces of

the dodecahedron (Jiang et al., 2018; Kyrilis et al., 2021). In another model called the ‘substitution model’, this ratio is 48 E2:12 E3 and E3BP (Hezaveh et al., 2017; Hiromasa et al., 2004). Additionally, according to both models, each E2 trimer is linked to an E1 tetramer made of two subunits each of E1 α and E1 β , which forms the outer shell of the PDHc (Ciszak et al., 2003; Gu et al., 2003; Miran et al., 1993; Stoops et al., 1997; C. Wang et al., 2024; Zhou, Liao, et al., 2001; Zhou, McCarthy, et al., 2001).

The PDHc bypass

In glucose-abundant conditions, the predominant energy generation pathway in yeast is fermentation, wherein pyruvate is preferentially converted in the cytosol to acetaldehyde and further to ethanol, and this phenomenon is referred to as the Crabtree effect (de Deken, 1966). It is somewhat surprising that fermentation is the preferred metabolic mode for yeast even though the yield of generated ATP from respiration is higher. However, in glucose-limited, aerobic conditions (where respiration is preferred), pyruvate catabolism takes place intramitochondrially, where PDHc converts pyruvate to acetyl-CoA, a reaction that lies at the interface of glycolysis and TCA cycle (Boubekeur et al., 1999; Pronk et al., 1996). Intramitochondrial acetyl-CoA is exclusively responsible for at least two metabolic processes apart from respiration, namely the synthesis of lipoic acid as well as the amino acids arginine and leucine (Flikweert et al., 1996; van Rossum et al., 2016).

In the absence of PDHc, rerouting of the respiratory pyruvate metabolism takes place, which is known as the PDHc bypass. This can occur by yeast carrying out multiple proxy reactions both in cytosol and mitochondria, that fulfil the role of PDHc, albeit imperfectly (Boubekeur et al., 1999; Pronk et al., 1994; van Rossum et al., 2016). In the absence of PDHc, instead of generating ethanol, pyruvate gets sequentially converted in cytosol to acetaldehyde, acetate and ultimately to acetyl-CoA, by the enzymes pyruvate decarboxylase, acetaldehyde dehydrogenase, and acetyl-CoA synthetase, respectively. This acetyl-CoA can act as a precursor for synthesis of lipids, sterols, lysine and as an acetyl donor for protein acetylation (Takahashi et al., 2006; van Rossum et al., 2016).

In yeast mitochondria, however, the deficiency of acetyl-CoA is partially fulfilled by an enzyme called Ach1 (acetyl-CoA hydrolase), which converts succinyl-CoA (a reaction intermediate of TCA cycle) to acetyl-CoA (Buu et al., 2003; Y. Chen et al., 2015; Fleck and Brock, 2009). The acetyl-CoA is further used for arginine, leucine and lipoate biosynthesis, but does not meet the entire demand for running TCA cycle and oxidative phosphorylation (van Rossum et al., 2016). As a substitution for insufficient TCA cycle flux, intermediates like citrate and α -ketoglutarate get additionally shuttled into the mitochondria and directly get fed into the TCA cycle.

These alternative pathways are commonly called anaplerotic reactions (Arnold and Finley, 2023; Xiberras et al., 2020). Therefore, the combined presence of both PDHc and Ach1 ensure robust generation of acetyl-CoA to meet mitochondrial needs (Boubekeur et al., 1999; van Rossum et al., 2016).

PDHc as a bifunctional enzyme

The main function of PDHc lies in metabolism where it acts as a frontier to respiration in mitochondria. However, as mentioned in section 1.2, the protein subunits Pda1, Pdb1 and Lpd1 were identified as a possible bifunctional proteins in yeast due to their presence close to the mtDNA in formaldehyde-crosslinked mitochondria (X. J. Chen et al., 2005; Kaufman et al., 2000). Furthermore, it was observed that these subunits were required for mtDNA stability in the cells (X. J. Chen et al., 2005). Apart from yeast, the components of PDHc have been identified in close proximity to mtDNA in various other eukaryotic as well as prokaryotic organisms. Among prokaryotes, the E2 subunit has been observed to bind to and regulate gene expression (Stein and Firshein, 2000; T. Walter and Aronson, 1999). In *Chlamydomonas reinhardtii*, the dihydrolipoamide acetyltransferase DLA2 (the E2 subunit) has been observed to exhibit moonlighting activity in chloroplast gene expression, by binding to mRNA in mixotrophic growth conditions (Bohne et al., 2013; Neusius et al., 2022). Similarly, in *Xenopus* oocyte mitochondria, the E2 subunit was found to associate with mtDNA upon metrizamide gradient analysis as well as immunoprecipitation studies, albeit without E1 and E3 subunits, which is rather surprising, as it suggests the independent functioning of E2 subunit in mtDNA association (Bogenhagen et al., 2003). Furthermore, the E2 subunit has also been co-purified with mtNucleoids in mammalian cells (Rajala et al., 2015). Nevertheless, the exact reason for the role of the PDHc in nucleic acid binding remains to be determined, and is open to investigation.

Therefore, this study aims at exploring the function of the PDHc as an mtDNA-binding enzyme in yeast, with an attempt to pinpoint the nature of its interaction at the molecular level.

1.7.2 Yme2

The endosymbiotic theory about the origin of mitochondria proposes that mitochondria arose as a result of a symbiotic relationship between ‘proto-mitochondrion’ and ‘proto-eukaryote’ (Gray, 1989; Sagan, 1967; Shafer et al., 1999). Eventually, over the course of evolution, the endosymbiont transferred parts of its DNA to the nucleus (Andersson et al., 1998). Meanwhile, this uptake of mtDNA by the nucleus has been well-documented for a number of eukaryotes, but questions involving

mechanisms of how this uptake happens and what role it plays in the metabolism and mitochondrial function, remain to be answered.

YME2 (Yeast Mitochondrial Escape protein 2) was first identified in a genetic screen, wherein its mutational inactivation led to escape of mtDNA from mitochondria to the nucleus (Hanekamp and Thorsness, 1996; Thorsness and Fox, 1993). It was one of the six nuclear-encoded genes discovered in this screen (*YME1-YME6*), the deletions of which accelerate the rate of mtDNA escape. Yme2 is an integral protein of the IMM that contains a putative single-spanning transmembrane domain, and exposes its N- and C-termini to the matrix and intermembrane space, respectively (Hanekamp and Thorsness, 1996; Leonhard et al., 2000). It has been previously observed that the deletion of Yme2 confers no collateral phenotype in yeast (Hanekamp and Thorsness, 1996; Thorsness and Fox, 1993). More recently, Yme2 was found to co-localize with mtDNA nucleoids and Yme2-GFP was used to visualize mitochondrial nucleoids (Hanekamp and Thorsness, 1996, 1999; Murlley et al., 2013; Park et al., 2006). Furthermore, Yme2 was also observed to be associated to the MIOREX complex (see section 1.3), presumably playing a role in the spatial environment of these large expressosome-like assemblies involved in mitochondrial gene expression (Kehrein et al., 2015). Although there is evidence about the topology and location of YME2 in the mitochondria, insight about its exact function in the mtNucleoids is largely unknown. This study, therefore, sheds light on the function of Yme2, based on a thorough mutational analysis of its sequence and putative structure.

2 Aim of this Study

The mtNucleoid is an mtDNA-containing complex essential for mitochondrial maintenance, gene expression, replication, and stability. However, its full composition remains elusive, with numerous associated factors and their roles still largely speculative. This research aims to investigate the mtDNA interactome from a biochemical perspective, focusing on two key candidates to uncover their specific roles within the context of the mtNucleoid.

The first objective of this study is to unravel the dual role of PDHc in mitochondria beyond its established metabolic functions. By characterizing its interaction with the mitochondrial genome, the study aims to elucidate its contribution to mtDNA maintenance and overall mitochondrial health.

The second objective is to characterize Yme2, a relatively understudied component of the mtNucleoid interactome. Using mutational analysis and structural characterization, this research will investigate Yme2's functional roles, its genetic interactions with mitochondrial protein biogenesis machinery, and its implications in mitochondrial genome stability.

By integrating these investigations, this work aims to enhance our understanding of the molecular dynamics and multifaceted roles of the mtDNA interactome, shedding light on the complex network underlying mitochondrial function.

3 Results

The mtNucleoid, replete with its interactome, has been long known to play a critical role in maintaining mitochondrial function. The research surrounding the role and dynamics of mtNucleoid is only beginning to prosper, owing to the advancements in scientific technology and imaging, as well as high throughput data generation. The mtNucleoid interactome, however, remains largely unexplored, with only limited research shedding light on its complex network. What we do know is, that it has a plethora of interacting factors that contribute together to efficient functioning of mtNucleoid as well as the mitochondria. The factors participating in mtNucleoid interactome have only been partly identified, with the presence of some of them being only a speculation. This study explores two such candidates, which have been previously identified to be a part of the mtNucleoid interactome, but their nature of interaction remains to be characterized.

In the first section, a well-known and characterized protein complex, the pyruvate dehydrogenase complex, is examined and its specificity of interaction with the mtDNA within the mtNucleoid is explored. The second part delves into a relatively lesser known, mtNucleoid-interacting protein called Yme2, and majorly focuses on its mutational characterization.

3.1 The Pyruvate Dehydrogenase Complex (PDHc)

The PDHc in yeast is a multi-subunit multi-enzyme complex that is composed of five subunits in yeast, which together assemble into three enzymatic centers, namely E1 (Pda1 and Pdb1), E2 (Lat1) and E3 (Lpd1 and Pdx1) (see section 1.7.1). PDHc forms an essential metabolic link between glycolysis and Krebs cycle, thereby driving mitochondrial respiration. It resides in the mitochondrial matrix, where it converts the incoming pyruvate (the end product of glycolysis) to acetyl-CoA, which further gets fed into TCA cycle. Recently, there has been evidence that the PDHc could potentially act as a bifunctional enzyme as it is observed to be associated to mtDNA (X. J. Chen et al., 2005; Kaufman et al., 2000; Rajala et al., 2015) (see section 1.7.1). However, the reason for this spatial proximity between PDHc and mtDNA remains largely elusive. This section explores and attempts to characterize the nature of association of PDHc to the mtDNA.

3.1.1 PDHc subunits contribute to overall mitochondrial health and integrity

Given the observed proximity of PDHc to mtDNA, an investigation into the effects of PDHc on mitochondrial health was initiated. Consequently, deletion strains for each subunit of the PDHc were subjected to growth analysis (fig. 5a). On fermentable medium (YPD), none of the deletion strains displayed a growth defect at 30°C, and only a weak growth phenotype at 37°C. On non fermentable medium (YPG), however, $\Delta pda1$, $\Delta pdb1$, $\Delta lat1$ and $\Delta pdx1$, exhibited a minor growth defect at 30°C, which worsened at thermally stressful temperature of 37°C. $\Delta lpd1$, however, was virtually dead on YPG, owing to its pleiotropic effects on the cells, due to the involvement of Lpd1 in multiple 2-oxo-acid dehydrogenase complexes, namely, α -ketoglutarate dehydrogenase complex (KGDHc), branched-chain keto acid dehydrogenase complex (BCKDc) and glycine decarboxylase complex (GDC). Considering that PDHc is a metabolic gatekeeper for aerobic respiration, these phenotypes were not entirely surprising.

It was next investigated whether the lack of strong growth defects of the single subunit deletions were due to acetyl-CoA being produced in alternative ways, that is, by Ach1, which converts succinyl-CoA to acetyl-CoA. In order to test this, a growth analysis was performed with double deletions of individual PDHc subunits and *ACH1* (fig. 5b). While $\Delta ach1$ itself had no obvious growth defects on fermentable and non-fermentable media, co-deletions of *ACH1* with PDHc subunits led to phenotypes that were more severe as compared to the single deletions, both on YPD and more so, on YPG media. The presence of a weak phenotype even on fermentable media points towards the fact that the double deletions of PDHc subunits and Ach1 exhibit growth defects that lie beyond mere respiratory growth.

It is known that PDHc is essential for cellular metabolism as it promotes efficient respiration, but whether it affects the overall mitochondrial health, remains to be answered. In this regard, petite analysis was carried out with the single deletion subunits of PDHc. Upon 8h of growth at 30°C, the petite frequencies of the single deletion subunits showed an expected WT-like level (mean WT petite frequency = 7.3%), but $\Delta pda1$ and $\Delta pdb1$ displayed a slightly higher petite frequency of 13.4% and 10.4%, respectively (fig. S1a). However, after 11h of growth at 37°C, the observed trends were considerably different. $\Delta pda1$ and $\Delta pdb1$ had a respective petite frequency of 77.2% and 79.2% (P-values = <0.001), whereas $\Delta lat1$ had a petite frequency of 61.3% (P-value = 0.005) in comparison to WT (38.4%) (fig. 5c). $\Delta pdx1$ however, had a WT-like petite frequency at both 30°C and 37°C. $\Delta lpd1$, on the other hand, was excluded from the analysis as this strain is petite by nature. Taken together, this indicated that $\Delta pda1$, $\Delta pdb1$ and $\Delta lat1$ had a higher tendency to form respiratory-deficient colonies as compared to WT, especially at higher

temperatures, which could be a consequence of mtDNA loss or instability, mtDNA mutations, metabolic inflexibility or due to overall debilitation of mitochondrial fitness.

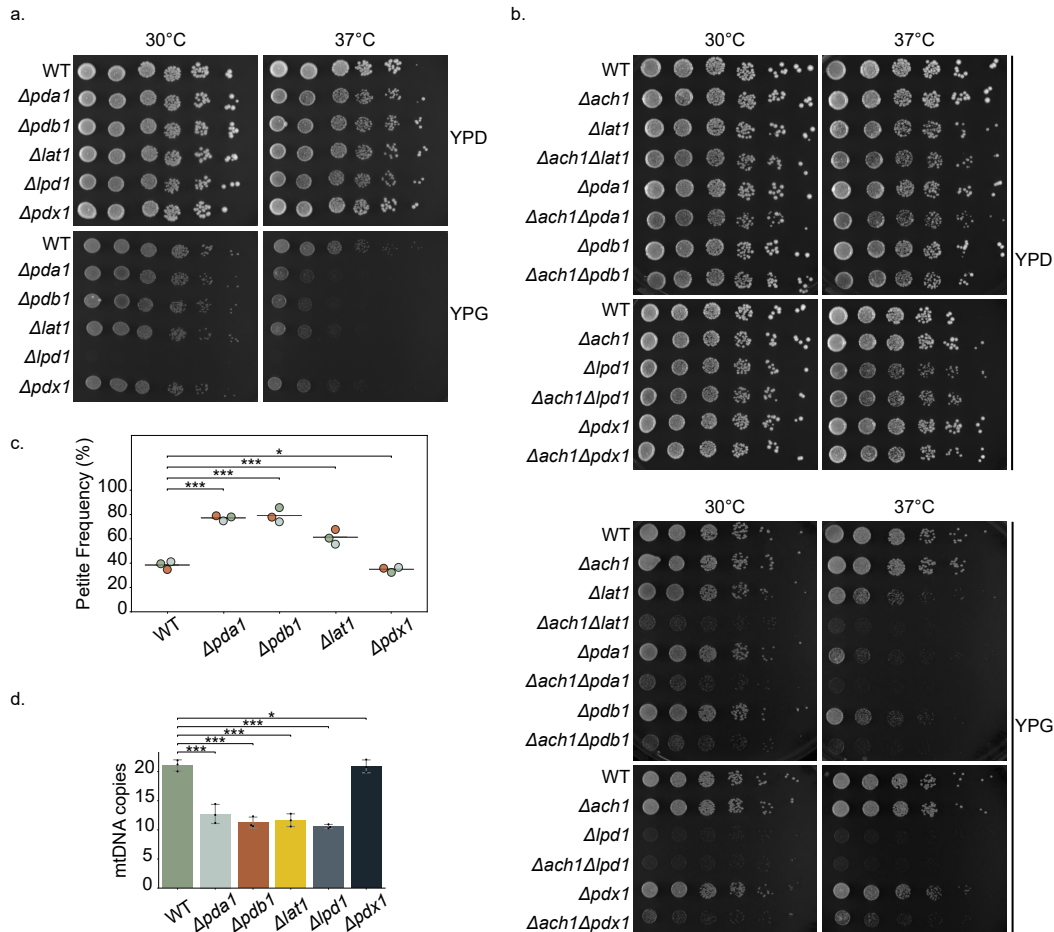


Figure 5: **Mitochondrial health is influenced by PDHc subunits.** (a,b) Growth test analysis showing the indicated strains spotted on fermentable YPD medium and non-fermentable YPG medium and at 30°C and 37°C and allowed to grow for 2 days. (c) Petite analysis of the indicated strains after growth at 37°C for 11 h. The strains were analyzed after 4 days of growth. (d) Quantitative PCR analysis after growth of indicated strains at 37°C for 11 h followed by calculation of mtDNA copy number for the indicated strains (The qPCR was performed by Johannes Hagen). (P-values: $p < 0.005$: ***, $p < 0.05$: **, $p < 0.5$: *).

3.1.2 PDHc functions in mtDNA maintenance

In order to exclude the possibility that the petite phenotype observed for PDHc deletion subunits was purely due to metabolic inflexibility, a petite analysis with $\Delta mpc1$ was performed. Mpc1, or Mitochondrial Pyruvate Carrier 1, is a protein responsible for facilitating pyruvate uptake into mitochondria. In the absence of Mpc1, pyruvate cannot be imported into mitochondria, resulting in a substrate deficit for the PDHc within the mitochondrial matrix. Consequently, the PDHc reaction is impaired, preventing the production of acetyl-CoA, despite the enzyme complex being intact and fully functional. By comparing the petite phenotype associated with PDHc subunit deletions to that observed in $\Delta mpc1$, an attempt was made to discern whether the phenotype arises exclusively from metabolic inflexibility (caused by either PDHc dysfunction or pyruvate unavailability) or results from factors that extend beyond the disruption of this metabolic reaction. Of note, the deletion of *MPC1* led to minor growth defect on YPG, possibly due to existence of accessory ways of pyruvate synthesis in mitochondria (fig. S1c). As deletion of *MPC1* causes the cells to be auxotrophic for valine synthesis (Bricker et al., 2012; Herzig et al., 2012; Timón-Gómez et al., 2013), $\Delta mpc1$ cells displayed a phenotype also on SC-Val at both 30°C and 37°C. Nevertheless, $\Delta mpc1$, which is expected to cause metabolic insufficiency of pyruvate and disruption of the conversion of pyruvate to acetyl-CoA in the mitochondria, displayed a petite frequency of 4.5% at 30°C and 35% at 37°C (fig. S1d (i) and (ii)), which was only marginally higher than WT. This indicated that the much higher petite frequency observed in the case of PDHc deletion subunits is rather due to a role of the PDHc that goes beyond adversities caused by interruption of this metabolic pathway.

To delve deeper into the cause of the petite phenotype exhibited by the deletions of PDHc complex, a qPCR analysis was performed after growing the respective deletion strains either at 30°C for 8h, or at 37°C for 11h. Upon calculating the amount of mtDNA copies each of the strains had, it was observed that at 37°C, where most PDHc deletion strains exhibited a stronger petite frequency, they also indeed had significantly lower number of mtDNA copies as compared to WT (fig. 5d). In contrast, $\Delta pdx1$, which showed WT-like petite frequency, also had similar amount of mtDNA copies as WT. This suggested that one of the main reasons for the strong petite phenotype and respiratory insufficiency for the aforementioned deletions was the loss of mtDNA copies upon growth at higher temperatures. Of note, at 30°C, all deletion strains had non-significant change in the amount of mtDNA in comparison to WT (fig. S1b).

Additionally, double deletion strains were also generated for enzymes E1 and E2, by deleting either Pda1 or Pdb1 with Lat1, to observe the changes that occur in the phenotypic behaviour when multiple enzymatic subunits of PDHc are deleted. Upon

performing the growth tests, it was observed that $\Delta lat1 \Delta pda1$ and $\Delta lat1 \Delta pdb1$ showed a marginally worse growth than the respective single deletions, on both YPD and YPG media (fig. S1e). Moreover, when petite analysis was performed with these strains, it was observed, that both double deletions exhibited slightly higher petite frequency as compared to respective single deletions (fig. S1f (i) and (ii)). This outcome was not entirely surprising, as the deletion of multiple subunits within the PDHc is likely to exacerbate cellular dysfunction compared to the deletion of a single subunit.

Collectively, the results were suggestive of the fact that the function of PDHc is not just limited to metabolism, but also lies in maintaining mtDNA, and by extension, overall mitochondrial health in yeast.

Considering that PDHc possibly associates with mtDNA and plays a role in mtDNA maintenance, it was proposed to further explore this association at a molecular and biochemical level to gain novel insights about the function of PDHc in mitochondria. Previously, peptide antibodies against Pdb1, Lat1, Lpd1 and Pdx1 were generated in our lab (by Julia Weisenseel), and antibody serum against Pda1 was obtained from the lab of Prof. Dr. Chris Meisinger (C. Walter et al., 2022). It has to be noted that the Anti-Pda1 antibody was not purified and had a very weak cross-reactive band just below the actual target band. Mitochondria were isolated and purified for WT, $\Delta pda1$, $\Delta pdb1$, $\Delta lat1$, $\Delta lpd1$ and $\Delta pdx1$ from cells grown in YPGal medium and the expression levels were checked for all the subunits of PDHc. As observed before on cell lysates (by Julia Weisenseel (fig. S2a)) and now in this study on purified mitochondria (fig. S2b), the levels of Pda1 in $\Delta pdb1$ were significantly less. Apart from this, all antibodies looked fairly clean and specific to the protein they were raised against. Therefore, the association of PDHc to mtDNA was explored further in order to gain better insights into this role of PDHc in mitochondria.

3.1.3 The role of PDHc in mtDNA maintenance is uncoupled from its metabolic function

Given that PDHc has a prime function in respiratory metabolism and an additional function in mtDNA maintenance, it was further investigated, on a catalytically inactive mutant level, whether these two functions were, in fact, coupled to each other. In this respect, catalytically dead mutants of the E1 α (Pda1) and the E2 (Lat1) enzymes were created.

The generation of catalytic dead mutant of Pda1 has been previously characterised in *E. coli*, wherein, the mutation of the residue G231, significantly reduced the specific activity of the PDHc (from 6.86 units/mg for the WT enzyme to 0.067 units/mg for the Pda1-G231 mutant) (Russell et al., 1992; Yi et al., 1996). In yeast,

this amino acid corresponds to G217, and therefore, a potentially catalytic dead PDHc mutant with Pda1^{G217A} was created. The mutant copy of Pda1 was inserted into the Leu2 locus of $\Delta pda1$ strain. Subsequently, a growth test analysis was performed in order to confirm whether Pda1^{G217A} mutant was indeed a catalytically inactive mutant. As expected, $\Delta pda1$ displayed a minor growth phenotype on YPD at 37°C and a drastic growth defect on YPG at 30°C and 37°C (fig. 6a). This growth defect was completely rescued when the WT copy of Pda1 was re-inserted into the Leu2 locus, but only partially rescued when the Pda1^{G217A} was re-incorporated, suggesting that the observed phenotype of $\Delta pda1$ strain could be a contribution of the lack of enzymatic activity as well as mtDNA maintenance by the PDHc. The mutant Pda1 displayed the growth phenotype partially similar to $\Delta pda1$, confirming its catalytic inactivity. Moreover, the expression levels of both Pda1^{WT} and Pda1^{G217A} strains were observed to be WT-like (fig. 6e(i)). Additionally, similar growth patterns were observed in $\Delta ach1 \Delta pda1$ background, where the re-insertion of Pda1^{WT} rescued the double deletion phenotype whereas the Pda1^{G217A} variant resulted in only minimal rescue (fig. 6f).

To see the effect of the mutant on mtDNA maintenance, a petite analysis was performed after growing the strains at 37°C for 11 h (fig. 6b). While $\Delta pda1$ had a petite frequency of 79%, which was in line with the previous observations, reinsertion of Pda1^{WT} rescued the petite frequency back to 42% which was similar to the WT control level. The startling effect, though was brought by the reincorporated catalytically inactive Pda1^{G217A} variant, which also rescued the petite frequency to 49%. This meant that while the mutant Pda1 rendered the enzyme metabolically inactive, it still rescued the petite phenotype to WT levels, thereby uncoupling the two functions of PDHc.

Likewise, to investigate the uncoupling of metabolic and mtDNA maintenance functions of PDHc, a catalytic-dead mutant of Lat1 (the core or E2 enzymatic center of the PDHc) was also generated. This mutant has been characterised in previous studies (Niu et al., 1990), and was created by making a double point mutant of Lat1 in the active site of the catalytic center of Lat1. This mutant (H455A/D459A) prevents the transfer of acetyl to a coenzyme A moiety, thereby impeding catalytic function of PDHc. In this study, the mutated copy of Lat1, i.e. Lat1^{H455A/D459A} was inserted into the HO locus of $\Delta lat1$ yeast background. When a growth analysis was performed with this mutant, it was observed that while re-insertion of Lat1^{WT} copy rescued the growth phenotype of $\Delta lat1$, the re-incorporation of the Lat1^{H455A/D459A} was detrimental to growth of the cells on YPG medium at 30°C and 37°C, and partly on fermentable medium at 37°C, much like the parent strain, $\Delta lat1$ (fig. 6c), confirming the catalytic inactivity of the $\Delta lat1 + Lat1^{\text{H455A/D459A}}$ strain. In conjunction, the Lat1^{WT} variant rescued the

Results: The Pyruvate Dehydrogenase Complex (PDHc)

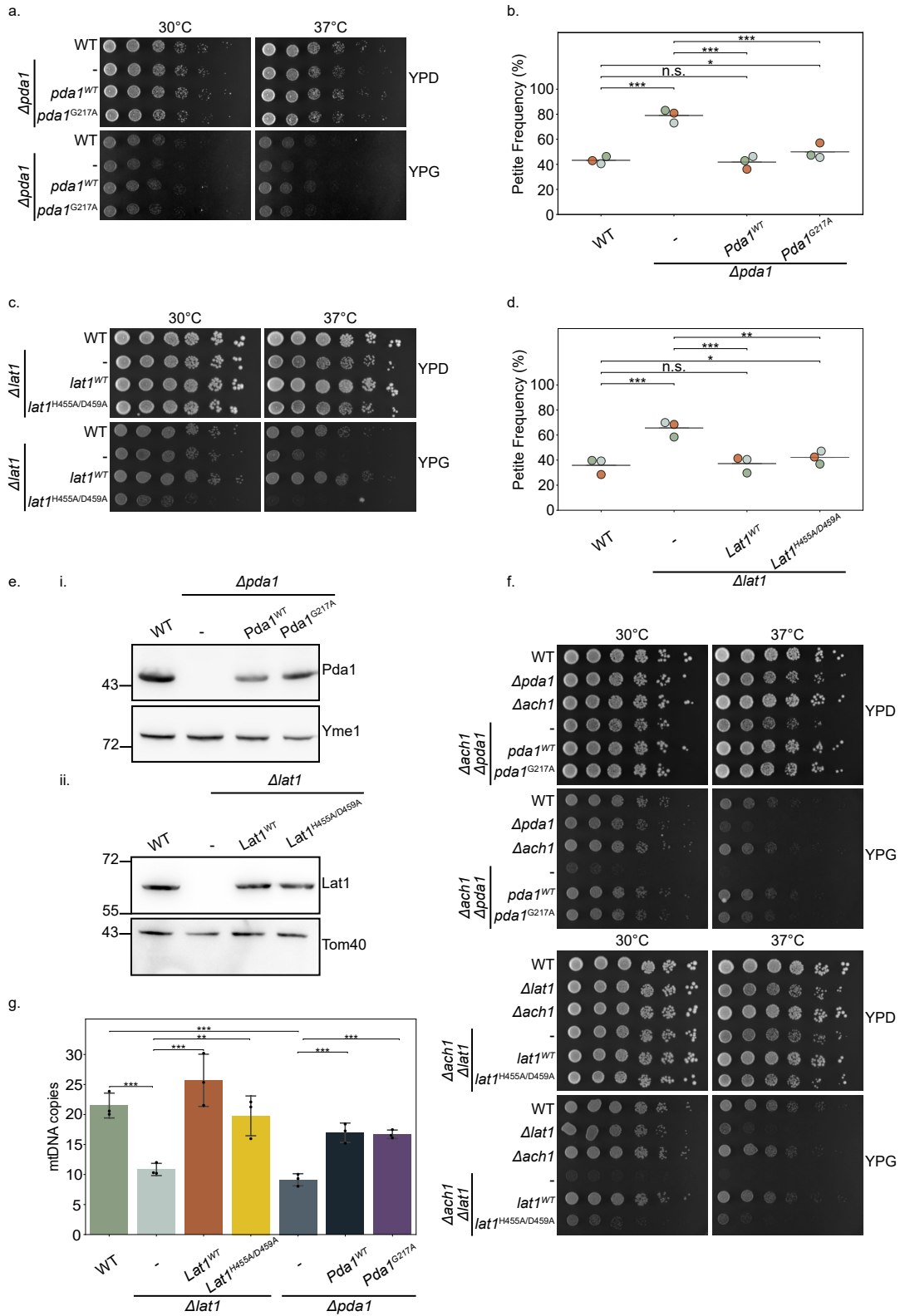


Figure 6: The metabolic role of PDHc is uncoupled from its function in mtNucleoid maintenance. (a) Growth tests showing the indicated strains on YPD and YPG after 1 day of growth. (b) Petite analysis of the indicated strains after growth at 37°C for 11 h. The strains were analyzed after 4 days of growth. P-values were calculated using unpaired t-test. (c) Growth tests showing the indicated strains on YPD and YPG after 2 days of growth. (d) Petite analysis of the indicated strains after growth at 37°C for 11 h. The strains were analyzed after 4 days of growth. P-values were calculated using unpaired t-test. (e) Western blot showing expression levels of the indicated strains from cell lysates, blotted with Lat1, Pda1, Yme1 and Tom40 antibodies. (f) Growth tests showing the indicated strains on YPD and YPG after 2 days of growth. (g) Quantitative PCR analysis (performed by Johannes Hagen) after growth of indicated strains at 37°C for 11 h followed by calculation of mtDNA copy number for the indicated strains. P-values were calculated using Welch's t-test. (P-values: $p < 0.005$: ***, $p < 0.05$: **, $p < 0.5$: *).

growth defect also in the $\Delta lat1 \Delta ach1$ background, whereas the $Lat1^{H455A/D459A}$ mutant did not, supporting the catalytic inactivity of the mutant (fig. 6f). Moreover, upon checking the expression levels of Lat1 in the aforementioned strains, it was seen that the $\Delta lat1 + Lat1^{WT}$ and $\Delta lat1 + Lat1^{H455A/D459A}$ had levels comparable to WT cells (fig. 6e(ii)).

To evaluate the coupling of the metabolic and mtDNA association functions of PDHc, petite analysis was performed with the $Lat1^{H455A/D459A}$ mutants after growth at 37°C for 11 h (fig. 6d). As expected, $\Delta lat1$ had a petite frequency of 65.6% (P-value=0.004) as compared to WT (35.8%). The $\Delta lat1 + Lat1^{WT}$ showed a complete rescue of petite frequency. Strikingly, the catalytic-dead mutant $\Delta lat1 + Lat1^{H455A/D459A}$ also showed a complete rescue of the petite frequency (37.2%), which was quite discernible from the inability of this mutant to rescue the growth phenotype of the $\Delta lat1$ strain.

Similar trends were observed when a quantitative PCR was performed after growing the cells at 37°C for 11 h. The catalytic mutants of both Lat1 and Pda1 rescued the mtDNA copy number to nearly WT-levels, despite being metabolically insufficient (fig. 6g). Taken together, these results showed that the function of PDHc as the metabolic gatekeeper to respiration in mitochondria is uncoupled from its role in maintaining mtDNA, and that this role brings a novel bifunctionality to this enzymatic complex.

3.1.4 Association of PDHc with the mitochondrial gene expression machinery

Following the establishment of a role for the PDHc in mtDNA maintenance, the molecular interactions of the PDHc were further explored at the biochemical level. To gain deeper insights into the proteins interacting with the PDHc within mitochondria, a co-immunoprecipitation (co-IP) experiment was conducted using PDHc subunits, followed by mass spectrometry analysis. Purified antibodies against Pdb1 (subunit of E1 enzymatic center) and Lat1 (E2 enzymatic center) were first tested with purified mitochondria for co-IP analysis. Unfortunately, the Anti-Pdb1 antibody was not suitable for co-IP assays (fig. S3a). The Anti-Lat1 antibody, however, proved to be ideal for co-IP. Next, for lysis of mitochondria, two different detergents, namely 1% digitonin and 0.5% NP-40, were tested. As seen in figure (fig. S3b), Lat1 co-IP worked in both conditions, that is, there was high enrichment of Lat1 in the elution fraction, compared to $\Delta lat1$, which was the negative control. When Abf2 (the mtNucleoid marker protein) was decorated on the same blot, it was observed that Abf2 was only enriched in the co-IP where mitochondria were lysed with 1% digitonin. Therefore, 1% digitonin was selected as the detergent for the co-IP that was further subjected to mass spectrometry analysis (fig. 7a). As expected, there was enrichment observed for Lat1, as well as for other subunits of PDHc, along with the mtNucleoid marker Abf2. Notably, a fraction of each protein was still present in the flowthrough fraction, suggesting the presence of residual PDHc subunits, either as part of an intact complex or in monomeric form. Furthermore, upon conducting mass spectrometry analysis (performed by PD Dr. Serena Schwenkert), it was observed that the subunits of PDHc were among the most enriched proteins (fig. 7b(left)). Abf2, and other mtNucleoid interactors were also highly enriched in the WT sample as compared to the $\Delta lat1$ sample (supplementary table B.7). GO term enrichment for biological processes revealed, furthermore, that the most significantly enriched proteins in WT sample compared to $\Delta lat1$ were proteins involved in mitochondrial genome maintenance, which supported the role of PDHc in mtDNA association (fig. 7b(right)).

A closer look at the molecular level was then taken at the interactome of PDHc, by performing an *in situ* assay called proximity labelling assay (fig. 7e). To achieve this, Pda1 was tagged with TurboID, an engineered biotin ligase enzyme used for proximity labelling (Branon et al., 2018; Kim and Kim, 2024), that enables identification of the *in vivo* proximal proteome of the tagged protein. TurboID, upon biotin induction, catalyzes biotinylation of neighboring proteins within an approximately 10 nm radius. These biotinylated proteins can be isolated using streptavidin-based affinity purification and subsequently identified through mass spectrometry. This approach, which allows high-resolution proteomic analysis of

suborganellar compartments with exceptional precision, was employed to identify proteins in close proximity to Pda1.

The proximity labelling assay was performed with log-phase grown cells, which were treated with biotin for 30 minutes prior to mitochondrial purification. As an additional control to a WT strain, a strain expressing a mitochondrial matrix-targeted freely-floating TurboID (Floaty-TurboID) was used, that would potentially biotinylate everything that comes in contact with it. There were two considerations that were needed to be taken into account. Firstly, that the growth analysis of Pda1-TurboID strain showed a minor phenotype on YPG medium at 37°C as compared to the WT (fig. S3c). In contrast, $\Delta pda1$, had a strong growth phenotype in the same conditions. Secondly, it was observed that the expression levels of Pda1-TurboID were also significantly lower than WT levels (fig. S3d), which could possibly explain the YPG phenotype. These results indicate that the TurboID tag may not have been optimal for maintaining the stability of Pda1. Nevertheless, the proximity labelling assay was carried out with WT, Pda1-TurboID and Floaty-TurboID strains, and the potential interacting proteins were purified by affinity purification with the streptavidin-conjugated magnetic beads. About 80% of the resulting elution samples were sent for mass spectrometry (performed by PD Dr. Serena Schwenkert), whereas the leftover 20% of the samples were subjected to western blotting. The resulting blot was decorated with antibodies against PDHc subunits, as well as HRP-conjugated streptavidin (fig. 7c). The blot revealed a distinct biotinylation pattern in the elution fractions of the Pda1-TurboID sample when probed with HRP-conjugated streptavidin. In contrast, the Floaty-TurboID strain exhibited a weaker but noticeably different biotinylation pattern in the elution fraction. As expected, all subunits of PDHc were enriched in the elution fraction of the Pda1-TurboID sample, with Lpd1 enrichment being the least apparent, possibly due to its involvement in multiple metabolic pathways.

The Mass spectrometry following proximity labelling assay revealed enrichment of PDHc subunits in Pda1-TurboID sample in comparison to both Floaty-TurboID and WT, as anticipated (fig. 7d, supplementary table B.8). Upon performing GO term analysis for biological processes, it was revealed that Pda1-TurboID sample also displayed enrichment of genes involved in mitochondrial gene expression and mitochondrial translation processes, when compared to both Floaty-TurboID and WT samples (fig. 7d (i) and (ii)). On the contrary, when Floaty-TurboID sample was compared with WT sample, proteins related to metabolism and biosynthesis were enriched, albeit not as strongly as Pda1-TurboID vs. Floaty-TurboID or WT (fig. 7d (iii)). In summary, it was clear that the highly enriched proteins which were found in immediate proximity to Pda1, and by extension to PDHc, belonged to the mitochondrial translation and gene expression categories, which include factors

Results: The Pyruvate Dehydrogenase Complex (PDHc)

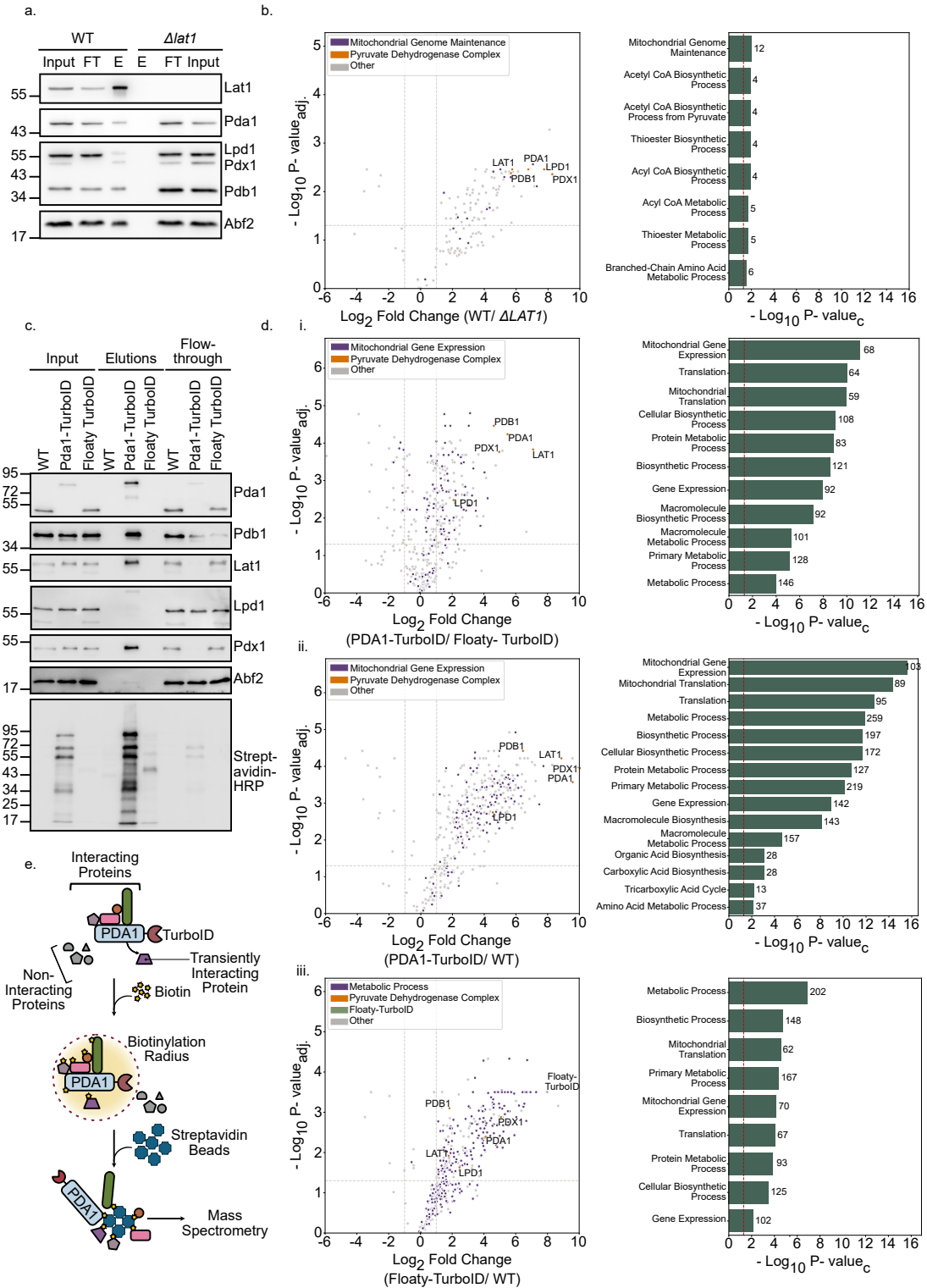


Figure 7: **The interacting partners of PDHc.** (a) Western blot showing co-IP performed with Anti-Lat1 antibody on purified mitochondria upon lysis with 1% digitonin. Input and flowthrough (FT) are 10%, and a sixth of the total elution (E) fraction was loaded on the gel. (b) Volcano plot (left) showing analysed mass spectrometry data, upon comparison of WT sample vs. $\Delta lat1$ (negative control). The top GO term for biological processes is highlighted in purple, and the most significant GO terms are displayed on the right, along with the $-\log_{10}$ corrected p-values as x-axis and number of genes belonging to the term highlighted next to the bar. (c) Proximity labelling assay performed with TurboID-tagged Pda1 with WT and Floaty-TurboID as controls. The input and flowthrough fractions are 1% whereas the elution (E) represents a sixth of the total amount used for the assay. The biotinylation patterns were observed after decorating the membranes with HRP-conjugated streptavidin. (d) (i),(ii),(iii) Volcano plots comparing the indicated strains with the top GO term highlighted in purple (left) and the significant GO terms and the number of associated genes in the barplot (right). The $-\log_{10}$ corrected p-values are plotted on the x-axis and number of genes belonging to the respective term are mentioned next to the bar. (e) Schematic showing the workflow of proximity labelling assay.

involved in MIOREX complex, mitoribosome, transcription and translation. This supported the idea of presence of PDHc in the mtNucleoid interactome, within the MIOREX complex, and its spatial proximity to proteins related to transcription and translation could likely mean that it resides close to proteins involved in the mitochondrial gene expression machinery.

3.1.5 PDHc subunits interact with mitochondrial RNA

In the previous section, it was observed that PDHc likely could be a member of the mtNucleoid interactome, possibly proximal to the mitochondrial gene expression machinery. To further examine this qualitatively, an experiment to test whether the solubility of the PDHc subunits changes upon RNase or DNase treatment, was performed. In this regard, mitochondrial isolation was performed from WT cultures grown in fermentable (YPD and YPGal), and non-fermentable (YPG) media. The mitochondria were solubilized, and then treated with 1 μg RNase I, after which they were subjected to centrifugation and separation of supernatant and pellet fractions. When the supernatant and pellet fractions were subjected to western blotting, it was observed that in the samples that were not treated with RNase I, the PDHc components (except Lpd1) were found either partially (Pda1 and Pdb1) or completely (Lat1 and Pdx1) in the pellet fraction (fig. 8a). Lpd1, on

the other hand, was completely soluble, and was observed to be in the supernatant after solubilization. However, treatment of solubilized mitochondria with RNase I resulted in a redistribution of the PDHc subunits, with a greater presence observed in the soluble fraction. Pda1, Pdb1, Lat1 and Pdx1 were observed to shift to the supernatant fraction, where the band intensity was now higher as compared to the control. This implied that the solubility of the PDHc subunits increased when wild-type mitochondria were treated with RNase I, leading to the degradation of mitochondrial RNA and the release of PDHc subunits into the supernatant fraction. Notably, this effect was observed across all tested media, indicating that the potential association between PDHc and mitochondrial RNA was independent of the carbon source (fig. 8a (i), (ii), (iii)).

In contrast, DNase I treatment of mitochondria did not result in any obvious changes in solubility for any of the proteins except the mtDNA packaging factor, Abf2 (fig. S4a). It has to be kept in mind that the total fractions before and after treatment with DNase I enzyme were not always equal, meaning that there was a likelihood of protease contamination in our DNase I, and that it wasn't the highest grade of purity. As a control however, a purified DNA plasmid and a purified mtRNA sample were treated with DNase I and RNase I, respectively, which revealed that the corresponding treatments worked (data not shown).

In addition to the solubility tests, mitochondria isolated from YPG media were analyzed using sucrose gradient centrifugation, which was followed by fractionating the gradient into 16 fractions (see Methods section 6.2.3: Sucrose Gradient Fractionation of lysed purified mitochondria with RNase treatment). These fractions were then examined by western blotting to track the migration of PDHc subunits within the gradient, based on their size and density. The subunits of the PDHc were detected in both lower molecular weight fractions (fractions 1–4) and higher molecular weight fractions (fractions 11–13) (fig. 8b). However, upon RNase I treatment of mitochondria prior to gradient centrifugation, the PDHc subunits were no longer observed in the higher molecular weight fractions, suggesting the existence of an RNase-associated form of the complex. A similar effect was seen on mitochondria isolated from YPD, which were subjected to sucrose gradient centrifugation (fig. S4b). On YPD, the PDHc subunits from higher molecular weight fractions (fractions 13-16), shifted to the lower molecular weight fractions when RNase I was added.

To visualize the localization of PDHc subunits in the absence of RNA, strains were constructed in which all subunits of PDHc were individually tagged with mNeonGreen (NG) in the WT background. After performing a growth analysis, it seemed that Pda1-NG, Pdb1-NG, Lpd1-NG and Pdx1-NG had no growth defects,

Results: The Pyruvate Dehydrogenase Complex (PDHc)

whereas Lat1-NG had a minor growth defect on non-fermentable (YPG) media at 37°C which was not as severe as $\Delta lat1$ (fig. S4c). However, it has to be noted that the expression levels of all NG-tagged strains were considerably less than the WT levels (fig. S4d). Nevertheless, microscopy was done to visualize the individual subunits. It was observed that Pda1-NG had a spotty localization with heterogenous intensity, which was classified as bright and dim spots (fig. 8c (i)). On an average, Pda1-NG formed 2.7 bright and 13.65 dim spots (fig. 8c (ii)).

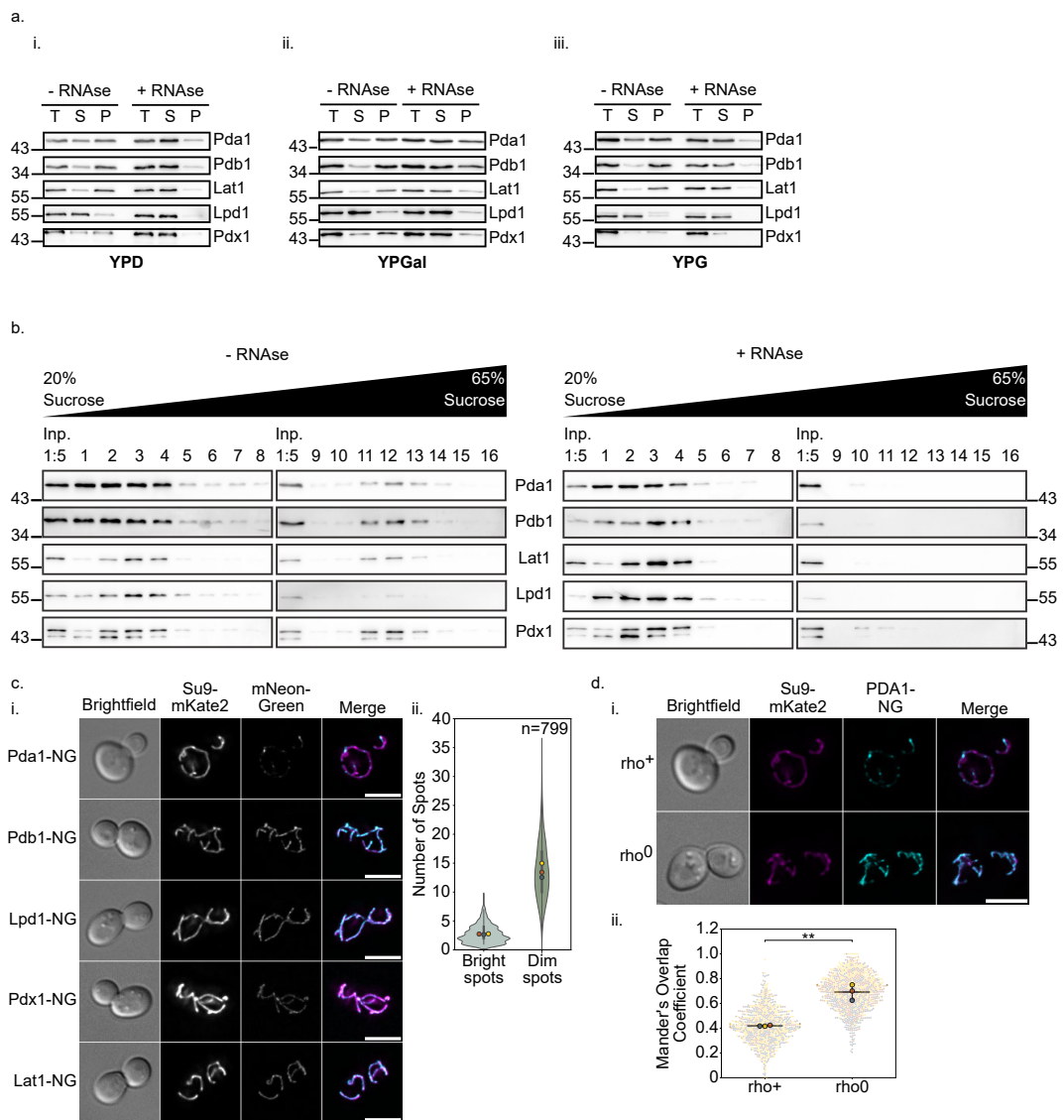


Figure 8: **PDHc associates with mitochondrial RNA.** (a) Solubility tests from the purified mitochondria of WT cells grown in YPD (i), YPGal (ii) and YPG (iii) media. The mitochondria were lysed with 1% digitonin and treated with 1 μ g RNase I, and subjected to SDS-PAGE and western blotting. T: Total; S: Supernatant; P: Pellet (b) Western blot showing sucrose gradient fractionation of isolated WT mitochondria from YPG-grown cells, upon treatment with 1 μ g RNase I. Inp: Input fraction (c) Microscopic images showing mNeonGreen tagged-PDHc subunits with Su9-mKate2 as mitochondrial network marker (performed by Felix Thoma) (i). The bright and dim spots for Pda1-NG calculated as described in Methods section 6.2.4 (ii). (d) (i) Microscopy showing distribution of Pda1-NG in rho+ vs rho0 cells (performed by Felix Thoma). Su9-mKate2 is the mitochondrial marker. (ii) The Mander's Overlap Coefficient calculated for the rho+ vs. rho0 cells as mentioned in Methods section 6.2.4. (P-values: $p < 0.005$: ***, $p < 0.05$: **, $p < 0.5$: *).

The other subunits, however, showed a rather dispersed distribution, with some foci that were not easily discernible (fig. 8c (i)). Nonetheless, the localization of Pda1-NG was further observed in absence of mitochondrial RNA, which was made possible by growing cells on medium containing ethidium bromide for a few days and by further screening for rho0 cells, which lack mtDNA and by extension, mitochondrial RNA. When the distribution of Pda1-NG was checked in rho0 cells, it was observed to be largely distributed throughout the mitochondrial network instead of appearing spotty (fig. 8d (i)). The distribution of Pda1-NG was also quantified using the Mander's Overlap Coefficient between Pda1-NG spots and Su9-mKate2 signal spread across the mitochondrial network (fig. 8d (ii)). In rho+ cells, which exhibited a spotty distribution of Pda1-NG, the Mander's coefficient was 0.42. In contrast, rho0 cells, where Pda1-NG showed a more uniform distribution, had a higher Mander's coefficient of 0.69, indicating a more homogeneous distribution of Pda1-NG within mitochondria of these cells.

Taken together, these results support that the PDHc is not only present inside the mtNucleoid, but also that it has a specific association towards the mtRNA. This was logically consistent with the data obtained from proximity labelling assay, wherein the components of mitochondrial gene expression machinery were enriched along with the PDHc subunits. Furthermore, as noted above, the role of PDHc in mtNucleoid maintenance is uncoupled to its metabolic function and the presence of PDHc is vital for the mitochondrial health.

3.2 Yme2 as a mtNucleoid interacting protein

The following section provides a functional description of an incompletely characterized mtNucleoid-interacting protein called Yme2. Yme2 (Yeast Mitochondrial Escape protein 2) is an integral yeast IMM protein of 96 kDa that exposes its N-terminus (32 kDa) to the matrix and C-terminus (60 kDa) to the IMS, with no known homologs in humans (Hanekamp and Thorsness, 1996; Leonhard et al., 2000) (see Introduction section 1.7.2). The deletion of Yme2 results in an increased rate of mtDNA escape from the mitochondria to nucleus (Hanekamp and Thorsness, 1996; Thorsness and Fox, 1993). Yme2 has been observed to co-localize with mtNucleoids and be a part of the MIOREX complex (Kehrein et al., 2015; Murley et al., 2013), wherein, its functional role remains elusive (fig. 9a). This section highlights the structural motifs present in Yme2 along with their mutational characterization and provides insights into the function of Yme2 in the mitochondria.

3.2.1 *YME2* exhibits a negative genetic interaction with members of the mitochondrial protein biogenesis machinery

Yme2 has previously been identified as a component of the MIOREX complex, which is linked to mitochondrial gene expression and protein biogenesis (Kehrein et al., 2015). To further investigate its functional role, the potential genetic interactions between *YME2* and key components of the mitochondrial protein biogenesis machinery were examined. A systematic large-scale genetic screen has previously revealed a genetic interaction between *YME2* and *MDM38*, an inner mitochondrial membrane (IMM) protein that aids in mitoribosome recruitment to the IMM by acting as a receptor (Costanzo et al., 2016; Usaj et al., 2017; van Leeuwen et al., 2016). This observation prompted the exploration of the genetic interactions of *YME2* with genes that code for other critical components of the mitochondrial protein biogenesis machinery, specifically the mitoribosome receptors at the IMM (*MDM38* and *MBA1*) and the membrane insertase *OXA1* (section 1.3.2). To test this, strains carrying deletions of *YME2* and/or *MDM38* were generated. Upon performing growth tests, it was apparent that deletion of *MDM38* conferred a growth defect in yeast on non-fermentable medium (YPG), whereas $\Delta yme2$ showed no obvious growth impairment on either fermentable (YPD) or non-fermentable (YPG) media (fig. 9b). The observed growth pattern of cells carrying deletions of *YME2* or *MDM38* was in agreement with prior findings (Bauerschmitt et al., 2010; Frazier et al., 2006; Hanekamp and Thorsness, 1996; Thorsness and Fox, 1993). In contrast, $\Delta yme2 \Delta mdm38$ cells displayed a strong growth defect even on YPD and were virtually incapable of growth on YPG, both

at 30 (fig. 9b) and 37°C (fig. S5).

Furthermore, since Mdm38 has been proposed to play a role in K^+/H^+ homeostasis (Nowikovsky et al., 2004), it was next examined whether the phenotype of $\Delta yme2\Delta mdm38$ cells was caused due to the role of Mdm38 as a ribosome receptor or its function in ion transport. In order to evaluate this, a growth analysis of the single and double deletions of *YME2* and *MDM38* was performed on media containing Nigericin, a K^+/H^+ ionophore, that has been previously observed to rescue the phenotype of $\Delta mdm38$ on YPG (fig. 9c). Expectedly, upon analysing the growth of $\Delta mdm38$ cells on Nigericin, it was indeed seen that their growth defect was restored. In contrast, the presence of Nigericin in the medium could not rescue the growth phenotype of $\Delta yme2\Delta mdm38$ on YPG. This indicated that the strong negative genetic interaction displayed by *YME2* and *MDM38* was not due

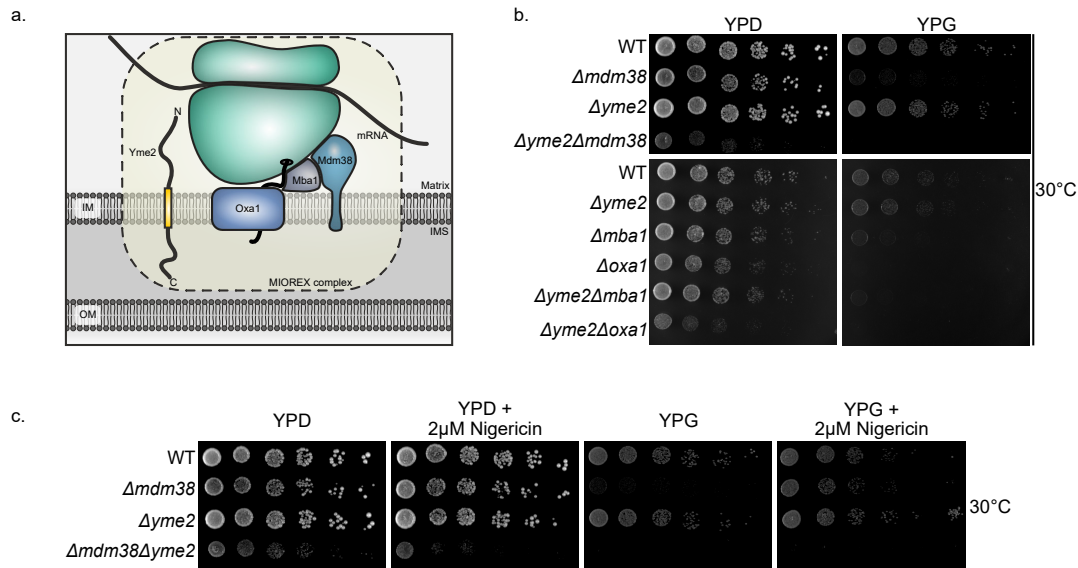


Figure 9: ***YME2* genetically interacts with mitochondrial protein biogenesis machinery.** (a) Schematic showing the presence of Yme2 in mitochondria, associated with the MIOREX complex. (b) Growth analysis of log-phase grown indicated strains showing genetic interactions of *YME2* with mitochondrial protein export machinery. The strains were spotted on YPD and YPG and allowed to grow at 30°C for 2 days (in case of $\Delta mdm38$, $\Delta yme2\Delta mdm38$) and 1 day (in case of $\Delta mba1$, $\Delta oxa1$, $\Delta yme2\Delta mba1$, $\Delta yme2\Delta oxa1$). (c) Growth tests showing the indicated strains grown at 30°C for 2 days on YPD and YPG without and with 2 μ M Nigericin. The figure was adapted from Sharma and Osman, 2022 and licensed under CC BY 4.0.

to the role of Mdm38 in K^+/H^+ homeostasis, but rather linked to the function of Mdm38 as a mitoribosome receptor.

Mdm38 has been known to physically interact with Mba1 and carry-out Oxa1-mediated insertion of mtDNA-encoded proteins upon accepting the mitoribosome at the IMM (Bauerschmitt et al., 2010). Therefore, it was further assessed whether *YME2* also genetically interacts with *MBA1* and/or *OXA1*. As anticipated, $\Delta yme2\Delta mba1$ and $\Delta yme2\Delta oxa1$ also exhibited a reduction in growth as compared to the respective single deletions, indicative of a negative genetic interaction between *YME2* and *MBA1* as well as *YME2* and *OXA1* (fig. 9b).

Taken together, these results suggested that the negative genetic interaction observed between *YME2* and mitochondrial protein biogenesis machinery additionally linked Yme2 to mitochondrial protein insertion, along with its association to the MIOREX complex.

3.2.2 The putative C-terminal Walker motifs are crucial for the function of Yme2

To delve deeper into the characterization of Yme2 and gain insight into its role in protein biogenesis, various bioinformatics tools were utilized. The putative structure of Yme2 was predicted using Alphafold (Jumper et al., 2021; Varadi et al., 2024), and the generated model, which was rather confident (average pLDDT score=78.48) revealed two distinct domains separated by an α -helix that corresponds to a putative transmembrane domain between residues 287 and 305 (average pLDDT > 70) (fig. 10a). The domain N-terminal to the transmembrane helix expanded from residues 46 until 286 (average pLDDT > 90), along with the first 45 amino acids constituting the predicted mitochondrial targeting sequence (MTS). The C-terminal domain, which lies on the opposite side of the transmembrane domain, is represented by residues 206 until 850 (average pLDDT>70). This was in line with the submitochondrial localization performed by Leonhard et al., 2000, wherein Yme2 was found to be integrated into the IMM, with parts of the protein present on both the matrix and the IMS side.

Upon careful analysis of the Yme2 amino acid sequence using a homology search based on 3D structure prediction, further understanding was obtained about the domains of Yme2 that protruded on either side of the IMM (fig. 10b) (Gabler et al., 2020; Meier and Söding, 2015; Söding et al., 2005; Zimmermann et al., 2018). The N-terminal matrix-facing domain of Yme2 was revealed to be a putative RNA-binding domain, namely the RNA Recognition Motif (RRM) (discussed in detail in Results section 3.2.5). The C-terminal IMS-facing domain was predicted to be similar to the AAA+ proteins, in that it had the putative Walker A and B

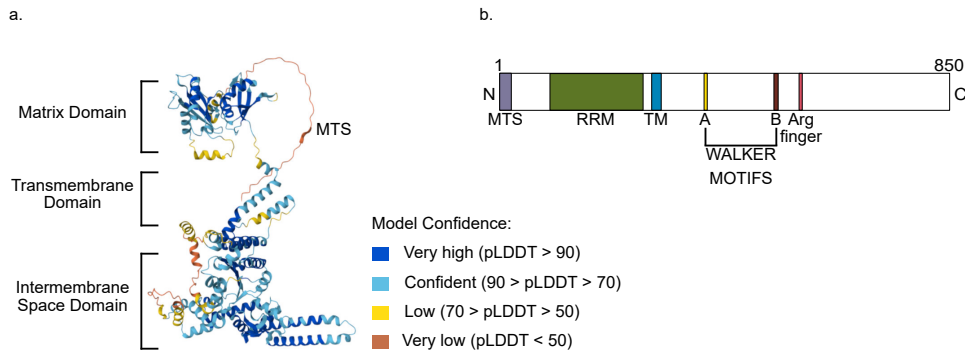


Figure 10: **Putative structure and motif architecture of Yme2.** (a) AlphaFold structural prediction of Yme2 sequence from *S. cerevisiae* S288C, showing the putative matrix-facing N-terminal, transmembrane and IMS-facing C-terminal domains. The colors represent the model confidence score, as calculated by the pLDDT parameter. (b) Schematic showing putative domain configuration of Yme2, highlighting a mitochondrial targeting sequence (MTS), RNA recognition motif (RRM), transmembrane domain (TM), Walker A and B motifs and arginine finger motif, as predicted *in silico* by HHPred. The figure was modified from Sharma and Osman, 2022 and licensed under CC BY 4.0.

motifs that are typically characteristic of P-loop ATPases (fig. 11a). The strongest similarities in the homology search were recognized among members of DNA-binding initiator clade of AAA+ proteins, which include origin recognition proteins and helicase-loading proteins, like Cdc6. Given that the Walker Motifs in Yme2 are predicted to exist in the IMS-facing region, which is devoid of any DNA or RNA, this finding was rather surprising.

The IMS domain of Yme2 was then further investigated on a structural level based on the prediction obtained from AlphaFold. This structure revealed the presence of features characteristic of AAA+ proteins, including a central β -sheet constituted by five β -strands arranged in a $\beta 5$ - $\beta 1$ - $\beta 4$ - $\beta 3$ - $\beta 2$ order, an additional region of homology connecting $\beta 4$ and $\beta 5$ (which included a hydrophilic glutamate at position 558 that could be regarded as Sensor I motif, and a putative Arginine finger at position 565), as well as a helical bundle situated C-terminal to the α - β - α sandwich (fig. 11c). This structural motif, taken together with the sequence analysis, divulged the positioning of the putative conserved Walker motifs of Yme2. The Walker A motif, which is usually found in the loop connecting $\beta 1$ and $\beta 2$, contains a conserved lysine residue which abolishes ATP binding, if mutated. For Yme2, this invariant lysine

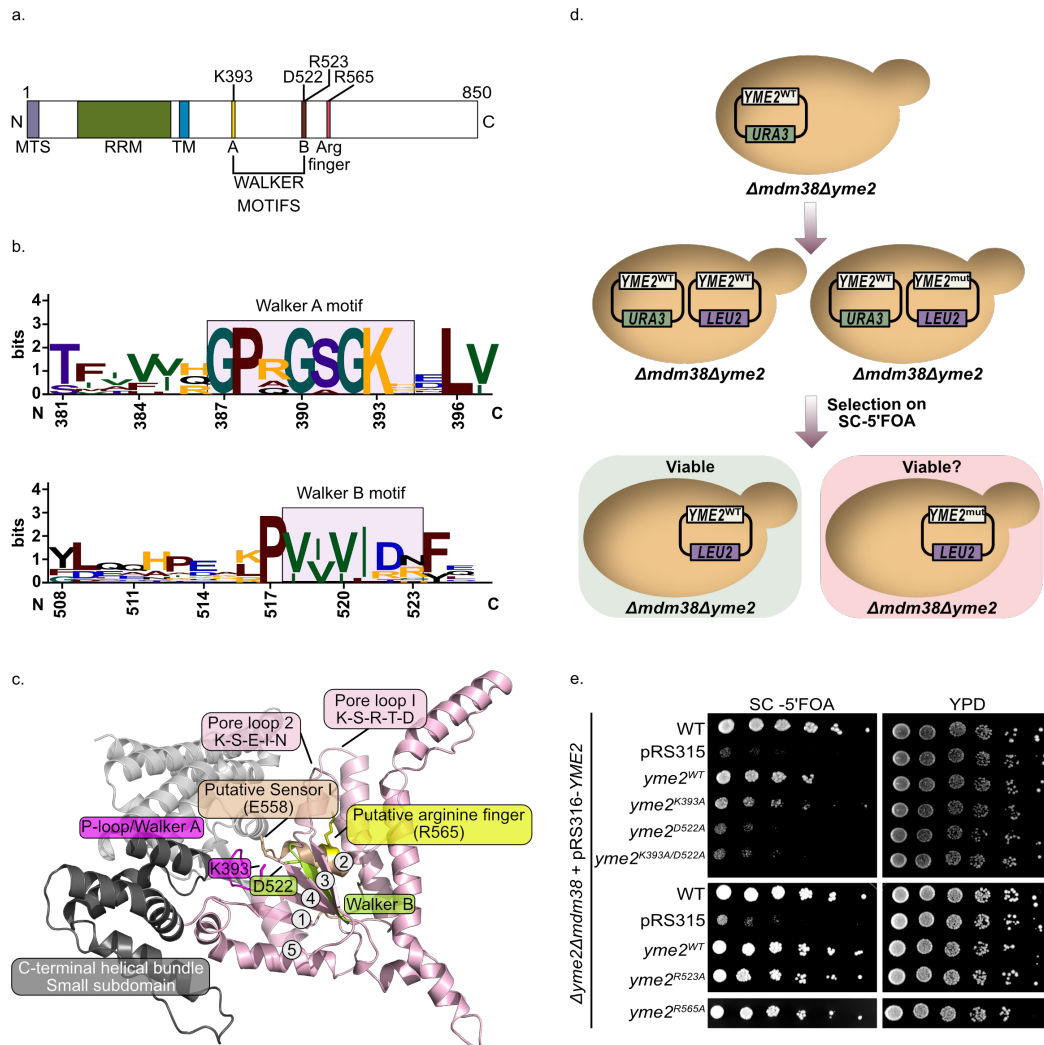


Figure 11: **Walker motifs of Yme2.** (a) Schematic representation of Yme2's predicted domain layout, with the specific residues targeted for mutation in this study. (b) Sequence logo from Weblogo (<https://weblogo.berkeley.edu/>) depicting conservation of Walker A and B motifs in the AAA+ domain of Yme2 across ten fungal species. (c) Putative structural model generated by Alphafold, of the AAA+ domain in Yme2 displaying key features, including the Walker A and B motifs, an Arginine finger, Pore loops 1 and 2, the Sensor I motif, and a helical bundle at the C-terminus. The numbered elements represent the location of β -sheets. The residues that were mutated are indicated. (d) Overview of the plasmid shuffle experimental setup. (e) Growth assay depicting the plasmid shuffle experiment, where the indicated strains were grown on SC-5'FOA and YPD for 2 days at 30°C. The figure was adapted from Sharma and Osman, 2022 and licensed under CC BY 4.0.

was at position 393 (fig. 11b, fig. S6b). The walker B motif of Yme2, which typically contains two conserved acidic residues (an aspartate and a glutamate), had an unusual replacement of glutamate by an arginine residue (consensus: hhhhDE; Yme2: hhhhDR) (fig. 11b, fig. S6b).

The importance of the AAA+ domain of Yme2 was next examined genetically by investigating the dispensability of Walker A and B motifs, as well as the Arginine finger to the function of Yme2. In this regard, Yme2 variants with Walker A (*yme2*^{K393A}), Walker B (*yme2*^{D522A}), Walker A/B (*yme2*^{K393A/D522A}), Walker B-Arginine (*yme2*^{R523A}) and Arginine-finger (*yme2*^{R565A}) mutations were generated (fig. 11a) and tested for their ability to rescue the $\Delta yme2 \Delta mdm38$ phenotype, via a plasmid shuffle experiment. In this assay, $\Delta yme2 \Delta mdm38$ cells expressing *YME2* from a centromeric plasmid containing a *URA3* marker (pRS316) were transformed with another plasmid containing a *LEU2* marker (pRS315), which harboured *YME2* either in the WT or mutated form (fig. 11d). These cells were further grown on SC medium containing 5'FOA, which selects for cells that have lost the plasmid with the *URA3* marker. This selection is achieved by killing of the cells that retained the *URA3* marker-plasmid, as in these cells, 5'FOA gets converted to a fatally toxic product by the Ura3 protein. Therefore, in this assay, it was observed that the $\Delta yme2 \Delta mdm38$ cells that contained the *yme2*^{WT} variant on the *LEU2*-containing plasmid, continued to rescue the growth of the double deletion mutant after the loss of the Ura3-containing plasmid (fig. 11e). Similar results were obtained for Walker B-Arginine (*yme2*^{R523A}) and Arginine-finger (*yme2*^{R565A}) mutants (at both 30°C and 37°C), indicating that these residues are not essential for Yme2's function in the absence of Mdm38 (fig. S6a, fig. 11e). Surprisingly, the Walker A and B mutants variants *yme2*^{K393A}, *yme2*^{D522A} and double mutant variant *yme2*^{K393A/D522A} were unable to efficiently rescue the growth phenotype associated with $\Delta yme2 \Delta mdm38$ cells (fig. 11e). It has to be noted that *yme2*^{K393A} mutant provided a weak rescue upon selection on SC-5'FOA medium at 30°C, which indicated that this specific mutation did not entirely abolish Yme2 function at this temperature. At 37°C, however, none of the Walker A and B variants (*yme2*^{K393A}, *yme2*^{D522A}, *yme2*^{K393A/D522A}) could rescue the growth of the cells lacking both Yme2 and Mdm38 (fig. S6a).

To confirm whether all the aforementioned Yme2 variants were expressed and the phenotypic rescue absent in Walker domains was not due to the lack of protein expression, $\Delta yme2$ cells expressing the mutant variants of Yme2 on a plasmid were subjected to Western blotting. The resulting membranes were decorated with Yme2 antibody serum (1:250) obtained from Dr. Peter Thorsness (Hanekamp and Thorsness, 1996), which detects C-terminal domain of Yme2 between residues at positions 586 and 850. The analyses revealed that all Yme2 mutants were

expressed to levels comparable to WT Yme2 (fig. S6c,d). Collectively, the results indicated that the putative Walker motifs of Yme2, which are characteristic of AAA+ proteins, are critical for the function of Yme2.

3.2.3 Yme2 exists as a multimeric complex

The predicted AAA+ fold of Yme2 and the importance of Walker motifs for Yme2 function prompted an examination of whether Yme2, like other AAA+ proteins, also exists as an oligomeric complex. This was first explored *in silico*, via Alphafold Multimer, wherein the sequence of Yme2 was submitted as an input to create a oligomeric structure (Abramson et al., 2024; Evans et al., 2021). Alphafold Multimer predicted a hexameric structure with a ring-like conformation (pTM score= 0.54), which is also common to other AAA+ proteins (fig. 12a).

To assess the Yme2 complex formation biochemically via Blue Native PAGE (BN-PAGE), TAP-tagged WT or Walker A or B mutated Yme2 variants were re-integrated into the *LEU2* locus of $\Delta yme2$ strain. As shown with a growth analysis in fig. S7a, the insertion of the TAP tag did not interfere with the Yme2 function, as indicated by undeterred growth of the cells in both WT and $\Delta mdm38$ background. Next, mitochondria were isolated from the TAP-tagged Yme2 variants, and steady state protein levels were determined. As indicated in fig. 12b, TAP-tagged Yme2^{WT}, Yme2^{K393A} and Yme2^{D522A} displayed comparable protein levels of Yme2, suggesting that the individual mutations did not result in protein instability. Contrastingly, however, TAP-tagged Yme2^{K393A/D522A} exhibited protein levels which were slightly destabilized, which only became apparent in isolated mitochondria. Nevertheless, BN-PAGE and Western blot analysis was performed on all the strains and a distinguishable Yme2-specific band was observed to run at a high molecular weight size similar to the size of dimeric complex V (approx. 1250kDa) (fig. 12c). This high molecular weight Yme2 band was also clearly visible for mitochondria which expressed the Walker A mutant of Yme2 (Yme2^{K393A}), but not for mitochondria that expressed the Walker B mutant of Yme2 (Yme2^{D522A}) wherein, there was a faint band seen, indicating that the complex formation was compromised in the Walker B mutant. Moreover, the high molecular weight band of Yme2 was virtually absent from the mitochondria expressing the Yme2 double mutant Yme2^{K393A/D522A} variant. The faint band could partially be due to slightly lower expression levels in case of Yme2^{K393A/D522A} mutant.

Based on the observation of Yme2 complex at the height of dimeric complex V in the BN-PAGE, the possibility of Yme2 forming a heteromeric complex with the complex V dimer was investigated. To test the same, $\Delta atp20$ strains were generated and the complex formation of Yme2 was observed in this strain on a BN-PAGE.

Atp20 is required for the dimerization of Complex V, and its deletion can lead to the dimeric complex V falling apart, as was indeed observed in the BN-PAGE gel stained with Coomassie staining solution (fig. S7c). The high molecular weight band formed by Yme2, on the other hand, was still apparent in the decorated

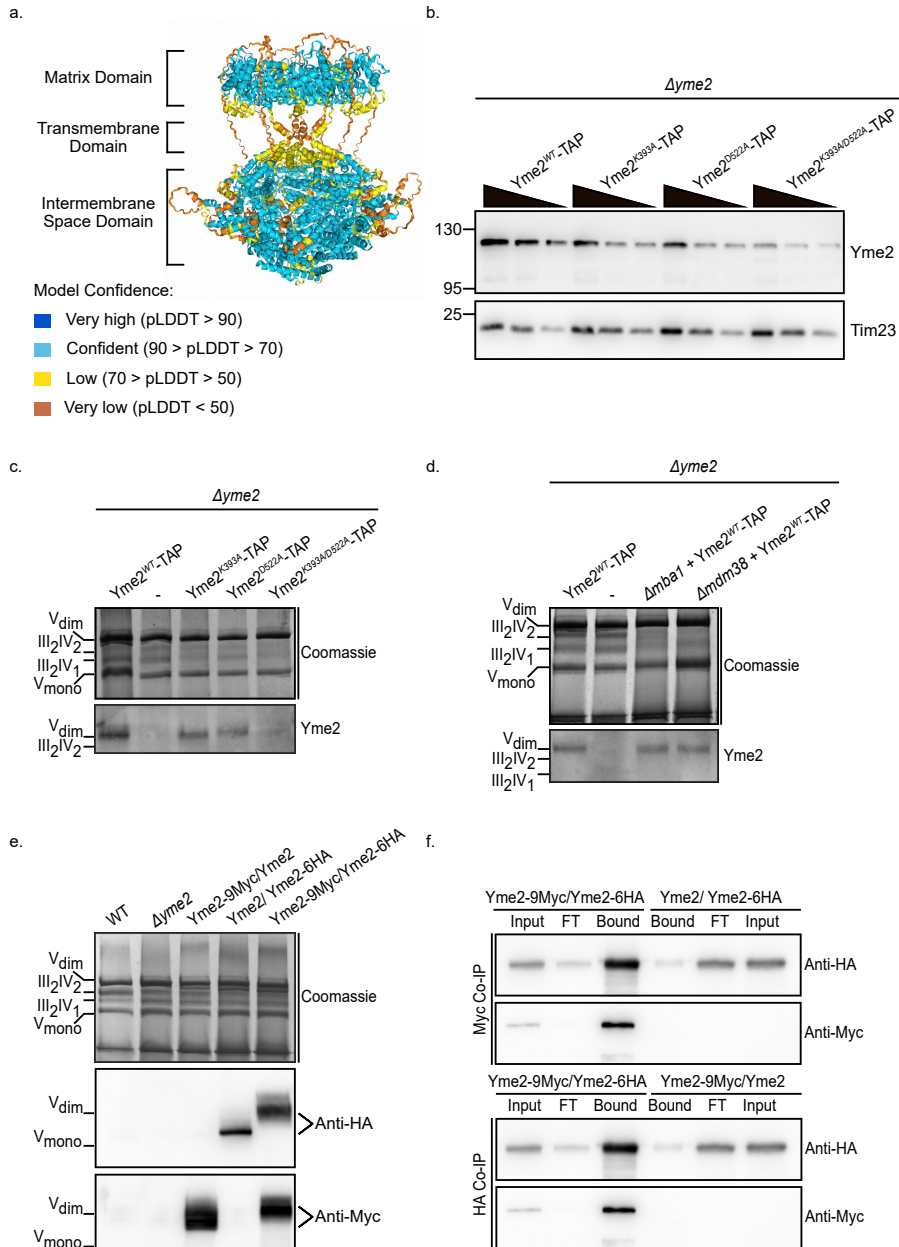


Figure 12: **Yme2 is a multimeric protein.** (a) Putative structure of the hexameric Yme2, as predicted by Alphafold Multimer (b) Western blot showing isolated mitochondria of the indicated strains depicting steady-state levels of Yme2 protein. (c,d) Western blot showing 100 μ g of isolated mitochondria from TAP-tagged Yme2 mutants separated on a 3%-13% BN-PAGE. (e) Diploid Yme2 strains with 9-Myc and/or 6-HA tags separated on a BN-PAGE and further subjected to western blotting. (f) Co-IP experiment performed with Anti-Myc (top) and Anti-HA (bottom) magnetic beads, depicting the presence of Yme2 as a homomer. Input and flowthrough (FT) are 1% and bound fractions are 50%. The figure was modified from Sharma and Osman, 2022 and licensed under CC BY 4.0.

Western blots. It was, hence, gathered from the BN-PAGE analysis that the high molecular weight band observed for Yme2 was not a heteromeric complex formed with Complex V dimer.

Additionally, given the genetic link between *YME2* and mitochondrial protein export machinery, the state of Yme2 complex formation in Δ *mdm38* and Δ *mba1* strains was further investigated (fig. 12d). No alteration was observed in complex formation by Yme2 on BN-PAGE when Mdm38 or Mba1 were lacking, which suggested that the Yme2 multimeric complex does not contain the receptors of the mitochondrial protein export machinery and the absence of these proteins does not compromise the formation of Yme2 complex through secondary effects.

It was then evaluated whether the Yme2 complex is rather a homo-oligomeric complex with multiple copies of Yme2. To test this, three diploid strains were generated which contained either a 9Myc or a 6HA- tagged allele of Yme2 along with an untagged Yme2 allele (Yme2-9Myc/Yme2 and Yme2/Yme2-6HA) and a strain where one allele of Yme2 was tagged with 9Myc and the other with 6HA (Yme2-9Myc/Yme2-6HA). To begin with, the respective strains showed no apparent growth defects, as well as no abnormalcy in steady state protein levels (fig. S7b,d). Mitochondria from these strains were isolated and analysed by BN-PAGE. As expected, Yme2 formed a high molecular weight band upon visualization for each strain. Interestingly, the double tagged version of Yme2 (Yme2-9Myc/Yme2-6HA) displayed a clear size shift in the Yme2 complex, indicating the presence of both tagged alleles in the complex (as opposed to single-tagged alleles for Yme2-9Myc/Yme2 and Yme2/Yme2-6HA strains) (fig. 12e). To gain further insight into this finding, isolated mitochondria from Yme2-9Myc/Yme2-6HA and Yme2/Yme2-6HA were subjected to Myc Co-IP. Surprisingly, Yme2-6HA efficiently co-precipitated with Yme2-9Myc from the Yme2-9Myc/Yme2-6HA strain, and not from the Yme2/Yme2-6HA strain which served as a control strain (fig. 12f).

Similar results were also obtained vice versa, meaning that Yme2-9Myc successfully co-purified with Yme2-6HA in an HA Co-IP from the mitochondria isolated from Yme2-9Myc/Yme2-6HA strain, but not from Yme2-9Myc/Yme2 strain.

Taken together, these results showed that Yme2 forms high molecular weight complexes which contained multiple copies of Yme2. Furthermore, the Yme2 complex formation is compromised when Walker B motif or both Walker motifs are mutated but not when only Walker A motif is mutated. The Yme2 complex formation is also not compromised when proteins of the mitochondrial protein export machinery are absent.

3.2.4 *In-vitro* purification of the Yme2 Walker domains

Having established that Yme2 contains Walker motifs characteristic of AAA+ proteins and that these motifs are essential for its functionality, the intermembrane space domain was purified *in-vitro* by expressing it in *E. coli*. For the expression, the 6xHis tag fused to a truncated Yme2 construct which had only the intermembrane space domain (residues Q356 to K850) was used (fig. S7e (i)). The purification was performed on a NiNTA column, and the eluted fractions were analyzed on a Coomassie-stained SDS gel. The purified protein had a concentration of 5.5 mg/ml.

The purified protein was further used to carryout ATPase assay in a kit-based method (ATPase/GTPase-Activity Assay Kit, Sigma-Aldrich, MAK113). The kit facilitates a colorimetric assay, which utilizes the intensity of the stable dark color formed when the dye malachite green reacts with free phosphates liberated during the ATPase reaction. As a positive control, purified apyrase enzyme (Sigma-Aldrich, A6410) was used. However, the assay revealed minimal to no detectable differences in ATPase activity between the negative control (buffer) and the purified Yme2 protein (data not shown). This result suggests either the absence of ATPase activity or that the assay conditions were insufficiently sensitive to provide conclusive results.

Furthermore, the purified C-terminal domain of Yme2 was used to affinity purify the Yme2 antibody from the antiserum obtained from the lab of Dr. Peter Thorsness (Hanekamp and Thorsness, 1996). For the antibody purification, the purified domain of Yme2 was coupled to CNBr-Sepharose 4B beads, and purification was carried out according to Methods section 6.2.3: Affinity purification of Yme2 antibody. After optimization, 1:1000 dilution in 5% milk (prepared in 1x TBS buffer) was chosen for the subsequent decorations (fig. S7e (ii)).

3.2.5 The putative N-terminal RNA binding domain is important for Yme2 function

The Yme2 structure presented by Alphafold along with the homology search of the protein sequence revealed the presence of a putative N-terminal RNA binding domain, which would be topologically facing the mitochondrial matrix (Gabler et al., 2020; Meier and Söding, 2015; Söding et al., 2005; Zimmermann et al., 2018). The RNA-binding domain, predicted from the residues 196 to 271, was further categorized *in silico* and was found to belong to the family of RNA Recognition Motifs (RRM). Yme2's predicted RRM domain is referred to as RRM2 domain in this study. This is because close examination of the Alphafold structure and the properties of RRM domains revealed that residues 45 to 187 of Yme2 adopt a conformation resembling an RRM domain. This finding raises the possibility of the presence of a previously unrecognized putative RRM domain that may have escaped detection from the bioinformatics softwares (fig. 13a). In order to avoid the confusion about the two putative RRM domains, they were renamed as RRM1 (consisting of amino acids V45-P187) and RRM2 (containing amino acids P196-N271), simply on the basis of their order in the sequence. Therefore, it has to be noted that the *in silico* predicted RRM domain, which is named as RRM2 domain in this study, is further discussed in this section, whereas the RRM1 domain is discussed in Results section 3.2.6.

The RRM domain typically contains a four-stranded anti-parallel β sheet, with two α helices packed against it. The fold takes an $\beta 1-\alpha 1-\beta 2-\beta 3-\alpha 2-\beta 4$ conformation, which is commonly referred to as the $\alpha\beta$ sandwich (Maris et al., 2005). Having mentioned the typical structure of the fold, it has to be considered that the RRM domains belong to an extremely vast family of proteins with equally variable domain architecture, for example, some proteins harboring RRM domains are characterized by the presence of additional β -strands and α -helices. But one common requisite for RRM domain-containing proteins is the presence of two conserved motifs, namely RNP1 (in $\beta 3$ strand) and RNP2 (in $\beta 1$ strand), wherein each motif has an invariant aromatic residue that interacts with the nucleotide bases of client RNA or DNA molecules (fig. 13c). Yme2 contains fungally-conserved RNP1 (amino acids A238-Y242) and RNP2 (amino acids I200-F204) motifs within the RRM2, wherein each motif contained a conserved aromatic residue (fig. 13b, fig. S8a).

First, the importance of the RRM2 domain for Yme2's function was tested via the plasmid shuffle experiment. In order to conduct the experiment, mutant *YME2* variants containing RNP1 (*yme2^{Y242A}*) and RNP2 (*yme2^{F204A}*) mutations, along with a double mutant (*yme2^{F204/Y242A}*) were generated. When the plasmid shuffle was performed, it was observed that the RNP2 mutation (*yme2^{F204A}*) completely restored the growth of $\Delta yme2\Delta mdm38$ cells, rendering itself dispensable to the

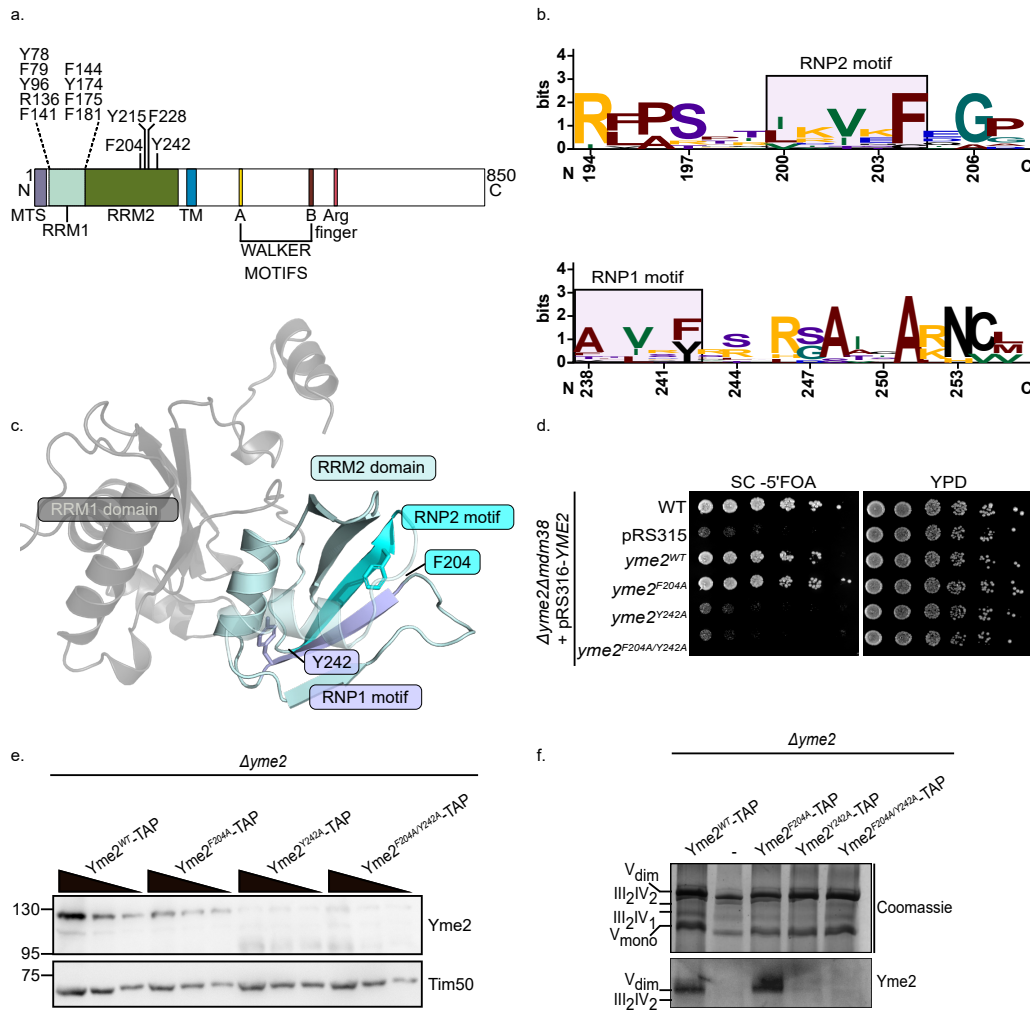


Figure 13: **Structural organization of RRM2 domain of Yme2.** (a) Schematic showing the predicted RRM domains of Yme2, highlighting specific residues targeted for mutation in this study. (b) Weblogo sequence logo (<https://weblogo.berkeley.edu/>) exhibiting the conservation of the RRM2 domain (comprising RNP1 and 2 motifs) across ten fungal species. (c) Key features of the RRM2 domain of Yme2, as predicted in the structural model from AlphaFold. The RRM2 domain consists of RNP1 and RNP2 motifs, with residues representing the mutations generated in the study. (d) Growth assay showing the plasmid shuffle experiment, where the indicated strains were grown on YPD and SC-5'FOA (to counter-select for the pRS316-URA3 plasmid) at 30°C for 2 days. (e) Steady-state levels of Yme2 in isolated mitochondria from the indicated strains, obtained after immunoblotting. (f) BN-PAGE (3%-13%) showing the Yme2 complex formation in the RRM2 mutants. The figure was modified from Sharma and Osman, 2022 and licensed under CC BY 4.0.

function of the RNP2 motif, and by extension, Yme2 (fig. 13d). The RNP1 (*yme2*^{Y242A}) mutation and the RNP1/2 double mutation (*yme2*^{F204/Y242A}), on the other hand, did not rescue the growth phenotype of the $\Delta yme2\Delta mdm38$ cells, rendering Yme2 non-functional, both at 30°C and 37°C (fig. 13d, fig. S8b). Based on this observation, it was concluded that the RRM2 domain was vital to the function of Yme2.

Next, it was investigated whether the Yme2 variants containing RRM2 mutations have a stable protein expression. In order to examine this, $\Delta yme2$ strains containing plasmid encoding either WT or mutant forms of Yme2, were generated. Upon performing Western blotting with cell lysates, it was observed that while Yme2^{F204A} variant accumulated to WT-like levels, the amounts of Yme2^{Y242A} and Yme2^{F204/Y242A} were undetectable (fig. S8e). Additionally, $\Delta yme2$ strains with *LEU2* locus-integrated TAP-tagged WT or mutant *YME2* versions were also generated, and the expression levels were assayed in the isolated mitochondria (fig. 13e). In agreement with the findings from the cell lysates, western blots from the TAP-tagged strains showed WT-like steady-state expression levels for Yme2^{F204A}, and strongly reduced and only residual levels for Yme2^{Y242A} and Yme2^{F204/Y242A} mutant variants, respectively. The complex formation in the aforementioned Yme2 variants was further evaluated by performing a BN-PAGE analysis, and as expected, it was observed that the Yme2^{F204A} variant formed a high molecular weight complex similar to the WT strain (fig. 13f). In contrast, no complexes were observed for strains with Yme2^{Y242A} and Yme2^{F204/Y242A} mutations. This pointed towards the fact that the stable expression and complex formation by Yme2 was affected by either disturbing the integrity of RNP1 fold which potentially causes a rapid degradation, or by abolishing RNA binding by the RRM2 domain.

It was established that the RNP1 and RNP2 mutants likely disrupted the RRM2 fold architecture, leading to unstable expression of Yme2. This instability may have contributed to their failure in rescuing the $\Delta yme2\Delta mdm38$ phenotype. Consequently, the search continued for a mutation that, while unable to rescue the $\Delta yme2\Delta mdm38$ growth defect, would still allow the expression of a stable protein. To address this, two aromatic residues within the RRM2 domain were selected, as RNA binding in RRM-domain-containing proteins frequently involves interactions mediated by aromatic residues. The selected aromatic residues protruded outward from the predicted structure of Yme2, and potentially displayed a higher probability of keeping the RRM fold intact and possibly binding RNA due to their aromaticity. The selected residues were Y215 and F228 (fig. S8f). Upon sequence analysis, it was observed that Y215 was also highly conserved among the fungal species (fig. S8c). Yme2 variants of these mutants (*yme2*^{Y215A} and *yme2*^{F228A}) were hence constructed and assayed for the plasmid shuffle experiment. Strikingly, *yme2*^{Y215A} resulted in

a non-functional Yme2 which led to its failure in rescuing the $\Delta yme2 \Delta mdm38$ phenotype at 30°C (fig. S8d). Nevertheless, when cell lysates of this variant in the $\Delta yme2$ background were subjected to SDS-PAGE and Western blotting, this variant produced a stably expressed protein whose levels were only marginally less than the Yme2^{WT} levels (fig. S8g). Contrastingly, $yme2^{F228A}$ rescued the double deletion phenotype efficiently and led to expression of a protein that was comparable to Yme2^{WT}, which meant that $yme2^{F228A}$ mutant was dispensable to the function of Yme2, unlike the $yme2^{Y215A}$ mutant, which abolished Yme2 function despite producing a stable protein.

Taken together, these results led to the conclusion that, indeed, the RRM2 domain was crucial for the function of Yme2 in the cells, as residues (Y242 and Y215) were identified which, when mutated, rendered Yme2 non-functional. However, for the $yme2^{Y242A}$ mutant, this could be attributed to destabilization of the RRM fold as the mutant Yme2 had a significantly lower expression as compared to Yme2^{WT}.

3.2.6 An additional N-terminal domain of Yme2 with features similar to the putative RRM2 domain

It was propounded in Results section 3.2.5 that a part of the N-terminal of Yme2 (residues P196-N271) was revealed via bioinformatics softwares to be a putative RRM domain (RRM2 domain of Yme2), the importance of which was then confirmed using genetic and biochemical assays. When the Alphafold structure of Yme2 was studied in depth, the other part of the N-terminal domain, which stretched from residues V45 until P187, appeared to fold into a conformation that was similar to the RRM2 domain. This domain was hence, named as the putative RRM1 domain. The RRM1 domain, like the RRM2 domain, had an $\alpha\beta$ sandwich structure with four anti-parallelly arranged β strands which stood against two α helices (fig. 14a). It was unknown why the RRM1 domain escaped *in silico* detection, although the presence of an accessory third α -helix sequence which conformationally resided completely outside the fold in the predicted structure, could be a possible reason. Nevertheless, to corroborate the claim of this stretch being another RRM domain, conserved RNP1 and 2 motifs were sought. It is known that RNP1 and 2 motifs form the β_3 and β_1 strand, respectively, and contain invariant aromatic amino acid residues that are involved in RNA binding. When the sequence of Yme2 was thoroughly checked, it was obvious that indeed, the RNP1 (amino acids R136-F144) and RNP2 (amino acids L76-N81) motifs were present (fig. 14a,b). Moreover, in both RNP1 and RNP2 motifs, there was a highly conserved aromatic amino acid that possessed an eerily similar pattern to the aromatic residues of the RRM2 domain (fig. S9a). Therefore, it was only logical to further investigate the RRM1

Results: Yme2 as a mtNucleoid interacting protein

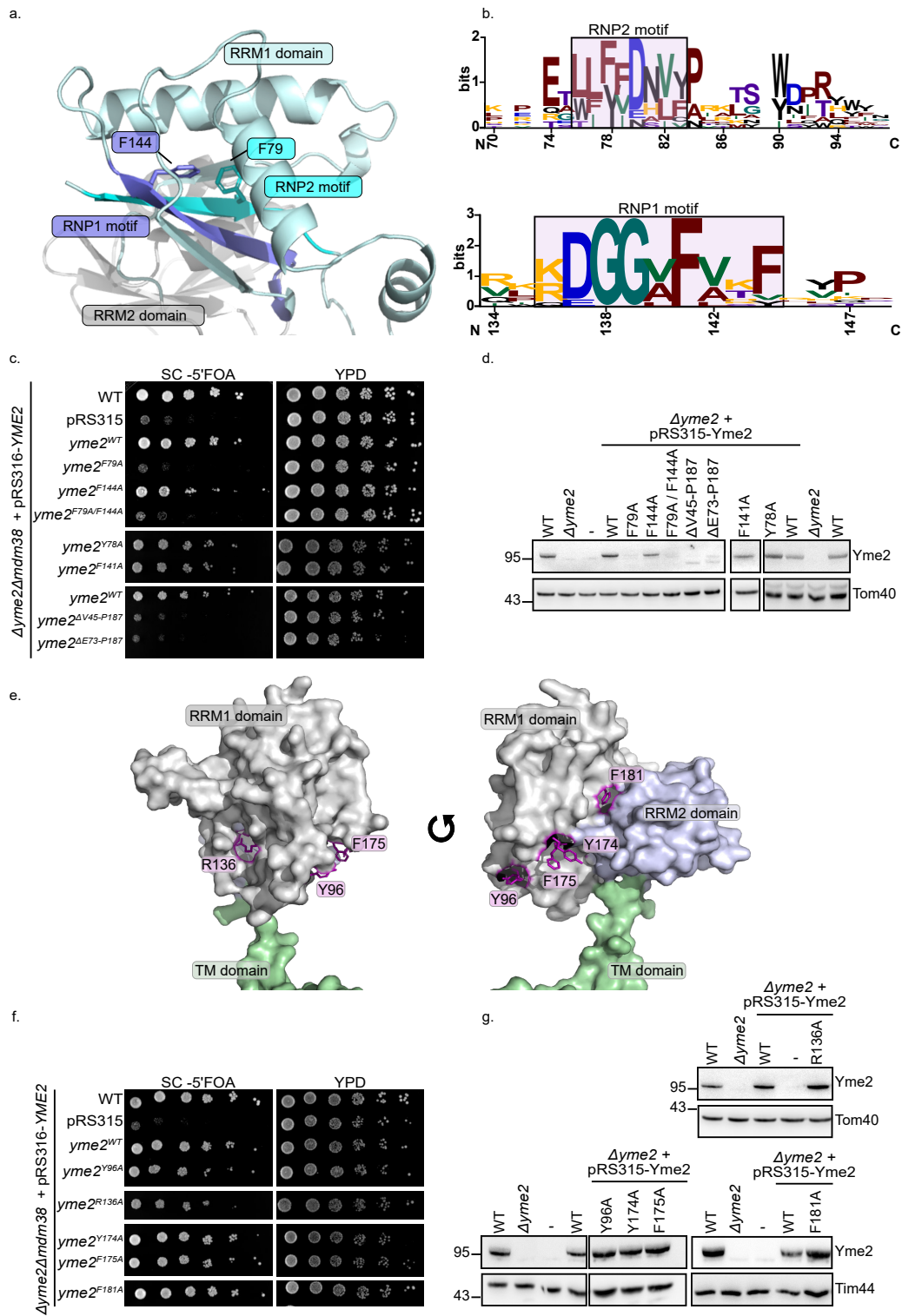


Figure 14: **Domain architecture of RRM1 domain of Yme2.** (a) The putative RRM1 domain obtained from the Alphafold structural prediction (b) Sequence logo from Weblogo (<https://weblogo.berkeley.edu/>) showing the conservation of the RRM1 domain (along with RNP1 and 2 motifs) among ten fungal species. (c,f) Plasmid shuffle experiment carried out in the RRM1 domain in the indicated strains, where they were grown at 30°C in YPD and SC-5'FOA (for counter-selection of the pRS316-Ura3 plasmid) for 2 days. (d,g) Steady-state levels of Yme2 in the cell lysates of indicated strains, upon immunoblotting and decoration with purified Yme2 antibody. Tom40 and Tim44 are loading controls. (e) Surface representation of the predicted Alphafold model of Yme2 N-terminal segment, highlighting the RRM1 domain and its residues that were mutated in the study.

domain for its essentiality in the function of Yme2.

Before delving deeper into the mutational analysis of the RNP motifs of the RRM1 domain, it was first investigated whether the entire domain was necessary at all. Therefore, two Yme2 variants with deletions of the entire RRM1 domain and a truncated version, were constructed, and subjected to the plasmid shuffle experiment. Both the variants (*yme2*^{ΔV45-P187} and *yme2*^{ΔE73-P187}) failed to rescue the growth defect of the *Δyme2Δmdm38* strain, suggesting that the RRM1 deletions rendered Yme2 non-functional (fig. 14c, fig. S9b). However, upon checking the steady-state protein levels of cell lysates from these deletion mutants generated in the *Δyme2* background, it was observed that Yme2 was stably expressed, albeit with a reduced levels as compared to Yme2^{WT} (fig. 14d). This pointed towards the fact that the availability of the RRM1 domain was crucial for the role of Yme2 in the cells.

Next, it was evaluated whether the mutants of RNP1 and 2 domains of RRM1 in Yme2 led to a restoration of growth of the *Δyme2Δmdm38* cells. To test this, the plasmid shuffle experiment was performed with mutations of the aromatic acid residues in RNP1 (*yme2*^{F144A}) and RNP2 (*yme2*^{F79A}) motifs. Unexpectedly, in the RRM1 domain, the mutation that caused a failure to restore the *Δyme2Δmdm38* growth was the mutation in RNP2 motif (*yme2*^{F79A}), unlike the RNP2 motif of the RRM2 domain (fig. 14c). Expression of the mutant *yme2*^{F144A} in the RNP1 motif of the RRM1 domain, however, led to a complete rescue in the growth phenotype, pointing towards a non-essential role in the function of Yme2. Additionally, the RNP1/2 double mutant (*yme2*^{F79A/F144A}) also failed to rescue the growth defect displayed by *Δyme2Δmdm38* cells at both 30 and 37°C (fig. S9b). When the Yme2 variants were transformed into *Δyme2* cells to assess their steady-state expression levels, it was rightfully observed that Yme2^{F79A} variant had minimal

to no expression, whereas the Yme2^{F144A} had a significant expression (although marginally less as compared to Yme2^{WT}) (fig. 14d). Astonishingly, the RNP motifs of RRM1 domain had yet another pair of highly invariant aromatic amino acids (F141 in RNP1; Y78 in RNP2), both of which protruded out of the respective β -strands in the opposite direction to the F79 and F144 residues (fig. S9c). When the *yme2*^{F141A} and *yme2*^{Y78A} variants were analysed in the plasmid shuffle assay, these mutants almost completely rescued the growth of $\Delta yme2 \Delta mdm38$ cells at 30°C, but failed to render Yme2 functional at 37°C (fig. 14c, fig. S9b). This suggested the evident cruciality of these motifs in a temperature-dependent manner. Furthermore, it was noteworthy to observe that both Yme2^{Y78A} and Yme2^{F141A} were expressed on a protein level in a WT-like manner, when cell lysates of these variants were assayed in a $\Delta yme2$ background (fig. 14d).

To further pursue the mutational characterization of the RRM1 domain, amino acids on the surface of the RRM1 domain were analyzed for those that protruded outward from the predicted structure and were either aromatic or positively charged by nature, as these were considered to have a potentially high likelihood of binding the client nucleic acid molecule. Few such residues were identified, namely, R136 (a conserved positively charged residue which also was located in the RNP1 motif), Y96 (located in the α 1 helix), and three residues located in the loop leading to the β 4 strand (Y174, F175 and F181) (fig. 14e). The last three residues were selected additionally to investigate their importance for Yme2 given their closeness to the RRM2 domain and to check whether these residues participated in both RRM domains working in conjunction. For all the aforementioned mutants, Yme2 variants were generated and plasmid shuffle experiment was performed. As seen in fig. 14f, only the *yme2*^{Y96A} and *yme2*^{R136A} variants seemed to partially rescue the phenotype, with the other variants able to rescue the phenotype fully, of the $\Delta yme2 \Delta mdm38$ cells. As anticipated, the partial rescue seen in case of *yme2*^{Y96A} and *yme2*^{R136A} variants was further reduced at 37°C, keeping up with the temperature-dependent vitality of the RRM1 domain (fig. S9b). Additionally, all the selected variants displayed WT-like expression levels when the cell lysates were analysed in the background of $\Delta yme2$ (fig. 14g).

In conclusion, it was evident that the RRM1 domain, which was unable to be detected by various prediction softwares, provides an indispensable role to the function of Yme2, especially at 37°C.

3.2.7 Mass Spectrometry analysis of the Yme2 interactome reveals presence of mtNucleoid proteins

After mutationally characterizing the domains of Yme2, the interactome of Yme2 was assessed biochemically. In this regard, a co-IP experiment was performed with the Myc-tagged Yme2 strain in WT background with an untagged WT strain as the negative control. The growth of the strains and expression of Yme2 were already assessed before (fig. S7b,d). After the Co-IP was performed in biological

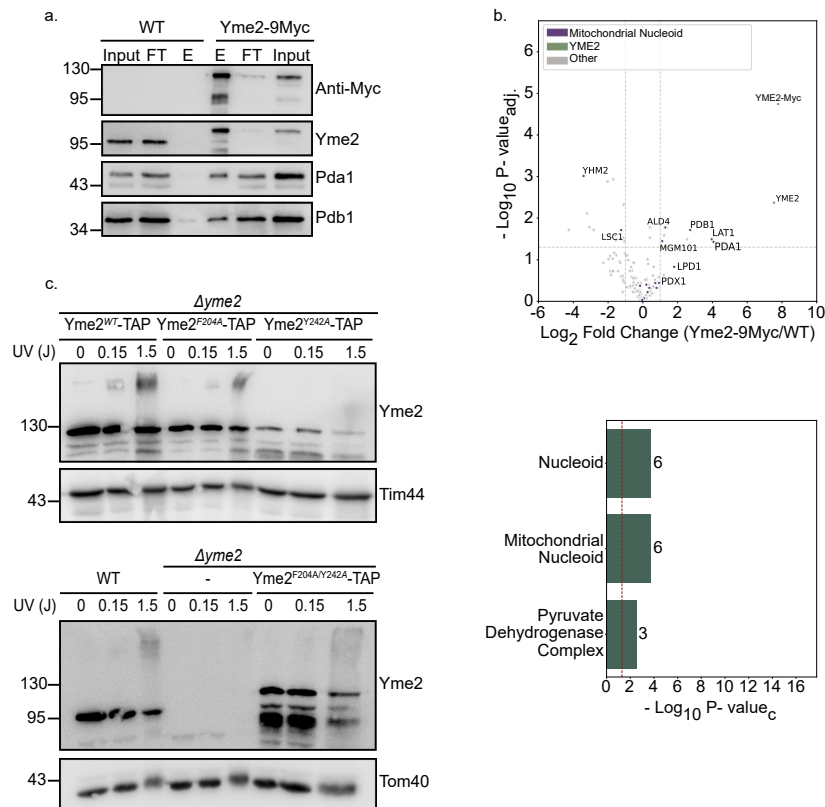


Figure 15: **Yme2 interactome has mtNucleoid-related proteins.** (a) Myc Co-IP experiment with Yme2-9Myc strain and WT strain as negative control. Input and flowthrough (FT) are 10% loaded. Elution (E) is a tenth of the total sample. (b) Volcano plot depicting the fold changes of the proteins detected in the Myc Co-IP experiment along with the GO terms highlighted, as shown (top) and a bar plot showing the top GO terms from the mass spectrometry data analysis, along with the number of associated proteins (bottom). (c) Western blot showing the UV crosslinking experiment performed with purified mitochondria of the indicated strains using UV at 254 nm, with varying intensities.

triplicates (fig. 15a), the samples were sent for mass spectrometry to investigate the candidates present in the Yme2 interactome, followed by a GO term analysis for biological components, using the total mitoproteome as the background set (fig. 15b) (supplementary table B.9). As anticipated, the top enriched GO terms belonged to the mtNucleoid and a mtNucleoid-associated protein complex, the pyruvate dehydrogenase complex. This further strengthened the idea of the presence of Yme2 in spatial proximity of mtNucleoid at a molecular level.

The presence of mtNucleoid-associated proteins as the molecular interactors of Yme2 along with the possession of putative RRM domains by Yme2, raised the possibility of Yme2 interacting with the mitochondrial nucleic acid molecules. In an attempt to photo-crosslink the potential nucleic acid molecules with Yme2, the isolated WT mitochondria were exposed to varying intensities of UV radiation at 254 nm. This wavelength is absorbed by the aromatic rings in both nucleic acids and proteins, allowing covalent bonding between the two molecules when exposed to UV light, and further stabilizing even transient interactions between nucleic acid and proteins. When the UV-crosslinked WT mitochondria were subjected to western blotting and decorated with anti-Yme2 antibody, a faint but detectable smear was observed which corresponded to a higher molecular size as compared to Yme2 (96 kDa) or the TAP-tagged Yme2 (130 kDa) (fig. 15c). This speculative crosslinked band was specific for the strains harbouring Yme2, and was absent from the $\Delta yme2$ strain. Moreover, the crosslink was also assessed in the RRM2 mutants of Yme2. The strains $yme2^{F204A}$ and $yme2^{F204A/Y242A}$ also showed the presence of crosslink, whereas in $yme2^{Y242A}$ the crosslink was apparently absent. This is a support for the idea of the physical link between Yme2 and the mtNucleoid.

Together, these results show that Yme2, an integral IMM protein, is mtNucleoid-associated and possesses distinct domains on either side of the IMM (AAA+ domain on the IMS side and RRM domain on the matrix-side), which are important for its role in mitochondria. Furthermore, the genetic link between *YME2* and the mitochondrial protein biogenesis machinery provides a strong foundation and offers key insights into its functional mechanisms.

4 Discussion

Mitochondria are double membrane-bound organelles present in eukaryotic cells that are responsible for producing ATP via OXPHOS. The ATP produced by mitochondria, in turn, is a driving force for majority of chemical reactions that occur within the cells. OXPHOS requires shuttling of electrons through five (four in yeast) multi-subunit complexes, which have a dual genetic origin (Barros and McStay, 2020; Hällberg and Larsson, 2014; Matus-Ortega et al., 2015; Overkamp et al., 2000). While most of the protein components of the ETC are encoded within the nucleus and are imported into the mitochondria, seven proteins (thirteen in humans) are mitochondrially-encoded and inserted into the IMM via the mitochondrial protein biogenesis machinery (Turk et al., 2013). The proteins encoded by mtDNA form the hydrophobic cores of the OXPHOS complexes, and hence are indispensable for the process of energy conversion. Therefore, mtDNA is a valuable and essential asset for the efficient functioning of mitochondria inside the cell (Priesnitz and Becker, 2018).

The mtDNA in yeast, apart from coding for seven subunits of ETC (namely, Cox1, Cox2, Cox3, Cytochrome B, Atp6, Atp8, Atp9), also encodes for a mitoribosomal protein Var1, 24 tRNAs, two RNA subunits that make up the mitoribosome (21S rRNA and 15S rRNA), and the RNA subunit of RNase P (Turk et al., 2013). Inside the mitochondria, the mtDNA resides within the mitochondrial matrix, and is organized into large nucleoprotein complexes called mtNucleoids (Lipinski et al., 2010; Williamson, 2002). Within the mtNucleoid, the mtDNA is packaged by an HMG box protein that has the ability to bend DNA, called Abf2 (Brewer et al., 2003; Friddle et al., 2004; Newman et al., 1996). Each mtNucleoid consists of a copy of packaged mtDNA, along with requisite protein machinery for transcription, translation and gene expression, as well as proteins involved in maintenance of mtDNA and related processes. The entire repertoire of factors which contain mtNucleoid, the mitoribosome and related gene expression and quality control proteins, together form large expressosome-like highly ordered assemblies known as the MIOREX complexes (Bogenghagen et al., 2014; Kehrein et al., 2015; Singh et al., 2020). In recent years, extensive research has focused on unraveling the components and mechanisms of MIOREX complexes, however, the complete MIOREX interactome remains largely unknown, with many of the protein partners and molecular mechanisms involved yet to be identified. In this study, two candidates are investigated, namely the PDHc and Yme2, which have been previously identified as part of the mtDNA interactome, but whose roles in these assemblies remain to be elucidated. Through exploration of the interaction dynamics of PDHc and mutational characterization of Yme2, novel insights into the mtDNA interactome were sought, with the aim of ushering this research further.

4.1 The Pyruvate Dehydrogenase Complex (PDHc)

The PDHc is a multi-subunit enzyme complex that resides in the mitochondrial matrix and plays a pivotal role in energy metabolism by converting pyruvate (the end product of glycolysis) to acetyl-CoA. The produced acetyl-CoA further serves as a substrate in the TCA cycle and leads to energy generation via OXPHOS. The size of fully assembled PDHc is up to 10 MDa in eukaryotes, which makes it one of the largest known complexes (Stoops et al., 1997; Zhou, Liao, et al., 2001; Zhou, McCarthy, et al., 2001). The conversion of pyruvate to acetyl-CoA takes place in a three-step reaction (see Introduction section 1.7.1) which requires three enzymatic centers, called E1, E2 and E3 (M. S. Patel et al., 2014). The shuttling of intermediates between the enzymatic centers takes place via the ‘swinging arm’ domain of the E2 center, which forms the core of the complex, and additionally acts a scaffold for the complete assembly of the pentagonal dodecahedron structure of the complex (Reed, 1974; Škerlová et al., 2021; Zdanowicz et al., 2024; Zhou, Liao, et al., 2001; Zhou, McCarthy, et al., 2001). The E1 subunits form a peripheral shell surrounding the oligomeric E2 core, which features E3 interspersed throughout the core. This arrangement imparts a dynamic and breathable character to the fully assembled complex, a characteristic crucial for facilitating its three-step catalytic process (Gu et al., 2003; M. S. Patel et al., 2014; Škerlová et al., 2021). In yeast, the enzymatic centers are made of multiple proteins, with E1 center constituted by Pda1 and Pdb1, E2 made up of Lat1 and E3 composed of Lpd1 and Pdx1.

4.1.1 Accessory Role of PDHc in Maintaining Mitochondrial Health

The PDHc acts as a gatekeeper to glucose metabolism, which makes it not only essential for respiratory processes, but also of utmost importance to cellular health. The importance of PDHc for yeast was apparent in this study, when deletion of individual PDHc subunits led to a growth phenotype on non-fermentable (YPG) media (especially at the stressful temperature of 37°C), where respiration is the prime source of energy generation. The growth defect exhibited upon individually deleting PDHc subunits worsened when additionally *ACH1* was deleted, which was understandable considering that Ach1 provides a partial PDHc bypass in the mitochondria by converting succinyl-CoA (a TCA cycle intermediate) to acetyl-CoA (Buu et al., 2003; Y. Chen et al., 2015; Fleck and Brock, 2009). In the absence of PDHc subunits, the acetyl-CoA produced by Ach1 is utilized for the biosynthesis of arginine, leucine, and lipoate, while also contributing partially to the functionality of the TCA cycle and OXPHOS (van Rossum et al., 2016). Therefore, the growth defect displayed by PDHc subunit deletion mutants (both with and without *ACH1*

deletion) points towards the vitality of PDHc in cellular metabolism.

This study explores a potential accessory role of PDHc in mtDNA maintenance within the mitochondria. PDHc subunits Pda1, Pdb1, and Lpd1 were identified in previous studies to be located in close proximity to mtDNA, upon performing formaldehyde-crosslinking of isolated mitochondria (Kaufman et al., 2000). When petite analysis for PDHc deletion subunits was performed on YPD (fermentable medium) at a thermally stressful temperature of 37°C, proteins of E1 (Pda1 and Pdb1) and E2 (Lat1) enzymatic centers were observed to have a significantly higher petite frequency than WT. The high petite frequency trends for Pda1 and Pdb1 were in line with the previously published findings on raffinose as a growth medium, where the respective null mutants were assayed for presence of respiratory-deficient (petite) colonies (X. J. Chen et al., 2005), underscoring the importance of PDHc in maintenance of mitochondrial health. The increased petite frequency in $\Delta pda1$, $\Delta pdb1$ and $\Delta lat1$ strains points towards their reduced respiratory competence, which could be attributed to mtDNA loss or instability. Of note, due to the involvement of Lpd1 in multiple complexes (like α -ketoglutarate dehydrogenase, glycine decarboxylase complex and branched-chain keto acid dehydrogenase complex), the deletion of Lpd1 causes severe growth defects owing to the multitude of pleiotropic effects within the cell. Therefore, as Lpd1 was incapable of growth on non-fermentable media, it was regarded by nature as petite and was excluded from the petite analysis.

To ascertain that this potential newfound role of PDHc in maintaining mitochondrial function is not due to metabolic inflexibility or lack of acetyl-CoA being produced in the mitochondria, petite analysis was also performed with $\Delta mpc1$, a strain which lacks the mitochondrial pyruvate transporter. Deletion of Mpc1 leads to lack of pyruvate uptake by mitochondria and results in accumulation of upstream metabolites and depletion of downstream TCA cycle intermediates (Bender et al., 2015; Bricker et al., 2012; Herzig et al., 2012), which could create a metabolic block due to lack of production of sufficient acetyl-CoA. While $\Delta mpc1$ displayed a petite frequency of 35% which was marginally higher than WT, the substantially high petite frequencies observed in case of PDHc subunit deletions (77.2% for $\Delta pda1$, 79.2% for $\Delta pdb1$, and 61.3% for $\Delta lat1$) were, in fact, suggestive of a role of PDHc that went beyond metabolism in mitochondria. In support of the same, the low amount of mtDNA copies in $\Delta pda1$, $\Delta pdb1$, $\Delta lat1$ and $\Delta lpd1$ reflected that mtDNA instability could be a probable explanation for the observed petite phenotype in PDHc individual subunit deletion mutants.

Given the well-documented role of the PDHc in metabolism and its auxiliary function in mtDNA maintenance, it was a reasonable hypothesis to investigate whether these two functions are interlinked. To address this, previously character-

ized catalytically inactive mutants of Pda1 (Pda1^{G217A}) and Lat1 (Lat1^{H455A/D459A}) were created in yeast and subjected to growth tests and petite assays (Niu et al., 1990; Russell et al., 1992; Yi et al., 1996). It was revealed, for both Pda1^{G217A} and Lat1^{H455A/D459A} mutants, that while yeast displayed a growth defect that was comparable with the phenotypes displayed by respective gene deletions, the petite frequencies were surprisingly rescued to almost WT-like levels. This divergence may indicate that although the catalytic inactivity affects growth of the cells due to metabolic defects, there is another mechanism at play, possibly unrelated to PDHc catalysis, that is responsible for the role of PDHc in mtDNA stability.

The possibility of the dual role of PDHc in mitochondria reinforces the idea of PDHc being a bifunctional enzyme, much like other metabolic enzymes, namely Ilv5, Hsp60, Kgd2 and Aco1. However, it has to be considered that not all bifunctional metabolic enzymes that were found crosslinked to mtDNA cause an mtDNA instability or respiratory insufficiency phenotype in the petite analysis (for example, Kgd1 and Kgd2) (X. J. Chen et al., 2005; Kaufman et al., 2000). Therefore, the observed trend for PDHc indicates an additional, specific role that is unrelated to its function in metabolism.

4.1.2 PDHc Associates with the Mitochondrial Gene Expression Machinery

The role of PDHc in maintaining mitochondrial health and mtDNA stability prompted the biochemical exploration of the specific nature of its interaction in the mtDNA interactome. It has been observed previously in bacteria that the PDHc subunits regulate gene expression. In *Bacillus subtilis*, PDHc-E2 subunit has been identified in binding to AT-rich regions of DNA close to the origin of replication, while the E1 β and E2 subunits are involved in regulating metabolic processes like sporulation (Gao et al., 2002; Stein and Firshein, 2000). Similarly, in *B. thuringiensis*, the PDHc-E2 subunit was found as a protein binding to the upstream region of prototoxin-producing genes, raising possibilities of the role of PDHc-E2 subunit in enhancing transcription (T. Walter and Aronson, 1999). Furthermore, recent evidence from *Chlamydomonas reinhardtii* has revealed a moonlighting function of DLA2, the E2 subunit of chloroplast PDHc, as an mRNA-binding protein under mixotrophic conditions, implicating its role in the regulation of gene expression (Bohne et al., 2013; Neusius et al., 2022). Aligned with the same, are the studies performed in higher eukaryotes, like mammals as well as *Xenopus* oocytes, where the PDHc-E2 subunit was found associated with mtDNA (Bogenhagen et al., 2003; Hensen et al., 2014; Rajala et al., 2015). Although PDHc subunits have been frequently observed in the mtDNA interactome, the underlying nature of this association remains obscure.

To investigate the basis of PDHc interaction with the mtDNA interactome, co-IP experiments were conducted using the Lat1 (E2 enzymatic center) antibody, which revealed that the most highly enriched proteins among the significantly enriched candidates belonged to the category of ‘mitochondrial genome maintenance’. This included proteins like the mtDNA packaging factor Abf2, the bifunctional metabolic enzymes Aco1 and Yhm2, mtDNA binding and repair proteins (Mgm101, Msh1, Mdj1 and Mip1), as well as mtRNA binders (Rpo41, Ccm1). This enrichment suggests a critical association between Lat1 and the processes essential for the stability and integrity of mitochondrial DNA or RNA, highlighting a potential role of PDHc in regulating mitochondrial genome function. To spatially validate and contextualize the aforementioned findings, a proximity labelling assay with TurboID-tagged Pda1 (E1 enzymatic center) was performed. Proximity labelling assay relies on proximity biotinylation, that is used to identify the *in vivo* proximal proteome for proteins of interest. This biotinylation is achieved by using an engineered biotin ligase enzyme called TurboID, which is fused to the protein of interest. Upon induction with biotin, TurboID biotinylates proteins within approximately 10 nm radius, which can be isolated and identified with Streptavidin-based affinity purification followed by mass spectrometry analysis. Therefore, TurboID provides a novel way of performing precision proteomics of suborganellar compartments (Branon et al., 2018; Kim and Kim, 2024). For Pda1-TurboID, mass spectrometry analysis following Streptavidin-based affinity purification identified interactions between Pda1-TurboID and factors associated with mitochondrial gene expression and translation, including proteins of the mitoribosome as well as those associated with transcription and translation machinery, among others. These processes converge to the hypothesis that PDHc could be involved more specifically in mtRNA binding or stability. Given the moonlighting activity of PDHc-E2 as an mRNA binder in *Chlamydomonas reinhardtii* chloroplasts, this was not entirely surprising (Bohne et al., 2013; Neusius et al., 2022). This finding can be further corroborated by a similar finding in HeLa cells, wherein PDHc-E2 was identified in a co-IP experiment with mitochondrial ribosome recycling factor, suggesting its presence in mitoribosome interactome (Hensen et al., 2014; Rorbach et al., 2008).

Moreover, additional evidence was provided by the solubility tests conducted in WT mitochondria, wherein treatment with RNase I released the subunits of PDHc from insoluble pellet fraction to the soluble supernatant fraction (except Lpd1, as it was completely in the supernatant fraction even in the control experiment). On the contrary, DNase I treatment resulted in almost no change in the solubilization of PDHc from pellet to supernatant. Extending this line of evidence, was the sucrose gradient fractionation performed from isolated mitochondria, which revealed the release of PDHc subunits from the heavier fractions and their almost-exclusive localization to the lighter fractions upon RNase I treatment. The observed trends

were consistent regardless of the media that was used to grow these cells from which the mitochondrial isolation was performed. Together, these observations underscore the connection between PDHc and the mitochondrial gene expression machinery, with a particular emphasis on its association with the mtRNA interactome.

The probability of the presence of PDHc in mtRNA interactome was additionally supported by microscopic visualization of mNeogreen-tagged Pda1 in yeast. In wild-type (WT) cells, Pda1-NG displayed a punctate localization pattern, which became more dispersed in rho0 cells, that are devoid of a mitochondrial genome. This suggested that the Pda1-NG spots may represent a visual pattern of PDA1 associated with its client RNA.

Collectively, these findings highlight an additional role for PDHc in mitochondrial genome maintenance, distinct from its well-established function in energy metabolism. The observed mtDNA instability phenotype in the absence of PDHc subunits suggests a potential link between the complex and the metabolic regulation of gene expression. This phenomenon, wherein metabolic enzymes exhibit dual roles—participating in metabolic pathways and coordinating gene expression levels to meet cellular demands—is well-documented (Cieřła, 2006). Notably, this study represents one of the first attempts to characterize the specific role of PDHc in mitochondrial genome regulation. Furthermore, biochemical experiments performed in this study provide pivotal insights into the specificity of interaction of PDHc subunits with mitochondrial gene expression machinery, linking the complex to the mtRNA interactome. This additional function of PDHc is reminiscent of the ‘moonlighting function’ of multiple metabolic enzymes, some of which were identified in screens for RNA-binding proteins, suggesting their involvement in post-transcriptional control (Jeffery, 2003; Scherrer et al., 2010; Tsvetanova et al., 2010). Along similar lines, due to its interactions with proteins that are involved in mitochondrial gene expression as well as mtDNA packaging, binding and repair, PDHc could have an under-explored role in linking mitochondrial metabolism with the regulation of gene expression, thereby contributing to mitochondrial genome stability. Given the evolutionarily conserved primary role of PDHc in metabolism, this additional function likely represents a secondary adaptation, highlighting the multifaceted nature of metabolic enzymes and their capacity to integrate metabolic and genetic processes in the cell.

4.1.3 Concluding Remarks

The experiments performed in this thesis highlight the possibility of PDHc acting as a bi-functional enzyme, with an accessory role linked to the mitochondrial genome, in addition to its role in cellular metabolism. While the exact function of PDHc in the interactome of mtDNA or mtRNA remains to be understood, the aforementioned

findings provide noteworthy observations that link PDHc to the mitochondrial gene expression machinery and mtRNA. Whether the PDHc modulates mitochondrial gene expression, or transcription or simply helps in maintaining the mtRNA integrity and stability, is not yet known. Moreover, the results of this research raise critical questions about the involvement of the fully-assembled PDHc or subcomplexes in this novel auxillary role. Therefore, the preliminary findings warrant further research to elucidate the process and the mechanism of PDHc's additional function in mitochondria.

Looking forward, this research could benefit from an attempt to recognize the identity of the client RNA molecule, via crosslinking and co-immunoprecipitation experiments (for example, iCLIP or RNA-immunoprecipitation) followed by sequencing the potentially bound RNA. Additionally, it would be worthy to perform an RNA sequencing experiment in different deletion subunits to observe how the entire mitochondrial RNA landscape is affected by the PDHc deletions. Even though the research on such sub-organellar processes adds an additional layer of technical complexity, it would be worthy to explore the potential nucleic acid partners of PDHc. In summary, this study establishes a strong foundation for elucidation and characterization of the role of PDHc in mitochondrial gene expression.

4.2 Yme2

YME2 (Yeast Mitochondrial Escape protein 2) is an integral IMM protein that was initially discovered through a genetic screen, where its deletion facilitated the transfer of mtDNA from mitochondria to the nucleus (Hanekamp and Thorsness, 1996; Leonhard et al., 2000; Thorsness and Fox, 1993). The mtDNA escape phenotype not only gave the protein its name, but also laid foundation for its importance in mitochondria. While it was observed that the single deletion of *YME2* confers no observable phenotype in yeast, its concomitant deletion with the proteins involved in mitochondrial protein biogenesis machinery (*MDM38*, *MBA1*, *OXA1*) leads to a severe growth defect even on fermentable media (YPD), where energy generation is not dependent on mitochondrial respiration. The most pronounced negative genetic interaction involving *YME2* occurs in $\Delta yme2\Delta mdm38$ mutants, which display a strong growth defect that cannot be alleviated by Nigericin supplementation, suggesting that this phenotype is more likely associated with Mdm38's function as a ribosome receptor rather than its role in maintaining K^+/H^+ homeostasis. These findings indicate that Yme2 and Mdm38 have partially overlapping roles that are critical for sustaining mitochondrial integrity and overall cellular functionality. Moreover, it is surprising to observe a severe growth phenotype displayed by $\Delta yme2\Delta mdm38$ on YPD, as it points towards a function of Mdm38 and/or Yme2 which extends beyond membrane integration of mtDNA-encoded proteins, prompting further research in elucidation of the Yme2's function in yeast.

4.2.1 The Characterization of Yme2 as a Potential AAA+ Protein Featuring RRM Domains

The genetic link of Yme2 with mitochondrial protein biogenesis machinery prompted insights to be obtained into the possible function of Yme2. Therefore, the putative domain organization of Yme2 was deduced using bioinformatics and mutational analyses, shedding light on its role in mitochondrial protein biogenesis. In addition to a putative TM domain, Yme2 is predicted to possess an IMS-facing AAA+ domain, as well matrix-facing RRM domains, all of which are essential for its function in the mitochondria.

Based on the AlphaFold structural prediction in this study, the IMS-facing C-terminal domain possessed by Yme2 adopts a AAA+ fold, and further *in silico* homology-based sequence analysis revealed the presence of Walker A and B motifs (typical structural motifs of P-loop ATPases) within the AAA+ domain. Among the AAA+ proteins, Yme2 showed the greatest similarity to members of the DNA-binding initiator clade, such as origin recognition proteins and helicase loader proteins. This observation was rather unexpected, considering the AAA+ domain's

location in the IMS, an environment where DNA or RNA is presumed to be absent. One feature that sets Yme2 apart from other AAA+ proteins is the presence of a positively-charged arginine residue in the Walker B motif (hhhhDR; h depicts a hydrophobic amino acid) instead of a negatively charged glutamic acid residue in the consensus sequence (hhhhDE; h depicts a hydrophobic amino acid) (Hanson and Whiteheart, 2005; Wendler et al., 2012). This substitution could potentially result in reduced or abolished catalytic activity of the AAA+ domain, as would be expected. Despite this inconsistency, mutational analysis confirmed that both Walker A and B motifs are indispensable for the function of Yme2. Furthermore, the detection of Yme2 within a high molecular weight complex comprising multiple copies of Yme2 is reminiscent of the known homo- or hetero-oligomeric structural organization displayed by AAA+ proteins (Miller and Enemark, 2016; Puchades et al., 2020; Snider et al., 2008). These findings raise critical questions about Yme2’s ability to hydrolyze nucleoside triphosphates and act as a motor, much like other AAA+ proteins. To address this, *in vitro* ATPase assays were conducted using the purified C-terminal AAA+ domain of Yme2, but no detectable ATPase activity was observed. This lack of activity could be attributed to technical limitations or the absence of a suitable substrate required to stimulate ATPase activity. Another plausible explanation could be the absence of Yme2’s N-terminal domain, suggesting that ATPase activity may require co-ordination between the two domains. Alternatively, it is also possible that the AAA+ domain inherently lacks ATPase activity, which would render the domain functionally redundant—a striking observation given its essential role in Yme2 function.

In addition to the putative AAA+ domain, *in silico* sequence analysis of Yme2 identified an N-terminal RRM domain (designated as RRM2 in this study), which was revealed to be critical for Yme2 function. Structural predictions from AlphaFold further validated the presence of the RRM2 domain and identified an additional RRM domain, termed RRM1 in this study, exhibiting a similar fold to RRM2. The RRM1 domain, in contrast to the RRM2 domain, likely evaded detection during *in silico* analysis due to the presence of an additional α -helix in its sequence, which spatially extended beyond the RRM1 fold. Nevertheless, extensive mutational analysis demonstrated that both putative RRM domains are essential for Yme2 functionality. However, only a limited number of analysed mutants were expressed at levels comparable to the wild type, suggesting that mutants with significantly reduced expression likely disrupted the structural integrity of the RRM fold of Yme2, possibly by impairing its RNA-binding capability.

RRM domains are well-characterized, structurally and functionally versatile motifs known to mediate interactions with DNA, RNA, or proteins (Maris et al., 2005). However, it remains unclear which of these molecules interact with the putative

RRM domains of Yme2. Studies by Kehrein et al., 2015 demonstrated the co-purification of Yme2 with the mitoribosome within the MIOREX complexes, further implicating the function of Yme2 in the mitochondrial protein biogenesis machinery. The RRM domains of Yme2 are likely positioned within the mitochondrial matrix to support this role. Whether these domains facilitate mitochondrial protein biogenesis by associating with mtDNA, mtRNA, the mitoribosome, or other components of the translation and biogenesis machinery remains unresolved, highlighting the need for a more detailed analysis of Yme2's interactome.

4.2.2 The mtNucleoid Association of Yme2

The presence of Yme2 in the MIOREX complex not only provided initial insights into its spatial positioning within the mitochondria, but also underscored the need for additional research for determination of its role in this space. Given the possibility of Yme2 binding to nucleic acids due to the presence of its RRM domains, UV crosslinking (254 nm) was performed in WT mitochondria, to biochemically visualize whether Yme2 formed crosslinks with its potentially nearby nucleic acids. It was consequently observed that Yme2^{WT} indeed appeared to form faint crosslinks, which seemed to be absent in the RRM2 domain mutant Yme2^{Y242A}. This finding provided an indicative evidence of the association of Yme2 with nucleic acids. Furthermore, mass spectrometry analysis of Yme2's interactome revealed that the most highly enriched proteins belonged to the 'mitochondrial nucleoid' GO term, which was in accordance with the previously observed co-localization of Yme2 and mtDNA (Murley et al., 2013). These results, along with the strong genetic interaction of *YME2* with *MDM38*, *MBA1* and *OXA1*, strongly allude to the role of Yme2 in the mitochondrial protein biogenesis.

4.2.3 The Proposed Working Model for the Putative Function of Yme2

The proposed role of Mdm38 as a ribosome receptor at the IMM (Bauerschmitt et al., 2010; Frazier et al., 2006) coupled with its robust genetic interaction with Yme2 provide noteworthy insights to the possible function of Yme2 in mitochondrial protein biogenesis. When the aforementioned findings are integrated with the observation that Yme2 is present close to the mtNucleoid in the MIOREX complex, a plausible hypothesis emerges, which has been conceptualized into a working model (fig. 16).

It is proposed that Yme2, through its putative RRM domains, could assist in mitochondrial protein translation by binding to either mRNAs or mitoribosomal rRNAs, and aid in tethering and positioning the translation apparatus at the

IMM. This anchoring mechanism by Yme2 could enhance efficient protein insertion, offering a probable explanation for the partially overlapping functions of Yme2 and Mdm38. In the absence of Mdm38 or Yme2, the remaining protein would still be adequate to fulfill this function, either fully or to a certain degree. On the contrary, in $\Delta yme2\Delta mdm38$ cells, the tethering and accurate positioning of the mitoribosome may be impaired to a degree that significantly disrupts protein insertion, leading to the observed strong growth defects. An alternative hypothesis could be that Yme2 interacts with mtDNA via its RRM domain, thereby aiding in the recruitment of mtDNA to the IMM, potentially facilitating the spatial co-ordination of transcription and translation.

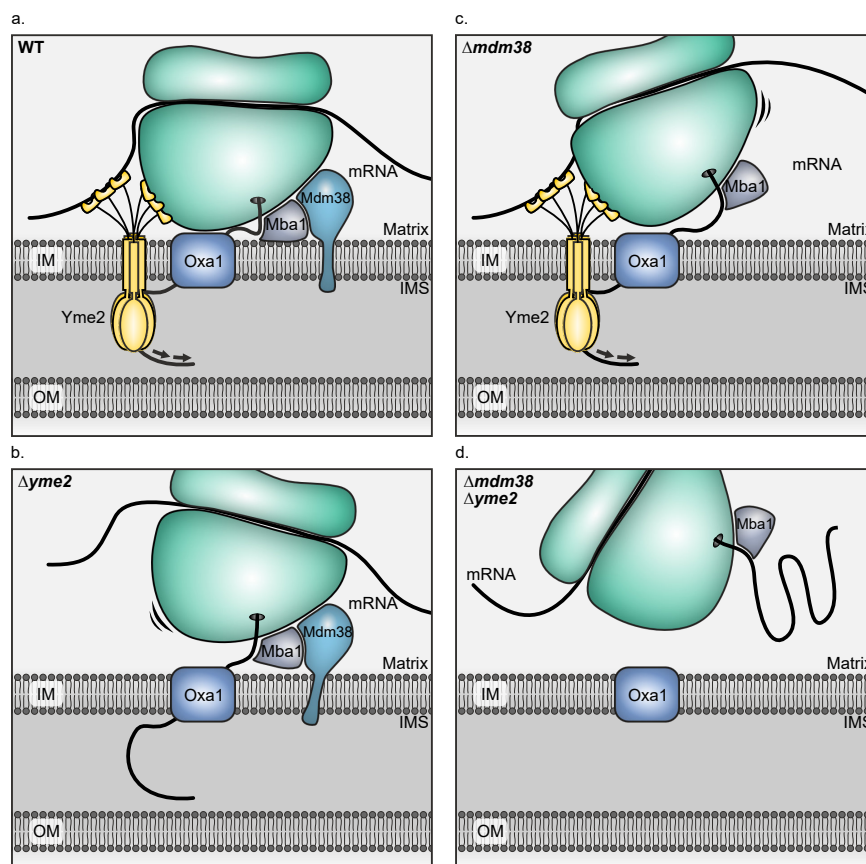


Figure 16: **The proposed working model for the function of Yme2.** A schematic showing the proposed working model for the probable function of Yme2 in WT (a), $\Delta yme2$ (b), $\Delta mdm38$ (c) and $\Delta yme2\Delta mdm38$ (d) cells. Mitochondrial compartments are indicated as follows: IM, Inner Membrane; OM, Outer Membrane; IMS, Intermembrane Space. Arrows show the possible Yme2-driven pulling force to aid in protein insertion into the IMM by Oxa1 insertase.

Meanwhile, via the presence of its AAA+ domains which, if assumed to possess an ATPase activity and acting as motors, an intriguing yet speculative idea could be that Yme2 aids in protein export by providing either a pulling force in the IMS or extracting stalled proteins from the Oxa1 insertase pore, similar to the role Msp1 and Cdc48 perform at the OMM (Mårtensson et al., 2019; Weidberg and Amon, 2018). The preliminary support to this idea could be given by overexpression of Yme2 with Gal1 (strong overexpression) or GalS (weak overexpression) promoters, where it would be expected that upon induction, Yme2 would overplay its role of protein extraction, disallowing efficient protein insertion and leading to a growth phenotype due to secondary effects. Indeed, when the experiment was performed, Yme2^{WT} overexpression appeared to cause growth defects in the yeast cells, while the overexpression of Walker A and B motif mutants of the AAA+ domain (Yme2^{K393A}, Yme2^{D522A}) supposedly alleviated the phenotype (fig. S10a,b). Although this finding is not a concrete explanation for the function of Yme2's AAA+ domain, it could lay groundwork for further research that is imperative to determine the presumed role of Yme2 in mitochondrial quality control.

Taken together, while the aforementioned findings do not define the exact role of Yme2, they do provide promising insights into its functional characterization. Through extensive mutational studies and supporting evidence from biochemical analyses, this thesis establishes a strong foundation for mechanistic elucidation of Yme2's role in mitochondrial protein biogenesis.

4.2.4 Concluding Remarks

This study investigates the genetic link between Yme2 and the mitochondrial protein biogenesis machinery, making a novel attempt to functionally characterize the protein through mutational and biochemical analyses. It was demonstrated in this research, that the *in silico*-predicted AAA+ and RRM domains of Yme2 are indispensable for its function, which may involve tethering the mitoribosome or the mtDNA in the MIOREX complex to the IMM. While the experiments conducted in this thesis provide a strong foundation for characterizing Yme2, several critical questions about its mitochondrial function remain to be answered. Whether the AAA+ domain of Yme2 exhibits ATPase activity, and if so, the specific substrates targeted for hydrolysis by Yme2, remains elusive. Additionally, regarding its RRM domains, it remains unclear whether the integrity of the RRM domains is necessary for the folding of Yme2 and if RNA binding plays a key role in promoting and stabilizing Yme2 complex formation and protein stability. Finally, the potential functional coupling of the AAA+ and RRM domains requires further investigation.

Furthermore, the pronounced growth defect observed in $\Delta yme2\Delta mdm38$ cells, even on fermentable medium, is unexpected if the sole function of Yme2 and/or Mdm38

is the efficient insertion mtDNA-encoded proteins. Exploring potential roles of Yme2 and Mdm38 beyond the biogenesis of mtDNA-encoded proteins represents an intriguing avenue for future research. Such investigations may yield valuable insights into the mechanisms underlying their mtDNA escape phenotype, offering a deeper understanding of mitochondrial function and contributing to the broader narrative of mitochondrial evolution.

5 Outlook

Mitochondrial nucleoids consist of packaged mtDNA, along with the essential protein machinery for transcription, translation, gene expression, and maintenance. These nucleoids, together with the mitoribosome and associated factors for gene expression and quality control, form highly organized assemblies known as MIOREX complexes. Despite extensive research, the full composition and mechanisms of the MIOREX interactome remain poorly understood. This study focuses on two key candidates, PDHc and Yme2, which are thought to be associated with the mtDNA interactome.

This work demonstrates that the PDHc, which is widely known for its conserved role in glucose metabolism, additionally has a function in mitochondrial gene expression. The biochemical analyses performed in this study further highlight its specific interactions with mitochondrial RNA, underscoring its identity as a bi-functional enzyme.

As a second objective, it is highlighted that Yme2, an inner mitochondrial membrane protein implicated in mitochondrial protein biogenesis, possesses an RNA recognition motif (RRM) and a AAA+ domain, as revealed through the extensive bioinformatics and mutational research conducted in this study. Additionally, Yme2 exhibits biochemical interactions with nucleoid-associated proteins, as well as genetic interactions with *MDM38*, *MBA1*, and *OXA1*, which links its function to the mitochondrial protein biogenesis machinery.

This thesis has provided significant insights into the mtDNA interactome, particularly by elucidating the roles of the PDHc and Yme2. By exploring the interaction dynamics of PDHc and characterizing Yme2's structural and functional attributes, novel links between these components and key mitochondrial processes, such as genome maintenance and protein biogenesis, have been established. These findings expand our understanding of the dual functionality of metabolic enzymes and highlight the intricate co-ordination between the mitochondrial genome and associated protein machinery. Despite these advances, many aspects of these interactions remain unresolved, offering exciting opportunities for further study.

Future research should focus on uncovering the candidates involved within the interactions identified in this study. Techniques such as iCLIP and advanced RNA-protein interaction mapping could provide deeper mechanistic insights into how PDHc contributes to mitochondrial gene expression and how Yme2 orchestrates its roles within the mtNucleoid and biogenesis pathways. Furthermore, a comprehensive characterization of the complete mtDNA interactome, including its lesser-known protein partners, could unveil additional regulatory mechanisms

underlying mitochondrial genome integrity and expression.

The findings presented in this thesis pave the way for future studies aimed at bridging fundamental mitochondrial biology with its impact on cellular health and disease. Given that disruptions in mitochondrial processes are implicated in a variety of disorders, from metabolic syndromes to neurodegeneration, understanding these molecular mechanisms holds the potential for developing novel therapeutic approaches. By further unraveling the complexities of the mtDNA interactome, we are advancing towards addressing critical questions in organelle biology and its relevance to human health.

6 Materials and Methods

6.1 Materials

The materials used in this study are mentioned in the Appendix B. The information about the sources of chemicals and reagents used is in supplementary table B.1. The composition of all the media used in this study is given in supplementary table B.2. The contents of the common buffers that were used or made are listed in supplementary table B.3. All special buffers are listed in the Methods section, as and when they are mentioned. The antibodies used in this thesis are listed along with their source in supplementary table B.4.

6.2 Methods

6.2.1 Strain generation and cloning

All yeast strains used in this study were generated in the W303 background. Single deletion strains and C-terminally tagged genes were constructed using toolbox PCR as previously described (Janke et al., 2004). The double deletion strains were constructed by mating the respective single deletion strains followed by tetrad dissection analysis. The catalytic mutant strains for *LAT1*, *PDA1* and *YME2* mutants were constructed by integrative transformation either in the *HO* locus or in the *LEU2* locus of the respective deletion backgrounds.

For plasmid shuffle, the parent strain was created by first deleting *YME2* in the WT background, followed by transformation with a rescue plasmid pRS316-*YME2*. Thereafter, *MDM38* was deleted, leading to the creation of the final (parent) strain $\Delta yme2\Delta mdm38 + \text{pRS316-Yme2}$. This strain was used for transformation with mutant copies of Yme2 on a plasmid pRS315, as and when indicated.

Rho0 strains were generated by growing the respective rho+ background strains for 4 days in YPD supplemented with 25 $\mu\text{g}/\text{ml}$ EtBr, with periodic dilution steps in order to keep the culture always in log phase. The cells were singly plated and isolated clones were subjected to multiple selection steps on YPD and YPG plates. The strains were confirmed by growth analysis and DAPI staining followed by microscopy.

Diploid strains were generated by mating the required haploid strains of opposing mating types on YPD for 2 h. Zygotes were then picked and isolated using the dissection scope, and allowed to form colonies. Zygotes were then tested against

mating type tester strains as well as WT strains and were replica-plated next day on SC-all media for the selection to take place.

The list of the yeast strains used in this study, along with their detailed genotypic description is listed in supplementary table B.5, whereas the plasmids generated and used in this study are described in supplementary table B.6. Additionally, the primers used for generation of plasmids and yeast strains are available on Osman Lab servers and Benchling.

6.2.2 Molecular and Cell Biology methods

Yeast Transformation

The yeast transformation protocol was performed with log-phase grown cells (OD_{600} 0.6-1.0). 5 ml of cells were harvested by centrifugation for 3 min at 3,000 g. The cell pellet was then resuspended in 100 mM LiAc, followed by centrifugation at 3,000 g for 3 min. The cell pellet was collected and to this pellet, the following reagents were added in the given order: 240 μ l 50% w/v PEG 3500, 34 μ l sterile water, 10 μ l pre-heated (95°C) 10 mg/ml Salmon sperm DNA and 36 μ l 1 M LiAc. The cells were then vortexed and all components were thoroughly mixed. To this, the DNA to be transformed was added (2 μ l for plasmid DNA; 40 μ l for PCR amplified fragment). The cells were briefly vortexed, and incubated at 30°C for 30 min at 400 rpm shaking. This was followed by their incubation at 42°C for 15 min with 400 rpm shaking (heat shock). Thereafter, the cells were spun down (3,000 g for 3 min) and directly plated on the required medium, or recovered in YPD medium for 2-3 hours before plating on the desired selection medium. The plates were incubated at 30°C for 1-2 days for colonies to grow.

Bacterial Transformation

The *E. coli* transformation was carried out with chemically competent cells stored at -80°C. The cells were thawed on ice for 15 min, to which 3 μ l of DNA to be transformed was added. The cells were incubated on ice for 30 min, after which they were subjected to heat shock at 42°C for 30 sec. The cells were then immediately transferred on ice and incubated for 5 min. This was followed by addition of 750 μ l LB-media to the cells, and recovery at 37°C for 45 min with 600 rpm shaking. Post-recovery, the cells were plated on LB+Ampicillin plates (100 μ g/ml) and incubated at 37°C overnight, for colonies to grow.

Agarose Gel Electrophoresis

Agarose gel electrophoresis was performed by dissolving 1% Agarose in 1X TAE buffer, and melting it by heating. The gel was then left to solidify for about 20 min at RT after adding a few drops of ethidium bromide. The gel was run in a gel running chamber at 120 V till the loading dye front migrated about 3/4th of the length of the gel. The separated nucleic acid bands were analyzed by exposing the gel to UV light, and the size of the bands was estimated according to the 1 kb plus molecular weight marker that was loaded along with the samples.

Growth Test Analysis

Growth test analysis was performed with log-phase grown cells in YPD. Equal number of cells (3.2×10^6) were taken for the strains for which the growth analysis was performed, washed in water and then serially diluted (1:50) six times in water. 3.5 μ l of the serially diluted cells were taken and spotted on fermentable (YPD) and non-fermentable (YPG) media, and additionally on special media as indicated in the respective figures. The plates were incubated at 30°C and 37°C to observe the phenotypes at optimal and thermally stressful temperatures, respectively, as some phenotypes become apparent only at 37°C. Pictures of the plates were taken after 24h (1 day), 48h (2 days) or even 72h (3 days) for some growth tests, and the phenotypes were further deduced.

Petite Assay

Petite analysis is an assay which provides a momentary glance and a quantitative insight into the ability of a strain to form respiratory-deficient colonies. The readout of the assay gives the proportion of respiratory-competent versus the respiratory-deficient cells in the respective strain, upon plating the cells onto YPG media with a low amount of glucose (0.1%). The glucose helps in kickstarting the growth of respiratory-deficient cells, which allows them to form smaller-sized ‘petite’ colonies, as opposed to the full-sized ‘grande’ colonies formed by the respiratory-efficient cells.

In order to carry out the petite assay, freshly streaked strains were grown overnight in 5 ml YPD, and were diluted the next morning to an OD_{600} of 0.01 in YPD, and grown to log-phase for 8 h at 30°C or 11 h at 37°C. After the cells reached log phase, 200 μ l of the culture was taken and diluted 10-fold in 1,800 μ l YPD. 1 ml of this dilution was used to measure the OD_{660} , and rest was further diluted 100-fold in water. From the final 1000-fold diluted culture, 200 cells were plated (calculated based on OD_{660}) on indicator plates, which are YPG plates with 0.1% Glucose. The cells were further allowed to grow and form colonies at 30°C for 4 days, after

which the amount of ‘petite’ and ‘grande’ colonies for each strain were counted, and petite frequency (percentage of cells forming ‘petite’ colonies) was determined. For statistical p-value deduction, unpaired t-test was performed.

Isolation of Yeast Genomic DNA from Cells

Log-phase grown cells equivalent to OD₆₀₀ 2.5 were harvested and centrifuged at 3,000 g for 3 min. The cell pellet was washed with water and re-harvested, before freezing at -80°C overnight. Next, cell pellet was thawed on ice and about 300 mg of 0.1 mm Zirconium beads (Carl Roth Catalog number N033.1) were added to the tube along with 200 µl of breaking buffer (2% v/v Triton X-100, 1% v/v SDS, 100 mM NaCl, 10 mM Tris pH 8.0, 1 mM EDTA pH 8.0). Additionally, 200 µl Phenol-Chloroform-Isoamylalcohol was added to the tube and the tube was vortexed in the multi-tube vortexer for 3 min at maximum speed. After vortexing, 200 µl of TE buffer was added to the tube and the contents were mixed rigorously by shaking. The tube was then subjected to centrifugation for 5 min at 20,000 g at RT, followed by aspiration and transfer of the aqueous (upper) phase of the supernatant into another tube. 1 ml of 100% ethanol was added to the aspirated supernatant and the contents were mixed by inverting. The tube was again centrifuged at 20,000 g for 3 min at RT. The supernatant was then discarded, and pellet was left to dry in order for the ethanol to evaporate completely. The pellet was resuspended in 400 µl TE buffer and was treated further with 30 µl of 1 mg/ml DNase-free RNase A (Thermo Scientific EN0531) by incubation at 37°C for 5 min. This was followed by addition of 10 µl 4 M ammonium acetate and then homogenously mixing the solution by inversion. 1 ml 100% ethanol was added thereafter in order to precipitate the DNA, and centrifugation was carried out for 3 min at 20,000 g at RT. The supernatant was then discarded and the pellet was allowed to dry, after which it was resuspended in 50 µl of DEPC-treated nuclease free water. The concentration of the isolated DNA was measured and it was further used for Quantitative PCR analysis.

Quantitative PCR (qPCR) and Determination of mtDNA copy number

Isolated DNA from yeast cells (in 3 biological replicates) was diluted upto 0.1 ng/µl and 2 µl of DNA was added into an 18 µl reaction mix containing 10 µl iTaq™ Universal SYBR Green Supermix (BioRad Catalog number 1725124), 0.8 µl each of forward and reverse primer, and 6.4 µl DEPC-treated nuclease-free water. The qPCR analysis was run on CFX96 Real-Time System with the following conditions: initial denaturation(95°C for 3 min), 39 cycles of denaturation(95°C for 30 sec), elongation (60°C for 30 sec) and signal detection. The melting curve was determined in the range of 60-95°C with 0.5°C increments and 5 sec intervals which was followed

by the signal readout. The C_t values were automatically determined by Biorad CFX 3.1 software. Absolute mtDNA copy number was quantified using the standards obtained from the 1 kb fragments of Cox1 (mitochondrial gene) and Act1 (nuclear gene) genes cloned into pUC19 vectors (Göke et al., 2020). Mean of the C_t values from three technical replicates was first calculated per biological replicate for each primer combination and the dC_t value was obtained by calculating the difference between Cox1 and Act1. Relative expression was then calculated by the square of $-dC_t$ value, which was then normalized to the mean of the relative expression of the three biological replicates of the WT sample. The number of mtDNA copies per sample were determined as performed by Göke et al., 2020. P-values were calculated with Welch's t-test (one-tailed) between the triplicates of WT and the respective mutant, assuming unequal variance.

6.2.3 Biochemical methods

SDS-PAGE and Western Blotting

The polyacrylamide gels were poured manually using the Biorad gel casting apparatus, and based on the experiment, different concentrations of acrylamide were used in order to create the suitable gel pore size. In this study, based on the requirement, 10%, 12%, and 16% gels were poured. The gels were run in 1X TGS buffer at 90 V for the first 10 min and then for 130 V till the desired resolution was achieved. The desired resolution was deciphered by loading a marker on the gel, which was the NEB Blue Protein standard (NEB, P7718L). After running the gel, either Western blotting or Coomassie staining was performed.

For Western blotting, the gel, the Whatman paper and the methanol-activated PVDF membrane were first soaked in 1X Towbin buffer, and then assembled in a blotting sandwich with the bottom to top order being- 2 Whatman papers, PVDF membrane, the gel with resolved proteins, 2 Whatman papers. The blotting was always performed for 90 min at 2 mA per cm^2 area of the blotting sandwich. Post-blotting, the membrane was re-activated in methanol, blocked in 5% Milk in 1X TBS for one hour at RT or overnight at 4°C. Subsequently, the primary antibody (prepared in 5% milk in 1X TBS) was decorated on the membrane for one hour at RT or overnight at 4°C. The membrane was then washed three times (10 min each time) with 1X TBS. The secondary antibody (always prepared fresh with 5% milk in TBS) was then decorated for one hour at RT or overnight at 4°C, followed by washing three times for 10 min each with 1X TBS. The immunoblotted proteins were then detected by chemiluminescence, after exposing the membrane to ECL I and II solutions.

For Coomassie staining, the gel was washed in water for a few minutes before

staining it with Coomassie staining solution overnight at RT. The gel was either directly analyzed and imaged, or incubated for the requisite amount of time with the destaining solution in order to make the background more transparent.

Cell lysates preparation for Immunoblotting

The protocol for the preparation of cell lysates was adapted from Kushnirov, 2000. Log-phase grown cells (2.5 OD_{600}) were centrifuged at 3,000 g for 3 minutes at RT. The pellets were washed and resuspended in 100 μl of water, to which 100 μl of 0.2 M NaOH was added in order to perform alkaline lysis. The cells were briefly vortexed and left undisturbed for 5 minutes at RT. This was followed by centrifugation at 3,000 g for 3 min at RT. The supernatant was then discarded and the cell pellet was resuspended in 1x Lämmli Buffer, and incubated at 95°C for 10 minutes, before separating the obtained proteins from lysed cells via SDS-PAGE.

Mitochondria isolation

Mitochondrial isolation (Mitoprep) was performed according to Basch et al., 2020. Each mitoprep was performed by growing 2 liters of cell culture in the indicated medium (YPD/YPGal/YPG) to log phase, and cell pellet was obtained by centrifugation at 3,000 g for 5 minutes at RT. The cells were washed once with water, and pelleted again, followed by determination of the wet weight of the cell pellet. The cell pellet was resuspended in 2 ml/g wet weight alkaline solution (100 mM Tris, 10 mM DTT) and incubated at 30°C for 10 minutes with 75 rpm shaking. The cell pellet was further resuspended in 6.6 ml/g wet weight Sphaeroplasts buffer (20 mM KH_2PO_4 pH 7.4, 1.2 M sorbitol) supplemented with Zymolyase T (6 mg/ml) after centrifugation, and incubated at 30°C for 30 min with 75 rpm shaking. After the sphaeroplast treatment, the cells, ideally devoid of an intact cell wall, were re-isolated by centrifugation. The sphaeroplasts were then dissolved in homogenization buffer (10 mM Tris pH 7.4, 0.6 M sorbitol, 1 mM EDTA, 0.2% bovine serum albumin (BSA), 1 mM PMSF) and mechanically disrupted on ice using a Dounce homogenizer. The homogenized cells were then centrifuged at 3,000 g for 5 minutes at 4°C. All further steps were performed on ice. The supernatant was collected and further centrifuged at 10,000 g for 10 minutes. This resulted in a mitochondria-containing pinkish-red pellet, which was further resuspended in SEM buffer (250 mM Sucrose, 1 mM EDTA, 10 mM MOPS-KOH pH 7.2), and then subjected to step gradient centrifugation over a sucrose cushion which consisted of SEM500 buffer (500 mM sucrose, 1 mM EDTA, 10 mM MOPS-KOH pH 7.2) at 13,000 g for 10 min (cite Morgenstern et al. 2017). The pellet was further resuspended in SEM buffer, aliquoted and shock frozen in liquid N_2 , after performing protein concentration determination using the Bradford's assay.

For checking the mitoprofile and the successful isolation of pure mitochondria, SDS gels and immunoblotting were performed with a concentration gradient of isolated mitochondria (for instance, 50 μg , 25 μg and 12.5 μg). For this, the pure mitochondria were thawed, centrifuged at 13,000 g for 10 min at 4°C, and mitochondrial pellet was resuspended in 1x Lämmli buffer. The samples were then heated at 95°C for 10 minutes, before being subjected to SDS PAGE and Western blotting.

Blue Native PAGE (BN-PAGE) analysis

The protocol for BN-PAGE was adapted from Wittig et al., 2006. The BN-PAGE was performed with 100 μg purified mitochondria. The mitochondrial pellet was resuspended in solubilization buffer (50 mM NaCl, 5 mM 6-aminohexanoic acid, 50 mM imidazole/HCl pH 7.0, 50 mM K_2HPO_4 pH 7.4, 10% (v/v) glycerol) containing 1.875% digitonin, and incubated for 20 min at 4°C. This was followed by centrifugation at 20,000 g for 20 min at 4°C, to obtain a cleared lysate. To the supernatant, 2 μl solubilization buffer with 2% Coomassie Brilliant Blue G-250 was added, and mixed thoroughly. The sample was then loaded onto a BN-PAGE gel at 4°C.

The BN-PAGE gel was a gradient gel representing acrylamide/bis-acrylamide concentrations of 3-13%, and was cast using a gradient mixer. The gel was solidified and stored overnight at 4°C in the 1x gel buffer (15 mM imidazole pH 7.0, 0.5 M 6-aminohexanoic acid). The following morning, the gel was taken out and loaded with 100 μg of freshly prepared mitochondrial sample at 4°C, and run for the first 30 min at 50 V with the deep blue cathode buffer and the anode buffer. Thereafter, the gel was run for about 2 hours at 200 V with the slightly blue cathode buffer and anode buffer, until the running front reached the bottom of the gel. After the gel was run, it was disassembled from the apparatus and subjected either to immunoblotting or Coomassie staining.

In order to perform immunoblotting, the gel was incubated first for a few minutes in 1x Towbin buffer. Western blotting was performed according to the section 6.2.3: SDS-PAGE and Western Blotting, except the fact that the blotting was done for 3 hours at 0.5 mA per cm^2 area of the blotting sandwich. The primary and secondary antibody decoration was done according to section 6.2.3: SDS-PAGE and Western Blotting. For the Coomassie staining, on the other hand, the gel was incubated twice in a fixing solution (40% methanol, 7% acetic acid) for 10 min each. This was followed by incubation of the gel overnight in Coomassie staining solution for the bands to be visible. If needed, the destaining solution was used to make the background transparent.

Lat1 Co-IP

The Lat1 Co-IP was performed with purified Lat1 antibody-coupled magnetic beads (Dynabeads™ M-270 Epoxy). The bead conjugation was done according to Cristea and Chait, 2011. 8 mg beads were washed and equilibrated for 15 minutes with 0.1 M sodium phosphate buffer pH 7.4, and then conjugated overnight at 30°C with 80 μ l of purified Lat1 antibody on a rotating wheel. The beads were then washed sequentially with 0.1 M sodium phosphate buffer (pH 7.4), 100 mM glycine-HCl, 10 mM Tris-HCl (pH 8.8), 100 mM triethylamine, PBS and 0.5% Triton X-100, as given in Cristea and Chait, 2011. The coupled beads were either used immediately or stored in PBS containing 0.02% NaN₃ at 4°C.

After bead conjugation, 2 mg purified mitochondria (in four replicates) for each sample were lysed for 30 min at 4°C by resuspension in lysis buffer (10 mM Tris-HCl pH 7.4, 150 mM NaCl, 1x Roche cOmplete™ with EDTA) supplemented with 1% Digitonin. The lysate was then cleared by centrifugation at 13,000 g for 10 minutes at 4°C. The cleared lysate was then added to lysis buffer-equilibrated Lat1 coupled beads, and further incubated at 4°C for 2 hours. After the binding step, the beads were washed three times with lysis buffer supplemented with 0.05% Digitonin, and then three times with detergent-free lysis buffer with higher salt (10 mM Tris-HCl pH 7.4, 250 mM NaCl, 1x Roche cOmplete™ with EDTA). After washing, the eluate was obtained by adding 1x Lämmli buffer and by heating the samples at 95°C for 10 minutes. The beads were then removed and 1/6th of each sample was separated for immunoblot analysis. The leftover sample was loaded on to SDS gels poured with a larger stacking gel. The gels were run at 90 V till the Lämmli buffer front reached a few millimetres into the resolving gel. The gel bands containing the stacked proteins were then cut with a fresh blade, and frozen at -20°C until they were subjected to protein extraction and analysis by mass spectrometry.

For the test analysis, the aforementioned protocol was followed with 500 μ g purified mitochondria, and lysis was performed with either 1% Digitonin or 0.5% NP-40 (fig. S3b).

Pdb1 Co-IP

The Pdb1 Co-IP was performed with purified Pdb1 antibody-coupled magnetic beads (Dynabeads™ M-270 Epoxy). The bead conjugation was done according to Cristea and Chait, 2011. 5 mg beads were washed and equilibrated for 15 minutes with 0.1 M sodium phosphate buffer pH 7.4, and then conjugated overnight at 30°C with 50 μ l of purified Pdb1 antibody on a rotating wheel. The beads were then washed sequentially as mentioned in section 6.2.3: Lat1 CoIP. The coupled beads were either used immediately or stored in PBS containing 0.02% NaN₃ at 4°C .

For the Co-IP, 500 μ g purified mitochondria were lysed for 30 min at 4°C by resuspension in lysis buffer (10 mM Tris-Hcl pH 7.4, 150 mM NaCl, 1x Roche cOmpleteTM with EDTA) supplemented with 1% Digitonin. The lysate was then cleared by centrifugation at 13,000 g for 10 minutes at 4°C, and further added to lysis buffer-equilibrated Pdb1 coupled beads, followed by incubation at 4°C for 2 hours. After the binding step, the beads were washed three times with lysis buffer supplemented with 0.05% Digitonin, and then three times with detergent-free lysis buffer with higher salt (10 mM Tris-Hcl pH 7.4, 250 mM NaCl, 1x Roche cOmpleteTM with EDTA). After washing, the eluate was obtained by adding 1x Lämmli buffer and by heating the samples at 95°C for 10 minutes, before separating the proteins on an SDS gel and analyzing them via immunoblotting.

c-Myc and HA Co-IP

For the immunoprecipitation with Myc or HA-tagged proteins, 2 mg purified mitochondria from the respective strains were lysed in a suitable lysis buffer (10 mM Tris-Hcl pH 7.4, 50 mM NaCl, 1x Roche cOmpleteTM with EDTA) with 2% digitonin. The lysis was performed for 30 min at 4°C. Subsequently, the obtained lysate was cleared by centrifugation at 13,000 g for 10 min at 4°C. The supernatant was then taken and incubated with equilibrated c-Myc (PierceTM) or HA (PierceTM) beads for 2 h at 4°C. This was followed by washing the beads three times with lysis buffer supplemented with 0.05% digitonin, after which the beads were again washed three times in lysis buffer devoid of any detergent. The bound proteins were then eluted with 1x Laemmli buffer and were separated on an SDS gel before being further subjected to immunoblotting.

Proximity Labelling Assay

The proximity labelling assay protocol was adapted from Salvatori et al., 2020. The assay was performed with purified mitochondria. Prior to the isolation of mitochondria, the log-phase grown cells were induced with 50 μ M Biotin (prepared in DMSO) for 30 minutes at 30°C. Mitochondrial isolation was performed as mentioned in section 6.2.3: Mitochondria isolation. 1 mg of mitochondria were used per sample for the assay. The assay was performed in triplicates for mass spectrometry analysis. The mitochondria were first resuspended in 100 μ l 1% SDS and incubated at 50°C for 5 minutes, after which lysis was performed by adding 900 μ l RIPA buffer (50 mM Tris-HCl pH 7.5, 150 mM NaCl, 1% w/v NP-40, 1 mM EDTA, 1 mM EGTA, 0.1% SDS, 0.5% sodium deoxycholate) along with 0.5 μ l Benzonase. The lysis was performed for 30 minutes at 4°C. This was followed by centrifuging the mitochondria at 16,000 g for 5 minutes. From the obtained lysate, the supernatant was taken out and added to 50 μ l of equilibrated PierceTM

magnetic Streptavidin beads, and further incubated for 1 h at 4°C. The beads were then washed three times with RIPA buffer, three times with TAP lysis buffer (50 mM HEPES-KOH pH 8.0, 100 mM KCl, 10% v/v Glycerol, 2 mM EDTA). In the last wash with TAP lysis buffer, 1/6th of the total volume was taken out to another tube, in order to perform immunoblotting. The rest of the beads were submitted for Mass Spectrometry analysis.

Sample preparation for Mass Spectrometry

The sample preparation for mass spectrometry analysis was done from either magnetic beads coupled to an antibody, which was bound to the target protein and its possible interactors; or from excised SDS gel bands that contained the eluted proteins after the Co-IP. The sample preparation method was performed by **PD Dr. Serena Schwenkert**.

On bead digest. The on-bead digest protocol was used in the case of proximity labelling assay. The beads were washed twice with 50 mM Tris (pH 7.5) and then with 50 mM Tris (pH 7.5) containing 2 M urea. For the initial trypsin digestion, the beads were resuspended in 160 μ l of 50 mM Tris (pH 7.5), 1 M urea, and 1 mM dithiothreitol (DTT), followed by the addition of 0.8 μ g of trypsin (Pierce, Thermo Scientific). The mixture was incubated at 25°C for 3 hours with continuous shaking. After incubation, the supernatant was collected, and the beads were washed twice with 120 μ l of 50 mM Tris (pH 7.5) and 1 M urea. The collected supernatants were combined with the trypsin digest. DTT was added to the pooled sample to a final concentration of 4 mM, and the sample was incubated at 25°C for 30 minutes with shaking. Iodoacetamide (IAA) was then added to a final concentration of 10 mM, and the sample was incubated at 25°C for 45 minutes in the dark with continuous shaking. An additional 1 μ g of trypsin was subsequently added, and a second digestion was carried out overnight at 25°C with continuous shaking.

Gel band extraction. Coomassie-stained gel pieces from Lat1 Co-IP as well as Myc Co-IP were excised, washed three times with water, and cut into small fragments. These gel pieces were washed twice for 10 min each with 20 mM ammonium bicarbonate (ABC) and acetonitrile (ACN). Proteins were reduced using 10 mM DTT at 56°C for 30 minutes, followed by a 10 min wash with ACN. Alkylation was performed using 55 mM IAA for 30 min in darkness. Samples were washed twice more, for 10 minutes each, with ABC and ACN before digestion with 0.3 μ g of trypsin at 37°C overnight. The resulting digested peptides were extracted sequentially with 5% formic acid (FA), 50% ACN, and 50% ACN with 1% FA, each for 15 minutes at 37°C. All extractions were pooled, and peptides were dried using a vacuum centrifuge. For peptide purification, home-made C18 stage tips (Rappsilber et al., 2003) were used. The tips were first activated with

100% methanol and equilibrated with 0.5% FA prior to loading the peptides. After loading, the tips were washed with 0.5% FA, and the peptides were eluted using 80% ACN with 0.1% FA.

Mass Spectrometry and Proteomics data analysis

The mass spectrometry was performed by **PD Dr. Serena Schwenkert**. For LC-MS/MS analysis, 1 μg of peptides was separated using a linear gradient ranging from 5% to 80% (v/v) ACN over 30 minutes at a constant flow rate of 250 nl/min on a nano-LC system (Ultimate 3000 RSLC, Thermo Fisher Scientific, Waltham, MA, USA). The system was equipped with an Acclaim Pepmap nano-trap column (C18, 100 \AA , 100 μm \times 2 cm) and an Acclaim Pepmap RSLC analytical column (C18, 100 \AA , 75 μm \times 50 cm), both from Thermo Fisher Scientific. The column temperature was maintained at 50°C throughout the run. MS/MS was conducted on an Impact II high-resolution Q-TOF (Bruker Daltonics, Bremen, Germany) using a CaptiveSpray nano-electrospray ionization (ESI) source (Bruker Daltonics). MS1 spectra were acquired with a mass range of m/z 200–2000 at a rate of 3 Hz, with the 18 most intense peaks selected for MS/MS analysis. The spectrum acquisition rate was intensity-dependent, varying from 4 to 16 Hz, and dynamic exclusion was set to 0.5 minutes.

Raw data were analyzed using MaxQuant software versions 2.4.2.0 (Lat1 Co-IP) and 2.4.14.0 (proximity labelling assay) (Cox and Mann, 2008). Peak lists were compared against the Yeast reference proteome from UniProt (www.uniprot.org). Oxidation (M) and Acetyl (Protein N-term) were considered as variable modifications, while Carbamidomethyl (C) was used as a fixed modification. All other parameters were set to default. Protein quantification was performed using the label-free quantification (LFQ) algorithm (Cox et al., 2014). Further analysis was carried out in Perseus versions 2.0.9.0 and 2.0.11 (Tyanova et al., 2016). To enhance dataset quality, potential contaminants, proteins identified solely by site modification, and reverse hits were excluded. Only protein groups quantifiable by the LFQ algorithm in at least two out of three replicates were retained. LFQ intensities were log₂-transformed, and missing values were imputed from a normal distribution within Perseus using standard settings.

For GO term analysis, log₂ fold change and adjusted $-\log_{10}$ p-value (after applying Benjamini-Hochberg corrections to the Welch's t-test) of the compared groups were calculated, and the dataset was filtered for candidates that were significant (that is, had an adjusted $-\log_{10}$ p-value of less than 0.05 and log₂ fold change greater than 1). The significant candidates were then analysed using the GO term finder on the Saccharomyces Genome Database (Cherry et al., 2012; <https://www.yeastgenome.org/>), with the available mitoproteome from (Morgenstern et al., 2017) as the background

gene set. The Saccharomyces Genome Database uses a hypergeometric distribution using a multiple hypothesis correction (Bonferroni correction) to calculate p-values and false discovery rates (FDR). The threshold for p-value was set to below 0.01. Thereafter, the GO terms were visualized and represented in the respective figures. The data including the identified candidates with their corresponding statistical significances (in terms of adjusted $-\log_{10}$ p-value) and \log_2 fold changes are listed in supplementary table B.7 (for Lat1 Co-IP), supplementary table B.9 (for Myc tag Co-IP) and supplementary table B.8 (for proximity labelling assay). The raw data obtained from the mass spectrometry analysis for each of the aforementioned supplementary table B.7, table B.8 and table B.9 are available on Osman Lab servers.

Solubility tests with RNase treatment

Solubility tests were performed with purified WT mitochondria isolated from cells grown on YPD, YPGal and YPG carbon sources. 1 mg mitochondria were taken from each medium, and resuspended in 400 μ l lysis buffer (10 mM Tris-HCl pH 7.4, 150 mM NaCl, 1x Roche cOmpleteTM with EDTA) supplemented with 1% digitonin. The mitochondria were then split into two tubes with 500 μ g mitochondria in each tube, and 5 μ l of RNase I was added to one tube. The other tube acted as a negative control. Lysis was then performed at 4°C for 30 min. As a control for the RNase treatment, 1 μ g of isolated total mitochondrial RNA was taken and dissolved in lysis buffer supplemented with RNase I, which was checked on an agarose gel post-lysis. 20 μ l of the lysate was then taken out as the ‘Total’ sample, 20 μ l was centrifuged at 13,000 g for 10 min at 4°C, from which the pellet and supernatant were then separated. The pellet was dissolved in 20 μ l of the lysis buffer. To all the samples, 4x Lämmli was added, and the proteins in the samples were separated by loading them on an SDS-PAGE, and analysed by immunoblotting.

Solubility tests with DNase treatment

Solubility tests were first carried out with purified WT mitochondria isolated from cells grown on YPGal. 200 μ g mitochondria were resuspended in 80 μ l of lysis buffer (10 mM Tris-HCl pH 7.4, 150 mM NaCl, 1x Roche cOmpleteTM with EDTA, 5 mM CaCl₂, 5 mM MgCl₂) supplemented with 1% digitonin. The mitochondria were then divided halfway, where 20 μ g/ μ l DNase I (dissolved in 5 mM CaCl₂) was added to one half. The lysis was carried out for 30 minutes at 4°C. As a control for the treatment, 0.5 μ g of a plasmid pRS315 was dissolved in the lysis buffer containing 20 μ g/ μ l DNase I. Post-lysis, from each sample, half of the volume was taken out as the ‘total’ sample, whereas the other half was subjected to

centrifugation at 13,000 g for 10 min at 4°C. After centrifugation, the supernatant and pellet were separated and equal amount of buffer was added to the pellet. All the samples were dissolved in 4x Lämmli, and the proteins were subjected to immunoblotting following separation on an SDS-PAGE.

Sucrose Gradient Fractionation of lysed purified mitochondria with RNase treatment

The sucrose gradient fractionation protocol was adapted from Kucej et al., 2008; Schrott and Osman, 2023. 7 mg mitochondria were resuspended in 3.5 ml lysis buffer (0.5% Nonidet P40, 0.5 M sucrose, 20 mM Tris-HCl pH 7.4, 2 mM EDTA, 50 mM NaCl, 7 mM β -mercaptoethanol, 1x Roche cOmpleteTM EDTA-free) and was split equally into two tubes. To one of the tubes, 1 μ l RNase I was added, and lysis was performed on ice for 5 minutes. After this, 1.5 ml of the lysate was overlaid on an 11-step sucrose gradient ranging from 20-65% sucrose, with 4.5% increments, each dissolved in 1 ml of gradient buffer (20 mM Tris-HCl pH 7.4, 50 mM NaCl, 2 mM EDTA, 7 mM β -mercaptoethanol, 1x Roche cOmpleteTM EDTA-free). The mitochondria were then ultracentrifuged on the sucrose gradient for 70 min at 110,000 g at 4°C in a swinging bucket rotor (Beckman SW 40 Ti). 250 μ l was saved as the 'Input' sample, which was diluted 6-fold with lysis buffer, and kept on ice. After the ultracentrifugation, 16 fractions of 750 μ l were collected from the top of the gradient. For protein analysis, 90 μ l of each fraction were used and added to 4x Lämmli buffer and incubated at 95°C for 10 min. 25 μ l of each fraction was loaded on an SDS-PAGE and subjected to immunoblotting.

Ni-NTA based Protein Purification

For the protein purification, the respective protein domain was first cloned into a suitable pETDuet vector with 6xHis tag attached to the target protein. After cloning and obtaining the desired clone, tests were performed to determine ideal conditions for the *E. coli* BL21 strain to express the said cloned domain. After the appropriate conditions were established, the culture was grown overnight in 2 L volume in LB + Amp broth, in order to obtain low log phase growth the following morning. The culture was then induced by IPTG in the specified conditions, after which the cell pellet was collected by centrifugation at 6,000 g for 10 min. The cell pellet was then resuspended in the lysis buffer (200 mM NaCl, 10 mM imidazole, 50 mM tris-HCl pH 7.4, 1 mM PMSF, 2 mg/ml lysozyme), and incubated at 4°C for 2 h 30 min with rotation. Subsequently, the lysate was sonicated three times on ice at 50% intensity with 50 pulses each time. The lysate was then cleared by a centrifugation step, and the supernatant was collected for purification.

The protein purification was carried out with a self-made apparatus that consisted

of two peristaltic pumps, econo-column and a flow adaptor. The Ni-NTA column was then packed into the econo-column in an airtight manner, with a set flow rate of 1 ml/min. After washing with water and equilibrating the column with the lysis buffer, the supernatant from the lysed culture was applied and circulated on it continuously for about 1 h 45 min. The column was then washed for 15-20 min with washing solution (200 mM NaCl, 20 mM Imidazole, 50 mM tris-HCl pH 8.0). The bound His-tagged protein was eluted into multiple 1 ml fractions by using elution buffer I (200 mM NaCl, 80 mM Imidazole, 50 mM tris-HCl pH 7.4) and elution buffer II (200 mM NaCl, 250 mM Imidazole, 50 mM tris-HCl pH 7.4). The whole setup was circulated with water to perform the washin thereafter.

Similar volumes of the collected fractions were run on an SDS gel, and coomassie-stained to determine the desired fraction where the purified protein was present.

If the purified protein was present in multiple fractions, the fractions were pooled and the buffer exchange was performed using Centricon columns to 1x TBS buffer. The final amount of protein was collected, concentration determined using Nanodrop and 0.02% of NaN_3 was added before storing the protein.

Affinity purification of Yme2 antibody

Yme2 antibody purification was performed using the freshly purified AAA+ domain of Yme2 (amino acids Q356-K850), as the antibody was designed against the amino acids 586-850 (Hanekamp and Thorsness, 1996). The serum was obtained from the **Thorsness lab**. The protocol of antibody purification was adapted from the lab of **Prof. Dr. Dejana Mokranjac**.

First, the purified Yme2 protein was coupled to CNBr-activated Sepharose 4B beads. Prior to coupling, the purified protein was first loaded onto a PD-10 column (GE Healthcare) which was equilibrated with column buffer (0.1 M NaHCO_3 , 0.5 M NaCl, pH 8.3). The protein was then collected in a new tube by passing the column buffer once again over the column. The protein was then ready to be coupled to the beads. Meanwhile, the CNBr-Sepharose beads were prepared by swelling the powder for 30 min at RT in 1 mM HCl, and then washing again with 1 mM HCl before transferring them to a disposable plastic column (Bio-Rad). The protein was then incubated with the beads for 1 h at RT with rotation, after which the column was washed again with column buffer after removing the unbound material. The column was blocked with 1 M ethanolamine pH 8.0 for 2 h at RT, after which the ethanolamine was drained. The column was then washed with three cycles of alternating pH: first with 0.1 M acetate, 0.5 M NaCl pH 4.0; and second with 0.1 M acetate, 0.5 M NaCl pH 8.0. The column was then stored in 0.05% NaN_3 until affinity purification of Yme2 antibody was carried out.

Next, affinity purification of the Yme2 antibody was performed. The column containing protein (antigen) coupled to CNBr-sepharose beads was first equilibrated with 10 mM Tris-HCl pH 7.5. The antibody serum was diluted six-fold with 10 mM Tris-HCl pH 7.5 and 1 mM PMSF, before it was loaded onto the column. The column was allowed to stand till the entire serum passed through it by gravity flow, and the flowthrough was collected. The column was then washed with 10 mM Tris-HCl pH 7.5 and then with 10 mM Tris-HCl pH 7.5 and 0.5 M NaCl. The elution was then done in three steps with buffers having three different pH values: 0.1 M citrate pH 4.0; 0.1 M glycine pH 2.5 and 0.1 M phosphate pH 12.5. During the three elution steps, 1 ml fractions were collected and immediately neutralized with 1 M Tris-HCl pH 8.8. The column was then washed with 0.1 M Tris pH 8.8 and stored in 0.05% NaN₃.

The collected fractions were then analyzed by testing them on PVDF membrane strips immunoblotted with WT and $\Delta yme2$ strains. For the decoration, the antibody fractions were diluted 1:1000 in 5% milk in 1x TBS buffer. The cleanest and most intense fraction was then selected and aliquots were made for further use and stored at -20°C.

UV Crosslinking

For UV Crosslinking, isolated mitochondria (50 μ g) were thawed on ice, and subjected to UV radiation (254 nm) on a cold block in a UV Stratalinker machine, for varying intensities (0 J, 0.15 J, 1.5 J). Thereafter, mitochondria were re-isolated by centrifugation and 1x Lämmli buffer was added to the tube, and the samples were subjected to SDS-PAGE and western blotting.

6.2.4 Microscopy and Image Processing

For microscopic visualization, cells were grown to log phase, centrifuged at 3,000 g for 3 min at RT. The cell pellet was washed in 1X PBS and cells were placed on IBIDI slides coated with 200 μ L of Concanavalin A (1 mg/ mL). Microscopy was performed with Nikon eclipse Ti2-E epi-fluorescence microscope using a 100x oil objective (RI = 1.518), and a prime 95b 25mm camera from Teledyne photometrics.

For imaging the mNeonGreen-tagged strains the following settings were used: Brightfield channel (Nikon preset: DIC, Exposure time: 100 ms; Lamp Intensity: 14.9%); Neon Green and mKate channels (Nikon preset: Neongreen-kate2 triggered mode with dual filter cube on single camera, Exposure time: 80 ms; Lamp Intensity: 15% for 575 nm and 75% for 511 nm).

The calculation of the intensity of Pda1-mNG spots was done using custom FIJI

and Python scripts by Felix Thoma. Single cells were automatically detected with Yeastmate and cropped into single images. Then, for each cell the mNeogreen signal was prepared for analysis with a 3D median filter. Both filters were used from the 3D fast filters Fiji plugin. Afterwards, the signal maxima were detected with the Fiji plugin ‘3D Maxima finder’, which could finally be fed into the ‘3D Spot segmentation’ plugin to analyze detect spots and measure their intensities in each channel. The measurements were saved as ‘.csv’ file for each cell individually and further analyzed in Python. To objectively determine which spot is considered a “bright” spot or a “dim” spot, a threshold of $2 \times \text{Median}$ of all spot intensities per cell was selected. Intensities of a spot above that threshold were scored as ‘bright’ and vice versa.

For a quantitative visualization of the Pda1-NG signal in rho+ vs. rho0 cells, Python was used. Mander’s Overlap Coefficient was calculated for mNeogreen signal across the mitochondria visualized with mKate2. Mitochondrial signal from the entire z-Stack was segmented with the MitoGraph software and signal intensities of both channels, mNeogreen and mKate2, were determined along the segmented coordinates. After auto thresholding (Li algorithm) both channels, Mander’s Overlap Coefficient between mNeogreen and mKate2 signals was calculated.

6.2.5 *In-silico* analysis of the Yme2 sequence

Multi-sequence alignment of Yme2 with 10 different fungal species was performed using MUSCLE (Madeira et al., 2019) and analyzed with Jalview (Waterhouse et al., 2009). The domain identification for Yme2 was predicted using HHPred and RRMdb (Gabler et al., 2020; Meier and Söding, 2015; Nowacka et al., 2019; Söding et al., 2005; Zimmermann et al., 2018). The sequence logos for the AAA+ and RRM domains were created using Weblogo (Crooks et al., 2004). The putative structure of Yme2 was predicted using Alphafold and Alphafold Multimer (Abramson et al., 2024; Jumper et al., 2021; Varadi et al., 2024).

A Supplementary Figures

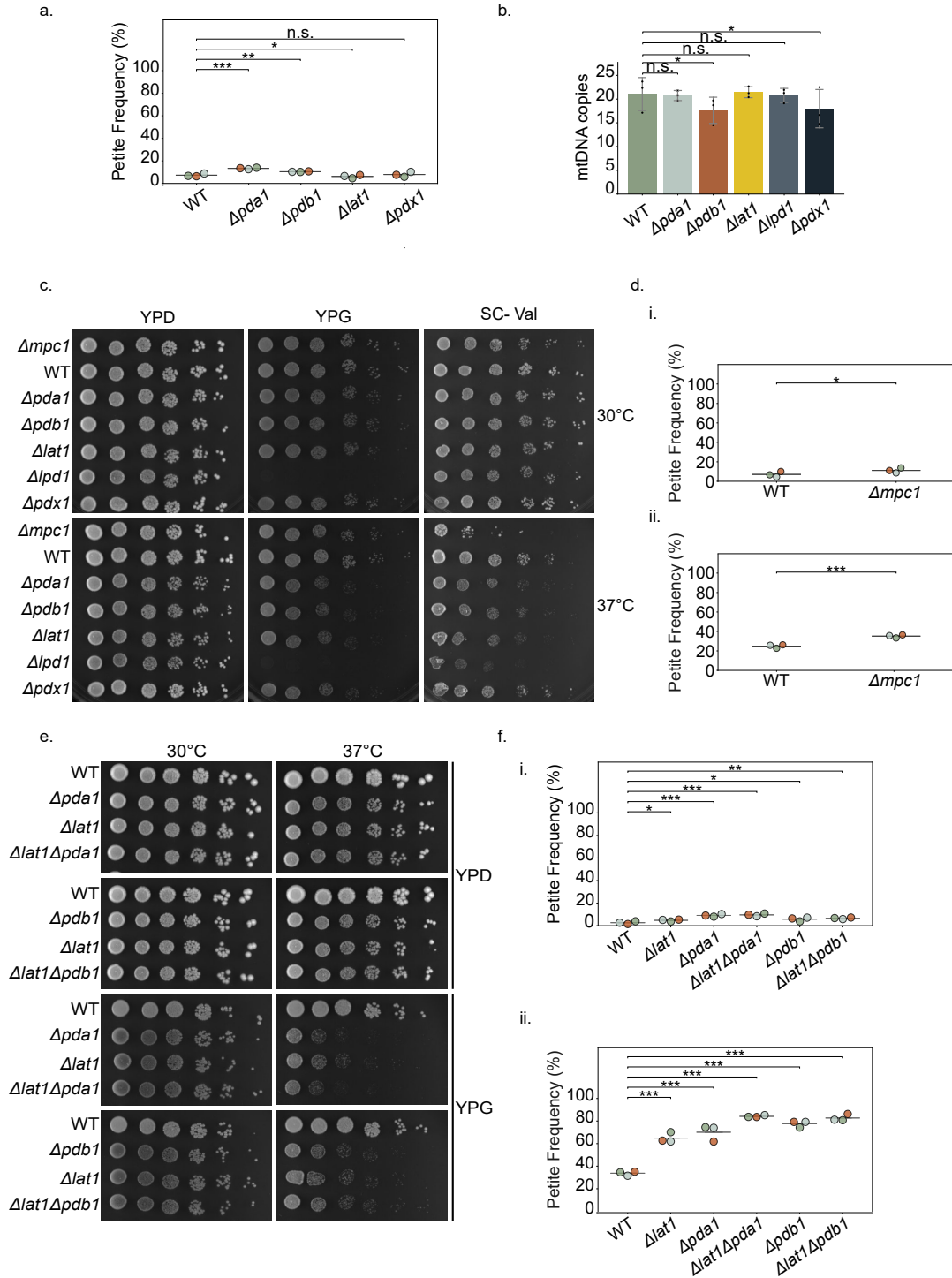


Figure S1: Mitochondrial health and maintenance of mtNucleoid is influenced by PDHc subunits. (a) Petite analysis of the indicated strains after growth at 30°C for 8 h. The strains were analyzed after 4 days of growth. P-values were calculated using unpaired t-test. (b) Quantitative PCR analysis (performed by Johannes Hagen) after growth of indicated strains at 30°C for 8 h, followed by calculation of mtDNA copy number for the indicated strains. P-values were calculated using Welch's t-test. (c) Growth test analysis showing the phenotypes displayed by $\Delta mpc1$ cells with respect to the deletions of PDHc subunits. The indicated strains were spotted on YPD, YPG and SC-Val media and allowed to grow at 30°C and 37°C for 2 days. (d) Petite analysis of the indicated strains after growth at 30°C for 8 h (i) and 37°C for 11 h (ii). The strains were analyzed after 4 days of growth. P-values were calculated using unpaired t-test. (e) Growth test analysis of the indicated strains displaying the effects of PDHc double subunit deletions on the cells. The strains were grown on YPD and YPG at 30°C and 37°C for 3 days. (f) Petite analysis of the indicated strains after growth at 30°C for 8 h (i) and 37°C for 11 h (ii). The strains were analyzed after 4 days of growth. P-values were calculated using unpaired t-test. P-values: $p < 0.005$: ***, $p < 0.05$: **, $p < 0.5$: *.

Supplementary Figures

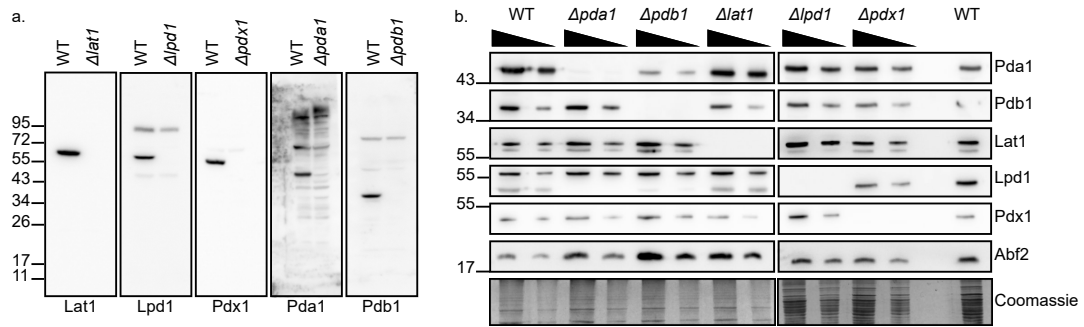


Figure S2: (a, b) Western blot from the purified PDHC antibodies generated by Julia Weisenseel and used in this study on cell lysates (a) and isolated mitochondria (50 and 25 μ g) (b). The unpurified Pda1 antibody serum was obtained from Prof. Dr. Chris Meisinger (C. Walter et al., 2022).

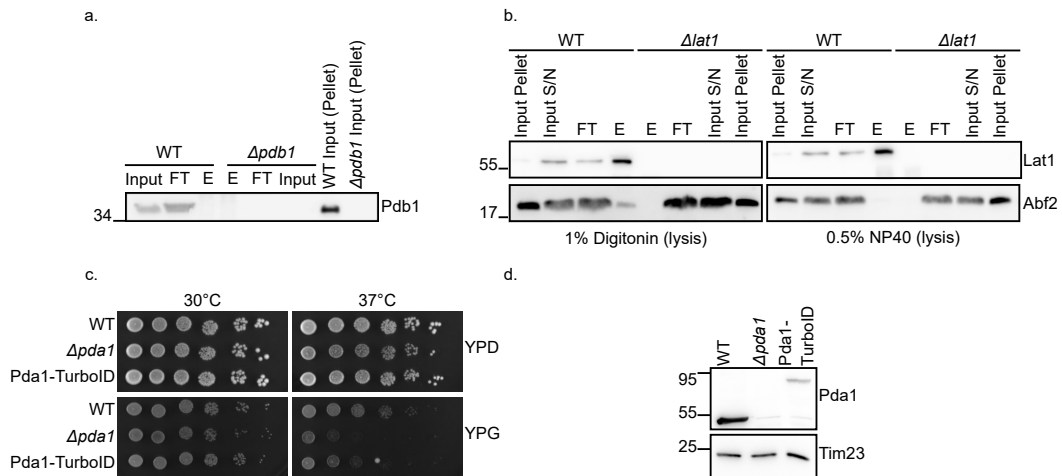


Figure S3: (a) Western blot showing co-IP performed with Anti-Pdb1 antibody on purified mitochondria. FT: Flowthrough; E: Elution. Input and FT are 4% loaded. (b) Western blot showing co-IP performed with Anti-Lat1 antibody on purified mitochondria upon lysis with 1% digitonin (left) and 0.5% NP-40 (right). FT: Flowthrough; E: Elution. Input and FT are 4% loaded. (c) Growth tests showing the indicated strains on YPD and YPG after 2 days of growth. (d) Western blot showing expression levels from cell lysates of indicated strains grown to log phase. Tim23 is the loading control.

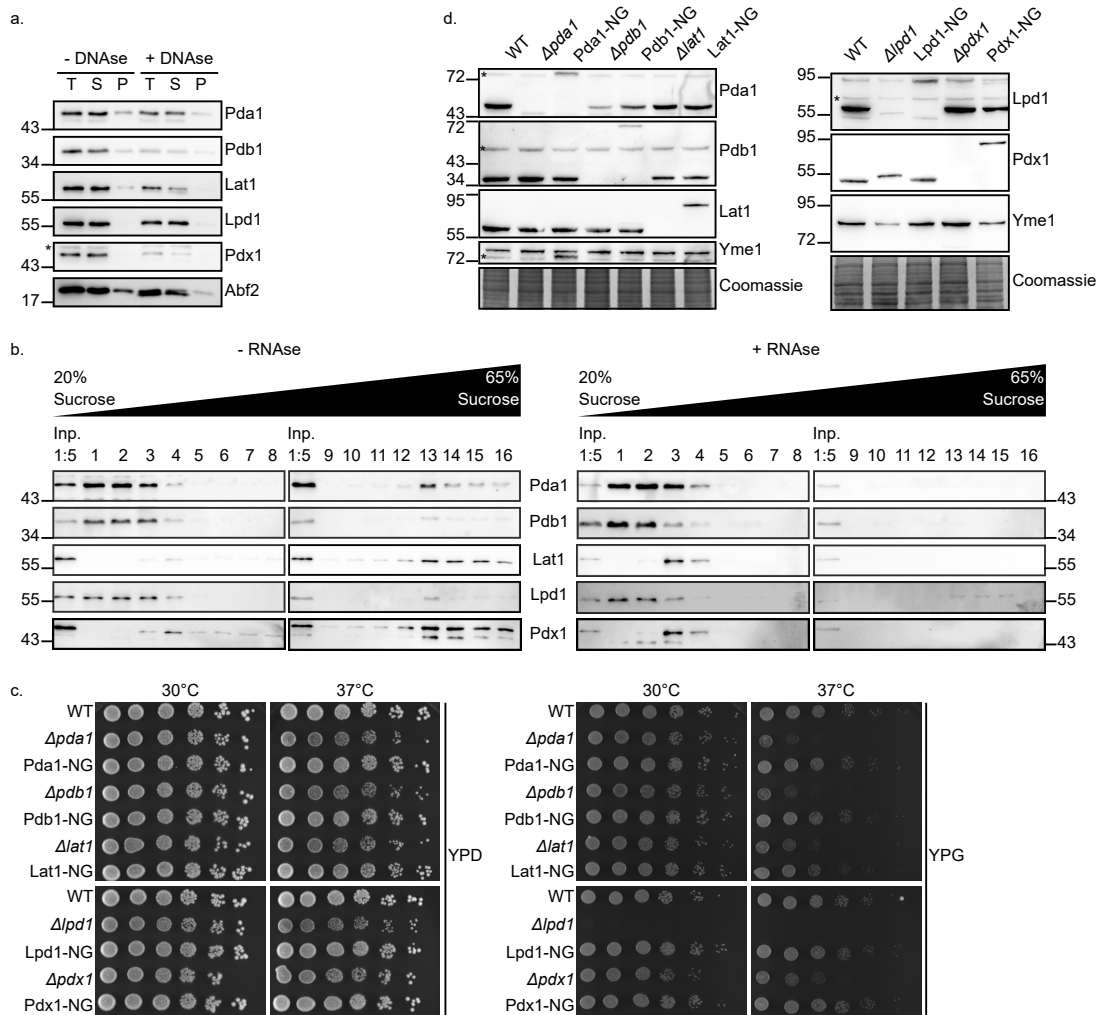


Figure S4: (a) Solubility tests from isolated WT mitochondria from YPGal-grown cells. The mitochondria were lysed with 1% digitonin and treated with 20 $\mu\text{g}/\mu\text{l}$ DNase I. The samples were further subjected to SDS-PAGE analysis and western blotting. T: Total; S: Supernatant; P: Pellet. (b) Sucrose gradient fractionation of isolated WT mitochondria from YPD-grown cells, with and without treatment with 1 μg RNase I. The image shows resolution of the fractions by SDS-PAGE and western blotting. Inp: Input fraction. (c) Growth test analysis showing the mNeonGreen-tagged PDHc subunit deletion strains grown on YPD and YPG at 30°C and 37°C for 2 days. (d) Expression levels of mNeonGreen-tagged PDHc subunit deletion strains after subjecting the respective cell lysates to western blotting.

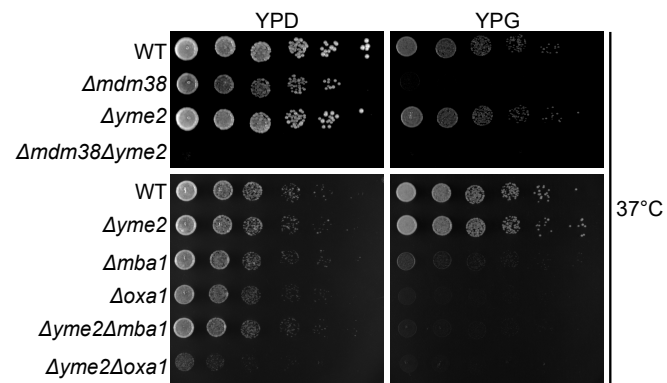


Figure S5: Growth test showing genetic interaction of *YME2* with mitochondrial protein biogenesis machinery, by growing the indicated strains on YPD and YPG at 37°C for 1 day (in case of $\Delta mba1$, $\Delta oxa1$, $\Delta yme2\Delta mba1$, $\Delta yme2\Delta oxa1$) and 2 days (in case of $\Delta mdm38$). The figure was adapted from Sharma and Osman, 2022 and licensed under CC BY 4.0.

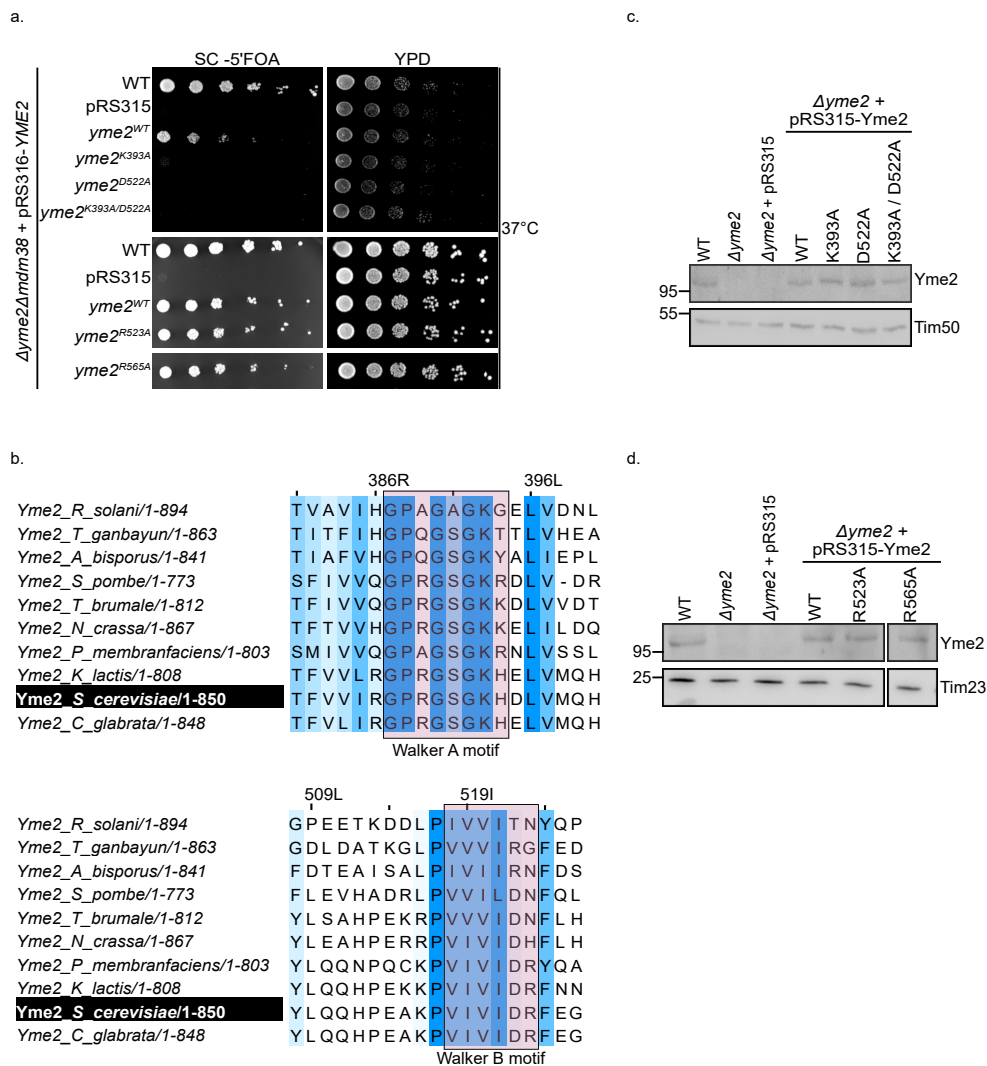


Figure S6: (a) Growth assay showing the AAA+ domain mutants analyzed by the plasmid shuffle experiment, upon growth at 37°C for 2 days on YPD and SC+5'FOA. (b) A schematic showing the alignment of multiple Yme2 sequences across ten fungal species using Jalview and the MUSCLE tool, with *S. cerevisiae* as the reference. Conservation of Walker A and B motifs in the AAA+ domain is depicted, with higher blue intensity showing greater residue conservation and respective motifs highlighted in red. (c,d) Expression levels revealed by western blotting for the indicated strains in $\Delta yme2$ background. The Yme2 decoration was performed with the unpurified antiserum. The figure was modified from Sharma and Osman, 2022 and licensed under CC BY 4.0.

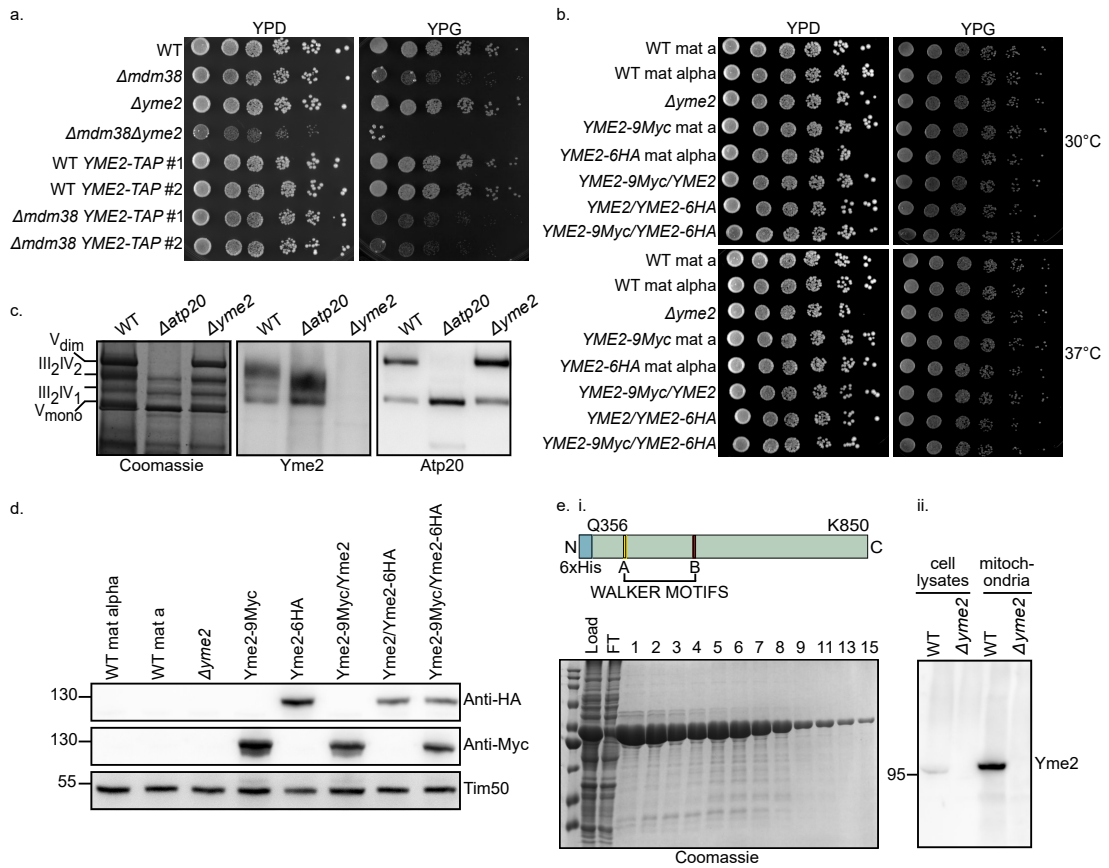


Figure S7: (a) Growth assay depicting the TAP-tagged *YME2* strains in WT and $\Delta m d m 3 8$ background. The indicated strains were spotted on YPD and incubated at 30°C for 2 days. (b) Growth tests showing the diploid strains with 9Myc and/or 6-HA-tagged *Yme2* strains, after growth on YPD and YPG at 30°C and 37°C for 2 days. (c) BN-PAGE analysis of indicated strains on a 3-13% gel, further followed by immunoblotting with *Yme2* and *Atp20* antibodies. (d) Western blot showing steady-state protein levels of cell lysates from diploid strains with 6HA and/or 9Myc tagged-*Yme2*. The *Yme2* antibody decoration was done with unpurified antiserum. (e) *Yme2* antibody purification from the obtained antiserum. The purified C-terminal of *Yme2* protein (i) was used to affinity purify the antibody for which the optimal concentration was determined to be 1:1000 in 5% milk in TBS (ii). The figure was modified from Sharma and Osman, 2022 and licensed under CC BY 4.0.

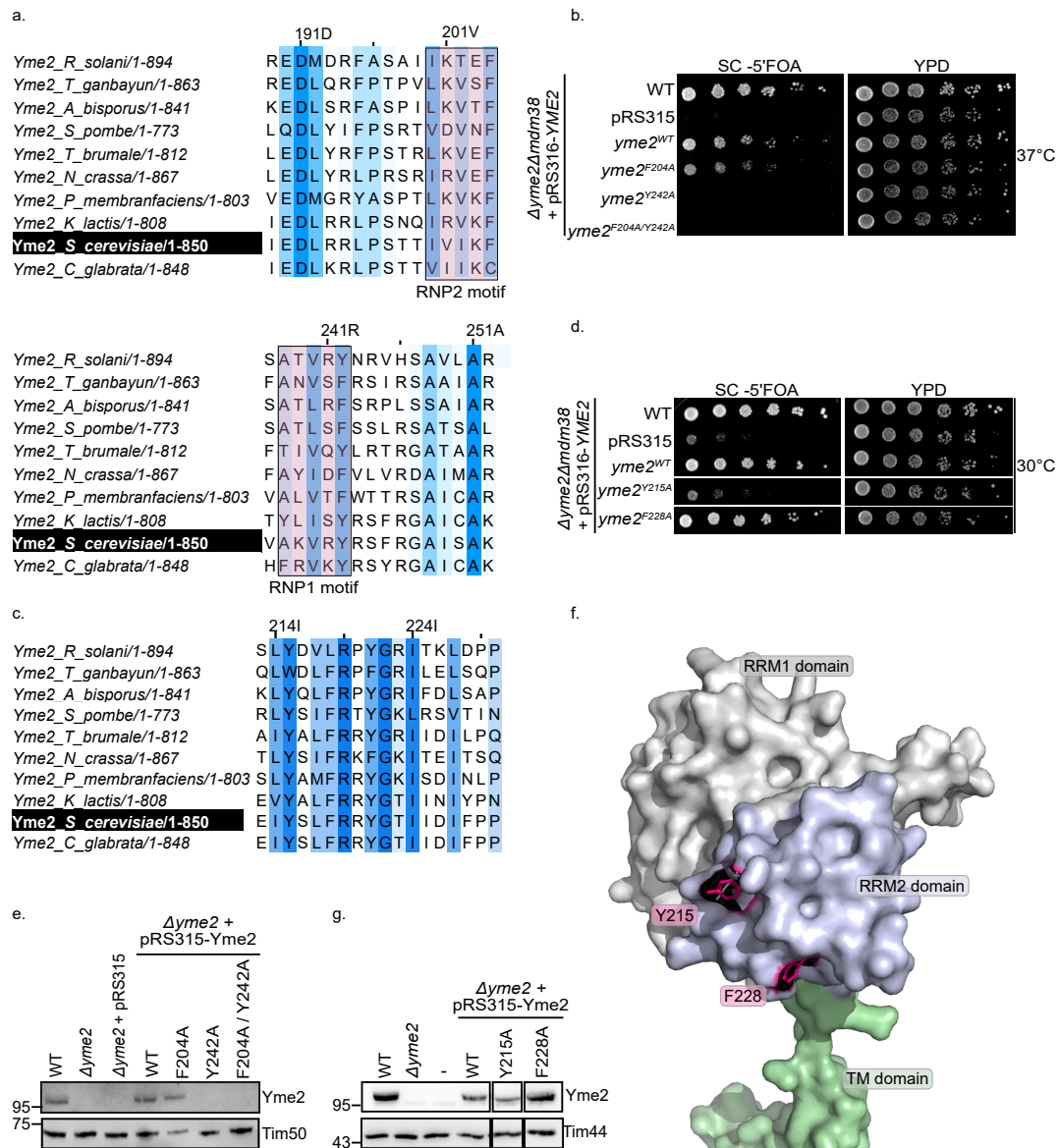


Figure S8: (a,c) Multiple sequence alignment of Yme2 using MUSCLE and Jalview, among ten fungal species showing the conservation of RRM2 domain, with the intensity of blue indicating the degree of conservation and the respective RNP motifs highlighted in red. Yme2 from *S. cerevisiae* is used as a reference. (b,d) Growth tests showing the RRM2 mutants analyzed by plasmid shuffle experiment, by growing them on YPD and SC-5'FOA for 2 days at indicated temperatures. (e,g) Steady-state protein levels of cell lysates from indicated Yme2 mutants upon immunoblotting, and decoration with purified Yme2 antibody. (f) Surface representation model showing the RRM2 domain with the mutated residues from RNP1 and RNP2 motifs highlighted in pink. The figure was modified from Sharma and Osman, 2022 and licensed under CC BY 4.0.

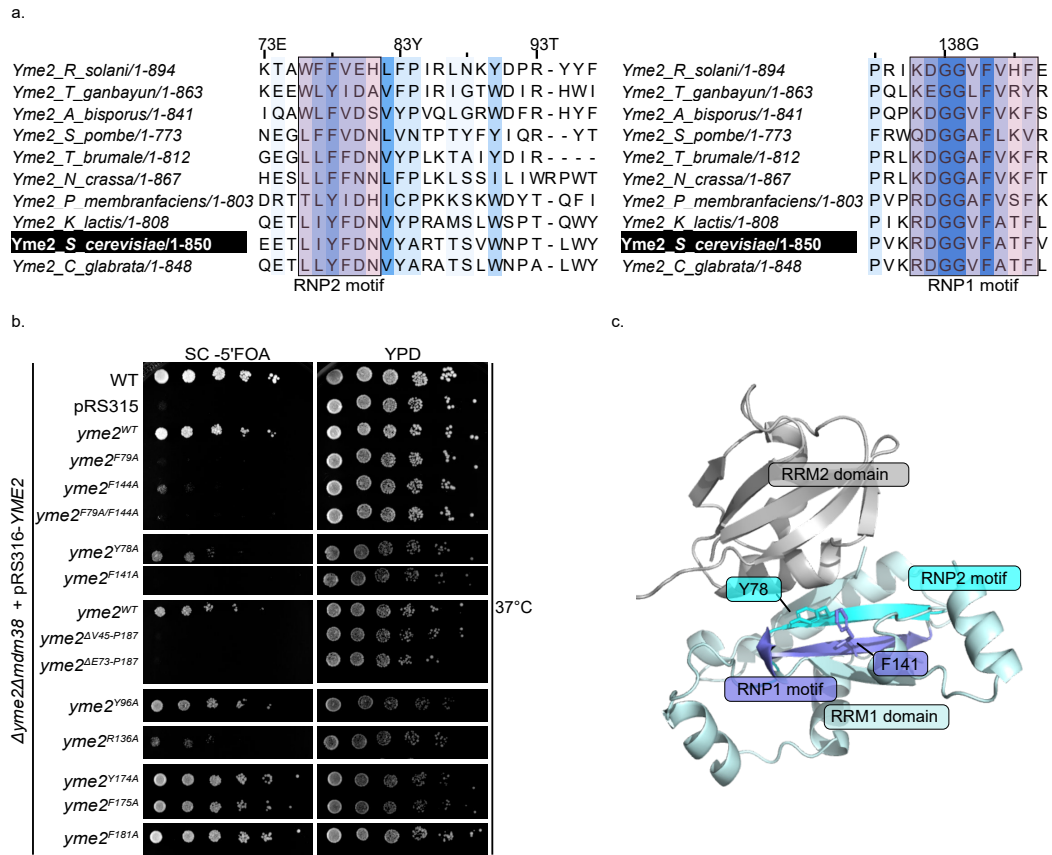


Figure S9: (a) Multiple sequence alignment of Yme2 using MUSCLE and Jalview, among ten fungal species showing the conservation of RRM1 domain, with the intensity of blue indicating the degree of conservation and the respective RNP1 and 2 motifs highlighted in red. Yme2 from *S. cerevisiae* is used as a reference. (b) Growth tests at 37°C showing the indicated mutants analyzed by plasmid shuffle experiment by growing them on SC-5'FOA for 2 days for counter-selection of the pRS316-Ura3 plasmid. (c) The predicted structural fold of RRM1 domain with designated RNP1 and RNP2 motifs. The figure was modified from Sharma and Osman, 2022 and licensed under CC BY 4.0.

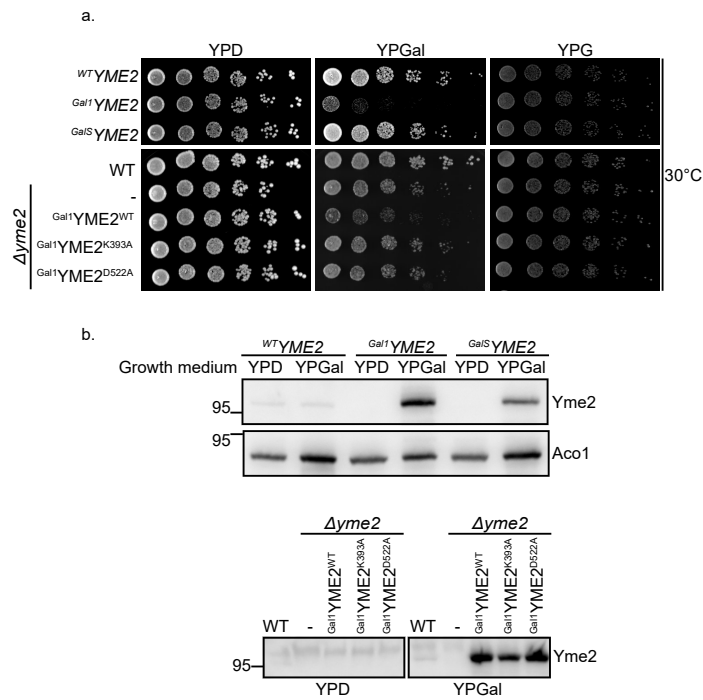


Figure S10: (a) Growth tests performed at 30°C indicating the endogenously overexpressed strains of WT or mutated forms of Yme2 with strong (Gal1) or relatively weak (GalS) overexpression promoters, upon overnight growth in YPD media and final spotting on the indicated media. The strains were allowed to grow for 2 days on the indicated plates. (b) Steady-state expression levels of the indicated WT or mutated forms of Yme2, upon growth in the indicated media. The strains were subjected to SDS-PAGE and immunoblotting, followed by decoration with purified Yme2 antibody. Aco1 was the loading control.

B Supplementary Tables

B.1 Chemicals and Reagents

Table B.1: Chemicals and Reagents

Chemical	Source	Chemical	Source
1 kb DNA ladder	NEB (N3200L)	LB broth	Sigma
5' Fluoroorotic acid	US Biological	Leucine	Carl Roth
6-aminohexanoic acid	Carl Roth	Lithium Acetate	Applichem
Acetic acid	Sigma	Luminol	Sigma
Acrylamide powder	Carl Roth	Lysozyme	Carl Roth
Acrylamide/ Bis-acrylamide solution 37.5:1	Carl Roth	Methanol	Sigma
Adenine	Applichem	Milk powder	Carl Roth
Agar	VWR	MOPS	Serva
Agarose	Sigma	NaN ₃	Carl Roth
Aluminum sulfate-18-hydrate	Applichem	Nigericin	EMD Milipore
Ammonium acetate	VWR	NP-40	Carl Roth
Ampicillin	Carl Roth	Orange G	
APS	Carl Roth	Orthophosphoric acid (85%)	Applichem
Benzonase	Sigma	Pancreatic peptone	VWR
Beta-mercaptoethanol	Sigma	P-coumaric acid	Sigma

Table B.1: Chemicals and Reagents

Chemical	Source	Chemical	Source
Biotin	Sigma	PEG 3000	VWR
Bis-acrylamide	Carl Roth	PEG 4000	Sigma
Blue prestained protein standard	NEB (P7718L)	Phenol-Chloroform-Isoamylalcohol	Carl Roth
Bromphenol Blue	Carl Roth	PMSF	Serva
BSA	Sigma	Potassium chloride	Carl Roth
Citric acid	Carl Roth	Potassium di-hydrogen phosphate	Carl Roth
c-Myc beads	Pierce (88842)	PVDF membrane	VWR
CNBr sepharose beads	Cytiva	RNase A	Thermo Scientific (EN0531)
Complete EDTA-free	Roche	RNase I	Thermo Scientific (EN0601)
Complete with EDTA	Roche	Salmon Sperm DNA	Applichem
Coomassie Brilliant Blue G-250	VWR	SDS	Carl Roth
D-Glucose monohydrate	VWR	Sodium acetate	Carl Roth
DEPC-treated nuclease free water	Carl Roth	Sodium chloride	Carl Roth
Digitonin	Applichem	Sodium deoxycholate	Carl Roth

Table B.1: Chemicals and Reagents

Chemical	Source	Chemical	Source
Di-potassium hydrogen phosphate	Carl Roth	Sodium di-hydrogen phosphate	VWR
Di-sodium hydrogen phosphate	Carl Roth	Sodium hydrogen-carbonate	Carl Roth
DMSO	Sigma	Sodium hydroxide	VWR
DNase I	Appllichem	Sorbitol	Sigma
Drop out mix	US Biological	Streptavidin beads	Pierce (88817)
DTT	Sigma	Sucrose	Carl Roth
Dynabeads M-270	Invitrogen (14301)	TEMED	Sigma
EDTA	VWR	Tricine	Carl Roth
EGTA	Carl Roth	Triethylamine	Merck
Ethanol	Sigma	Tris	Sigma
Ethanolamine	Sigma	Triton X-100	VWR
Ethidium Bromide	Carl Roth	Uracil	VWR
Galactose	Carl Roth	Yeast extract	VWR
Glycerol	VWR	Yeast nitrogen base	Carl Roth
Glycine	Roth	Zymolyase 20T	amsbio
HA-beads	Pierce (88836)	HCl	Carl Roth
HEPES	Carl Roth	Histidine	Carl Roth
Hydrogen peroxide	Merck	Imidazole	Carl Roth
IPTG	Carl Roth		

B.2 Growth Media Composition

Table B.2: Growth Media used in this Study

Medium	Components	Amount (1 l)	pH
YPD	Yeast extract	10 g	5.5
	Bacto Peptone	20 g	
	Glucose	20 g	
	Adenin	40 mg	
YPG	Yeast extract	10 g	5.5
	Peptone	20 g	
	Adenin	40 mg	
	Glycerol	37.8 g	
YPGal	Yeast extract	10 g	5.5
	Bacto Peptone	20 g	
	Galactose	20 g	
	Adenin	40 mg	
SC-all	Yeast Nitrogen Base	6.7 g	5.5
	Glucose	20 g	
SC + all	Yeast Nitrogen Base	6.7 g	5.5
	Drop out mix-Uracil	1.92 g	
	Uracil	50 mg	
	Glucose	20 g	
Indicator plates	Yeast extract	10 g	5.5
	Bacto Peptone	20 g	
	Adenin	40 mg	
	Glycerol	37.8 g	
	Glucose	1 g	
LB Broth	Tryptone	10 g	7.0
	Yeast extract	5 g	
	NaCl	5 g	

B.3 Buffer Composition

Table B.3: Composition of Buffers used in this Study

Buffer	Components	Concentration
1x TAE	Tris EDTA Glacial Acetic Acid pH	40 mM 1 mM 20 mM 8.3
1x TGS	Tris Glycine SDS pH	25 mM 192 mM 0.1 % 8.3
1x TBS	Tris NaCl pH	50 mM 150 mM 7.6
1x Towbin	Tris Glycine SDS Methanol pH	25 mM 192 mM 0.05 % 20 % 8.3
Laemmli Buffer	Tris/HCl SDS Glycerol β -Mercaptoethanol Bromphenol Blue pH	60 mM 2 % 8 % 2.5 % 0.0025 % 6.8
Coomassie Staining Solution	Aluminum sulfate-18-hydrate Ethanol Coomassie Brilliant Blue G-250 Orthophosphoric acid (85 %)	5 % 10 % 0.02 % 2 %
Luminol Stock solution	Luminol DMSO	4.4 % 100 ml
p-Coumaric acid solution	p-Coumaric acid DMSO	1.5 % 100 ml
ECL I (100 ml)	Tris-HCl Luminol stock solution p-Coumaric acid stock solution pH	0.1 M 1 ml 0.44 ml 8.5
ECL II (100 ml)	Tris-HCl	0.1 M

Table B.3: Composition of Buffers used in this study

Buffer	Components	Concentration
	Hydrogen peroxide (30 %) pH	60 μ l 8.5
Bradford's reagent (1:1)	Coomassie Brilliant Blue G-250 HCl	0.03 % 2 M
Deep Blue Cathode Buffer B	Tricine Imidazole Coomassie Brilliant Blue G-250 pH	50 mM 7.5 mM 0.02 % 7.0
Slightly Blue Cathode Buffer B/10	Tricine Imidazole Coomassie Brilliant Blue G-250 pH	50 mM 7.5 mM 0.002 % 7.0
Anode Buffer	Imidazole pH	25 mM 7.0
PBS	NaCl KCl Na ₂ HPO ₄ KH ₂ PO ₄ pH	137 mM 2.7 mM 10 mM 1.8 mM 7.4
0.1 M Sodium Phosphate buffer (100 ml)	NaH ₂ PO ₄ Na ₂ HPO ₄ pH	1M (77.4 ml) 1M (22.6 ml) 7.4
TE buffer	Tris-HCl EDTA pH	10 mM 1 mM 8.0

B.4 Antibodies

Table B.4: Antibodies used in this Study

Antibodies	Source
Abf2	Osman lab (Simon Schrott)
Aco1	Osman lab
Anti-HA	Osman lab (Abcam)
Strep-HRP	Osman lab (Thermo)
Anti-Myc	Osman lab (Sigma)
Atp20	Reichert lab
Lat1	Osman lab (Julia Weisenseel)
Lpd1	Osman lab (Julia Weisenseel)
Pda1	Meisinger lab
Pdb1	Osman lab (Julia Weisenseel)
Pdx1	Osman lab (Julia Weisenseel)
Tim23	Mokranjac lab
Tim44	Osman lab
Tim50	Mokranjac lab
Tom40	Osman lab
Yme1	Mokranjac lab
Yme2	Generated by Thorsness lab, purified in this study

B.5 Yeast Strains

Table B.5: Yeast Strains used in this study

Strain Name	Strain description	Genotype	Mating type	Source
yCO272	Wild-type	<i>leu2-3,112 can1-100 ura3-1 his3-11,15</i>	a	W303
yCO273	Wild-type	<i>leu2-3,112 can1-100 ura3-1 his3-11,15</i>	alpha	W303
yCO380	WT mtLacO	<i>leu2-3,112 can1-100 ura3-1 his3-11,15 mt-LacO</i>	a	W303
yCO381	WT mtLacO	<i>leu2-3,112 can1-100 ura3-1 his3-11,15 mt-LacO</i>	alpha	W303
yCO630	$\Delta pda1$	<i>leu2-3,112 can1-100 ura3-1 his3-11,15 mt-LacO $\Delta pda1::hphNT1$</i>	a	Ananthi
yCO622	$\Delta pdb1$	<i>leu2-3,112 can1-100 ura3-1 his3-11,15 mt-LacO $\Delta pdb1::kanMX4$</i>	a	Ananthi
yCO626	$\Delta lat1$	<i>leu2-3,112 can1-100 ura3-1 his3-11,15 mt-LacO $\Delta lat1::NATNT2$</i>	a	Ananthi
yCO659	$\Delta lpd1$	<i>leu2-3,112 can1-100 ura3-1 his3-11,15 mt-LacO $\Delta lpd1::hphNT1$</i>	a	Ananthi
yCO632	$\Delta pdx1$	<i>leu2-3,112 can1-100 ura3-1 his3-11,15 mt-LacO $\Delta pdx1::hphNT1$</i>	a	Ananthi
yCO655	$\Delta ach1$	<i>leu2-3,112 can1-100 ura3-1 his3-11,15 mt-LacO $\Delta ach1::NATNT2$</i>	a	Veronika Iskra
yCO798	$\Delta ach1\Delta lat1$	<i>leu2-3,112 can1-100 ura3-1 his3-11,15 mt-LacO $\Delta ach1::NATNT2$ $\Delta lat1::hphNT1$</i>	a	Veronika Iskra
yCO772	$\Delta ach1\Delta pda1$	<i>leu2-3,112 can1-100 ura3-1 his3-11,15 mt-LacO $\Delta ach1::kanMX4$ $\Delta pda1::hphNT1$</i>	a	Veronika Iskra
yCO774	$\Delta ach1\Delta pdb1$	<i>leu2-3,112 can1-100 ura3-1 his3-11,15 mt-LacO $\Delta ach1::kanMX4$ $\Delta pdb1::hphNT1$</i>	a	Veronika Iskra
yCO770	$\Delta ach1\Delta lpd1$	<i>leu2-3,112 can1-100 ura3-1 his3-11,15 mt-LacO $\Delta ach1::kanMX4$ $\Delta lpd1::hphNT1$</i>	a	Veronika Iskra

Table B.5: Yeast Strains used in the Study

Strain Name	Strain description	Genotype	Mating type	Source
yCO776	$\Delta ach1\Delta pdx1$	<i>leu2-3,112 can1-100 ura3-1 his3-11,15 mt-LacO $\Delta ach1::kanMX4$ $\Delta pdx1::hphNT1$</i>	a	Veronika Iskra
yNS252	$\Delta lat1\Delta pda1$	<i>leu2-3,112 can1-100 ura3-1 his3-11,15 mt-LacO $\Delta lat1::NATNT2$ $\Delta pda1::kanMX4$</i>	a	Nupur Sharma
yNS255	$\Delta lat1\Delta pdb1$	<i>leu2-3,112 can1-100 ura3-1 his3-11,15 mt-LacO $\Delta lat1::NATNT2$ $\Delta pdb1::kanMX4$</i>	a	Nupur Sharma
yNS299	$\Delta mpc1$	<i>leu2-3,112 can1-100 ura3-1 his3-11,15 mt-LacO $\Delta mpc1::hphNT1$</i>	a	Nupur Sharma
yCO813	$\Delta lat1 + HO::Lat1^{WT}$	<i>leu2-3,112 can1-100 ura3-1 his3-11,15 mt-LacO $\Delta lat1::hphNT1$ $HO::Lat1^{WT}-kanMX4$</i>	a	Veronika Iskra
yCO818	$\Delta lat1 + HO::Lat1^{H455A/D459A}$	<i>leu2-3,112 can1-100 ura3-1 his3-11,15 mt-LacO $\Delta lat1::hphNT1$ $HO::Lat1^{H455A/D459A}-kanMX4$</i>	a	Veronika Iskra
yCO816	$\Delta ach1\Delta lat1 + HO::Lat1^{WT}$	<i>leu2-3,112 can1-100 ura3-1 his3-11,15 mt-LacO $\Delta ach1::NATNT2$ $\Delta lat1::hphNT1$ $HO::Lat1^{WT}-kanMX4$</i>	a	Veronika Iskra
yCO975	$\Delta ach1\Delta lat1 + HO::Lat1^{H455A/D459A}$	<i>leu2-3,112 can1-100 ura3-1 his3-11,15 mt-LacO $\Delta ach1::NATNT2$ $\Delta lat1::hphNT1$ $HO::Lat1^{H455A/D459A}-kanMX4$</i>	a	Veronika Iskra
yNS337	$\Delta pda1 + Leu2::Pda1^{WT}$	<i>leu2-3,112 can1-100 ura3-1 his3-11,15 pda1::hphNT1 $Leu2::Pda1^{WT}$</i>	a	Nupur Sharma/ Johannes Hagen
yNS339	$\Delta pda1\Delta ach1 + Leu2::Pda1^{WT}$	<i>leu2-3,112 can1-100 ura3-1 his3-11,15 pda1::hphNT1 $ach1::KanMX4$ $Leu2::Pda1^{WT}$</i>	a	Nupur Sharma/ Johannes Hagen

Table B.5: Yeast Strains used in the Study

Strain Name	Strain description	Genotype	Mating type	Source
yNS341	$\Delta pda1 +$ <i>Leu2::Pda1^{G217A}</i>	<i>leu2-3,112 can1-100 ura3-1</i> <i>his3-11,15 pda1::hphNT1</i> <i>Leu2::Pda1^{G217A}</i>	a	Nupur Sharma/ Jo- hannes Hagen
yNS343	$\Delta pda1\Delta ach1 +$ <i>Leu2::Pda1^{G217A}</i>	<i>leu2-3,112 can1-100 ura3-1</i> <i>his3-11,15 pda1::hphNT1</i> <i>ach1::KanMX4 Leu2::Pda1^{G217A}</i>	a	Nupur Sharma/ Jo- hannes Hagen
yNS308	<i>PDA1-TurboID</i>	<i>leu2-3,112 can1-100 ura3-1 his3-11,15</i> <i>mt-LacO Pda1-TurboID-</i> <i>kanMX4</i>	a	Nupur Sharma/ Jo- hannes Hagen
yMQY006	<i>Floaty-TurboID</i>	<i>leu2-3,112 can1-100 ura3-1 his3-11,15</i> <i>mt-LacO HO::Cup1-Su9-</i> <i>TurboID-kanMX4</i>	a	Mengqiao Yang
yNS276	<i>PDA1-mNeonGreen</i> <i>Su9-mKate2</i>	<i>leu2-3,112 can1-100 ura3-1 his3-11,15</i> <i>mt-LacO Pda1-mNeongreen-</i> <i>kanMX4 HO::PrPGK1-Su9-</i> <i>mKate2</i>	a	Felix Thoma
yNS277	<i>PDB1-mNeonGreen</i> <i>Su9-mKate2</i>	<i>leu2-3,112 can1-100 ura3-1 his3-11,15</i> <i>mt-LacO Pdb1-mNeongreen-</i> <i>kanMX4 HO::PrPGK1-Su9-</i> <i>mKate2</i>	alpha	Felix Thoma
yNS278	<i>LPD1-mNeonGreen</i> <i>Su9-mKate2</i>	<i>leu2-3,112 can1-100 ura3-1 his3-11,15</i> <i>mt-LacO Lpd1-mNeongreen-</i> <i>kanMX4 HO::PrPGK1-Su9-</i> <i>mKate2</i>	a	Felix Thoma
yNS279	<i>PDX1-mNeonGreen</i> <i>Su9-mKate2</i>	<i>leu2-3,112 can1-100 ura3-1 his3-11,15</i> <i>mt-LacO Pdx1-mNeongreen-</i> <i>kanMX4 HO::PrPGK1-Su9-</i> <i>mKate2</i>	a	Felix Thoma
yNS280	<i>LAT1-mNeonGreen</i> <i>Su9-mKate2</i>	<i>leu2-3,112 can1-100 ura3-1 his3-11,15</i> <i>mt-LacO Lat1-mNeongreen-</i> <i>kanMX4 HO::PrPGK1-Su9-</i> <i>mKate2</i>	a	Felix Thoma

Table B.5: Yeast Strains used in the Study

Strain Name	Strain description	Genotype	Mating type	Source
yCO1105	$\Delta pda1$ <i>rho0</i>	<i>leu2-3,112 can1-100 ura3-1 his3-11,15 pda1::hphNT1 mt-rho0</i>	a	Paul Retzer
yCO520	$\Delta yme2$	<i>leu2-3,112 trp1-1 can1-100 ura3-1 ADE2-1 his3-11,15 $\Delta yme2::NatNT2$</i>	a	Timotheus Fischer
yCO521	$\Delta mdm38$	<i>leu2-3,112 can1-100 ura3-1 his3-11,15 $\Delta mdm38::hphNT1$</i>	a	Timotheus Fischer
yCO522	$\Delta yme2\Delta mdm38$	<i>leu2-3,112 can1-100 ura3-1 his3-11,15 $\Delta mdm38::hphNT1$ $\Delta yme2::NatNT2$</i>	a	Timotheus Fischer
yCO536	$\Delta mba1$	<i>leu2-3,112 can1-100 ura3-1 his3-11,15 $\Delta mba1::hphNT1$</i>	alpha	Christof Osman
yCO537	$\Delta yme2\Delta mba1$	<i>leu2-3,112 can1-100 ura3-1 his3-11,15 $\Delta mba1::hphNT1$ $\Delta yme2::NatNT2$</i>	alpha	Christof Osman
yCO541	$\Delta oxa1$	<i>leu2-3,112 can1-100 ura3-1 his3-11,15 $\Delta oxa1::hphNT1$</i>	alpha	Alicia Gas-sauer
yCO542	$\Delta yme2\Delta oxa1$	<i>leu2-3,112 can1-100 ura3-1 his3-11,15 $\Delta yme2::NatNT2$ $\Delta oxa1::hphNT1$</i>	alpha	Alicia Gas-sauer
yNS041	$\Delta yme2 + pCO216_YME2$	<i>leu2-3,112 trp1-1 can1-100 ura3-1 ADE2-1 his3-11,15 $\Delta yme2::NatNT2$ pRS316-YME2-Ura3</i>	a	Nupur Sharma
yNS046	<i>YME2-9Myc</i>	<i>leu2-3,112 can1-100 ura3-1 his3-11,15 Yme2-9Myc-kanMX4</i>	a	Nupur Sharma
yNS050	$\Delta yme2\Delta mdm38 + pCO216_YME2$	<i>leu2-3,112 can1-100 ura3-1 his3-11,15 $\Delta mdm38::hphNT1$ $\Delta yme2::NatNT2$ pRS316-YME2-Ura3</i>	a	Nupur Sharma
yNS053	$\Delta yme2\Delta mdm38 + pCO216_YME2 + pCO033$	<i>leu2-3,112 can1-100 ura3-1 his3-11,15 $\Delta mdm38::hphNT1$ $\Delta yme2::NatNT2$ pRS316-YME2-Ura3 pRS315-Leu2</i>	a	Nupur Sharma

Table B.5: Yeast Strains used in the Study

Strain Name	Strain description	Genotype	Mating type	Source
yNS054	$\Delta yme2\Delta mdm38 +$ $pCO216_YME2 +$ $pCO033_YME2$	$leu2-3,112$ $can1-100$ $ura3-1$ $his3-11,15$ $\Delta mdm38::hphNT1$ $\Delta yme2::NatNT2$ $pRS316-YME2-$ $Ura3$ $pRS315-Yme2-Leu2$	a	Nupur Sharma
yNS055	$\Delta yme2\Delta mdm38 +$ $pCO216_YME2 +$ $pCO033_YME2^{K393A}$	$leu2-3,112$ $can1-100$ $ura3-1$ $his3-11,15$ $\Delta mdm38::hphNT1$ $\Delta yme2::NatNT2$ $pRS316-Yme2-$ $Ura3$ $pRS315-Yme2^{K393A}-Leu2$	a	Nupur Sharma
yNS056	$\Delta yme2\Delta mdm38 +$ $pCO216_YME2 +$ $pCO033_YME2^{D522A}$	$leu2-3,112$ $can1-100$ $ura3-1$ $his3-11,15$ $\Delta mdm38::hphNT1$ $\Delta yme2::NatNT2$ $pRS316-Yme2-$ $Ura3$ $pRS315-Yme2^{D522A}-Leu2$	a	Nupur Sharma
yNS057	$\Delta yme2\Delta mdm38 +$ $pCO216_YME2 +$ $pCO033_YME2^{K393A/D522A}$	$leu2-3,112$ $can1-100$ $ura3-1$ $his3-11,15$ $\Delta mdm38::hphNT1$ $\Delta yme2::NatNT2$ $pRS316-Yme2-$ $Ura3$ $pRS315-Yme2^{K393A/D522A}-$ $Leu2$	a	Nupur Sharma
yNS068	$\Delta yme2 +$ $Leu2::Yme2-TAP$	$leu2-3,112$ $trp1-1$ $can1-100$ $ura3-1$ $ADE2-1$ $his3-11,15$ $\Delta yme2::NatNT2$ $Leu2::$ $Yme2-$ $TAP-Ura3$	a	Nupur Sharma
yNS071	$\Delta yme2 +$ $Leu2::Yme2^{K393A}-$ TAP	$leu2-3,112$ $trp1-1$ $can1-100$ $ura3-1$ $ADE2-1$ $his3-11,15$ $\Delta yme2::NatNT2$ $Leu2::$ $Yme2^{K393A}-TAP-Ura3$	a	Nupur Sharma
yNS072	$\Delta yme2 +$ $Leu2::Yme2^{D522A}-$ TAP	$leu2-3,112$ $trp1-1$ $can1-100$ $ura3-1$ $ADE2-1$ $his3-11,15$ $\Delta yme2::NatNT2$ $Leu2::$ $Yme2^{D522A}-TAP-Ura3$	a	Nupur Sharma
yNS074	$\Delta yme2 + Leu2::$ $Yme2^{K393A/D522A}-$ TAP	$leu2-3,112$ $trp1-1$ $can1-100$ $ura3-1$ $ADE2-1$ $his3-11,15$ $\Delta yme2::NatNT2$ $Leu2::$ $Yme2^{K393A/D522A}-TAP-Ura3$	a	Nupur Sharma
yNS131	$\Delta yme2\Delta mdm38 +$ $pCO216_YME2+$ $pCO033_YME2^{F204A}$	$leu2-3,112$ $can1-100$ $ura3-1$ $his3-11,15$ $\Delta mdm38::hphNT1$ $\Delta yme2::NatNT2$ $pRS316-Yme2$ $pRS315-Yme2^{F204A}-Leu2$	a	Nupur Sharma

Table B.5: Yeast Strains used in the Study

Strain Name	Strain description	Genotype	Mating type	Source
yNS132	$\Delta yme2 \Delta mdm38 +$ $pCO216_YME2 +$ $pCO033_YME2^{Y242A}$	$leu2-3,112$ $can1-100$ $ura3-1$ $his3-11,15$ $\Delta mdm38::hphNT1$ $\Delta yme2::NatNT2$ $pRS316-Yme2$ $pRS315-Yme2^{Y242A}-Leu2$	a	Nupur Sharma
yNS133	$\Delta yme2 \Delta mdm38 +$ $pCO216_YME2 +$ $pCO033_YME2^{F204A/Y242A}$	$leu2-3,112$ $can1-100$ $ura3-1$ $his3-11,15$ $\Delta mdm38::hphNT1$ $\Delta yme2::NatNT2$ $pRS316-Yme2$ $pRS315-Yme2^{F204A/Y242A}-Leu2$	a	Nupur Sharma
yNS146	$\Delta yme2 \Delta mba1 +$ $Leu2::Yme2-TAP$	$leu2-3,112$ $trp1-1$ $can1-100$ $ura3-1$ $ADE2-1$ $his3-11,15$ $\Delta yme2::NatNT2$ $\Delta mba1::$ $hphNT1$ $Leu2::$ $Yme2-TAP-$ $Ura3$	a	Nupur Sharma
yNS150	$\Delta yme2 \Delta mdm38 +$ $Leu2::Yme2-TAP$	$leu2-3,112$ $trp1-1$ $can1-100$ $ura3-1$ $ADE2-1$ $his3-11,15$ $\Delta yme2::NatNT2$ $\Delta mdm38::$ $hphNT1$ $Leu2::$ $Yme2-TAP-Ura3$	a	Nupur Sharma
yNS158	$\Delta yme2 \Delta mdm38 +$ $pCO216_YME2 +$ $pCO033_YME2^{R523A}$	$leu2-3,112$ $can1-100$ $ura3-1$ $his3-11,15$ $\Delta mdm38::hphNT1$ $\Delta yme2::NatNT2$ $pRS316-Yme2-$ $Ura3$ $pRS315-Yme2^{R523A}-Leu2$	a	Nupur Sharma
yNS160	$\Delta yme2 \Delta mdm38 +$ $pCO216_YME2 +$ $pCO033_YME2^{R565A}$	$leu2-3,112$ $can1-100$ $ura3-1$ $his3-11,15$ $\Delta mdm38::hphNT1$ $\Delta yme2::NatNT2$ $pRS316-Yme2-$ $Ura3$ $pRS315-Yme2^{R565A}-Leu2$	a	Nupur Sharma
yNS162	$\Delta yme2 +$ $Leu2::Yme2^{F204A}-$ TAP	$leu2-3,112$ $trp1-1$ $can1-100$ $ura3-1$ $ADE2-1$ $his3-11,15$ $\Delta yme2::NatNT2$ $Leu2::$ $Yme2^{F204A}-TAP-Ura3$	a	Nupur Sharma
yNS163	$\Delta yme2 +$ $Leu2::Yme2^{Y242A}-$ TAP	$leu2-3,112$ $trp1-1$ $can1-100$ $ura3-1$ $ADE2-1$ $his3-11,15$ $\Delta yme2::NatNT2$ $Leu2::$ $Yme2^{Y242A}-TAP-Ura3$	a	Nupur Sharma
yNS164	$\Delta yme2 +$ $Leu2::Yme2^{F204A/Y242A}-$ TAP	$leu2-3,112$ $trp1-1$ $can1-100$ $ura3-1$ $ADE2-1$ $his3-11,15$ $\Delta yme2::NatNT2$ $Leu2::$ $Yme2^{F204A/Y242A}-TAP-Ura3$	a	Nupur Sharma

Table B.5: Yeast Strains used in the Study

Strain Name	Strain description	Genotype	Mating type	Source
yNS171	<i>YME2-6HA</i>	<i>leu2-3,112 can1-100 ura3-1 his3-11,15 Yme2-6HA-NatNT2</i>	alpha	Nupur Sharma
yNS172	<i>YME2-9Myc/YME2-6HA</i>	<i>leu2-3,112 can1-100 ura3-1 his3-11,15 Yme2-9Myc-kanMX4/Yme2-6HA-NatNT2</i>	diploid	Nupur Sharma
yNS173	<i>YME2-9Myc/YME2</i>	<i>leu2-3,112 can1-100 ura3-1 his3-11,15 Yme2-9Myc-kanMX4/Yme2</i>	diploid	Nupur Sharma
yNS174	<i>YME2-6HA/YME2</i>	<i>leu2-3,112 can1-100 ura3-1 his3-11,15 Yme2-6HA-NatNT2/Yme2</i>	diploid	Nupur Sharma
yNS175	$\Delta yme2 + pCO033$	<i>leu2-3,112 can1-100 ura3-1 his3-11,15 $\Delta yme2::NatNT2$ pRS315-Leu2</i>	a	Nupur Sharma
yNS176	$\Delta yme2 + pCO033_YME2$	<i>leu2-3,112 can1-100 ura3-1 his3-11,15 $\Delta yme2::NatNT2$ pRS315-Yme2-Leu2</i>	a	Nupur Sharma
yNS177	$\Delta yme2 + pCO033_YME2^{K393A}$	<i>leu2-3,112 can1-100 ura3-1 his3-11,15 $\Delta yme2::NatNT2$ pRS315-Yme2^{K393A}-Leu2</i>	a	Nupur Sharma
yNS178	$\Delta yme2 + pCO033_YME2^{D522A}$	<i>leu2-3,112 can1-100 ura3-1 his3-11,15 $\Delta yme2::NatNT2$ pRS315-Yme2^{D522A}-Leu2</i>	a	Nupur Sharma
yNS179	$\Delta yme2 + pCO033_YME2^{K393A/D522A}$	<i>leu2-3,112 can1-100 ura3-1 his3-11,15 $\Delta yme2::NatNT2$ pRS315-Yme2^{K393A/D522A}-Leu2</i>	a	Nupur Sharma
yNS180	$\Delta yme2 + pCO033_YME2^{F204A}$	<i>leu2-3,112 can1-100 ura3-1 his3-11,15 $\Delta yme2::NatNT2$ pRS315-Yme2^{F204A}-Leu2</i>	a	Nupur Sharma
yNS181	$\Delta yme2 + pCO033_YME2^{Y242A}$	<i>leu2-3,112 can1-100 ura3-1 his3-11,15 $\Delta yme2::NatNT2$ pRS315-Yme2^{Y242A}-Leu2</i>	a	Nupur Sharma
yNS182	$\Delta yme2 + pCO033_YME2^{F204A/Y242A}$	<i>leu2-3,112 can1-100 ura3-1 his3-11,15 $\Delta yme2::NatNT2$ pRS315-Yme2^{F204A/Y242A}-Leu2</i>	a	Nupur Sharma

Table B.5: Yeast Strains used in the Study

Strain Name	Strain description	Genotype	Mating type	Source
yNS183	$\Delta yme2 +$ <i>pCO033_YME2^{R523A}</i>	<i>leu2-3,112 can1-100 ura3-1 his3-11,15</i> $\Delta yme2::NatNT2$ <i>pRS315-Yme2^{R523A}-Leu2</i>	a	Nupur Sharma
yNS185	$\Delta yme2 +$ <i>pCO033_YME2^{R565A}</i>	<i>leu2-3,112 can1-100 ura3-1 his3-11,15</i> $\Delta yme2::NatNT2$ <i>pRS315-Yme2^{R565A}-Leu2</i>	a	Nupur Sharma
yNS080	$\Delta atp20$	<i>leu2-3,112 can1-100 ura3-1 his3-11,15</i> $\Delta atp20::kanMX4$	a	Nupur Sharma
yNS031	<i>Gal1 YME2</i>	<i>leu2-3,112 can1-100 ura3-1 his3-11,15</i> Gal1 promoter- <i>yme2</i>	a	Nupur Sharma
yNS032	<i>GalS YME2</i>	<i>leu2-3,112 can1-100 ura3-1 his3-11,15</i> GalS promoter- <i>yme2</i>	a	Nupur Sharma
yNS107	$\Delta yme2 + Leu2::Gal1$ promoter- <i>Yme2^{K393A}-TAP</i>	<i>leu2-3,112 can1-100 ura3-1 his3-11,15</i> $\Delta yme2::NatNT2$ <i>Leu2::Gal1-Yme2^{K393A}-TAP</i>	a	Nupur Sharma
yNS109	$\Delta yme2 + Leu2::Gal1$ promoter- <i>Yme2^{D522A}-TAP</i>	<i>leu2-3,112 can1-100 ura3-1 his3-11,15</i> $\Delta yme2::NatNT2$ <i>Leu2::Gal1-Yme2^{D522A}-TAP</i>	a	Nupur Sharma
yNS111	$\Delta yme2 + Leu2::Gal1$ promoter- <i>Yme2^{K393A/D522A}-TAP</i>	<i>leu2-3,112 can1-100 ura3-1 his3-11,15</i> $\Delta yme2::NatNT2$ <i>Leu2::Gal1-Yme2^{K393A/D522A}-TAP</i>	a	Nupur Sharma
yNS200	$\Delta yme2\Delta mdm38 +$ <i>pCO216_YME2 +</i> <i>pCO033_YME2^{F79A}</i>	<i>leu2-3,112 can1-100 ura3-1 his3-11,15</i> $\Delta mdm38::hphNT1$ $\Delta yme2::NatNT2$ <i>pRS316-Yme2-Ura3</i> <i>pRS315-Yme2^{F79A}-Leu2</i>	a	Jasmin Forster
yNS204	$\Delta yme2 +$ <i>pCO033_YME2^{F79A}</i>	<i>leu2-3,112 can1-100 ura3-1 his3-11,15</i> $\Delta yme2::NatNT2$ <i>pRS315-Yme2^{F79A}-Leu2</i>	a	Jasmin Forster
yNS201	$\Delta yme2\Delta mdm38 +$ <i>pCO216_YME2 +</i> <i>pCO033_YME2^{F144A}</i>	<i>leu2-3,112 can1-100 ura3-1 his3-11,15</i> $\Delta mdm38::hphNT1$ $\Delta yme2::NatNT2$ <i>pRS316-Yme2-Ura3</i> <i>pRS315-Yme2^{F144A}-Leu2</i>	a	Jasmin Forster
yNS205	$\Delta yme2 +$ <i>pCO033_YME2^{F144A}</i>	<i>leu2-3,112 can1-100 ura3-1 his3-11,15</i> $\Delta yme2::NatNT2$ <i>pRS315-Yme2^{F144A}-Leu2</i>	a	Jasmin Forster

Table B.5: Yeast Strains used in the Study

Strain Name	Strain description	Genotype	Mating type	Source
yNS202	$\Delta yme2 \Delta mdm38 +$ $pCO216_YME2 +$ $pCO033_$ $YME2^{\Delta V45-P187}$	$leu2-3,112$ $can1-100$ $ura3-1$ $his3-11,15$ $\Delta mdm38::hphNT1$ $\Delta yme2::NatNT2$ $pRS316-Yme2-$ $Ura3$ $pRS315-Yme2^{\Delta V45-P187}-$ $Leu2$	a	Jasmin Forster
yNS206	$\Delta yme2 + pCO033_$ $YME2^{\Delta V45-P187}$	$leu2-3,112$ $can1-100$ $ura3-1$ $his3-$ $11,15$ $\Delta yme2::NatNT2$ $pRS315-$ $Yme2^{\Delta V45-P187}-Leu2$	a	Jasmin Forster
yNS203	$\Delta yme2 \Delta mdm38 +$ $pCO216_YME2 +$ $pCO033_$ $YME2^{\Delta E73-P187}$	$leu2-3,112$ $can1-100$ $ura3-1$ $his3-11,15$ $\Delta mdm38::hphNT1$ $\Delta yme2::NatNT2$ $pRS316-Yme2-$ $Ura3$ $pRS315-Yme2^{\Delta E73-P187}-$ $Leu2$	a	Jasmin Forster
yNS207	$\Delta yme2 + pCO033_$ $YME2^{\Delta E73-P187}$	$leu2-3,112$ $can1-100$ $ura3-1$ $his3-$ $11,15$ $\Delta yme2::NatNT2$ $pRS315-$ $Yme2^{\Delta E73-P187}-Leu2$	a	Jasmin Forster
yNS208	$\Delta yme2 \Delta mdm38 +$ $pCO216_YME2 +$ $pCO033_YME2^{Y78A}$	$leu2-3,112$ $can1-100$ $ura3-1$ $his3-11,15$ $\Delta mdm38::hphNT1$ $\Delta yme2::NatNT2$ $pRS316-Yme2-$ $Ura3$ $pRS315-Yme2^{Y78A}-Leu2$	a	Jasmin Forster
yNS212	$\Delta yme2 +$ $pCO033_YME2^{Y78A}$	$leu2-3,112$ $can1-100$ $ura3-1$ $his3-$ $11,15$ $\Delta yme2::NatNT2$ $pRS315-$ $Yme2^{Y78A}-Leu2$	a	Jasmin Forster
yNS209	$\Delta yme2 \Delta mdm38 +$ $pCO216_YME2 +$ $pCO033_YME2^{R136A}$	$leu2-3,112$ $can1-100$ $ura3-1$ $his3-11,15$ $\Delta mdm38::hphNT1$ $\Delta yme2::NatNT2$ $pRS316-Yme2-$ $Ura3$ $pRS315-Yme2^{R136A}-Leu2$	a	Jasmin Forster
yNS213	$\Delta yme2 +$ $pCO033_YME2^{R136A}$	$leu2-3,112$ $can1-100$ $ura3-1$ $his3-$ $11,15$ $\Delta yme2::NatNT2$ $pRS315-$ $Yme2^{R136A}-Leu2$	a	Jasmin Forster
yNS210	$\Delta yme2 \Delta mdm38 +$ $pCO216_YME2 +$ $pCO033_YME2^{F141A}$	$leu2-3,112$ $can1-100$ $ura3-1$ $his3-11,15$ $\Delta mdm38::hphNT1$ $\Delta yme2::NatNT2$ $pRS316-Yme2-$ $Ura3$ $pRS315-Yme2^{F141A}-Leu2$	a	Jasmin Forster
yNS214	$\Delta yme2 +$ $pCO033_YME2^{F141A}$	$leu2-3,112$ $can1-100$ $ura3-1$ $his3-$ $11,15$ $\Delta yme2::NatNT2$ $pRS315-$ $Yme2^{F141A}-Leu2$	a	Jasmin Forster

Table B.5: Yeast Strains used in the Study

Strain Name	Strain description	Genotype	Mating type	Source
yNS211	$\Delta yme2\Delta mdm38 +$ $pCO216_YME2 +$ $pCO033_YME2^{F79A/F144A}$	$leu2-3,112$ $can1-100$ $ura3-1$ $his3-11,15$ $\Delta mdm38::hphNT1$ $\Delta yme2::NatNT2$ $pRS316-Yme2-$ $Ura3$ $pRS315-Yme2^{F79A/F144A}-$ $Leu2$	a	Jasmin Forster
yNS215	$\Delta yme2 + pCO033_YME2^{F79A/F144A}$	$leu2-3,112$ $can1-100$ $ura3-1$ $his3-$ $11,15$ $\Delta yme2::NatNT2$ $pRS315-$ $Yme2^{F79A/F144A}-Leu2$	a	Jasmin Forster
yNS219	$\Delta yme2\Delta mdm38 +$ $pCO216_YME2 +$ $pCO033_YME2^{Y96A}$	$leu2-3,112$ $can1-100$ $ura3-1$ $his3-11,15$ $\Delta mdm38::hphNT1$ $\Delta yme2::NatNT2$ $pRS316-Yme2-$ $Ura3$ $pRS315-Yme2^{Y96A}-Leu2$	a	Anna Maria Melyshi
yNS220	$\Delta yme2\Delta mdm38 +$ $pCO216_YME2 +$ $pCO033_YME2^{Y174A}$	$leu2-3,112$ $can1-100$ $ura3-1$ $his3-11,15$ $\Delta mdm38::hphNT1$ $\Delta yme2::NatNT2$ $pRS316-Yme2-$ $Ura3$ $pRS315-Yme2^{Y174A}-Leu2$	a	Anna Maria Melyshi
yNS221	$\Delta yme2\Delta mdm38 +$ $pCO216_YME2 +$ $pCO033_YME2^{F175A}$	$leu2-3,112$ $can1-100$ $ura3-1$ $his3-11,15$ $\Delta mdm38::hphNT1$ $\Delta yme2::NatNT2$ $pRS316-Yme2-$ $Ura3$ $pRS315-Yme2^{F175A}-Leu2$	a	Anna Maria Melyshi
yNS222	$\Delta yme2\Delta mdm38 +$ $pCO216_YME2 +$ $pCO033_YME2^{F181A}$	$leu2-3,112$ $can1-100$ $ura3-1$ $his3-11,15$ $\Delta mdm38::hphNT1$ $\Delta yme2::NatNT2$ $pRS316-Yme2-$ $Ura3$ $pRS315-Yme2^{F181A}-Leu2$	a	Anna Maria Melyshi
yNS223	$\Delta yme2\Delta mdm38 +$ $pCO216_YME2 +$ $pCO033_YME2^{Y215A}$	$leu2-3,112$ $can1-100$ $ura3-1$ $his3-11,15$ $\Delta mdm38::hphNT1$ $\Delta yme2::NatNT2$ $pRS316-Yme2-$ $Ura3$ $pRS315-Yme2^{Y215A}-Leu2$	a	Anna Maria Melyshi
yNS225	$\Delta yme2\Delta mdm38 +$ $pCO216_YME2 +$ $pCO033_YME2^{F228A}$	$leu2-3,112$ $can1-100$ $ura3-1$ $his3-11,15$ $\Delta mdm38::hphNT1$ $\Delta yme2::NatNT2$ $pRS316-Yme2-$ $Ura3$ $pRS315-Yme2^{F228A}-Leu2$	a	Anna Maria Melyshi

B.6 List of Plasmids

All plasmids were made in *E. coli* DH5 α strain background. Details about plasmid construction and the related primers are available on Osman Lab servers and Benchling.

Table B.6: Plasmids used in this study

Plasmid Name	Description	Construction	Source	Bacterial Marker	Yeast Marker
pCO021	pFA6a-kanMX6	-	Janke et al., 2004	Amp	kanMX
pCO033	pRS315	centromeric plasmid with yeast Leu2 marker	Addgene	Amp	Leu2
pCO059	pFA6a-NATNT2	-	Janke et al., 2004	Amp	NatNT2
pCO074	pFA6a-hphNT1	-	Janke et al., 2004	Amp	hPhNT1
pCO075	pETDUET-1	6XHis tag containing expression plasmid	Millipore Sigma (Novagen)	Amp	
pCO216	pRS316-Yme2 ^{WT}	Yme2 amplified from W303 genomic DNA and cloned via BamHI+HindIII	Christof Osman	Amp	Ura3
pCO341	pYM18 plasmid with 9XMyC tag	-	Janke et al., 2004	Amp	kanMX
pCO572	pCO337-TurboID	TurboID cloned from pMQY016 into pYM14	Nupur Sharma	Amp	kanMX
pCO611	Yeast integrative plasmid in the Leu2 locus	pCO466 and pCO492 cloned with pCO327 backbone	Simon Schrott	Amp	Ura3
pNS019	pRS315-Yme2 ^{WT}	Yme2 amplified from pco216 and cloned into pco033	Nupur Sharma	Amp	Leu2
pNS020	pRS315-Yme2 ^{K393A}	Site-directed mutagenesis on pNS019	Nupur Sharma	Amp	Leu2
pNS022	pRS315-Yme2 ^{D522A}	Site-directed mutagenesis on pNS019	Nupur Sharma	Amp	Leu2

Table B.6: Plasmids used in this study

Plasmid Name	Description	Construction	Source	Bacterial Marker	Yeast Marker
pNS024	pRS315-Yme2 ^{K393A/D522A}	Site-directed mutagenesis on pNS019	Nupur Sharma	Amp	Leu2
pNS026	pCO611-Yme2 ^{WT} -TAP	Yme2 ^{WT} -TAP amplified from TAP-tagged YME2 yeast strain genomic DNA (yNS019); YME2 terminator amplified from W303 genomic DNA; further cloned into pCO611 backbone	Nupur Sharma	Amp	Ura3
pNS029	pCO611-Yme2 ^{K393A} -TAP	Site-directed mutagenesis on pNS026	Nupur Sharma	Amp	Ura3
pNS030	pCO611-Yme2 ^{D522A} -TAP	Site-directed mutagenesis on pNS026	Nupur Sharma	Amp	Ura3
pNS032	pCO611-Yme2 ^{K393A/D522A} -TAP	Site-directed mutagenesis on pNS026	Nupur Sharma	Amp	Ura3
pNS037	pCO611-Gal1Yme2 ^{WT} -TAP	Gal1Yme2 ^{WT} amplified from yNS031 yeast strain genomic DNA and further cloned into pCO611 backbone	Nupur Sharma	Amp	Ura3
pNS039	pCO611-Gal1Yme2 ^{K393A} -TAP	Site-directed mutagenesis on pNS037	Nupur Sharma	Amp	Ura3
pNS041	pCO611-Gal1Yme2 ^{D522A} -TAP	Site-directed mutagenesis on pNS037	Nupur Sharma	Amp	Ura3
pNS047	6XHis-Yme2 ^{Q356-end}	Yme2 ^{Q356-end} cloned in pCO075 (pETDUET1 with 6XHis)	Nupur Sharma	Amp	-
pNS049	pRS315-Yme2 ^{F204A}	Site-directed mutagenesis on pNS019	Nupur Sharma	Amp	Leu2
pNS051	pRS315-Yme2 ^{Y242A}	Site-directed mutagenesis on pNS019	Nupur Sharma	Amp	Leu2

Table B.6: Plasmids used in this study

Plasmid Name	Description	Construction	Source	Bacterial Marker	Yeast Marker
pNS053	pRS315-Yme2 ^{F204A/Y242A}	Site-directed mutagenesis on pNS019	Nupur Sharma	Amp	Leu2
pNS065	pRS315-Yme2 ^{R523A}	Site-directed mutagenesis on pNS019	Nupur Sharma	Amp	Leu2
pNS067	pRS315-Yme2 ^{R565A}	Site-directed mutagenesis on pNS019	Nupur Sharma	Amp	Leu2
pNS069	pCO611-Yme2 ^{F204A} -TAP	Site-directed mutagenesis on pNS026	Nupur Sharma	Amp	Ura3
pNS070	pCO611-Yme2 ^{Y242A} -TAP	Site-directed mutagenesis on pNS026	Nupur Sharma	Amp	Ura3
pNS071	pCO611-Yme2 ^{F204A/Y242A} -TAP	Site-directed mutagenesis on pNS026	Nupur Sharma	Amp	Ura3
pNS072	pRS315-Yme2 ^{F79A}	Site-directed mutagenesis on pNS019	Jasmin Forster	Amp	Leu2
pNS073	pRS315-Yme2 ^{F144A}	Site-directed mutagenesis on pNS019	Jasmin Forster	Amp	Leu2
pNS074	pRS315-Yme2 ^{δV45-P187}	Site-directed mutagenesis on pNS019	Jasmin Forster	Amp	Leu2
pNS076	pRS315-Yme2 ^{δE73-P187}	Site-directed mutagenesis on pNS019	Jasmin Forster	Amp	Leu2
pNS078	pRS315-Yme2 ^{Y78A}	Site-directed mutagenesis on pNS019	Jasmin Forster	Amp	Leu2
pNS079	pRS315-Yme2 ^{R136A}	Site-directed mutagenesis on pNS019	Jasmin Forster	Amp	Leu2
pNS080	pRS315-Yme2 ^{F141A}	Site-directed mutagenesis on pNS019	Jasmin Forster	Amp	Leu2
pNS081	pRS315-Yme2 ^{F79A144A}	Site-directed mutagenesis on pNS019	Jasmin Forster	Amp	Leu2

B.7 Mass Spectrometry data from Lat1 Co-immunoprecipitation

The raw data obtained from the Mass Spectrometry analysis is available on Osman Lab servers. For the following table, all identified candidates are listed along with their P-values (on a $-\log_{10}$ scale), as well as fold changes (on a \log_2 scale), as calculated from four replicates. The $-\log_{10}$ P-values and \log_2 fold changes are listed upon comparison of WT sample against the $\Delta lat1$ sample.

Table B.7: Candidates identified in Lat1 Mass Spectrometry (WT vs. $\Delta lat1$)

P-value	Fold change	Gene Names	Protein IDs	Protein Names
4.71	8.19	<i>PDX1</i>	P16451	Pyruvate dehydrogenase complex protein X component, mitochondrial
4.87	8.06	<i>LPD1</i>	P09624	Dihydrolipoyl dehydrogenase, mitochondrial
7.86	7.99	<i>MRPL11</i>	P36521	54S ribosomal protein L11, mitochondrial
6.03	7.33	<i>MGM101</i>	P32787	Mitochondrial genome maintenance protein MGM101
3.60	6.99	<i>MNP1</i>	P53163	54S ribosomal protein L12, mitochondrial
4.46	6.80	<i>PDA1</i>	P16387	Pyruvate dehydrogenase E1 component subunit alpha, mitochondrial
3.74	6.72	<i>PET54</i>	P10834	Protein PET54
3.07	6.46	<i>ABF2</i>	Q02486	ARS-binding factor 2, mitochondrial
4.76	5.99	<i>LAT1</i>	P12695	Dihydrolipoyllysine-residue acetyltransferase component of pyruvate dehydrogenase complex, mitochondrial
4.59	5.98	<i>RPO41</i>	P13433	DNA-directed RNA polymerase, mitochondrial
2.41	5.92	<i>ATP2</i>	P00830	ATP synthase subunit beta, mitochondrial
4.84	5.83	<i>HMO1</i>	Q03973	High mobility group protein 1
4.66	5.81	<i>PDB1</i>	P32473	Pyruvate dehydrogenase E1 component subunit beta, mitochondrial
4.22	5.81	<i>AAC1</i>	P04710	ADP,ATP carrier protein 1
5.06	5.81	<i>MRP51</i>	Q02950	37S ribosomal protein MRP51, mitochondrial
5.16	5.76	<i>NFS1</i>	P25374	Cysteine desulfurase, mitochondrial
5.08	5.72	<i>RIP1</i>	P08067	Cytochrome b-c1 complex subunit Rieske, mitochondrial
2.54	5.67	<i>POR1</i>	P04840	Mitochondrial outer membrane protein porin 1

Table B.7: Candidates identified in Lat1 Mass Spectrometry (WT vs. $\Delta lat1$)

P-value	Fold change	Gene Names	Protein IDs	Protein Names
4.40	5.50	<i>MSH1</i>	P25846	DNA mismatch repair protein MSH1, mitochondrial
4.71	5.45	<i>MIP1</i>	P15801	DNA polymerase gamma
4.68	5.41	<i>KAR2</i>	P16474	78 kDa glucose-regulated protein homolog
2.11	5.37	<i>ATP1</i>	P07251	ATP synthase subunit alpha, mitochondrial
4.09	5.31	<i>TCB1</i>	Q12466	Tricalbin-1
5.09	5.21	<i>NDE1</i>	P40215	External NADH-ubiquinone oxidoreductase 1, mitochondrial
4.13	5.15	<i>TCB3</i>	Q03640	Tricalbin-3
2.76	4.98	<i>CYT1</i>	P07143	Cytochrome c1, heme protein, mitochondrial
3.93	4.93	<i>COX2</i>	P00410	Cytochrome c oxidase subunit 2
4.68	4.92	<i>CST9</i>	Q06032	Chromosome stability protein 9
4.71	4.78	<i>ILV1</i>	P00927	Threonine dehydratase, mitochondrial
4.22	4.78	<i>SLS1</i>	P42900	Sigma-like sequence protein 1, mitochondrial
3.78	4.65	<i>ALD4</i>	P46367	Potassium-activated aldehyde dehydrogenase, mitochondrial
3.04	4.59	<i>MRPL9</i>	P31334	54S ribosomal protein L9, mitochondrial
5.28	4.57	<i>YHM2</i>	Q04013	Citrate/oxoglutarate carrier protein
2.17	4.57	<i>COR1</i>	P07256	Cytochrome b-c1 complex subunit 1, mitochondrial
3.16	4.53	<i>ACO1</i>	P19414	Aconitate hydratase, mitochondrial
3.39	4.51	<i>DLD1</i>	P32891	D-lactate dehydrogenase [cytochrome] 1, mitochondrial
4.68	4.51	<i>RSM28</i>	Q03430	37S ribosomal protein RSM28, mitochondrial
3.26	4.49	<i>CCE1</i>	Q03702	Cruciform cutting endonuclease 1, mitochondrial
4.40	4.48	<i>SSB1</i>	P11484	Heat shock protein SSB1;Heat shock protein SSB2
2.53	4.44	<i>COX1</i>	P00401	Cytochrome c oxidase subunit 1
3.35	4.38	<i>COQ9</i>	Q05779	Ubiquinone biosynthesis protein COQ9, mitochondrial
4.05	4.30	<i>PHB2</i>	P50085	Prohibitin-2
2.66	4.29	<i>OLE1</i>	P21147	Acyl-CoA desaturase 1

Table B.7: Candidates identified in Lat1 Mass Spectrometry (WT vs. $\Delta lat1$)

P-value	Fold change	Gene Names	Protein IDs	Protein Names
3.60	4.28	<i>MRPL22</i>	P53881	54S ribosomal protein L22, mitochondrial
2.21	4.22	<i>QCR2</i>	P07257	Cytochrome b-c1 complex subunit 2, mitochondrial
2.68	4.18	<i>TOM70</i>	P07213	Mitochondrial import receptor subunit TOM70
1.69	4.12	<i>SDH1</i>	Q00711	Succinate dehydrogenase [ubiquinone] flavoprotein subunit, mitochondrial
5.07	4.08	<i>ATP10</i>	P18496	Mitochondrial ATPase complex subunit ATP10
2.74	3.95	<i>XDJ1</i>	P39102	DnaJ protein homolog XDJ1
2.92	3.91	<i>MRF1</i>	P30775	Peptide chain release factor 1, mitochondrial
3.31	3.87	<i>TOP2</i>	P06786	DNA topoisomerase 2
2.05	3.87	<i>COQ6</i>	P53318	Ubiquinone biosynthesis monooxygenase COQ6, mitochondrial
3.79	3.86	<i>MTF2</i>	P10849	Mitochondrial transcription factor 2
2.18	3.81	<i>ILV3</i>	P39522	Dihydroxy-acid dehydratase, mitochondrial
3.57	3.72	<i>HFD1</i>	Q04458	Fatty aldehyde dehydrogenase HFD1
4.35	3.67	<i>PET127</i>	P32606	Putative mitochondrial translation system component PET127
1.33	3.67	<i>ATP4</i>	P05626	ATP synthase subunit 4, mitochondrial
3.24	3.64	<i>OAC1</i>	P32332	Mitochondrial oxaloacetate transport protein
2.08	3.64	<i>MRPS17</i>	Q03246	37S ribosomal protein S17, mitochondrial
2.06	3.64	<i>YKL077W</i>	P36081	Uncharacterized protein YKL077W
3.50	3.63	<i>MRPL1</i>	Q04599	54S ribosomal protein L1, mitochondrial
2.94	3.62	<i>PET9</i>	P18239	ADP,ATP carrier protein 2
1.54	3.62	<i>ATP3</i>	P38077	ATP synthase subunit gamma, mitochondrial
1.55	3.57	<i>NUC1</i>	P08466	Mitochondrial nuclease
3.73	3.53	<i>LEU4</i>	P06208	2-isopropylmalate synthase
3.15	3.51	<i>WBP1</i>	P33767	Dolichyl-diphosphooligosaccharide-protein glycosyltransferase subunit WBP1
2.18	3.46	<i>NAM9</i>	P27929	37S ribosomal protein NAM9, mitochondrial

Table B.7: Candidates identified in Lat1 Mass Spectrometry (WT vs. $\Delta lat1$)

P-value	Fold change	Gene Names	Protein IDs	Protein Names
3.42	3.46	<i>MYO5</i>	Q04439	Myosin-5
1.97	3.45	<i>RSM7</i>	P47150	37S ribosomal protein S7, mitochondrial
1.79	3.43	<i>HSP42</i>	Q12329	Heat shock protein 42
2.48	3.42	<i>ILV6</i>	P25605	Acetolactate synthase small subunit, mitochondrial
1.27	3.42	<i>ATP5</i>	P09457	ATP synthase subunit 5, mitochondrial
1.55	3.36	<i>GUT2</i>	P32191	Glycerol-3-phosphate dehydrogenase, mitochondrial
3.62	3.35	<i>SLC1</i>	P33333	Probable 1-acyl-sn-glycerol-3-phosphate acyltransferase
2.62	3.32	<i>YDJ1</i>	P25491	Mitochondrial protein import protein MAS5
4.03	3.30	<i>LSC2</i>	P53312	Succinyl-CoA ligase [ADP-forming] subunit beta, mitochondrial
2.64	3.30	<i>MRPL8</i>	P22353	54S ribosomal protein L8, mitochondrial
2.96	3.22	<i>MIR1</i>	P23641	Mitochondrial phosphate carrier protein; Mitochondrial phosphate carrier protein, N-terminally processed
1.94	3.22	<i>TEF1</i>	P02994	Elongation factor 1-alpha
1.59	3.14	<i>PHB1</i>	P40961	Prohibitin-1
2.14	3.14	<i>HSP60</i>	P19882	Heat shock protein 60, mitochondrial
1.51	3.13	<i>SDH2</i>	P21801	Succinate dehydrogenase [ubiquinone] iron-sulfur subunit, mitochondrial
2.66	3.11	<i>RSM22</i>	P36056	37S ribosomal protein S22, mitochondrial
1.96	3.10	<i>ALT1</i>	P52893	Probable alanine aminotransferase, mitochondrial
1.49	3.10	<i>MAE1</i>	P36013	NAD-dependent malic enzyme, mitochondrial
1.38	3.02	<i>MRPL10</i>	P36520	54S ribosomal protein L10, mitochondrial
3.05	3.02	<i>MIC60</i>	P36112	MICOS complex subunit MIC60
1.28	2.97	<i>MRPS5</i>	P33759	37S ribosomal protein S5, mitochondrial
2.02	2.96	<i>GGC1</i>	P38988	Mitochondrial GTP/GDP carrier protein 1
3.70	2.94	<i>ARP4</i>	P80428	Actin-related protein 4
1.96	2.92	<i>SSC1</i>	P0CS90	Heat shock protein SSC1, mitochondrial
1.43	2.89	<i>VMA2</i>	P16140	V-type proton ATPase subunit B

Table B.7: Candidates identified in Lat1 Mass Spectrometry (WT vs. $\Delta lat1$)

P-value	Fold change	Gene Names	Protein IDs	Protein Names
2.65	2.88	<i>MRPL17</i>	P36528	54S ribosomal protein L17, mitochondrial
2.21	2.85	<i>RVB1</i>	Q03940	RuvB-like protein 1
1.63	2.84	<i>MRPL7</i>	P36519	54S ribosomal protein L7, mitochondrial
1.56	2.81	<i>MHR1</i>	Q06630	Mitochondrial homologous recombination protein 1
2.44	2.78	<i>SEC61</i>	P32915	Protein transport protein SEC61
2.24	2.76	<i>LIP5</i>	P32875	Lipoyl synthase, mitochondrial
2.55	2.76	<i>IRC3</i>	Q06683	Putative ATP-dependent helicase IRC3
1.23	2.74	<i>COQ5</i>	P49017	2-methoxy-6-polyprenyl-1,4-benzoquinol methylase, mitochondrial
1.54	2.69	<i>NDI1</i>	P32340	Rotenone-insensitive NADH-ubiquinone oxidoreductase, mitochondrial
2.66	2.69	<i>RPM2</i>	Q02773	Ribonuclease P protein component, mitochondrial
1.57	2.64	<i>SSH1</i>	P38353	Sec sixty-one protein homolog
1.47	2.63	<i>GAL1</i>	P04385	Galactokinase
1.45	2.61	<i>MRPL15</i>	P36523	54S ribosomal protein L15, mitochondrial
2.80	2.60	<i>RTN1</i>	Q04947	Reticulon-like protein 1
1.54	2.45	<i>SHM1</i>	P37292	Serine hydroxymethyltransferase, mitochondrial
2.25	2.43	<i>TCB2</i>	P48231	Tricalbin-2
1.06	2.38	<i>MSS116</i>	P15424	ATP-dependent RNA helicase MSS116, mitochondrial
1.63	2.37	<i>MRP1</i>	P10662	37S ribosomal protein MRP1, mitochondrial
1.90	2.24	<i>VAR1</i>	P02381	Ribosomal protein VAR1, mitochondrial
2.56	2.23	<i>AEP3</i>	Q12089	ATPase expression protein 3
1.92	2.14	<i>ELO3</i>	P40319	Elongation of fatty acids protein 3
1.02	2.09	<i>MRPL35</i>	Q06678	54S ribosomal protein L35, mitochondrial
2.09	1.97	<i>YER077C</i>	P40050	Uncharacterized protein YER077C
1.79	1.95	<i>INO80</i>	P53115	Putative DNA helicase INO80
1.56	1.93	<i>RSM24</i>	Q03976	37S ribosomal protein S24, mitochondrial

Table B.7: Candidates identified in Lat1 Mass Spectrometry (WT vs. $\Delta lat1$)

P-value	Fold change	Gene Names	Protein IDs	Protein Names
1.86	1.91	<i>ILV2</i>	P07342	Acetolactate synthase catalytic subunit, mitochondrial
2.11	1.90	<i>KGD1</i>	P20967	2-oxoglutarate dehydrogenase, mitochondrial
2.69	1.87	<i>ACT1</i>	P60010	Actin
0.90	1.85	<i>FSF1</i>	Q12029	Probable mitochondrial transport protein FSF1
0.62	1.82	<i>MRP4</i>	P32902	37S ribosomal protein MRP4, mitochondrial
1.50	1.81	<i>MRPL24</i>	P36525	54S ribosomal protein L24, mitochondrial
1.26	1.72	<i>TIM23</i>	P32897	Mitochondrial import inner membrane translocase subunit TIM23
3.29	1.68	<i>MDJ1</i>	P35191	DnaJ homolog 1, mitochondrial
1.59	1.68	<i>CCM1</i>	P48237	Mitochondrial group I intron splicing factor CCM1
0.44	1.60	<i>PMA1</i>	P05030	Plasma membrane ATPase 1
0.66	1.57	<i>OM45</i>	P16547	Mitochondrial outer membrane protein OM45
0.40	1.29	<i>MRPL3</i>	P36516	54S ribosomal protein L3, mitochondrial
0.80	1.27	<i>ILV5</i>	P06168	Ketol-acid reductoisomerase, mitochondrial
0.40	1.27	<i>MRPL40</i>	P36534	54S ribosomal protein L40, mitochondrial
0.30	0.72	<i>SRP54</i>	P20424	Signal recognition particle subunit SRP54
0.15	0.57	<i>GAL7</i>	P08431	Galactose-1-phosphate uridylyltransferase
0.41	0.47	<i>KGD2</i>	P19262	Dihydrolipoyllysine-residue succinyltransferase component of 2-oxoglutarate dehydrogenase complex, mitochondrial
0.36	0.39	<i>HEM15</i>	P16622	Ferrochelatase, mitochondrial
0.04	0.18	<i>TY2B-LR1</i>	P0C2J3	Transposon Ty2-LR1 Gag-Pol polyprotein
0.29	-0.47	<i>TY1B-H</i>	O13535	Transposon Ty1-H Gag-Pol polyprotein
0.43	-0.63	<i>HTZ1</i>	Q12692	Histone H2A.Z
0.51	-1.89	<i>TY1B-BL</i>	Q12490	Transposon Ty1-BL Gag-Pol polyprotein

Table B.7: Candidates identified in Lat1 Mass Spectrometry (WT vs. $\Delta lat1$)

P-value	Fold change	Gene Names	Protein IDs	Protein Names
1.85	-1.93	<i>PIL1</i>	P53252	Sphingolipid long chain base-responsive protein PIL1
2.17	-1.94	<i>LSP1</i>	Q12230	Sphingolipid long chain base-responsive protein LSP1
1.05	-2.18	<i>RPL40B</i>	P0CH09	Ubiquitin-60S ribosomal protein L40
0.52	-2.49	<i>TAO3</i>	P40468	Cell morphogenesis protein PAG1

B.8 Mass Spectrometry data from Proximity Labelling Assay

The raw data obtained from the Mass Spectrometry analysis is available on Osman Lab servers. For the following table, all identified candidates are listed along with their P-values (on a $-\log_{10}$ scale), as well as fold changes (on a \log_2 scale), as calculated from three replicates. The $-\log_{10}$ P-values and \log_2 fold changes are listed upon comparison of Pda1-TurboID (Pda1-T) vs. WT, Pda1-TurboID (Pda1-T) vs. Floaty-TurboID (Floaty-T), and Floaty-TurboID (Floaty-T) vs. WT samples.

Table B.8: Candidates identified in proximity labelling assay followed by Mass Spectrometry

Gene names	Protein IDs	Pda1-T vs. WT		Pda1-T vs. Floaty-T		Floaty-T vs. WT	
		P-value	Fold change	P-value	Fold change	P-value	Fold change
TurboID	TurboID	5.54	9.56	4.01	1.58	5.11	7.99
PDX1	P16451	4.97	10.04	4.97	4.96	3.63	5.07
PDA1	P16387	4.30	9.58	5.92	5.48	2.90	4.10
LAT1	P12695	5.65	8.87	5.09	7.09	2.30	1.78
PPA2	P28239	4.29	8.54	1.91	6.67	0.54	1.88
ATP7	P30902	5.18	8.29	5.15	1.37	4.87	6.93
COQ1	P18900	5.17	8.28	4.51	0.99	4.92	7.29
RSM25	P40496	5.08	7.73	4.40	1.00	4.81	6.73
RSM7	P47150	3.35	7.47	5.44	1.55	2.96	5.92
PRX1	P34227	4.35	7.25	3.32	0.81	4.12	6.44
ILV5	P06168	5.19	7.19	1.34	0.63	4.69	6.56
RIM1	P32445	3.67	7.18	2.03	2.21	4.07	4.97
MDL2	P33311	5.37	7.02	5.02	5.16	3.59	1.85
HSP60	P19882	3.55	6.85	1.04	0.18	3.49	6.67
RDL2	Q08742	5.51	6.75	5.37	1.95	4.84	4.80
HSP10	P38910	4.32	6.61	2.28	0.40	4.18	6.21
AIM17	P23180	3.05	6.57	4.37	3.33	1.91	3.25
ALD4	P46367	5.51	6.53	3.99	0.82	5.21	5.71
ATP14	Q12349	3.90	6.52	4.08	1.68	3.35	4.84
PDB1	P32473	6.37	6.44	6.20	4.62	3.98	1.83
COX4	P04037	3.40	6.42	1.07	1.27	3.63	5.15
ATP5	P09457	4.71	6.38	5.21	1.43	4.26	4.95
AAT1	Q01802	4.06	6.35	1.05	-0.14	4.07	6.49
ADH3	P07246	3.22	6.33	0.27	0.29	3.64	6.04
MRPL3	P36516	3.67	6.32	3.55	0.79	3.43	5.53
MAS2	P11914	5.73	6.26	4.84	1.13	5.33	5.13
MDH1	P17505	3.37	6.18	4.05	0.95	3.08	5.23
PET123	P17558	4.00	6.15	2.80	0.54	3.83	5.62
IDH2	P28241	5.19	6.14	2.61	0.50	5.11	5.63
MRP51	Q02950	4.62	6.11	4.95	2.03	3.92	4.08
ATP2	P00830	5.25	6.06	1.04	0.35	4.77	5.71
ATP12	P22135	5.29	6.04	4.28	0.83	5.02	5.20
SDH8	P38345	4.02	6.03	4.23	1.06	3.67	4.97
MRM1	P25270	4.16	5.99	2.15	-0.56	4.25	6.55
RSM10	Q03201	7.26	5.98	4.92	2.00	6.32	3.97
MSD1	P15179	3.46	5.91	3.74	1.29	3.02	4.63
LYS12	P40495	3.93	5.90	2.90	0.58	3.74	5.32
AIM9	P40053	4.44	5.90	4.17	1.52	3.92	4.38
COX6	P00427	3.37	5.86	5.41	1.94	2.70	3.92
MRP21	P38175	4.36	5.82	2.42	0.54	4.13	5.28
ILV3	P39522	4.60	5.81	0.11	-0.09	4.61	5.91
CPR3	P25719	3.71	5.81	5.57	1.85	3.05	3.96
CIR1	P42940	2.51	5.77	5.19	2.22	1.77	3.56
MRPS28	P21771	3.57	5.71	6.99	1.50	3.05	4.20

Table B.8: Candidates identified in proximity labelling assay followed by Mass Spectrometry

Gene names	Protein IDs	Pda1-T vs. WT		Pda1-T vs. Floaty-T		Floaty-T vs. WT	
		P-value	Fold change	P-value	Fold change	P-value	Fold change
MHR1	Q06630	3.90	5.67	2.43	3.96	1.39	1.71
MRP1	P10662	4.01	5.63	6.20	1.56	3.45	4.06
MIS1	P09440	4.23	5.61	3.12	0.62	4.01	5.00
MGM101	P32787	3.56	5.61	4.52	0.78	3.30	4.83
MRPL36	P36531	4.44	5.60	4.28	0.99	4.08	4.60
ALT1	P52893	3.24	5.60	4.22	4.74	0.65	0.85
BIO2	P32451	7.52	5.58	3.51	-1.14	6.46	6.72
SSC1	P0CS90	3.97	5.55	0.75	-0.47	4.36	6.03
RSM19	P53733	4.18	5.53	1.68	0.95	4.42	4.58
MRP4	P32902	4.67	5.53	3.39	0.90	4.27	4.63
TIM44	Q01852	3.63	5.52	3.99	-0.85	3.88	6.36
SDH1	Q00711	2.78	5.51	0.97	0.44	2.70	5.06
IDP1	P21954	3.89	5.50	1.48	0.94	4.31	4.55
MSE1	P48525	4.51	5.48	2.86	0.85	4.23	4.63
LIP5	P32875	3.08	5.46	4.35	0.45	2.94	5.00
AIM32	Q04689	4.01	5.43	4.40	0.80	3.73	4.62
MDM38	Q08179	4.51	5.42	5.51	-1.25	4.86	6.66
QCR2	P07257	2.87	5.41	1.80	0.63	2.64	4.78
MZM1	Q03429	2.68	5.39	3.16	2.92	1.40	2.46
RSM28	Q03430	4.53	5.38	5.06	-1.06	4.84	6.43
MRPL17	P36528	3.47	5.36	3.32	2.21	2.49	3.15
ATP10	P18496	3.04	5.35	1.94	0.44	2.87	4.90
MRPL40	P36534	4.48	5.31	3.34	1.40	3.82	3.91
SDH7	Q04401	4.83	5.30	3.25	0.41	4.68	4.89
KGD1	P20967	3.57	5.29	4.33	0.66	3.35	4.63
ZIM17	P42844	4.09	5.26	1.33	2.77	1.15	2.49
LSC1	P53598	3.81	5.20	0.11	0.05	3.95	5.15
ATP3	P38077	4.60	5.19	4.11	1.23	4.15	3.96
NFS1	P25374	4.25	5.17	2.33	1.53	3.37	3.64
COQ3	P27680	3.24	5.14	3.30	1.19	2.79	3.95
ATP11	P32453	4.62	5.10	3.91	1.25	4.06	3.86
PET127	P32606	4.09	5.05	3.23	1.07	3.60	3.98
MRPL15	P36523	3.73	5.05	2.11	3.78	0.76	1.27
YMR31	P19955	3.77	5.03	0.90	1.77	1.53	3.26
MRPL11	P36521	4.17	5.03	3.01	0.42	4.00	4.60
MRPS35	P53292	3.03	5.02	4.80	2.37	2.00	2.65
ACO1	P19414	3.71	5.01	0.01	-0.01	3.97	5.01
NFU1	P32860	4.21	4.98	3.84	1.53	3.47	3.45
MRPL20	P22354	6.26	4.96	4.09	3.34	2.79	1.62
YGR021W	P53212	4.40	4.96	3.06	1.85	3.26	3.11
RIP1	P08067	2.71	4.95	1.76	1.68	1.99	3.27
MSS116	P15424	2.49	4.95	2.64	-0.23	2.57	5.18
MRF1	P30775	3.91	4.94	3.41	3.32	1.67	1.62
MAE1	P36013	3.39	4.93	4.17	1.31	2.87	3.62
SDH2	P21801	5.91	4.92	0.82	1.81	1.42	3.11
PKP2	P53170	5.08	4.91	1.67	-0.59	4.74	5.51
TRX3	P25372	6.25	4.91	1.85	2.45	1.83	2.46
MRPL13	Q02204	2.70	4.86	4.46	1.03	2.31	3.83
REX2	P54964	3.39	4.85	2.38	0.31	3.27	4.54
ABF2	Q02486	3.63	4.85	4.83	3.65	1.36	1.19
MRPL38	P35996	4.25	4.84	2.60	3.49	1.10	1.36
INH1	P01097	0.87	4.81	0.70	3.85	0.73	0.96
CBP3	P21560	4.81	4.80	1.21	0.12	4.75	4.68
MRX9	Q07349	3.14	4.79	6.93	-3.88	4.14	8.68
RSM22	P36056	3.69	4.79	1.91	0.38	3.50	4.40

Table B.8: Candidates identified in proximity labelling assay followed by Mass Spectrometry

Gene names	Protein IDs	Pda1-T vs. WT		Pda1-T vs. Floaty-T		Floaty-T vs. WT	
		P-value	Fold change	P-value	Fold change	P-value	Fold change
MRPS18	P42847	3.58	4.78	5.60	1.00	3.18	3.78
YOR022C	Q12204	3.04	4.76	4.68	-0.83	3.30	5.59
RMD9	P53140	3.07	4.75	2.05	0.34	2.94	4.40
RSM26	P47141	4.82	4.73	3.94	4.04	1.01	0.69
SDH5	Q08230	2.34	4.72	1.68	2.22	1.26	2.50
KGD2	P19262	3.85	4.72	2.45	0.77	3.44	3.95
MRPS5	P33759	3.44	4.71	4.68	0.68	3.18	4.03
LSC2	P53312	2.94	4.69	2.01	0.72	2.62	3.97
ILV2	P07342	4.22	4.64	0.22	0.05	4.14	4.59
CCM1	P48237	4.45	4.63	3.84	-0.70	4.70	5.33
MRPS17	Q03246	3.73	4.62	2.27	1.06	3.35	3.57
YME1	P32795	6.35	4.62	4.56	-0.98	6.78	5.60
PTC7	P38797	3.31	4.59	3.76	4.14	0.37	0.46
MEF1	P25039	2.91	4.56	2.65	1.36	2.32	3.20
LPD1	P09624	3.05	4.55	2.99	2.09	1.93	2.46
SHM1	P37292	4.32	4.54	2.19	1.50	2.90	3.04
IMG1	P25626	4.11	4.52	3.42	1.36	3.40	3.16
HEM15	P16622	4.61	4.50	2.96	2.60	2.39	1.90
PET54	P10834	3.65	4.49	2.61	2.87	1.38	1.63
MRPL22	P53881	3.34	4.44	1.52	2.36	1.18	2.09
SDH4	P37298	4.44	4.41	0.51	-0.04	4.48	4.45
MET7	Q08645	4.12	4.40	1.28	2.21	1.22	2.19
SSQ1	Q05931	3.73	4.40	4.75	2.75	2.06	1.65
AIM41	Q12032	3.09	4.39	4.50	2.02	2.08	2.37
MRP13	P12686	3.42	4.38	3.05	0.25	3.32	4.12
CIT1	P00890	4.80	4.36	0.61	0.10	4.64	4.27
MRPL31	P14063	2.64	4.36	3.15	2.78	1.07	1.59
MRP7	P12687	4.49	4.30	2.43	2.28	2.51	2.02
IMO32	P53219	5.24	4.30	3.24	2.97	1.82	1.34
IDH1	P28834	2.10	4.28	1.41	1.68	1.19	2.60
MGE1	P38523	2.98	4.28	1.99	0.94	2.71	3.34
OAC1	P32332	6.15	4.27	0.03	0.01	6.67	4.26
RSM24	Q03976	3.26	4.25	3.13	3.25	0.84	1.00
DLD2	P46681	4.02	4.20	4.75	2.88	1.98	1.32
MSC6	Q08818	2.37	4.17	2.65	-0.66	2.59	4.84
RPM2	Q02773	2.69	4.16	3.04	4.23	0.04	-0.07
NAM9	P27929	2.98	4.15	3.52	1.30	2.33	2.85
MRPL23	Q12487	4.06	4.15	2.82	3.08	1.06	1.07
FUM1	P08417	3.93	4.13	1.19	0.39	3.56	3.74
GCV3	P39726	3.01	4.12	1.37	2.43	0.84	1.69
AIM22	P47051	5.75	4.11	2.43	3.57	0.39	0.54
GUT2	P32191	3.50	4.10	1.43	-0.36	3.59	4.46
COX2	P00410	3.99	4.09	0.46	0.11	3.83	3.98
MSR1	P38714	4.03	4.07	1.18	0.20	3.87	3.86
MAS1	P10507	4.37	4.06	4.15	-1.08	4.76	5.13
CIR2	Q08822	4.65	4.03	2.00	1.31	2.92	2.72
ARG2	P40360	4.05	4.02	2.39	2.65	1.26	1.37
CST9	Q06032	3.05	4.01	2.67	1.10	2.44	2.91
ALD5	P40047	3.31	4.01	2.13	2.47	1.22	1.53
SLS1	P42900	1.81	4.01	0.60	0.31	1.66	3.70
PUT2	P07275	3.00	4.00	2.66	1.44	2.14	2.56
TUF1	P02992	2.61	4.00	0.20	0.18	2.83	3.82
CYC1	P00044	1.38	3.98	0.47	1.86	0.88	2.13
TIM50	Q02776	4.29	3.95	4.57	-1.05	4.68	5.00
IBA57	P47158	5.59	3.95	3.16	2.61	1.98	1.33

Table B.8: Candidates identified in proximity labelling assay followed by Mass Spectrometry

Gene names	Protein IDs	Pda1-T vs. WT		Pda1-T vs. Floaty-T		Floaty-T vs. WT	
		P-value	Fold change	P-value	Fold change	P-value	Fold change
MRPL37	P36532	2.43	3.94	4.64	2.55	0.99	1.39
MRPL25	P23369	3.62	3.93	3.15	2.23	1.90	1.70
PTC6	P25646	3.32	3.91	3.55	2.67	1.34	1.24
FMP46	P36141	3.54	3.90	4.38	2.05	2.23	1.85
VAR1	P02381	4.06	3.87	3.32	1.79	3.53	2.08
PIC2	P40035	4.25	3.86	3.91	2.11	2.67	1.76
CYM1	P32898	4.37	3.85	4.47	0.74	4.00	3.12
MTG2	P38860	3.60	3.84	5.67	2.51	1.87	1.33
NDE1	P40215	3.21	3.84	2.98	-1.67	3.84	5.51
MDJ1	P35191	2.43	3.81	1.42	1.63	1.25	2.18
MRPL6	P32904	2.99	3.80	4.39	2.73	1.08	1.07
YOR131C	Q12486	3.20	3.79	2.18	1.38	2.35	2.41
GUF1	P46943	3.94	3.76	1.82	1.49	2.18	2.27
HXT6	P39003	1.38	3.75	0.94	2.25	1.12	1.50
MRPL1	Q04599	3.28	3.73	2.38	2.09	1.49	1.64
YLF2	P38746	5.58	3.73	2.27	2.07	1.97	1.66
ETR1	P38071	2.81	3.71	1.88	1.77	1.43	1.94
MRPL33	P20084	2.61	3.71	2.65	2.73	0.67	0.98
YLR290C	Q05892	2.25	3.71	3.64	2.13	1.12	1.58
MRPL8	P22353	3.03	3.70	2.74	2.58	0.96	1.12
NGL1	Q08213	3.26	3.65	2.39	2.23	1.28	1.42
MRP20	P32387	2.82	3.64	2.71	0.83	2.39	2.81
ACH1	P32316	3.60	3.64	2.90	2.17	2.48	1.47
MSF1	P08425	5.17	3.64	3.19	2.62	1.61	1.01
COQ8	P27697	3.29	3.63	1.27	0.81	2.55	2.82
AIM45	Q12480	2.80	3.61	3.82	2.61	1.08	1.00
CBS2	P14905	2.66	3.61	2.65	0.44	2.44	3.17
HEM1	P09950	3.86	3.59	0.48	0.64	2.03	2.95
COQ5	P49017	2.50	3.59	1.92	0.80	2.04	2.79
GTF1	P53260	3.29	3.57	3.47	2.76	0.89	0.81
AIM23	P47015	5.00	3.54	1.49	1.57	1.79	1.98
ICP55	P40051	4.75	3.54	0.61	0.23	4.81	3.31
MRPS9	P38120	3.05	3.54	7.44	3.13	0.45	0.41
MRPL9	P31334	3.92	3.52	4.19	1.37	3.02	2.15
FAU1	P40099	3.91	3.51	2.29	2.47	0.97	1.04
MTF2	P10849	6.06	3.42	0.10	-0.02	5.79	3.44
OCT1	P35999	3.58	3.42	3.28	-0.49	3.83	3.92
AFG1	P32317	2.83	3.40	1.94	-0.27	2.95	3.68
MRPL27	P36526	5.52	3.40	2.63	1.42	3.18	1.98
MRPL19	P53875	5.49	3.40	1.71	1.60	1.84	1.79
YHB1	P39676	1.73	3.39	4.79	2.63	0.36	0.76
HSP78	P33416	4.20	3.39	1.64	0.35	4.10	3.04
CBP6	P07253	5.53	3.38	0.94	1.74	0.87	1.64
MRPL7	P36519	3.14	3.36	1.94	1.50	1.84	1.86
ILV1	P00927	3.58	3.36	1.44	1.12	2.11	2.24
PIM1	P36775	2.87	3.36	2.62	2.84	0.87	0.52
ADK2	P26364	3.95	3.35	3.36	1.91	2.15	1.44
NDI1	P32340	2.24	3.32	1.67	-0.72	2.49	4.05
MRPL50	P53724	3.11	3.32	4.30	2.57	0.90	0.75
MMF1	P40185	4.83	3.32	3.48	2.83	0.82	0.49
COX1	P00401	1.28	3.28	2.25	-0.30	1.39	3.58
MCT1	Q12283	3.35	3.28	3.18	2.37	1.11	0.91
COX15	P40086	2.52	3.24	5.13	-1.97	3.31	5.21
MOD5	P07884	3.74	3.22	2.44	1.29	2.52	1.93
CYT1	P07143	2.68	3.21	1.29	-0.68	2.84	3.89

Table B.8: Candidates identified in proximity labelling assay followed by Mass Spectrometry

Gene names	Protein IDs	Pda1-T vs. WT		Pda1-T vs. Floaty-T		Floaty-T vs. WT	
		P-value	Fold change	P-value	Fold change	P-value	Fold change
CDC9	P04819	4.69	3.18	2.67	1.41	2.74	1.77
MST1	P07236	2.96	3.16	1.88	1.81	1.12	1.35
MRPL10	P36520	4.95	3.13	6.22	3.05	0.29	0.09
APE2	P32454	2.43	3.13	1.03	0.20	2.30	2.93
aI2	P03876	2.83	3.08	2.56	0.40	2.59	2.68
MRPS12	P53732	2.16	3.05	3.67	1.74	1.01	1.31
PKP1	P40530	4.08	3.04	2.43	1.64	1.88	1.39
MRP17	P28778	3.10	3.02	1.67	1.60	1.23	1.42
ECM31	P38122	2.67	3.01	0.90	1.00	1.40	2.01
AIM24	P47127	2.26	2.95	6.48	-2.57	3.28	5.52
YPT1	P01123	3.20	2.95	2.80	1.43	1.94	1.52
IFM1	P25038	3.46	2.95	3.89	1.69	2.15	1.26
JAC1	P53193	3.66	2.95	2.19	1.85	1.23	1.10
PET130	P47065	3.61	2.92	3.27	1.76	1.79	1.16
RRG1	Q12167	2.38	2.92	3.23	-1.12	2.87	4.04
MCX1	P38323	2.76	2.91	1.58	1.23	1.48	1.68
GLR1	P41921	3.83	2.90	4.04	1.41	2.58	1.50
NAM2	P11325	2.91	2.90	1.65	0.88	2.06	2.02
YDR061W	Q12298	2.29	2.89	2.43	0.83	1.75	2.06
RRF1	P38771	4.28	2.89	2.28	1.83	1.36	1.06
GEP3	Q08622	1.92	2.88	0.93	0.65	1.42	2.23
RPL20B	P0CX24	3.11	2.87	0.79	1.26	0.94	1.62
ATP4	P05626	3.90	2.87	0.40	0.86	1.02	2.01
MRPL35	Q06678	3.74	2.84	1.68	0.89	2.62	1.96
CAT2	P32796	3.44	2.84	2.32	-0.39	3.68	3.22
MCR1	P36060	4.37	2.82	1.23	1.20	1.56	1.62
MRPL4	P36517	3.06	2.81	2.01	1.46	1.50	1.35
PCS60	P38137	3.35	2.76	1.66	0.93	2.16	1.83
CRS1	P53852	1.98	2.72	1.21	1.34	1.90	1.38
VAS1	P07806	5.15	2.72	1.56	1.08	2.12	1.63
ILV6	P25605	1.91	2.71	1.04	1.36	0.71	1.35
RPL9A	P05738	3.17	2.70	2.30	1.17	1.96	1.53
MRPL49	P40858	3.09	2.68	0.57	0.33	3.28	2.35
MSY1	P48527	1.93	2.68	1.84	1.33	0.93	1.34
SSH1	P38353	1.20	2.66	0.82	-0.30	1.34	2.97
ISU1	Q03020	2.52	2.65	2.87	1.61	1.06	1.04
MSS2	P40990	2.15	2.64	3.69	1.53	0.97	1.11
HNT1	Q04344	2.80	2.63	4.34	2.16	0.58	0.47
MRPL44	P19956	3.02	2.62	1.22	0.53	2.39	2.10
COR1	P07256	3.68	2.62	0.71	-0.63	3.01	3.25
MSS51	P32335	2.05	2.61	0.52	0.13	1.97	2.48
PIF1	P07271	2.62	2.61	3.29	-0.91	3.11	3.53
ARG5,6	Q01217	5.10	2.61	1.30	0.19	4.57	2.42
ATP25	Q03153	2.35	2.56	2.84	1.42	1.13	1.14
PIS1	P06197	1.15	2.56	0.97	2.06	0.62	0.50
RPL33A	P05744	2.57	2.54	1.95	1.51	0.96	1.04
DIA4	P38705	2.25	2.54	3.28	1.64	0.85	0.90
MRPS8	Q03799	3.33	2.53	4.75	1.78	1.39	0.75
PST2	Q12335	4.94	2.51	0.40	0.37	2.24	2.14
SEC4	P07560	2.36	2.50	2.24	1.17	1.29	1.33
PET111	P08468	2.56	2.47	4.36	-1.69	3.40	4.16
SOD2	P00447	2.53	2.44	4.11	0.92	1.79	1.52
MRS1	P07266	3.38	2.42	1.26	1.39	0.86	1.03
ERG6	P25087	1.79	2.42	3.44	-0.79	2.21	3.21
CBS1	P14066	0.80	2.40	0.01	-0.03	1.45	2.43

Table B.8: Candidates identified in proximity labelling assay followed by Mass Spectrometry

Gene names	Protein IDs	Pda1-T vs. WT		Pda1-T vs. Floaty-T		Floaty-T vs. WT	
		P-value	Fold change	P-value	Fold change	P-value	Fold change
TES1	P41903	1.03	2.39	0.35	0.90	1.44	1.49
YJL147C	P47007	2.70	2.39	2.01	0.83	1.88	1.56
JEN1	P36035	0.94	2.38	0.81	2.00	0.42	0.38
SPF1	P39986	2.66	2.37	0.51	0.55	1.47	1.83
OLE1	P21147	2.19	2.37	1.52	0.79	1.44	1.58
SLM3	Q12093	4.68	2.36	1.68	1.80	0.50	0.57
RSM23	Q01163	2.85	2.36	0.79	0.86	1.21	1.50
CDS1	P38221	2.08	2.36	2.15	1.25	0.96	1.11
MRPL24	P36525	2.22	2.35	4.74	1.46	0.93	0.89
FMP40	Q08968	2.70	2.33	1.73	0.92	1.61	1.42
MTG1	Q03151	3.48	2.33	1.65	0.70	2.37	1.63
RHO1	P06780	1.34	2.32	0.04	-0.04	1.30	2.36
SAC1	P32368	3.14	2.32	0.62	-0.21	3.10	2.53
YML6	P51998	2.50	2.31	2.74	1.39	1.14	0.93
GRX2	P17695	2.16	2.31	3.39	0.85	1.50	1.46
RPL11B	Q3E757	2.50	2.31	2.90	1.12	1.43	1.19
AIM10	P39965	3.15	2.30	2.11	1.31	1.31	1.00
SOV1	Q04748	2.86	2.27	2.00	1.28	1.16	0.99
FAA1	P30624	2.26	2.27	0.38	0.51	1.21	1.76
MSS18	P08593	3.02	2.26	6.36	1.89	0.65	0.38
YME2	P32843	2.67	2.24	2.67	-0.81	3.19	3.05
ISM1	P48526	2.71	2.24	0.66	0.58	1.51	1.65
YER077C	P40050	2.05	2.21	2.64	-1.64	3.17	3.85
AIM25	P47140	3.03	2.19	4.63	-1.49	3.87	3.68
MTO1	P53070	2.54	2.16	1.98	2.14	0.01	0.02
RPO41	P13433	1.61	2.15	2.62	-1.11	2.20	3.26
RPS6B	P0CX38	1.58	2.15	0.53	1.00	0.52	1.15
POS5	Q06892	2.81	2.13	0.75	0.14	2.77	1.99
ISA2	Q12425	1.66	2.10	0.08	-0.10	1.81	2.21
MRH4	P53166	2.69	2.10	0.52	0.24	2.28	1.86
PDH1	Q12428	2.79	2.08	0.92	0.92	1.38	1.16
RPS11B	P0CX48	1.20	2.06	0.10	0.23	2.09	1.83
DUS1	P53759	2.73	2.05	3.02	0.92	1.72	1.13
TDH2	P00358	3.06	2.05	3.44	1.01	1.89	1.03
YLR283W	Q05867	1.25	2.02	2.97	1.39	0.34	0.64
RRG9	P40156	2.84	2.02	0.87	0.44	1.99	1.59
LYS4	P49367	2.18	2.02	2.78	1.27	0.83	0.75
RPS8B	P0CX40	4.12	1.96	0.25	0.38	1.23	1.59
MRPL39	P36533	1.20	1.95	0.63	0.78	1.05	1.18
ATP15	P21306	2.38	1.94	0.33	0.14	2.25	1.80
COX5A	P00424	0.91	1.92	0.46	0.94	0.98	0.98
LCB2	P40970	1.60	1.91	1.23	0.49	1.16	1.41
ERG3	P32353	2.66	1.86	0.18	0.27	1.20	1.59
ARG7	Q04728	0.89	1.85	0.03	-0.09	2.00	1.93
PUS9	Q12069	1.98	1.83	2.75	1.23	0.62	0.60
TAM41	P53230	3.44	1.83	2.31	-1.02	3.56	2.85
EXO5	P38289	1.90	1.83	0.92	0.55	1.20	1.28
YSA1	Q01976	3.15	1.80	0.17	0.19	1.66	1.61
TY1B-PL	Q12414	3.71	1.77	1.46	0.70	2.28	1.08
HXT7	P39004	3.24	1.75	0.21	0.06	3.27	1.69
PTC5	Q12511	3.18	1.75	0.11	-0.09	2.30	1.83
BAT1	P38891	2.88	1.74	0.65	-0.26	3.02	2.00
YNR040W	P53736	0.73	1.74	1.04	-2.35	2.43	4.09
MTF1	P14908	1.19	1.73	0.58	0.45	0.77	1.28
RRG8	Q06109	1.09	1.72	0.76	0.77	0.47	0.95

Table B.8: Candidates identified in proximity labelling assay followed by Mass Spectrometry

Gene names	Protein IDs	Pda1-T vs. WT		Pda1-T vs. Floaty-T		Floaty-T vs. WT	
		P-value	Fold change	P-value	Fold change	P-value	Fold change
MGR2	Q02889	1.13	1.70	0.06	0.11	1.63	1.59
MSM1	P22438	1.69	1.69	1.40	0.60	1.05	1.09
BBC1	P47068	1.35	1.69	0.32	0.44	1.11	1.25
FMP41	P53889	1.67	1.69	1.04	0.48	1.16	1.20
CHO2	P05374	0.74	1.69	0.22	0.58	1.63	1.11
ACO2	P39533	2.89	1.68	0.65	0.66	0.95	1.01
RSM18	P40033	1.38	1.67	0.70	0.82	1.26	0.85
STT3	P39007	1.47	1.65	0.76	-0.44	1.64	2.09
GEP5	Q12393	1.33	1.62	0.08	0.09	1.01	1.53
PET112	P33893	4.98	1.60	2.36	0.48	3.47	1.12
LEU9	Q12166	2.47	1.60	2.80	0.97	1.05	0.62
YHM2	Q04013	4.82	1.56	1.39	0.19	5.10	1.37
BCS1	P32839	1.55	1.54	0.62	0.79	0.66	0.75
LIP2	Q06005	0.83	1.53	0.36	0.78	0.81	0.75
DSS1	P39112	1.62	1.53	1.92	1.24	0.21	0.28
CLD1	P53264	1.47	1.51	0.13	0.24	0.93	1.27
AIM39	Q08223	1.56	1.50	2.56	-1.19	2.47	2.69
YCP4	P25349	0.77	1.50	0.67	0.91	0.21	0.60
IFA38	P38286	1.24	1.50	0.76	-0.37	1.44	1.87
YNR021W	P53723	1.13	1.49	2.15	1.10	0.25	0.40
GAL2	P13181	3.69	1.49	0.53	0.14	4.03	1.34
DFM1	Q12743	2.22	1.47	0.05	-0.05	1.54	1.52
TCM62	P38228	1.45	1.47	0.05	0.05	1.14	1.42
RIM2	P38127	1.38	1.47	0.10	0.12	0.97	1.35
OXA1	P39952	4.06	1.46	1.77	0.99	0.82	0.47
DUG1	P43616	1.62	1.46	2.41	1.30	0.12	0.16
ISA1	Q07821	1.86	1.35	1.68	0.63	0.92	0.72
ATP16	Q12165	1.30	1.34	1.57	1.14	0.14	0.21
CBP2	P03874	0.51	1.31	0.20	0.58	0.64	0.73
PET8	P38921	1.17	1.31	0.04	0.03	1.28	1.27
FMP52	P40008	0.56	1.28	0.03	-0.04	0.57	1.32
aI3	P03877	1.10	1.27	0.13	0.21	1.19	1.06
MMT1	Q03218	0.94	1.26	0.12	0.23	0.50	1.02
SAM35	P14693	2.53	1.25	0.42	-0.19	3.31	1.44
COX10	P21592	0.45	1.25	1.15	-2.44	1.96	3.69
SEC61	P32915	0.60	1.25	0.01	-0.02	1.29	1.26
RPL25	P04456	0.76	1.24	0.18	0.35	0.68	0.89
YPR114W	Q06107	1.11	1.23	0.29	0.48	0.62	0.75
ATP1	P07251	2.99	1.22	1.23	-0.20	3.11	1.42
LEU4	P06208	2.50	1.22	4.83	-0.68	3.24	1.90
EHD3	P28817	1.51	1.22	0.04	-0.02	1.41	1.24
GAL1	P04385	1.36	1.20	0.08	0.15	0.60	1.05
MSK1	P32048	3.76	1.20	1.47	0.74	0.86	0.46
SED4	P25365	2.30	1.19	0.36	0.22	1.41	0.98
YTA12	P40341	1.30	1.15	2.73	-2.10	3.39	3.25
AIM19	P40502	4.35	1.15	0.57	-0.29	2.55	1.43
MIR1	P23641	3.01	1.12	1.28	-0.45	2.83	1.56
ARH1	P48360	2.23	1.11	0.04	-0.05	1.10	1.16
PET9	P18239	2.21	1.09	1.08	-0.58	2.43	1.67
PMA1	P05030	3.15	1.00	1.78	-0.75	2.91	1.75
FOL1	P53848	2.16	0.99	1.49	-0.88	3.20	1.87
GAL7	P08431	0.61	0.98	0.31	-0.77	0.64	1.75
MEU1	Q07938	0.61	0.97	0.16	0.20	0.60	0.77
YMR252C	Q04814	0.49	0.96	0.23	0.46	0.43	0.50
YHL018W	P38744	0.75	0.92	0.14	0.21	0.67	0.71

Table B.8: Candidates identified in proximity labelling assay followed by Mass Spectrometry

Gene names	Protein IDs	Pda1-T vs. WT		Pda1-T vs. Floaty-T		Floaty-T vs. WT	
		P-value	Fold change	P-value	Fold change	P-value	Fold change
MSS1	P32559	1.21	0.91	0.01	-0.01	0.84	0.92
VPS21	P36017	1.16	0.89	0.12	0.04	1.05	0.84
YFR045W	P43617	1.41	0.89	0.64	0.62	0.20	0.27
MSW1	P04803	0.50	0.86	0.39	0.45	0.23	0.41
AIM34	Q03673	1.29	0.83	0.93	-2.67	1.22	3.49
MSH1	P25846	0.37	0.82	1.22	-0.24	0.50	1.07
POR1	P04840	3.74	0.80	0.51	-0.06	4.90	0.86
AEP2	P22136	0.86	0.79	0.44	-0.31	1.08	1.11
RPL17A	P05740	0.50	0.79	0.30	-0.43	1.26	1.22
MMT2	Q08970	0.39	0.76	1.29	-2.24	5.67	3.00
YJR003C	P47084	1.05	0.75	0.05	0.06	1.25	0.69
SLC1	P33333	0.62	0.75	0.04	-0.05	0.66	0.80
SLM5	P25345	0.59	0.73	0.23	-0.13	0.66	0.86
SUV3	P32580	1.29	0.72	0.17	0.15	0.63	0.58
NAT2	P37293	0.51	0.72	2.36	-2.64	2.55	3.35
RML2	P32611	0.26	0.71	5.17	-1.33	0.86	2.04
CCE1	Q03702	0.54	0.69	0.84	-0.49	1.07	1.18
STE24	P47154	0.68	0.68	0.58	0.37	0.24	0.31
CBR1	P38626	0.50	0.68	0.84	-0.89	2.05	1.57
ASC1	P38011	0.47	0.66	0.58	-0.81	2.24	1.47
YDL177C	Q12257	1.04	0.64	0.26	-0.38	0.72	1.01
SCS2	P40075	0.70	0.61	1.37	-0.36	1.12	0.96
MIP1	P15801	0.48	0.60	1.80	-1.75	2.42	2.35
NNR2	P36059	0.91	0.56	0.20	0.20	0.30	0.36
GAL10	P04397	0.39	0.54	0.21	-0.13	0.47	0.67
SAP1	P39955	0.37	0.45	0.51	-0.57	0.65	1.02
NTA1	P40354	0.74	0.40	1.91	-0.73	1.86	1.13
YML020W	Q03722	0.28	0.33	1.57	-1.10	1.72	1.43
YDR336W	Q05473	1.02	0.32	0.59	-0.47	1.12	0.79
ODC1	Q03028	0.40	0.30	4.25	-3.08	3.55	3.38
RTN1	Q04947	0.67	0.23	0.79	-0.84	0.97	1.06
AAC1	P04710	0.14	0.23	0.89	-3.08	0.94	3.31
MFB1	Q04922	0.15	0.21	0.44	-0.35	0.42	0.56
AEP3	Q12089	0.08	0.16	0.36	-0.63	0.51	0.78
INA17	Q02888	0.11	0.15	1.01	-3.43	1.04	3.58
RPS14A	P06367	0.05	0.15	0.07	-0.16	0.09	0.30
SAL1	D6W196	0.31	0.13	1.64	-1.06	1.60	1.18
PHB2	P50085	0.03	0.04	2.05	-2.08	2.26	2.12
PHO88	P38264	0.19	-0.24	1.34	-1.30	1.47	1.06
RAS2	P01120	0.09	-0.25	0.78	-0.80	0.24	0.55
CDC19	P00549	0.21	-0.43	0.75	-0.67	0.11	0.24
TEF1	P02994	2.10	-0.44	3.43	-1.70	3.10	1.26
ACT1	P60010	1.70	-0.56	2.07	-1.23	1.36	0.67
CWP1	P28319	0.99	-0.71	0.73	0.98	1.16	-1.69
RPL10	P41805	0.60	-0.89	1.46	-1.72	0.91	0.82
RPS31	P05759	5.65	-1.66	4.45	-1.63	0.15	-0.03
MRH1	Q12117	3.12	-1.69	4.39	-1.77	0.17	0.08
RNQ1	P25367	1.81	-1.78	0.28	0.16	2.07	-1.94
RPL34A	P87262	0.80	-2.01	0.70	-1.21	0.25	-0.80
RPL15A	P05748	0.86	-2.37	0.89	-2.44	0.26	0.08
PYC1	P11154	4.56	-2.58	4.05	-2.16	1.99	-0.42
LSP1	Q12230	3.01	-2.59	1.33	-1.66	0.80	-0.94
DUR1,2	P32528	2.84	-2.67	1.95	-1.66	1.82	-1.01
ARC1	P46672	4.95	-2.77	2.72	-0.83	4.52	-1.95
SEC28	P40509	5.13	-3.33	0.24	0.16	3.64	-3.49

Table B.8: Candidates identified in proximity labelling assay followed by Mass Spectrometry

Gene names	Protein IDs	Pda1-T vs. WT		Pda1-T vs. Floaty-T		Floaty-T vs. WT	
		P-value	Fold change	P-value	Fold change	P-value	Fold change
PYC2	P32327	3.54	-3.62	3.28	-3.20	1.90	-0.43
ACC1	Q00955	6.21	-3.69	5.46	-3.25	2.52	-0.44
RPA43	P46669	5.79	-4.75	5.79	-1.64	5.04	-3.11
HFA1	P32874	5.02	-6.46	4.70	-5.91	2.10	-0.55

B.9 Mass Spectrometry data from Myc tag Co-immunoprecipitation

The raw data obtained from the Mass Spectrometry analysis is available on Osman Lab servers. For the following table, all identified candidates are listed along with their P-values (on a $-\log_{10}$ scale), as well as fold changes (on a \log_2 scale), as calculated from four replicates. The $-\log_{10}$ P-values and \log_2 fold changes are listed upon comparison of Yme2-9Myc sample against the WT sample.

Table B.9: Candidates identified in Myc tag Mass Spectrometry (Yme2-9Myc vs. WT)

P-value	Fold change	Gene Names	Protein IDs	Protein Names
0.00	7.79	Yme2- Myc	-	-
0.00	7.54	YME2	P32843	Mitochondrial escape protein 2
0.04	4.06	PDA1	P16387	Pyruvate dehydrogenase E1 component subunit alpha, mitochondrial
0.03	3.96	LAT1	P12695	Dihydrolipoyllysine-residue acetyltransferase component of pyruvate dehydrogenase complex, mitochondrial
0.02	2.72	PDB1	P32473	Pyruvate dehydrogenase E1 component subunit beta, mitochondrial
0.02	2.55	MRPL11	P36521	54S ribosomal protein L11, mitochondrial
0.10	1.80	LPD1	P09624	Dihydrolipoyl dehydrogenase, mitochondrial
0.00	1.40	PET127	P32606	Putative mitochondrial translation system component PET127
0.00	1.30	RMD9	P53140	Protein RMD9, mitochondrial
0.01	1.29	ALD4	P46367	Potassium-activated aldehyde dehydrogenase, mitochondrial
0.00	1.22	IDH2	P28241	Isocitrate dehydrogenase [NAD] subunit 2, mitochondrial
0.16	1.20	MIC60	P36112	MICOS complex subunit MIC60
0.02	1.12	MGM101	P32787	Mitochondrial genome maintenance protein MGM101
0.26	0.93	PDX1	P16451	Pyruvate dehydrogenase complex protein X component, mitochondrial
0.19	0.91	TCB3	Q03640	Tricalbin-3
0.40	0.89	YTA12	P40341	Mitochondrial respiratory chain complexes assembly protein YTA12
0.24	0.85	TUF1	P02992	Elongation factor Tu, mitochondrial
0.40	0.78	ILV5	P06168	Ketol-acid reductoisomerase, mitochondrial
0.28	0.72	IDH1	P28834	Isocitrate dehydrogenase [NAD] subunit 1, mitochondrial
0.24	0.69	CIT1	P00890	Citrate synthase, mitochondrial
0.07	0.62	POR1	P04840	Mitochondrial outer membrane protein porin 1
0.30	0.61	LSC2	P53312	Succinyl-CoA ligase [ADP-forming] subunit beta, mitochondrial
0.36	0.59	NFS1	P25374	Cysteine desulfurase, mitochondrial

Table B.9: Candidates identified in Myc tag Mass Spectrometry (Yme2-9Myc vs. WT)

P-value	Fold change	Gene Names	Protein IDs	Protein Names
0.11	0.58	TCB1	Q12466	Tricalbin-1
0.56	0.53	RPM2	Q02773	Ribonuclease P protein component, mitochondrial
0.41	0.48	OMS1	Q06668	Methyltransferase OMS1, mitochondrial
0.43	0.43	YPP1	P46951	Cargo-transport protein YPP1
0.66	0.41	KAR2	P16474	78 kDa glucose-regulated protein homolog
0.02	0.40	BAT1	P38891	Branched-chain-amino-acid aminotransferase, mitochondrial
0.00	0.40	NUC1	P08466	Mitochondrial nuclease
0.35	0.38	KGD1	P20967	2-oxoglutarate dehydrogenase, mitochondrial
0.26	0.34	ILV2	P07342	Acetolactate synthase catalytic subunit, mitochondrial
0.06	0.31	MDJ1	P35191	DnaJ homolog 1, mitochondrial
0.57	0.29	MIS1	P09440	C-1-tetrahydrofolate synthase, mitochondrial;Methylenetetrahydrofolate dehydrogenase;Methenyltetrahydrofolate cyclohydrolase;Formyltetrahydrofolate synthetase
0.50	0.27	RPO41	P13433	DNA-directed RNA polymerase, mitochondrial
0.03	0.27	PHB2	P50085	Prohibitin-2
0.15	0.23	PHB1	P40961	Prohibitin-1
0.17	0.21	TIM50	Q02776	Mitochondrial import inner membrane translocase subunit TIM50
0.76	0.21	NAM9	P27929	37S ribosomal protein NAM9, mitochondrial
0.28	0.20	KGD2	P19262	Dihydrolipoyllysine-residue succinyltransferase component of 2-oxoglutarate dehydrogenase complex, mitochondrial
0.64	0.18	ILV3	P39522	Dihydroxy-acid dehydratase, mitochondrial
0.21	0.13	TIM44	Q01852	Mitochondrial import inner membrane translocase subunit TIM44
0.71	0.09	YME1	P32795	Mitochondrial inner membrane i-AAA protease supercomplex subunit YME1
0.80	0.07	HSP60	P19882	Heat shock protein 60, mitochondrial
0.91	0.05	YDJ1	P25491	Mitochondrial protein import protein MAS5
0.96	0.02	CIR2	Q08822	Probable electron transfer flavoprotein-ubiquinone oxidoreductase, mitochondrial
0.98	0.00	DSS1	P39112	Exoribonuclease II, mitochondrial
0.98	-0.01	MDL2	P33311	ATP-dependent permease MDL2, mitochondrial
0.89	-0.04	ACO1	P19414	Aconitate hydratase, mitochondrial
0.80	-0.04	QCR2	P07257	Cytochrome b-c1 complex subunit 2, mitochondrial
0.92	-0.05	MDH1	P17505	Malate dehydrogenase, mitochondrial

Table B.9: Candidates identified in Myc tag Mass Spectrometry (Yme2-9Myc vs. WT)

P-value	Fold change	Gene Names	Protein IDs	Protein Names
0.81	-0.06	SHY1	P53266	Cytochrome oxidase assembly protein SHY1
0.71	-0.11	NDE1	P40215	External NADH-ubiquinone oxidoreductase 1, mitochondrial
0.28	-0.12	ATP2	P00830	ATP synthase subunit beta, mitochondrial
0.60	-0.12	MRPL3	P36516	54S ribosomal protein L3, mitochondrial
0.63	-0.13	SSC1	P0CS90	Heat shock protein SSC1, mitochondrial
0.53	-0.16	MRPL40	P36534	54S ribosomal protein L40, mitochondrial
0.34	-0.16	ATP1	P07251	ATP synthase subunit alpha, mitochondrial
0.84	-0.17	FUM1	P08417	Fumarate hydratase, mitochondrial
0.45	-0.19	COR1	P07256	Cytochrome b-c1 complex subunit 1, mitochondrial
0.53	-0.20	MDM38	Q08179	Mitochondrial distribution and morphology protein 38
0.64	-0.22	MYO2	P19524	Myosin-2
0.43	-0.27	MSS116	P15424	ATP-dependent RNA helicase MSS116, mitochondrial
0.23	-0.28	CBP3	P21560	Protein CBP3, mitochondrial
0.71	-0.29	PUT2	P07275	Delta-1-pyrroline-5-carboxylate dehydrogenase, mitochondrial
0.46	-0.31	TIM54	P47045	Mitochondrial import inner membrane translocase subunit TIM54
0.28	-0.38	YSP2	Q06681	GRAM domain-containing protein YSP2
0.15	-0.40	NDI1	P32340	Rotenone-insensitive NADH-ubiquinone oxidoreductase, mitochondrial
0.51	-0.46	MRPL22	P53881	54S ribosomal protein L22, mitochondrial
0.41	-0.47	MIA40	P36046	Mitochondrial intermembrane space import and assembly protein 40
0.18	-0.48	TY1B-H	O13535	Transposon Ty1-H Gag-Pol polyprotein
0.09	-0.52	MRPL17	P36528	54S ribosomal protein L17, mitochondrial
0.04	-0.53	COX1	P00401	Cytochrome c oxidase subunit 1
0.26	-0.53	RML2	P32611	54S ribosomal protein RML2, mitochondrial
0.17	-0.54	DLD1	P32891	D-lactate dehydrogenase [cytochrome] 1, mitochondrial
0.17	-0.54	PET54	P10834	Protein PET54
0.49	-0.57	AFG3	P39925	Mitochondrial respiratory chain complexes assembly protein AFG3
0.33	-0.58	ILV1	P00927	Threonine dehydratase, mitochondrial
0.09	-0.62	COX2	P00410	Cytochrome c oxidase subunit 2
0.13	-0.64	SDH1	Q00711	Succinate dehydrogenase [ubiquinone] flavoprotein subunit, mitochondrial

Table B.9: Candidates identified in Myc tag Mass Spectrometry (Yme2-9Myc vs. WT)

P-value	Fold change	Gene Names	Protein IDs	Protein Names
0.08	-0.67	GUT2	P32191	Glycerol-3-phosphate dehydrogenase, mitochondrial
0.33	-0.70	MRPL4	P36517	54S ribosomal protein L4, mitochondrial
0.30	-0.73	ASM4	Q05166	Nucleoporin ASM4
0.09	-0.74	HMG1	P12683	3-hydroxy-3-methylglutaryl-coenzyme A reductase 1
0.05	-0.84	CYT1	P07143	Cytochrome c1, heme protein, mitochondrial
0.05	-0.90	PET9	P18239	ADP,ATP carrier protein 2
0.32	-0.91	MRP7	P12687	54S ribosomal protein L2, mitochondrial
0.03	-0.93	TRM1	P15565	tRNA (guanine(26)-N(2))-dimethyltransferase, mitochondrial
0.04	-1.04	MIR1	P23641	Mitochondrial phosphate carrier protein;Mitochondrial phosphate carrier protein, N-terminally processed
0.02	-1.06	AAC1	P04710	ADP,ATP carrier protein 1
0.25	-1.06	ATP4	P05626	ATP synthase subunit 4, mitochondrial
0.00	-1.10	TEF1	P02994	Elongation factor 1-alpha
0.22	-1.12	MRPL15	P36523	54S ribosomal protein L15, mitochondrial
0.00	-1.12	SAM1	P10659	S-adenosylmethionine synthase 1;S-adenosylmethionine synthase 2
0.18	-1.15	OAC1	P32332	Mitochondrial oxaloacetate transport protein
0.23	-1.15	GGC1	P38988	Mitochondrial GTP/GDP carrier protein 1
0.47	-1.16	LEU4	P06208	2-isopropylmalate synthase
0.02	-1.25	LSC1	P53598	Succinyl-CoA ligase [ADP-forming] subunit alpha, mitochondrial
0.02	-1.25	NUP170	P38181	Nucleoporin NUP170
0.19	-1.27	MRPL35	Q06678	54S ribosomal protein L35, mitochondrial
0.08	-1.29	FKS1	P38631	1,3-beta-glucan synthase component FKS1
0.05	-1.36	GAL7	P08431	Galactose-1-phosphate uridylyltransferase
0.14	-1.43	MRPL1	Q04599	54S ribosomal protein L1, mitochondrial
0.05	-1.53	COX15	P40086	Cytochrome c oxidase assembly protein COX15
0.01	-1.55	MSC6	Q08818	Meiotic sister-chromatid recombination protein 6, mitochondrial
0.00	-1.58	VMA2	P16140	V-type proton ATPase subunit B
0.02	-1.65	NOP58	Q12499	Nucleolar protein 58
0.00	-1.71	PIL1	P53252	Sphingolipid long chain base-responsive protein PIL1
0.15	-1.72	RPL4B	P49626	60S ribosomal protein L4-B;60S ribosomal protein L4-A
0.07	-1.73	GAL1	P04385	Galactokinase

Table B.9: Candidates identified in Myc tag Mass Spectrometry (Yme2-9Myc vs. WT)

P-value	Fold change	Gene Names	Protein IDs	Protein Names
0.11	-1.74	HSP42	Q12329	Heat shock protein 42
0.14	-1.75	RPL6A	Q02326	60S ribosomal protein L6-A
0.17	-1.84	RPL7B	Q12213	60S ribosomal protein L7-B;60S ribosomal protein L7-A
0.10	-1.87	RIP1	P08067	Cytochrome b-c1 complex subunit Rieske, mitochondrial
0.04	-1.89	ATP3	P38077	ATP synthase subunit gamma, mitochondrial
0.01	-1.89	GAL10	P04397	Bifunctional protein GAL10;UDP-glucose 4-epimerase;Aldose 1-epimerase
0.05	-1.98	NUP157	P40064	Nucleoporin NUP157
0.00	-2.03	ACT1	P60010	Actin
0.07	-2.27	RPL2B	P0CX46	60S ribosomal protein L2-B;60S ribosomal protein L2-A
0.01	-2.83	SDH2	P21801	Succinate dehydrogenase [ubiquinone] iron-sulfur subunit, mitochondrial
0.00	-3.07	RPP0	P05317	60S acidic ribosomal protein P0
0.01	-3.22	LSP1	Q12230	Sphingolipid long chain base-responsive protein LSP1
0.00	-3.41	YHM2	Q04013	Citrate/oxoglutarate carrier protein
0.00	-4.26	POM152	P39685	Nucleoporin POM152

Curriculum vitae



NUPUR SHARMA

Personal Info

✉ nupur121995@gmail.com

☎ +49-15171320388

🌐 [linkedin.com/in/nupursharma1995](https://www.linkedin.com/in/nupursharma1995)

🏠 München, Germany

Model Organisms

Yeast- *S. cerevisiae*

Bacteria- *E.coli*, *B.subtilis*,
M.smegmatis

Bacteriophages

Worms- *C.elegans*

Mammalian cells

Technical Skills

Molecular Biology Techniques (DNA and RNA)

Protein Biochemistry, Expression and Purification

Proteomics- Mass Spectrometry sample preparation and Data analysis using Max Quant

Assays- Bacteriophage, ATP Production, mitochondrial isolation & manipulation

Microscopy- Light, DIC, Fluorescence

Software Skills

Structural Biology- Pymol, MAESTRO, RosettaFold, AlphaFold

Programming Languages- Python, SQL, HTML

Graphic Design- Adobe InDesign, Affinity Designer, CorelDRAW, Adobe Illustrator

Traceability Tool- Benchling

MS Office Suite

Professional Experience

04.2020- Present **Molecular and Cell Biologist (PhD Student)**

AG Osman, Ludwig Maximilians University (LMU), Munich, Germany

Project Title- Unraveling novel roles in the mitochondrial DNA interactome: Functional insights into the Pyruvate dehydrogenase complex and Yme2

Publication- Sharma, Nupur and Osman, Christof. Biological Chemistry, vol. 403, no. 8-9, 2022, pp. 807-817. <https://doi.org/10.1515/hsz-2021-0398>

04.2019-10.2019 **Molecular and Cell Biologist (Master's Dissertation)**

AG Bramkamp, LMU, Munich, Germany

Project Title- The role of a bacterial dynamin-like protein in phage defence

10.2018-03.2020 **Working Student (Wissenschaftlicher Hilfsarbeiterin)**

Eisbach Bio GmbH, Munich, Germany (03.2019-03.2020)

Protein recombinant expression and biochemistry.

AG Korn, Klinikum Rechts der Isar, Munich, Germany (10.2018-12.2019)

Genotyping of mice tails and confirmation of strain identity for experimental validation.

Faculty of Biology, LMU, Munich, Germany (10.2018-10.2019)

Tutoring 'Introduction to Lab Sciences and Methods' course to incoming master's students.

Social Contributions

2024- **PhD Representative**

2025 Faculty of Biology, LMU, Munich, Germany

2022- **Vice President, Student Council**

2024 Life Sciences Munich Graduate School (LSM), LMU, Munich, Germany

🔗 Mental Health Outreach Initiative

🔗 Networking Events Organizer

🔗 Mentorship Agreement

🔗 Onboarding Initiative

2023- **Retreat Organizer**

2024 AG Osman (LMU) & AG Ott (University of Gothenburg); Tjarnö Marine Laboratory, Sweden (2024)

AG Osman (LMU); Zillertal, Austria (2023)

LSM Graduate School (LMU); Munich (2021)

2015- **Organizer**

2014 Blood Donation Camp- National Service Scheme, Ministry of Youth Affairs and Sports, Government of India, India

UK-India Education and Research Initiative, Study India Programme, India

Science Communications Contributions

2021- **Head, Newsletter Committee**

2024 LSM Graduate School, LMU, Munich, Germany

2014- **Editor-in-Chief & Design Editor**

2016 Science Journal- EUREKA University of Delhi, New Delhi, India

Workshops

2023 Scientific Writing

2023 Industrial Pharma Management

2021 Global Manufacturing Practices

2020 Good Scientific Practices

Education

2017-19 Master's in Biology, LMU, Munich, Germany (1,03)

2016-17 M.Sc (Microbiology), University of Delhi, New Delhi, India (78.3%)

2013-16 B.Sc Honours (Microbiology), University of Delhi, New Delhi, India (82.04%)

Languages

English (Native)

German (B1- intermediate)

D Publications

A part of this study has been published by the author in the following publication.

Sharma, N. and Osman, C. (2022). Yme2, a putative RNA recognition motif and AAA+ domain containing protein, genetically interacts with the mitochondrial protein export machinery. *Biological Chemistry*, 403(8-9), 807-817. <https://doi.org/10.1515/hsz-2021-0398>.

** Figures published in the aforementioned manuscript have also been adapted fully, or in part, in this thesis (Licensed under CC BY 4.0).

Bibliography

- Abramson, J., Adler, J., Dunger, J., Evans, R., Green, T., Pritzel, A., Ronneberger, O., Willmore, L., Ballard, A. J., Bambrick, J., Bodenstein, S. W., Evans, D. A., Hung, C.-C., O'Neill, M., Reiman, D., Tunyasuvunakool, K., Wu, Z., Žemgulytė, A., Arvaniti, E., . . . Jumper, J. M. (2024). Accurate structure prediction of biomolecular interactions with alphafold 3. *Nature*, *630*(8016), 493–500. <https://doi.org/10.1038/s41586-024-07487-w>
- Acín-Pérez, R., Fernández-Silva, P., Peleato, M. L., Pérez-Martos, A., & Enriquez, J. A. (2008). Respiratory active mitochondrial supercomplexes. *Molecular cell*, *32*(4), 529–539. <https://doi.org/10.1016/j.molcel.2008.10.021>
- Amunts, A., Brown, A., Bai, X.-C., Llácer, J. L., Hussain, T., Emsley, P., Long, F., Murshudov, G., Scheres, S. H. W., & Ramakrishnan, V. (2014). Structure of the yeast mitochondrial large ribosomal subunit. *Science (New York, N.Y.)*, *343*(6178), 1485–1489. <https://doi.org/10.1126/science.1249410>
- Andersson, S. G., Zomorodipour, A., Andersson, J. O., Sicheritz-Pontén, T., Alsmark, U. C., Podowski, R. M., Näslund, A. K., Eriksson, A. S., Winkler, H. H., & Kurland, C. G. (1998). The genome sequence of rickettsia prowazekii and the origin of mitochondria. *Nature*, *396*(6707), 133–140. <https://doi.org/10.1038/24094>
- Arlt, H., Tauer, R., Feldmann, H., Neupert, W., & Langer, T. (1996). The yta10–12 complex, an aaa protease with chaperone-like activity in the inner membrane of mitochondria. *Cell*, *85*(6), 875–885. [https://doi.org/10.1016/s0092-8674\(00\)81271-4](https://doi.org/10.1016/s0092-8674(00)81271-4)
- Arnold, P. K., & Finley, L. W. S. (2023). Regulation and function of the mammalian tricarboxylic acid cycle. *Journal of Biological Chemistry*, *299*(2), 102838. <https://doi.org/10.1016/j.jbc.2022.102838>
- Baile, M. G., & Claypool, S. M. (2013). The power of yeast to model diseases of the powerhouse of the cell. *Frontiers in bioscience (Landmark edition)*, *18*(1), 241–278. <https://doi.org/10.2741/4098>
- Barros, M. H., & McStay, G. P. (2020). Modular biogenesis of mitochondrial respiratory complexes. *Mitochondrion*, *50*, 94–114. <https://doi.org/10.1016/j.mito.2019.10.008>
- Basch, M., Wagner, M., Rolland, S., Carbonell, A., Zeng, R., Khosravi, S., Schmidt, A., Aftab, W., Imhof, A., Wagener, J., Conradt, B., & Wagener, N. (2020). Msp1 cooperates with the proteasome for extraction of arrested mitochondrial import intermediates. *Molecular Biology of the Cell*, *31*(8), 753–767. <https://doi.org/10.1091/mbc.E19-06-0329>
- Bauerschmitt, H., Mick, D. U., Deckers, M., Vollmer, C., Funes, S., Kehrein, K., Ott, M., Rehling, P., & Herrmann, J. M. (2010). Ribosome-binding

- proteins mdm38 and mba1 display overlapping functions for regulation of mitochondrial translation. *Molecular Biology of the Cell*, 21(12), 1937–1944. <https://doi.org/10.1091/mbc.e10-02-0101>
- Becker, T., Gebert, M., Pfanner, N., & van der Laan, M. (2009). Biogenesis of mitochondrial membrane proteins. *Current Opinion in Cell Biology*, 21(4), 484–493. <https://doi.org/10.1016/j.ceb.2009.04.002>
- Bender, T., Pena, G., & Martinou, J.-C. (2015). Regulation of mitochondrial pyruvate uptake by alternative pyruvate carrier complexes. *The EMBO Journal*, 34(7), 911–924. <https://doi.org/10.15252/emboj.201490197>
- Bieri, P., Greber, B. J., & Ban, N. (2018). High-resolution structures of mitochondrial ribosomes and their functional implications. *Current opinion in structural biology*, 49, 44–53. <https://doi.org/10.1016/j.sbi.2017.12.009>
- Boczonadi, V., & Horvath, R. (2014). Mitochondria: Impaired mitochondrial translation in human disease. *The international journal of biochemistry & cell biology*, 48(100), 77–84. <https://doi.org/10.1016/j.biocel.2013.12.011>
- Bogenghagen, D. F., Martin, D. W., & Koller, A. (2014). Initial steps in rna processing and ribosome assembly occur at mitochondrial dna nucleoids. *Cell metabolism*, 19(4), 618–629. <https://doi.org/10.1016/j.cmet.2014.03.013>
- Bogenghagen, D. F., Wang, Y., Shen, E. L., & Kobayashi, R. (2003). Protein components of mitochondrial dna nucleoids in higher eukaryotes. *Molecular & cellular proteomics : MCP*, 2(11), 1205–1216. <https://doi.org/10.1074/mcp.M300035-MCP200>
- Bohne, A.-V., Schwarz, C., Schottkowski, M., Lidschreiber, M., Piotrowski, M., Zerges, W., & Nickelsen, J. (2013). Reciprocal regulation of protein synthesis and carbon metabolism for thylakoid membrane biogenesis. *PLoS biology*, 11(2), e1001482. <https://doi.org/10.1371/journal.pbio.1001482>
- Bonekamp, N. A., Jiang, M., Motori, E., Garcia Villegas, R., Koolmeister, C., Atanassov, I., Mesaros, A., Park, C. B., & Larsson, N.-G. (2021). High levels of tfam repress mammalian mitochondrial dna transcription in vivo. *Life science alliance*, 4(11). <https://doi.org/10.26508/lsa.202101034>
- Böttlinger, L., & Becker, T. (2012). Protein quality control in the intermembrane space of mitochondria. *Journal of molecular biology*, 424(5), 225–226. <https://doi.org/10.1016/j.jmb.2012.10.013>
- Boubekeur, S., Bunoust, O., Camougrand, N., Castroviejo, M., Rigoulet, M., & Guérin, B. (1999). A mitochondrial pyruvate dehydrogenase bypass in the yeast *saccharomyces cerevisiae*. *The Journal of biological chemistry*, 274(30), 21044–21048. <https://doi.org/10.1074/jbc.274.30.21044>
- Branon, T. C., Bosch, J. A., Sanchez, A. D., Udeshi, N. D., Svinkina, T., Carr, S. A., Feldman, J. L., Perrimon, N., & Ting, A. Y. (2018). Efficient proximity

- labeling in living cells and organisms with turboid. *Nature Biotechnology*, *36*(9), 880–887. <https://doi.org/10.1038/nbt.4201>
- Bratic, A., & Larsson, N.-G. (2013). The role of mitochondria in aging. *The Journal of clinical investigation*, *123*(3), 951–957. <https://doi.org/10.1172/JCI64125>
- Brewer, L. R., Friddle, R., Noy, A., Baldwin, E., Martin, S. S., Corzett, M., Balhorn, R., & Baskin, R. J. (2003). Packaging of single dna molecules by the yeast mitochondrial protein abf2p. *Biophysical journal*, *85*(4), 2519–2524. [https://doi.org/10.1016/S0006-3495\(03\)74674-8](https://doi.org/10.1016/S0006-3495(03)74674-8)
- Bricker, D. K., Taylor, E. B., Schell, J. C., Orsak, T., Boutron, A., Chen, Y.-C., Cox, J. E., Cardon, C. M., van Vranken, J. G., Dephoure, N., Redin, C., Boudina, S., Gygi, S. P., Brivet, M., Thummel, C. S., & Rutter, J. (2012). A mitochondrial pyruvate carrier required for pyruvate uptake in yeast, drosophila, and humans. *Science (New York, N.Y.)*, *337*(6090), 96–100. <https://doi.org/10.1126/science.1218099>
- Busch, K. B., Kowald, A., & Spelbrink, J. N. (2014). Quality matters: How does mitochondrial network dynamics and quality control impact on mtdna integrity? *Philosophical transactions of the Royal Society of London. Series B, Biological sciences*, *369*(1646), 20130442. <https://doi.org/10.1098/rstb.2013.0442>
- Butenko, A., Lukeš, J., Speijer, D., & Wideman, J. G. (2024). Mitochondrial genomes revisited: Why do different lineages retain different genes? *BMC biology*, *22*(1), 15. <https://doi.org/10.1186/s12915-024-01824-1>
- Buu, L.-M., Chen, Y.-C., & Lee, F.-J. S. (2003). Functional characterization and localization of acetyl-coa hydrolase, ach1p, in saccharomyces cerevisiae. *The Journal of biological chemistry*, *278*(19), 17203–17209. <https://doi.org/10.1074/jbc.M213268200>
- Chen, X., Prosser, R., Simonetti, S., Sadlock, J., Jagiello, G., & Schon, E. A. (1995). Rearranged mitochondrial genomes are present in human oocytes. *American Journal of Human Genetics*, *57*(2), 239–247.
- Chen, X. J., Wang, X., & Butow, R. A. (2007). Yeast aconitase binds and provides metabolically coupled protection to mitochondrial dna. *Proceedings of the National Academy of Sciences*, *104*(34), 13738–13743. <https://doi.org/10.1073/pnas.0703078104>
- Chen, X. J., Wang, X., Kaufman, B. A., & Butow, R. A. (2005). Aconitase couples metabolic regulation to mitochondrial dna maintenance. *Science (New York, N.Y.)*, *307*(5710), 714–717. <https://doi.org/10.1126/science.1106391>
- Chen, Y., Zhang, Y., Siewers, V., & Nielsen, J. (2015). Ach1 is involved in shuttling mitochondrial acetyl units for cytosolic c2 provision in saccharomyces cerevisiae lacking pyruvate decarboxylase. *FEMS yeast research*, *15*(3). <https://doi.org/10.1093/femsyr/fov015>

- Cherry, J. M., Hong, E. L., Amundsen, C., Balakrishnan, R., Binkley, G., Chan, E. T., Christie, K. R., Costanzo, M. C., Dwight, S. S., Engel, S. R., Fisk, D. G., Hirschman, J. E., Hitz, B. C., Karra, K., Krieger, C. J., Miyasato, S. R., Nash, R. S., Park, J., Skrzypek, M. S., ... Wong, E. D. (2012). Saccharomyces genome database: The genomics resource of budding yeast. *Nucleic acids research*, *40*(Database issue), D700–5. <https://doi.org/10.1093/nar/gkr1029>
- Cieřła, J. (2006). Metabolic enzymes that bind rna: Yet another level of cellular regulatory network? *Acta biochimica Polonica*, *53*(1), 11–32.
- Ciszak, E. M., Korotchkina, L. G., Dominiak, P. M., Sidhu, S., & Patel, M. S. (2003). Structural basis for flip-flop action of thiamin pyrophosphate-dependent enzymes revealed by human pyruvate dehydrogenase. *The Journal of biological chemistry*, *278*(23), 21240–21246. <https://doi.org/10.1074/jbc.M300339200>
- Cogliati, S., Enriquez, J. A., & Scorrano, L. (2016). Mitochondrial cristae: Where beauty meets functionality. *Trends in biochemical sciences*, *41*(3), 261–273. <https://doi.org/10.1016/j.tibs.2016.01.001>
- Costanzo, M., VanderSluis, B., Koch, E. N., Baryshnikova, A., Pons, C., Tan, G., Wang, W., Usaj, M., Hanchard, J., Lee, S. D., Pelechano, V., Styles, E. B., Billmann, M., van Leeuwen, J., van Dyk, N., Lin, Z.-Y., Kuzmin, E., Nelson, J., Piotrowski, J. S., ... Boone, C. (2016). A global genetic interaction network maps a wiring diagram of cellular function. *Science (New York, N.Y.)*, *353*(6306). <https://doi.org/10.1126/science.aaf1420>
- Cox, J., Hein, M. Y., Lubner, C. A., Paron, I., Nagaraj, N., & Mann, M. (2014). Accurate proteome-wide label-free quantification by delayed normalization and maximal peptide ratio extraction, termed maxlq. *Molecular & Cellular Proteomics*, *13*(9), 2513–2526. <https://doi.org/10.1074/mcp.M113.031591>
- Cox, J., & Mann, M. (2008). Maxquant enables high peptide identification rates, individualized p.p.b.-range mass accuracies and proteome-wide protein quantification. *Nature Biotechnology*, *26*(12), 1367–1372. <https://doi.org/10.1038/nbt.1511>
- Cristea, I. M., & Chait, B. T. (2011). Conjugation of magnetic beads for immunopurification of protein complexes. *Cold Spring Harbor protocols*, *2011*(5), pdb.prot5610. <https://doi.org/10.1101/pdb.prot5610>
- Crooks, G. E., Hon, G., Chandonia, J.-M., & Brenner, S. E. (2004). Weblogo: A sequence logo generator. *Genome research*, *14*(6), 1188–1190. <https://doi.org/10.1101/gr.849004>
- de Deken, R. H. (1966). The crabtree effect: A regulatory system in yeast. *Journal of general microbiology*, *44*(2), 149–156. <https://doi.org/10.1099/00221287-44-2-149>

- Desai, N., Brown, A., Amunts, A., & Ramakrishnan, V. (2017). The structure of the yeast mitochondrial ribosome. *Science (New York, N.Y.)*, *355*(6324), 528–531. <https://doi.org/10.1126/science.aal2415>
- Deshwal, S., Fiedler, K. U., & Langer, T. (2020). Mitochondrial proteases: Multifaceted regulators of mitochondrial plasticity. *Annual review of biochemistry*, *89*, 501–528. <https://doi.org/10.1146/annurev-biochem-062917-012739>
- Diffley, J. F., & Stillman, B. (1991). A close relative of the nuclear, chromosomal high-mobility group protein hmg1 in yeast mitochondria. *Proceedings of the National Academy of Sciences*, *88*(17), 7864–7868. <https://doi.org/10.1073/pnas.88.17.7864>
- DL Nelson, AL Lehninger, MM Cox. (2008). *Lehninger principles of biochemistry*. <https://scholar.google.com/citations?user=dgccdxxmaaaa&hl=en&oi=sra>
- Ekstrand, M. I., Falkenberg, M., Rantanen, A., Park, C. B., Gaspari, M., Hulthenby, K., Rustin, P., Gustafsson, C. M., & Larsson, N.-G. (2004). Mitochondrial transcription factor a regulates mtdna copy number in mammals. *Human molecular genetics*, *13*(9), 935–944. <https://doi.org/10.1093/hmg/ddh109>
- Erzberger, J. P., & Berger, J. M. (2006). Evolutionary relationships and structural mechanisms of aaa+ proteins. *Annual Review of Biophysics and Biomolecular Structure*, *35*(1), 93–114. <https://doi.org/10.1146/annurev.biophys.35.040405.101933>
- Evans, R., O'Neill, M., Pritzel, A., Antropova, N., Senior, A., Green, T., Žídek, A., Bates, R., Blackwell, S., Yim, J., Ronneberger, O., Bodenstern, S., Zielinski, M., Bridgland, A., Potapenko, A., Cowie, A., Tunyasuvunakool, K., Jain, R., Clancy, E., ... Hassabis, D. (2021). *Protein complex prediction with alphafold-multimer*. <https://doi.org/10.1101/2021.10.04.463034>
- Fernandez-Vizarra, E., & Zeviani, M. (2021). Mitochondrial disorders of the oxphos system. *FEBS letters*, *595*(8), 1062–1106. <https://doi.org/10.1002/1873-3468.13995>
- Fleck, C. B., & Brock, M. (2009). Re-characterisation of *saccharomyces cerevisiae* ach1p: Fungal coa-transferases are involved in acetic acid detoxification. *Fungal genetics and biology : FG & B*, *46*(6-7), 473–485. <https://doi.org/10.1016/j.fgb.2009.03.004>
- Flikweert, M. T., van der Zanden, L., Janssen, W. M. T. M., YDE STEENSMA, H., van Dijken, J. P., & Pronk, J. T. (1996). Pyruvate decarboxylase: An indispensable enzyme for growth of *saccharomyces cerevisiae* on glucose. *Yeast*, *12*(3), 247–257. [https://doi.org/10.1002/\(SICI\)1097-0061\(19960315\)12:3<247::AID-YEA911>3.0.CO;2-I](https://doi.org/10.1002/(SICI)1097-0061(19960315)12:3<247::AID-YEA911>3.0.CO;2-I)
- Frazier, A. E., Taylor, R. D., Mick, D. U., Warscheid, B., Stoepel, N., Meyer, H. E., Ryan, M. T., Guiard, B., & Rehling, P. (2006). Mdm38 interacts with ribosomes and is a component of the mitochondrial protein export

- machinery. *The Journal of Cell Biology*, 172(4), 553–564. <https://doi.org/10.1083/jcb.200505060>
- Frey, T. G., & Mannella, C. A. (2000). The internal structure of mitochondria. *Trends in biochemical sciences*, 25(7), 319–324. [https://doi.org/10.1016/S0968-0004\(00\)01609-1](https://doi.org/10.1016/S0968-0004(00)01609-1)
- Frey, T. G., Renken, C. W., & Perkins, G. A. (2002). Insight into mitochondrial structure and function from electron tomography. *Biochimica et biophysica acta*, 1555(1-3), 196–203. [https://doi.org/10.1016/S0005-2728\(02\)00278-5](https://doi.org/10.1016/S0005-2728(02)00278-5)
- Friddle, R. W., Klare, J. E., Martin, S. S., Corzett, M., Balhorn, R., Baldwin, E. P., Baskin, R. J., & Noy, A. (2004). Mechanism of dna compaction by yeast mitochondrial protein abf2p. *Biophysical journal*, 86(3), 1632–1639. [https://doi.org/10.1016/S0006-3495\(04\)74231-9](https://doi.org/10.1016/S0006-3495(04)74231-9)
- Gabaldón, T., & Huynen, M. A. (2007). From endosymbiont to host-controlled organelle: The hijacking of mitochondrial protein synthesis and metabolism. *PLoS computational biology*, 3(11), e219. <https://doi.org/10.1371/journal.pcbi.0030219>
- Gabler, F., Nam, S.-Z., Till, S., Mirdita, M., Steinegger, M., Söding, J., Lupas, A. N., & Alva, V. (2020). Protein sequence analysis using the mpi bioinformatics toolkit. *Current protocols in bioinformatics*, 72(1), e108. <https://doi.org/10.1002/cpbi.108>
- Gao, H., Jiang, X., Pogliano, K., & Aronson, A. I. (2002). The e1beta and e2 subunits of the bacillus subtilis pyruvate dehydrogenase complex are involved in regulation of sporulation. *Journal of Bacteriology*, 184(10), 2780–2788. <https://doi.org/10.1128/JB.184.10.2780-2788.2002>
- Gates, S. N., & Martin, A. (2020). Stairway to translocation: Aaa+ motor structures reveal the mechanisms of atp-dependent substrate translocation. *Protein Science : A Publication of the Protein Society*, 29(2), 407–419. <https://doi.org/10.1002/pro.3743>
- Gerdes, F., Tatsuta, T., & Langer, T. (2012). Mitochondrial aaa proteases — towards a molecular understanding of membrane-bound proteolytic machines. *Biochimica et Biophysica Acta (BBA) - Molecular Cell Research*, 1823(1), 49–55. <https://doi.org/10.1016/j.bbamcr.2011.09.015>
- Gerhold, J. M., Cansiz-Arda, Ş., Löhmus, M., Engberg, O., Reyes, A., van Rennes, H., Sanz, A., Holt, I. J., Cooper, H. M., & Spelbrink, J. N. (2015). Human mitochondrial dna-protein complexes attach to a cholesterol-rich membrane structure. *Scientific Reports*, 5(1), 15292. <https://doi.org/10.1038/srep15292>
- Gey, U., Czupalla, C., Hoflack, B., Rödel, G., & Krause-Buchholz, U. (2008). Yeast pyruvate dehydrogenase complex is regulated by a concerted activity of two kinases and two phosphatases. *The Journal of biological chemistry*, 283(15), 9759–9767. <https://doi.org/10.1074/jbc.M708779200>

- Gilkerson, R. W., Selker, J. M. L., & Capaldi, R. A. (2003). The cristal membrane of mitochondria is the principal site of oxidative phosphorylation. *FEBS letters*, *546*(2-3), 355–358. [https://doi.org/10.1016/s0014-5793\(03\)00633-1](https://doi.org/10.1016/s0014-5793(03)00633-1)
- Glynn, S. E. (2017). Multifunctional mitochondrial aaa proteases. *Frontiers in molecular biosciences*, *4*, 34. <https://doi.org/10.3389/fmolb.2017.00034>
- Göke, A., Schrott, S., Mizrak, A., Belyy, V., Osman, C., & Walter, P. (2020). Mrx6 regulates mitochondrial dna copy number in *saccharomyces cerevisiae* by engaging the evolutionarily conserved lon protease pim1. *Molecular Biology of the Cell*, *31*(7), 527–545. <https://doi.org/10.1091/mbc.E19-08-0470>
- Gray, M. W. (1989). Origin and evolution of mitochondrial dna. *Annual review of cell biology*, *5*, 25–50. <https://doi.org/10.1146/annurev.cb.05.110189.000325>
- Gray, M. W. (2014). The pre-endosymbiont hypothesis: A new perspective on the origin and evolution of mitochondria. *Cold Spring Harbor perspectives in biology*, *6*(3). <https://doi.org/10.1101/cshperspect.a016097>
- Gray, M. W. (2015). Mosaic nature of the mitochondrial proteome: Implications for the origin and evolution of mitochondria. *Proceedings of the National Academy of Sciences*, *112*(33), 10133–10138. <https://doi.org/10.1073/pnas.1421379112>
- Greber, B. J., & Ban, N. (2016). Structure and function of the mitochondrial ribosome. *Annual review of biochemistry*, *85*, 103–132. <https://doi.org/10.1146/annurev-biochem-060815-014343>
- Gruschke, S., Gröne, K., Heublein, M., Hölz, S., Israel, L., Imhof, A., Herrmann, J. M., & Ott, M. (2010). Proteins at the polypeptide tunnel exit of the yeast mitochondrial ribosome. *The Journal of biological chemistry*, *285*(25), 19022–19028. <https://doi.org/10.1074/jbc.M110.113837>
- Gu, Y., Zhou, Z. H., McCarthy, D. B., Reed, L. J., & Stoops, J. K. (2003). 3d electron microscopy reveals the variable deposition and protein dynamics of the peripheral pyruvate dehydrogenase component about the core. *Proceedings of the National Academy of Sciences*, *100*(12), 7015–7020. <https://doi.org/10.1073/pnas.0732060100>
- Habbane, M., Montoya, J., Rhouda, T., Sbaoui, Y., Radallah, D., & Emperador, S. (2021). Human mitochondrial dna: Particularities and diseases. *Biomedicines*, *9*(10). <https://doi.org/10.3390/biomedicines9101364>
- Hällberg, B. M., & Larsson, N.-G. (2014). Making proteins in the powerhouse. *Cell metabolism*, *20*(2), 226–240. <https://doi.org/10.1016/j.cmet.2014.07.001>
- Hanekamp, T., & Thorsness, P. E. (1996). Inactivation of yme2/rna12, which encodes an integral inner mitochondrial membrane protein, causes increased escape of dna from mitochondria to the nucleus in *saccharomyces cerevisiae*. *Molecular and cellular biology*, *16*(6), 2764–2771. <https://doi.org/10.1128/MCB.16.6.2764>

- Hanekamp, T., & Thorsness, P. E. (1999). Ynt20, a bypass suppressor of yme1 yme2, encodes a putative 3'-5' exonuclease localized in mitochondria of *Saccharomyces cerevisiae*. *Current Genetics*, *34*(6), 438–448. <https://doi.org/10.1007/s002940050418>
- Hansen, K. G., & Herrmann, J. M. (2019). Transport of proteins into mitochondria. *The Protein Journal*, *38*(3), 330–342. <https://doi.org/10.1007/s10930-019-09819-6>
- Hanson, P. I., & Whiteheart, S. W. (2005). Aaa+ proteins: Have engine, will work. *Nature Reviews Molecular Cell Biology*, *6*(7), 519–529. <https://doi.org/10.1038/nrm1684>
- Harper, N. J., Burnside, C., & Klinge, S. (2023). Principles of mitoribosomal small subunit assembly in eukaryotes. *Nature*, *614*(7946), 175–181. <https://doi.org/10.1038/s41586-022-05621-0>
- Harris, R. A., Bowker-Kinley, M. M., Huang, B., & Wu, P. (2002). Regulation of the activity of the pyruvate dehydrogenase complex. *Advances in Enzyme Regulation*, *42*, 249–259. [https://doi.org/10.1016/s0065-2571\(01\)00061-9](https://doi.org/10.1016/s0065-2571(01)00061-9)
- He, J., Cooper, H. M., Reyes, A., Di Re, M., Sembongi, H., Litwin, T. R., Gao, J., Neuman, K. C., Fearnley, I. M., Spinazzola, A., Walker, J. E., & Holt, I. J. (2012). Mitochondrial nucleoid interacting proteins support mitochondrial protein synthesis. *Nucleic Acids Research*, *40*(13), 6109–6121. <https://doi.org/10.1093/nar/gks266>
- Hell, K., Neupert, W., & Stuart, R. A. (2001). Oxa1p acts as a general membrane insertion machinery for proteins encoded by mitochondrial DNA. *The EMBO Journal*, *20*(6), 1281–1288. <https://doi.org/10.1093/emboj/20.6.1281>
- Hensen, F., Cansiz, S., Gerhold, J. M., & Spelbrink, J. N. (2014). To be or not to be a nucleoid protein: A comparison of mass-spectrometry based approaches in the identification of potential mtDNA-nucleoid associated proteins. *Biochimie*, *100*, 219–226. <https://doi.org/10.1016/j.biochi.2013.09.017>
- Herzig, S., Raemy, E., Montessuit, S., Veuthey, J.-l., Zamboni, N., Westermann, B., Edmund R. S. Kunji, & Martinou, J.-C. (2012). Identification and functional expression of the mitochondrial pyruvate carrier. *American Association for the Advancement of Science*. https://www.science.org/doi/10.1126/science.1218530?url_ver=Z39.88-2003&rfr_id=ori:rid:crossref.org&rfr_dat=cr_pub%20%20pubmed
- Hezaveh, S., Zeng, A.-P., & Jandt, U. (2017). Investigation of core structure and stability of human pyruvate dehydrogenase complex: A coarse-grained approach. *ACS Omega*, *2*(3), 1134–1145. <https://doi.org/10.1021/acsomega.6b00386>
- Hiromasa, Y., Fujisawa, T., Aso, Y., & Roche, T. E. (2004). Organization of the cores of the mammalian pyruvate dehydrogenase complex formed by e2

- and e2 plus the e3-binding protein and their capacities to bind the e1 and e3 components. *The Journal of biological chemistry*, 279(8), 6921–6933. <https://doi.org/10.1074/jbc.M308172200>
- Imbard, A., Boutron, A., Vequaud, C., Zater, M., de Lonlay, P., de Baulny, H. O., Barnerias, C., Miné, M., Marsac, C., Saudubray, J.-M., & Brivet, M. (2011). Molecular characterization of 82 patients with pyruvate dehydrogenase complex deficiency. structural implications of novel amino acid substitutions in e1 protein. *Molecular genetics and metabolism*, 104(4), 507–516. <https://doi.org/10.1016/j.ymgme.2011.08.008>
- Iovine, J. C., Claypool, S. M., & Alder, N. N. (2021). Mitochondrial compartmentalization: Emerging themes in structure and function. *Trends in biochemical sciences*, 46(11), 902–917. <https://doi.org/10.1016/j.tibs.2021.06.003>
- Itoh, Y., Andréll, J., Choi, A., Richter, U., Maiti, P., Best, R. B., Barrientos, A., Battersby, B. J., & Amunts, A. (2021). Mechanism of membrane-tethered mitochondrial protein synthesis. *Science (New York, N.Y.)*, 371(6531), 846–849. <https://doi.org/10.1126/science.abe0763>
- Iyer, L. M., Leipe, D. D., Koonin, E. V., & Aravind, L. (2004). Evolutionary history and higher order classification of aaa+ atpases. *Journal of Structural Biology*, 146(1-2), 11–31. <https://doi.org/10.1016/j.jsb.2003.10.010>
- Jakubke, C., Roussou, R., Maiser, A., Schug, C., Thoma, F., Bunk, D., Hörl, D., Leonhardt, H., Walter, P., Klecker, T., & Osman, C. (2021). Cristae-dependent quality control of the mitochondrial genome. *Science advances*, 7(36), eabi8886. <https://doi.org/10.1126/sciadv.abi8886>
- James, A. G., Cook, R. M., West, S. M., & Lindsay, J. G. (1995). The pyruvate dehydrogenase complex of *saccharomyces cerevisiae* is regulated by phosphorylation. *FEBS letters*, 373(2), 111–114. [https://doi.org/10.1016/0014-5793\(95\)01020-f](https://doi.org/10.1016/0014-5793(95)01020-f)
- Janke, C., Magiera, M. M., Rathfelder, N., Taxis, C., Reber, S., Maekawa, H., Moreno-Borchart, A., Doenges, G., Schwob, E., Schiebel, E., & Knop, M. (2004). A versatile toolbox for pcr-based tagging of yeast genes: New fluorescent proteins, more markers and promoter substitution cassettes. *Yeast*, 21(11), 947–962. <https://doi.org/10.1002/yea.1142>
- Jeffery, C. J. (2003). Moonlighting proteins: Old proteins learning new tricks. *Trends in Genetics*, 19(8), 415–417. [https://doi.org/10.1016/S0168-9525\(03\)00167-7](https://doi.org/10.1016/S0168-9525(03)00167-7)
- Jia, L., Dienhart, M., Schramp, M., McCauley, M., Hell, K., & Stuart, R. A. (2003). Yeast oxal interacts with mitochondrial ribosomes: The importance of the c-terminal region of oxal. *The EMBO Journal*, 22(24), 6438–6447. <https://doi.org/10.1093/emboj/cdg624>
- Jiang, J., Baiesc, F. L., Hiromasa, Y., Yu, X., Hui, W. H., Dai, X., Roche, T. E., & Zhou, Z. H. (2018). Atomic structure of the e2 inner core of human

- pyruvate dehydrogenase complex. *Biochemistry*, 57(16), 2325–2334. <https://doi.org/10.1021/acs.biochem.8b00357>
- Jourdain, A. A., Boehm, E., Maundrell, K., & Martinou, J.-C. (2016). Mitochondrial rna granules: Compartmentalizing mitochondrial gene expression. *The Journal of Cell Biology*, 212(6), 611–614. <https://doi.org/10.1083/jcb.201507125>
- Jumper, J., Evans, R., Pritzel, A., Green, T., Figurnov, M., Ronneberger, O., Tunyasuvunakool, K., Bates, R., Žídek, A., Potapenko, A., Bridgland, A., Meyer, C., Kohl, S. A. A., Ballard, A. J., Cowie, A., Romera-Paredes, B., Nikolov, S., Jain, R., Adler, J., . . . Hassabis, D. (2021). Highly accurate protein structure prediction with alphafold. *Nature*, 596(7873), 583–589. <https://doi.org/10.1038/s41586-021-03819-2>
- Karlberg, O., Canbäck, B., Kurland, C. G., & Andersson, S. G. E. (2000). The dual origin of the yeast mitochondrial proteome. *Yeast*, 1(3), 170–187. [https://doi.org/10.1002/1097-0061\(20000930\)17:3<170::AID-YEA25>3.0.CO;2-V](https://doi.org/10.1002/1097-0061(20000930)17:3<170::AID-YEA25>3.0.CO;2-V)
- Kaufman, B. A., Newman, S. M., Hallberg, R. L., Slaughter, C. A., Perlman, P. S., & Butow, R. A. (2000). In organello formaldehyde crosslinking of proteins to mtdna: Identification of bifunctional proteins. *Proceedings of the National Academy of Sciences*, 97(14), 7772–7777. <https://doi.org/10.1073/pnas.140063197>
- Kaufman, B. A., Durisic, N., Mativetsky, J. M., Costantino, S., Hancock, M. A., Grutter, P., & Shoubridge, E. A. (2007). The mitochondrial transcription factor tfam coordinates the assembly of multiple dna molecules into nucleoid-like structures. *Molecular Biology of the Cell*, 18(9), 3225–3236. <https://doi.org/10.1091/mbc.e07-05-0404>
- Kaufman, B. A., Kolesar, J. E., Perlman, P. S., & Butow, R. A. (2003). A function for the mitochondrial chaperonin hsp60 in the structure and transmission of mitochondrial dna nucleoids in *saccharomyces cerevisiae*. *The Journal of Cell Biology*, 163(3), 457–461. <https://doi.org/10.1083/jcb.200306132>
- Kaushal, P. S., Sharma, M. R., Booth, T. M., Haque, E. M., Tung, C.-S., Sanbonmatsu, K. Y., Spremulli, L. L., & Agrawal, R. K. (2014). Cryo-em structure of the small subunit of the mammalian mitochondrial ribosome. *Proceedings of the National Academy of Sciences*, 111(20), 7284–7289. <https://doi.org/10.1073/pnas.1401657111>
- Kehrein, K., Schilling, R., Möller-Hergt, B. V., Wurm, C. A., Jakobs, S., Lamkemeyer, T., Langer, T., & Ott, M. (2015). Organization of mitochondrial gene expression in two distinct ribosome-containing assemblies. *Cell reports*, 10(6), 843–853. <https://doi.org/10.1016/j.celrep.2015.01.012>
- Kieth Porter. (2011). Cil_11397, myotis lucifugus. <https://doi.org/10.7295/W9CIL11397>

- Kim, H. B., & Kim, K.-E. (2024). Precision proteomics with turboid: Mapping the suborganelle landscape. *The Korean journal of physiology & pharmacology : official journal of the Korean Physiological Society and the Korean Society of Pharmacology*, 28(6), 495–501. <https://doi.org/10.4196/kjpp.2024.28.6.495>
- Kotiadis, V. N., Duchon, M. R., & Osellame, L. D. (2014). Mitochondrial quality control and communications with the nucleus are important in maintaining mitochondrial function and cell health. *Biochimica et biophysica acta*, 1840(4), 1254–1265. <https://doi.org/10.1016/j.bbagen.2013.10.041>
- Krause-Buchholz, U., Gey, U., Wünschmann, J., Becker, S., & Rödel, G. (2006). Yil042c and yor090c encode the kinase and phosphatase of the *saccharomyces cerevisiae* pyruvate dehydrogenase complex. *FEBS letters*, 580(11), 2553–2560. <https://doi.org/10.1016/j.febslet.2006.04.002>
- Kucej, M., Kucejova, B., Subramanian, R., Chen, X. J., & Butow, R. A. (2008). Mitochondrial nucleoids undergo remodeling in response to metabolic cues. *Journal of cell science*, 121(11), 1861–1868. <https://doi.org/10.1242/jcs.028605>
- Kukat, C., Davies, K. M., Wurm, C. A., Spähr, H., Bonekamp, N. A., Köhl, I., Joos, F., Polosa, P. L., Park, C. B., Posse, V., Falkenberg, M., Jakobs, S., Köhlbrandt, W., & Larsson, N.-G. (2015). Cross-strand binding of tfam to a single mtdna molecule forms the mitochondrial nucleoid. *Proceedings of the National Academy of Sciences*, 112(36), 11288–11293. <https://doi.org/10.1073/pnas.1512131112>
- Kukat, C., Wurm, C. A., Spähr, H., Falkenberg, M., Larsson, N.-G., & Jakobs, S. (2011). Super-resolution microscopy reveals that mammalian mitochondrial nucleoids have a uniform size and frequently contain a single copy of mtdna. *Proceedings of the National Academy of Sciences*, 108(33), 13534–13539. <https://doi.org/10.1073/pnas.1109263108>
- Kummer, E., & Ban, N. (2021). Mechanisms and regulation of protein synthesis in mitochondria. *Nature Reviews Molecular Cell Biology*, 22(5), 307–325. <https://doi.org/10.1038/s41580-021-00332-2>
- Kurland, C. G., & Andersson, S. G. (2000). Origin and evolution of the mitochondrial proteome. *Microbiology and molecular biology reviews : MMBR*, 64(4), 786–820. <https://doi.org/10.1128/MMBR.64.4.786-820.2000>
- Kushnirov, V. V. (2000). Rapid and reliable protein extraction from yeast. *Yeast*, 16(9), 857–860. [https://doi.org/10.1002/1097-0061\(20000630\)16:9<857::AID-YEA561>3.0.CO;2-B](https://doi.org/10.1002/1097-0061(20000630)16:9<857::AID-YEA561>3.0.CO;2-B)
- Kyrilis, F. L., Semchonok, D. A., Skolidis, I., Tüting, C., Hamdi, F., O'Reilly, F. J., Rappsilber, J., & Kastiris, P. L. (2021). Integrative structure of a 10-megadalton eukaryotic pyruvate dehydrogenase complex from native cell

- extracts. *Cell Reports*, *34*(6), 108727. <https://doi.org/10.1016/j.celrep.2021.108727>
- Lane, N., & Martin, W. (2010). The energetics of genome complexity. *Nature*, *467*(7318), 929–934. <https://doi.org/10.1038/nature09486>
- Lang, B. F., Gray, M. W., & Burger, G. (1999). Mitochondrial genome evolution and the origin of eukaryotes. *Annual review of genetics*, *33*, 351–397. <https://doi.org/10.1146/annurev.genet.33.1.351>
- Larsson, N.-G. (2010). Somatic mitochondrial dna mutations in mammalian aging. *Annual review of biochemistry*, *79*, 683–706. <https://doi.org/10.1146/annurev-biochem-060408-093701>
- Lasserre, J.-P., Dautant, A., Aiyar, R. S., Kucharczyk, R., Glatigny, A., Tribouillard-Tanvier, D., Rytka, J., Blondel, M., Skoczen, N., Reynier, P., Pitayu, L., Rötig, A., Delahodde, A., Steinmetz, L. M., Dujardin, G., Procaccio, V., & Di Rago, J.-P. (2015). Yeast as a system for modeling mitochondrial disease mechanisms and discovering therapies. *Disease Models & Mechanisms*, *8*(6), 509–526. <https://doi.org/10.1242/dmm.020438>
- Lee, J., Oh, S., Bhattacharya, S., Zhang, Y., Florens, L., Washburn, M. P., & Workman, J. L. (2020). The plasticity of the pyruvate dehydrogenase complex confers a labile structure that is associated with its catalytic activity. *PLOS ONE*, *15*(12), e0243489. <https://doi.org/10.1371/journal.pone.0243489>
- Leonhard, K., Guiard, B., Pellicchia, G., Tzagoloff, A., Neupert, W., & Langer, T. (2000). Membrane protein degradation by aaa proteases in mitochondria: Extraction of substrates from either membrane surface. *Molecular cell*, *5*(4), 629–638. [https://doi.org/10.1016/s1097-2765\(00\)80242-7](https://doi.org/10.1016/s1097-2765(00)80242-7)
- Leonhard, K., Herrmann, J. M., Stuart, R. A., Mannhaupt, G., Neupert, W., & Langer, T. (1996). Aaa proteases with catalytic sites on opposite membrane surfaces comprise a proteolytic system for the atp-dependent degradation of inner membrane proteins in mitochondria. *The EMBO Journal*, *15*(16), 4218–4229. <https://doi.org/10.1002/j.1460-2075.1996.tb00796.x>
- Levytskyy, R. M., Bohovych, I., & Khalimonchuk, O. (2017). Metalloproteases of the inner mitochondrial membrane. *Biochemistry*, *56*(36), 4737–4746. <https://doi.org/10.1021/acs.biochem.7b00663>
- Lipinski, K. A., Kaniak-Golik, A., & Golik, P. (2010). Maintenance and expression of the s. cerevisiae mitochondrial genome—from genetics to evolution and systems biology. *Biochimica et biophysica acta*, *1797*(6-7), 1086–1098. <https://doi.org/10.1016/j.bbabi.2009.12.019>
- Madeira, F., Park, Y. m., Lee, J., Buso, N., Gur, T., Madhusoodanan, N., Basutkar, P., Tivey, A. R. N., Potter, S. C., Finn, R. D., & Lopez, R. (2019). The embl-ebi search and sequence analysis tools apis in 2019. *Nucleic acids research*, *47*(W1), W636–W641. <https://doi.org/10.1093/nar/gkz268>

- Mannella, C. A. (2006). Structure and dynamics of the mitochondrial inner membrane cristae. *Biochimica et biophysica acta*, *1763*(5-6), 542–548. <https://doi.org/10.1016/j.bbamcr.2006.04.006>
- Maris, C., Dominguez, C., & Allain, F. H.-T. (2005). The rna recognition motif, a plastic rna-binding platform to regulate post-transcriptional gene expression. *The FEBS journal*, *272*(9), 2118–2131. <https://doi.org/10.1111/j.1742-4658.2005.04653.x>
- Mårtensson, C. U., Priesnitz, C., Song, J., Ellenrieder, L., Doan, K. N., Boos, F., Floerchinger, A., Zufall, N., Oeljeklaus, S., Warscheid, B., & Becker, T. (2019). Mitochondrial protein translocation-associated degradation. *Nature*, *569*(7758), 679–683. <https://doi.org/10.1038/s41586-019-1227-y>
- Matus-Ortega, M. G., Cárdenas-Monroy, C. A., Flores-Herrera, O., Mendoza-Hernández, G., Miranda, M., González-Pedrajo, B., Vázquez-Meza, H., & Pardo, J. P. (2015). New complexes containing the internal alternative nadh dehydrogenase (nd1) in mitochondria of *saccharomyces cerevisiae*. *Yeast*, *32*(10), 629–641. <https://doi.org/10.1002/yea.3086>
- McBride, H. M., Neuspiel, M., & Wasiak, S. (2006). Mitochondria: More than just a powerhouse. *Current biology : CB*, *16*(14), R551–60. <https://doi.org/10.1016/j.cub.2006.06.054>
- McDowell, M. A., Heimes, M., & Sinning, I. (2021). Structural and molecular mechanisms for membrane protein biogenesis by the oxal1 superfamily. *Nature structural & molecular biology*, *28*(3), 234–239. <https://doi.org/10.1038/s41594-021-00567-9>
- Meier, A., & Söding, J. (2015). Automatic prediction of protein 3d structures by probabilistic multi-template homology modeling. *PLoS computational biology*, *11*(10), e1004343. <https://doi.org/10.1371/journal.pcbi.1004343>
- Miller, J. M., & Enemark, E. J. (2016). Fundamental characteristics of aaa+ protein family structure and function. *Archaea (Vancouver, B.C.)*, *2016*, 9294307. <https://doi.org/10.1155/2016/9294307>
- Miran, S. G., Lawson, J. E., & Reed, L. J. (1993). Characterization of pdh beta 1, the structural gene for the pyruvate dehydrogenase beta subunit from *saccharomyces cerevisiae*. *Proceedings of the National Academy of Sciences*, *90*(4), 1252–1256. <https://doi.org/10.1073/pnas.90.4.1252>
- Möller-Hergt, B. V., Carlström, A., Stephan, K., Imhof, A., & Ott, M. (2018). The ribosome receptors mrx15 and mba1 jointly organize cotranslational insertion and protein biogenesis in mitochondria. *Molecular Biology of the Cell*, *29*(20), 2386–2396. <https://doi.org/10.1091/mbc.E18-04-0227>
- Morgenstern, M., Stiller, S. B., Lübbert, P., Peikert, C. D., Dannenmaier, S., Drepper, F., Weill, U., Höß, P., Feuerstein, R., Gebert, M., Bohnert, M., van der Laan, M., Schuldiner, M., Schütze, C., Oeljeklaus, S., Pfanner, N.,

- Wiedemann, N., & Warscheid, B. (2017). Definition of a high-confidence mitochondrial proteome at quantitative scale. *Cell reports*, *19*(13), 2836–2852. <https://doi.org/10.1016/j.celrep.2017.06.014>
- Mounolou, J. C., Jakob, H., & Slonimski, P. P. (1966). Mitochondrial dna from yeast "petite" mutants: Specific changes in buoyant density corresponding to different cytoplasmic mutations. *Biochemical and Biophysical Research Communications*, *24*(2), 218–224. [https://doi.org/10.1016/0006-291X\(66\)90723-6](https://doi.org/10.1016/0006-291X(66)90723-6)
- Murley, A., Lackner, L. L., Osman, C., West, M., Voeltz, G. K., Walter, P., & Nunnari, J. (2013). Er-associated mitochondrial division links the distribution of mitochondria and mitochondrial dna in yeast. *eLife*, *2*, e00422. <https://doi.org/10.7554/eLife.00422>
- Neupert, W. (2015). A perspective on transport of proteins into mitochondria: A myriad of open questions. *Journal of molecular biology*, *427*(6 Pt A), 1135–1158. <https://doi.org/10.1016/j.jmb.2015.02.001>
- Neusius, D., Kleinknecht, L., Teh, J. T., Ostermeier, M., Kelterborn, S., Eirich, J., Hegemann, P., Finkemeier, I., Bohne, A.-V., & Nickelsen, J. (2022). Lysine acetylation regulates moonlighting activity of the e2 subunit of the chloroplast pyruvate dehydrogenase complex in chlamydomonas. *The Plant journal : for cell and molecular biology*, *111*(6), 1780–1800. <https://doi.org/10.1111/tpj.15924>
- Newman, S. M., Zelenaya-Troitskaya, O., Perlman, P. S., & Butow, R. A. (1996). Analysis of mitochondrial dna nucleoids in wild-type and a mutant strain of *saccharomyces cerevisiae* that lacks the mitochondrial hmg box protein abf2p. *Nucleic acids research*, *24*(2), 386–393. <https://doi.org/10.1093/nar/24.2.386>
- Niu, X. D., Stoops, J. K., & Reed, L. J. (1990). Overexpression and mutagenesis of the catalytic domain of dihydrolipoamide acetyltransferase from *saccharomyces cerevisiae*. *Biochemistry*, *29*(37), 8614–8619. <https://doi.org/10.1021/bi00489a017>
- Nowacka, M., Boccaletto, P., Jankowska, E., Jarzynka, T., Bujnicki, J. M., & Dunin-Horkawicz, S. (2019). Rrmdb-an evolutionary-oriented database of rna recognition motif sequences. *Database : the journal of biological databases and curation*, *2019*. <https://doi.org/10.1093/database/bay148>
- Nowikovsky, K., Froschauer, E. M., Zsurka, G., Samaj, J., Reipert, S., Kolisek, M., Wiesenberger, G., & Schweyen, R. J. (2004). The letm1/yol027 gene family encodes a factor of the mitochondrial k⁺ homeostasis with a potential role in the wolf-hirschhorn syndrome. *The Journal of biological chemistry*, *279*(29), 30307–30315. <https://doi.org/10.1074/jbc.M403607200>
- Nunnari, J., & Suomalainen, A. (2012). Mitochondria: In sickness and in health. *Cell*, *148*(6), 1145–1159. <https://doi.org/10.1016/j.cell.2012.02.035>

- Opalińska, M., & Jańska, H. (2018). Aaa proteases: Guardians of mitochondrial function and homeostasis. *Cells*, *7*(10). <https://doi.org/10.3390/cells7100163>
- O'Rourke, T. W., Doudican, N. A., Mackereth, M. D., Doetsch, P. W., & Shadel, G. S. (2002). Mitochondrial dysfunction due to oxidative mitochondrial dna damage is reduced through cooperative actions of diverse proteins. *Molecular and cellular biology*, *22*(12), 4086–4093. <https://doi.org/10.1128/MCB.22.12.4086-4093.2002>
- Osman, C., Noriega, T. R., Okreglak, V., Fung, J. C., & Walter, P. (2015). Integrity of the yeast mitochondrial genome, but not its distribution and inheritance, relies on mitochondrial fission and fusion. *Proceedings of the National Academy of Sciences*, *112*(9), E947–56. <https://doi.org/10.1073/pnas.1501737112>
- Ott, M., Amunts, A., & Brown, A. (2016). Organization and regulation of mitochondrial protein synthesis. *Annual review of biochemistry*, *85*, 77–101. <https://doi.org/10.1146/annurev-biochem-060815-014334>
- Ott, M., & Herrmann, J. M. (2010). Co-translational membrane insertion of mitochondrially encoded proteins. *Biochimica et biophysica acta*, *1803*(6), 767–775. <https://doi.org/10.1016/j.bbamcr.2009.11.010>
- Ott, M., Prestele, M., Bauerschmitt, H., Funes, S., Bonnefoy, N., & Herrmann, J. M. (2006). Mba1, a membrane-associated ribosome receptor in mitochondria. *The EMBO Journal*, *25*(8), 1603–1610. <https://doi.org/10.1038/sj.emboj.7601070>
- Overkamp, K. M., Bakker, B. M., Kötter, P., van Tuijl, A., de Vries, S., van Dijken, J. P., & Pronk, J. T. (2000). In vivo analysis of the mechanisms for oxidation of cytosolic nadh by *saccharomyces cerevisiae* mitochondria. *Journal of Bacteriology*, *182*(10), 2823–2830. <https://doi.org/10.1128/JB.182.10.2823-2830.2000>
- Park, S., Hanekamp, T., Thorsness, M. K., & Thorsness, P. E. (2006). Yme2p is a mediator of nucleoid structure and number in mitochondria of the yeast *saccharomyces cerevisiae*. *Current genetics*, *50*(3), 173–182. <https://doi.org/10.1007/s00294-006-0087-9>
- Patel, K. P., O'Brien, T. W., Subramony, S. H., Shuster, J., & Stacpoole, P. W. (2012). The spectrum of pyruvate dehydrogenase complex deficiency: Clinical, biochemical and genetic features in 371 patients. *Molecular genetics and metabolism*, *106*(3), 385–394. <https://doi.org/10.1016/j.ymgme.2012.03.017>
- Patel, M. S., & Korotchkina, L. G. (2006). Regulation of the pyruvate dehydrogenase complex. *Biochemical Society transactions*, *34*(Pt 2), 217–222. <https://doi.org/10.1042/BST20060217>
- Patel, M. S., Nemeria, N. S., Furey, W., & Jordan, F. (2014). The pyruvate dehydrogenase complexes: Structure-based function and regulation. *Journal*

- of Biological Chemistry*, 289(24), 16615–16623. <https://doi.org/10.1074/jbc.R114.563148>
- Pfeffer, S., Woellhaf, M. W., Herrmann, J. M., & Förster, F. (2015). Organization of the mitochondrial translation machinery studied in situ by cryoelectron tomography. *Nature communications*, 6, 6019. <https://doi.org/10.1038/ncomms7019>
- Preuss, M., Leonhard, K., Hell, K., Stuart, R. A., Neupert, W., & Herrmann, J. M. (2001). Mba1, a novel component of the mitochondrial protein export machinery of the yeast *saccharomyces cerevisiae*. *The Journal of Cell Biology*, 153(5), 1085–1096. <https://doi.org/10.1083/jcb.153.5.1085>
- Priesnitz, C., & Becker, T. (2018). Pathways to balance mitochondrial translation and protein import. *Genes & Development*, 32(19-20), 1285–1296. <https://doi.org/10.1101/gad.316547.118>
- Pronk, J. T., Wenzel, T. J., Luttik, M. A., Klaassen, C. C., Scheffers, W. A., Steensma, H. Y., & van Dijken, J. P. (1994). Energetic aspects of glucose metabolism in a pyruvate-dehydrogenase-negative mutant of *saccharomyces cerevisiae*. *Microbiology*, 140 (Pt 3)(3), 601–610. <https://doi.org/10.1099/00221287-140-3-601>
- Pronk, J. T., YDE STEENSMA, H., & van Dijken, J. P. (1996). Pyruvate metabolism in *saccharomyces cerevisiae*. *Yeast*, 12(16), 1607–1633. [https://doi.org/10.1002/\(SICI\)1097-0061\(199612\)12:16<textless>1607::AID-YEA70<textgreater>3.0.CO;2-4](https://doi.org/10.1002/(SICI)1097-0061(199612)12:16<textless>1607::AID-YEA70<textgreater>3.0.CO;2-4)
- Puchades, C., Sandate, C. R., & Lander, G. C. (2020). The molecular principles governing the activity and functional diversity of aaa+ proteins. *Nature Reviews Molecular Cell Biology*, 21(1), 43–58. <https://doi.org/10.1038/s41580-019-0183-6>
- Raimundo, N., Baysal, B. E., & Shadel, G. S. (2011). Revisiting the tca cycle: Signaling to tumor formation. *Trends in molecular medicine*, 17(11), 641–649. <https://doi.org/10.1016/j.molmed.2011.06.001>
- Rajala, N., Hensen, F., Wessels, H. J. C. T., Ives, D., Gloerich, J., & Spelbrink, J. N. (2015). Whole cell formaldehyde cross-linking simplifies purification of mitochondrial nucleoids and associated proteins involved in mitochondrial gene expression. *PLOS ONE*, 10(2), e0116726. <https://doi.org/10.1371/journal.pone.0116726>
- Rappsilber, J., Ishihama, Y., & Mann, M. (2003). Stop and go extraction tips for matrix-assisted laser desorption/ionization, nanoelectrospray, and lc/ms sample pretreatment in proteomics. *Analytical chemistry*, 75(3), 663–670. <https://doi.org/10.1021/ac026117i>
- Rathore, S., Berndtsson, J., Marin-Buera, L., Conrad, J., Carroni, M., Brzezinski, P., & Ott, M. (2019). Cryo-em structure of the yeast respiratory supercomplex.

- Nature Structural & Molecular Biology*, 26(1), 50–57. <https://doi.org/10.1038/s41594-018-0169-7>
- Reed, L. J. (1974). Multienzyme complexes. *Accounts of Chemical Research*, 7(2), 40–46. <https://doi.org/10.1021/ar50074a002>
- Reed, L. J. (1981). Regulation of mammalian pyruvate dehydrogenase complex by a phosphorylation–dephosphorylation cycle* *this work was supported in part by grant gm06590 from the u.s. public health service. In R. W. Estabrook & P. Srere (Eds.), *Current topics in cellular regulation : Biological cycles* (pp. 95–106, Vol. 18). Academic Press. <https://doi.org/10.1016/B978-0-12-152818-8.50012-8>
- Rehling, P., Brandner, K., & Pfanner, N. (2004). Mitochondrial import and the twin-pore translocase. *Nature Reviews Molecular Cell Biology*, 5(7), 519–530. <https://doi.org/10.1038/nrm1426>
- Reinders, J., Zahedi, R. P., Pfanner, N., Meisinger, C., & Sickmann, A. (2006). Toward the complete yeast mitochondrial proteome: Multidimensional separation techniques for mitochondrial proteomics. *Journal of proteome research*, 5(7), 1543–1554. <https://doi.org/10.1021/pr050477f>
- Rinaldi, T., Dallabona, C., Ferrero, I., Frontali, L., & Bolotin-Fukuhara, M. (2010). Mitochondrial diseases and the role of the yeast models. *FEMS yeast research*, 10(8), 1006–1022. <https://doi.org/10.1111/j.1567-1364.2010.00685.x>
- Rorbach, J., Richter, R., Wessels, H. J., Wydro, M., Pekalski, M., Farhoud, M., Kühl, I., Gaisne, M., Bonnefoy, N., Smeitink, J. A., Lightowlers, R. N., & Chrzanowska-Lightowlers, Z. M. A. (2008). The human mitochondrial ribosome recycling factor is essential for cell viability. *Nucleic acids research*, 36(18), 5787–5799. <https://doi.org/10.1093/nar/gkn576>
- Russell, G. C., Machado, R. S., & Guest, J. R. (1992). Overproduction of the pyruvate dehydrogenase multienzyme complex of escherichia coli and site-directed substitutions in the e1p and e2p subunits. *Biochemical Journal*, 287 (Pt 2)(Pt 2), 611–619. <https://doi.org/10.1042/bj2870611>
- Sagan, L. (1967). On the origin of mitosing cells. *Journal of theoretical biology*, 14(3), 255–274. [https://doi.org/10.1016/0022-5193\(67\)90079-3](https://doi.org/10.1016/0022-5193(67)90079-3)
- Salvatori, R., Aftab, W., Forne, I., Imhof, A., Ott, M., & Singh, A. P. (2020). Mapping protein networks in yeast mitochondria using proximity-dependent biotin identification coupled to proteomics. *STAR protocols*, 1(3), 100219. <https://doi.org/10.1016/j.xpro.2020.100219>
- Schägger, H. (2001). Respiratory chain supercomplexes. *IUBMB life*, 52(3-5), 119–128. <https://doi.org/10.1080/15216540152845911>
- Scherrer, T., Mittal, N., Janga, S. C., & Gerber, A. P. (2010). A screen for rna-binding proteins in yeast indicates dual functions for many enzymes. *PLOS ONE*, 5(11), e15499. <https://doi.org/10.1371/journal.pone.0015499>

- Schrott, S., & Osman, C. (2023). Two mitochondrial hmg-box proteins, cim1 and abf2, antagonistically regulate mtdna copy number in *saccharomyces cerevisiae*. *Nucleic Acids Research*, *51*(21), 11813–11835. <https://doi.org/10.1093/nar/gkad849>
- Seraphim, T. V., & Houry, W. A. (2020). Aaa+ proteins. *Current biology : CB*, *30*(6), R251–R257. <https://doi.org/10.1016/j.cub.2020.01.044>
- Shadel, G. S. (1999). Yeast as a model for human mtdna replication. *American Journal of Human Genetics*, *65*(5), 1230–1237. <https://doi.org/10.1086/302630>
- Shadel, G. S. (2005). Mitochondrial dna, aconitase 'wraps' it up. *Trends in biochemical sciences*, *30*(6), 294–296. <https://doi.org/10.1016/j.tibs.2005.04.007>
- Shafer, K. S., Hanekamp, T., White, K. H., & Thorsness, P. E. (1999). Mechanisms of mitochondrial dna escape to the nucleus in the yeast *saccharomyces cerevisiae*. *Current genetics*, *36*(4), 183–194. <https://doi.org/10.1007/s002940050489>
- Sharma, N., & Osman, C. (2022). Yme2, a putative rna recognition motif and aaa+ domain containing protein, genetically interacts with the mitochondrial protein export machinery. *Biological chemistry*, *403*(8-9), 807–817. <https://doi.org/10.1515/hsz-2021-0398>
- Shi, Y., Dierckx, A., Wanrooij, P. H., Wanrooij, S., Larsson, N.-G., Wilhelmsson, L. M., Falkenberg, M., & Gustafsson, C. M. (2012). Mammalian transcription factor a is a core component of the mitochondrial transcription machinery. *Proceedings of the National Academy of Sciences*, *109*(41), 16510–16515. <https://doi.org/10.1073/pnas.1119738109>
- Sickmann, A., Reinders, J., Wagner, Y., Joppich, C., Zahedi, R., Meyer, H. E., Schönfisch, B., Perschil, I., Chacinska, A., Guiard, B., Rehling, P., Pfanner, N., & Meisinger, C. (2003). The proteome of *saccharomyces cerevisiae* mitochondria. *Proceedings of the National Academy of Sciences*, *100*(23), 13207–13212. <https://doi.org/10.1073/pnas.2135385100>
- Singh, A. P., Salvatori, R., Aftab, W., Kohler, A., Carlström, A., Forne, I., Imhof, A., & Ott, M. (2020). Molecular connectivity of mitochondrial gene expression and oxphos biogenesis. *Molecular cell*, *79*(6), 1051–1065.e10. <https://doi.org/10.1016/j.molcel.2020.07.024>
- Škerlová, J., Berndtsson, J., Nolte, H., Ott, M., & Stenmark, P. (2021). Structure of the native pyruvate dehydrogenase complex reveals the mechanism of substrate insertion. *Nature communications*, *12*(1), 5277. <https://doi.org/10.1038/s41467-021-25570-y>
- Smeitink, J. A., Zeviani, M., Turnbull, D. M., & Jacobs, H. T. (2006). Mitochondrial medicine: A metabolic perspective on the pathology of oxidative phospho-

- rylation disorders. *Cell Metabolism*, 3(1), 9–13. <https://doi.org/10.1016/j.cmet.2005.12.001>
- Smith, P. M., Fox, J. L., & Winge, D. R. (2012). Biogenesis of the cytochrome bc(1) complex and role of assembly factors. *Biochimica et biophysica acta*, 1817(2), 276–286. <https://doi.org/10.1016/j.bbabi.2011.11.009>
- Snider, J., Thibault, G., & Houry, W. A. (2008). The aaa+ superfamily of functionally diverse proteins. *Genome biology*, 9(4), 216. <https://doi.org/10.1186/gb-2008-9-4-216>
- Söding, J., Biegert, A., & Lupas, A. N. (2005). The hhpred interactive server for protein homology detection and structure prediction. *Nucleic acids research*, 33(Web Server issue), W244–8. <https://doi.org/10.1093/nar/gki408>
- Song, J., Herrmann, J. M., & Becker, T. (2021). Quality control of the mitochondrial proteome. *Nature Reviews Molecular Cell Biology*, 22(1), 54–70. <https://doi.org/10.1038/s41580-020-00300-2>
- Song, J., Pfanner, N., & Becker, T. (2018). Assembling the mitochondrial atp synthase. *Proceedings of the National Academy of Sciences*, 115(12), 2850–2852. <https://doi.org/10.1073/pnas.1801697115>
- Spinelli, J. B., & Haigis, M. C. (2018). The multifaceted contributions of mitochondria to cellular metabolism. *Nature Cell Biology*, 20(7), 745–754. <https://doi.org/10.1038/s41556-018-0124-1>
- Steele, T. E., & Glynn, S. E. (2019). Mitochondrial aaa proteases: A stairway to degradation. *Mitochondrion*, 49, 121–127. <https://doi.org/10.1016/j.mito.2019.07.012>
- Stehling, O., Wilbrecht, C., & Lill, R. (2014). Mitochondrial iron-sulfur protein biogenesis and human disease. *Biochimie*, 100, 61–77. <https://doi.org/10.1016/j.biochi.2014.01.010>
- Stein, A., & Firshein, W. (2000). Probable identification of a membrane-associated repressor of bacillus subtilis dna replication as the e2 subunit of the pyruvate dehydrogenase complex. *Journal of Bacteriology*, 182(8), 2119–2124. <https://doi.org/10.1128/JB.182.8.2119-2124.2000>
- Stoops, J. K., Baker, T. S., Schroeter, J. P., Kolodziej, S. J., Niu, X. D., & Reed, L. J. (1992). Three-dimensional structure of the truncated core of the saccharomyces cerevisiae pyruvate dehydrogenase complex determined from negative stain and cryoelectron microscopy images. *The Journal of biological chemistry*, 267(34), 24769–24775.
- Stoops, J. K., Cheng, R. H., Yazdi, M. A., Maeng, C. Y., Schroeter, J. P., Klueppelberg, U., Kolodziej, S. J., Baker, T. S., & Reed, L. J. (1997). On the unique structural organization of the saccharomyces cerevisiae pyruvate dehydrogenase complex. *The Journal of biological chemistry*, 272(9), 5757–5764. <https://doi.org/10.1074/jbc.272.9.5757>

- Suomalainen, A., & Nunnari, J. (2024). Mitochondria at the crossroads of health and disease. *Cell*, *187*(11), 2601–2627. <https://doi.org/10.1016/j.cell.2024.04.037>
- Szyrach, G., Ott, M., Bonnefoy, N., Neupert, W., & Herrmann, J. M. (2003). Ribosome binding to the oxa1 complex facilitates co-translational protein insertion in mitochondria. *The EMBO Journal*, *22*(24), 6448–6457. <https://doi.org/10.1093/emboj/cdg623>
- Takahashi, H., McCaffery, J. M., Irizarry, R. A., & Boeke, J. D. (2006). Nucleo-cytosolic acetyl-coenzyme a synthetase is required for histone acetylation and global transcription. *Molecular cell*, *23*(2), 207–217. <https://doi.org/10.1016/j.molcel.2006.05.040>
- Tatsuta, T. (2009). Protein quality control in mitochondria. *Journal of biochemistry*, *146*(4), 455–461. <https://doi.org/10.1093/jb/mvp122>
- Taylor, R. W., & Turnbull, D. M. (2005). Mitochondrial dna mutations in human disease. *Nature reviews. Genetics*, *6*(5), 389–402. <https://doi.org/10.1038/nrg1606>
- Thorsness, P. E., & Fox, T. D. (1993). Nuclear mutations in *saccharomyces cerevisiae* that affect the escape of dna from mitochondria to the nucleus. *Genetics*, *134*(1), 21–28. <https://doi.org/10.1093/genetics/134.1.21>
- Timón-Gómez, A., Nývltová, E., Abriata, L. A., Vila, A. J., Hosler, J., & Barrientos, A. (2018). Mitochondrial cytochrome c oxidase biogenesis: Recent developments. *Seminars in cell & developmental biology*, *76*, 163–178. <https://doi.org/10.1016/j.semcdb.2017.08.055>
- Timón-Gómez, A., Proft, M., & Pascual-Ahuir, A. (2013). Differential regulation of mitochondrial pyruvate carrier genes modulates respiratory capacity and stress tolerance in yeast. *PLOS ONE*, *8*(11), e79405. <https://doi.org/10.1371/journal.pone.0079405>
- Tsvetanova, N. G., Klass, D. M., Salzman, J., & Brown, P. O. (2010). Proteome-wide search reveals unexpected rna-binding proteins in *saccharomyces cerevisiae*. *PLOS ONE*, *5*(9). <https://doi.org/10.1371/journal.pone.0012671>
- Tuppen, H. A. L., Blakely, E. L., Turnbull, D. M., & Taylor, R. W. (2010). Mitochondrial dna mutations and human disease. *Biochimica et biophysica acta*, *1797*(2), 113–128. <https://doi.org/10.1016/j.bbabi.2009.09.005>
- Turk, E. M., Das, V., Seibert, R. D., & Andrusis, E. D. (2013). The mitochondrial rna landscape of *saccharomyces cerevisiae*. *PloS one*, *8*(10), e78105. <https://doi.org/10.1371/journal.pone.0078105>
- Tyanova, S., Temu, T., & Cox, J. (2016). The maxquant computational platform for mass spectrometry-based shotgun proteomics. *Nature Protocols*, *11*(12), 2301–2319. <https://doi.org/10.1038/nprot.2016.136>

- Uhlinger, D. J., Yang, C. Y., & Reed, L. J. (1986). Phosphorylation-dephosphorylation of pyruvate dehydrogenase from bakers' yeast. *Biochemistry*, *25*(19), 5673–5677. <https://doi.org/10.1021/bi00367a049>
- Usaj, M., Tan, Y., Wang, W., VanderSluis, B., Zou, A., Myers, C. L., Costanzo, M., Andrews, B., & Boone, C. (2017). Thecellmap.org: A web-accessible database for visualizing and mining the global yeast genetic interaction network. *G3: Genes/Genomes/Genetics*, *7*(5), 1539–1549. <https://doi.org/10.1534/g3.117.040220>
- van Leeuwen, J., Pons, C., Mellor, J. C., Yamaguchi, T. N., Friesen, H., Koschwanez, J., Ušaj, M. M., Pechlaner, M., Takar, M., Ušaj, M., VanderSluis, B., Andrusiak, K., Bansal, P., Baryshnikova, A., Boone, C. E., Cao, J., Cote, A., Gebbia, M., Horecka, G., . . . Boone, C. (2016). Exploring genetic suppression interactions on a global scale. *Science (New York, N.Y.)*, *354*(6312). <https://doi.org/10.1126/science.aag0839>
- van Rossum, H. M., Kozak, B. U., Niemeijer, M. S., Duine, H. J., Luttik, M. A. H., Boer, V. M., Kötter, P., Daran, J.-M. G., van Maris, A. J. A., & Pronk, J. T. (2016). Alternative reactions at the interface of glycolysis and citric acid cycle in *saccharomyces cerevisiae*. *FEMS yeast research*, *16*(3). <https://doi.org/10.1093/femsyr/fow017>
- Varadi, M., Bertoni, D., Magana, P., Paramval, U., Pidruchna, I., Radhakrishnan, M., Tsenkov, M., Nair, S., Mirdita, M., Yeo, J., Kovalevskiy, O., Tunyasuvunakool, K., Laydon, A., Židek, A., Tomlinson, H., Hariharan, D., Abrahamson, J., Green, T., Jumper, J., . . . Velankar, S. (2024). Alphafold protein structure database in 2024: Providing structure coverage for over 214 million protein sequences. *Nucleic acids research*, *52*(D1), D368–D375. <https://doi.org/10.1093/nar/gkad1011>
- Vyas, S., Zaganjor, E., & Haigis, M. C. (2016). Mitochondria and cancer. *Cell*, *166*(3), 555–566. <https://doi.org/10.1016/j.cell.2016.07.002>
- Walker, J. E., Saraste, M., Runswick, M. J., & Gay, N. J. (1982). Distantly related sequences in the alpha- and beta-subunits of atp synthase, myosin, kinases and other atp-requiring enzymes and a common nucleotide binding fold. *The EMBO Journal*, *1*(8), 945–951. <https://doi.org/10.1002/j.1460-2075.1982.tb01276.x>
- Walter, C., Marada, A., & Meisinger, C. (2022). Monitoring checkpoints of metabolism and protein biogenesis in mitochondria by phos-tag technology. *Journal of Proteomics*, *252*, 104430. <https://doi.org/10.1016/j.jprot.2021.104430>
- Walter, T., & Aronson, A. (1999). Specific binding of the e2 subunit of pyruvate dehydrogenase to the upstream region of *bacillus thuringiensis* protoxin genes. *The Journal of biological chemistry*, *274*(12), 7901–7906. <https://doi.org/10.1074/jbc.274.12.7901>

- Wang, C., Ma, C., Chang, S., Wu, H., Yan, C., Chen, J., Wu, Y., An, S., Xu, J., Han, Q., Jiang, Y., Jiang, Z., Gao, H., Zhang, X., & Chang, Y. (2024). *Architecture of intact mammalian pyruvate dehydrogenase complex revealed by in-situ structural analysis*. <https://doi.org/10.1101/2024.02.01.578502>
- Wang, F., Zhang, D., Zhang, D., Li, P., & Gao, Y. (2021). Mitochondrial protein translation: Emerging roles and clinical significance in disease. *Frontiers in Cell and Developmental Biology*, *9*, 675465. <https://doi.org/10.3389/fcell.2021.675465>
- Waterhouse, A. M., Procter, J. B., Martin, D. M. A., Clamp, M., & Barton, G. J. (2009). Jalview version 2—a multiple sequence alignment editor and analysis workbench. *Bioinformatics (Oxford, England)*, *25*(9), 1189–1191. <https://doi.org/10.1093/bioinformatics/btp033>
- Weidberg, H., & Amon, A. (2018). Mitocpr-a surveillance pathway that protects mitochondria in response to protein import stress. *Science (New York, N.Y.)*, *360*(6385). <https://doi.org/10.1126/science.aan4146>
- Wendler, P., Ciniawsky, S., Kock, M., & Kube, S. (2012). Structure and function of the aaa+ nucleotide binding pocket. *Biochimica et Biophysica Acta (BBA) - Molecular Cell Research*, *1823*(1), 2–14. <https://doi.org/10.1016/j.bbamcr.2011.06.014>
- Wiedemann, N., & Pfanner, N. (2017). Mitochondrial machineries for protein import and assembly. *Annual review of biochemistry*, *86*, 685–714. <https://doi.org/10.1146/annurev-biochem-060815-014352>
- Wiese, M., & Bannister, A. J. (2020). Two genomes, one cell: Mitochondrial-nuclear coordination via epigenetic pathways. *Molecular metabolism*, *38*, 100942. <https://doi.org/10.1016/j.molmet.2020.01.006>
- Williamson, D. (2002). The curious history of yeast mitochondrial dna. *Nature reviews. Genetics*, *3*(6), 475–481. <https://doi.org/10.1038/nrg814>
- Wittig, I., Braun, H.-P., & Schägger, H. (2006). Blue native page. *Nature Protocols*, *1*(1), 418–428. <https://doi.org/10.1038/nprot.2006.62>
- Woellhaf, M. W., Sommer, F., Schroda, M., & Herrmann, J. M. (2016). Proteomic profiling of the mitochondrial ribosome identifies atp25 as a composite mitochondrial precursor protein. *Molecular Biology of the Cell*, *27*(20), 3031–3039. <https://doi.org/10.1091/mbc.E16-07-0513>
- Woodson, J. D., & Chory, J. (2008). Coordination of gene expression between organellar and nuclear genomes. *Nature Reviews Genetics*, *9*(5), 383–395. <https://doi.org/10.1038/nrg2348>
- Xiberras, J., Klein, M., Prosch, C., Malubhoy, Z., & Nevoigt, E. (2020). Anaplerotic reactions active during growth of *saccharomyces cerevisiae* on glycerol. *FEMS yeast research*, *20*(1). <https://doi.org/10.1093/femsyr/foz086>

- Yi, J., Nemeria, N., McNally, A., Jordan, F., Machado, R. S., & Guest, J. R. (1996). Effect of substitutions in the thiamin diphosphate-magnesium fold on the activation of the pyruvate dehydrogenase complex from *Escherichia coli* by cofactors and substrate. *The Journal of biological chemistry*, *271*(52), 33192–33200. <https://doi.org/10.1074/jbc.271.52.33192>
- Zdanowicz, R., Afanasyev, P., Pruška, A., Harrison, J. A., Giese, C., Boehringer, D., Leitner, A., Zenobi, R., & Glockshuber, R. (2024). Stoichiometry and architecture of the human pyruvate dehydrogenase complex. *Science advances*, *10*(29), eadn4582. <https://doi.org/10.1126/sciadv.adn4582>
- Zelenaya-Troitskaya, O., Newman, S. M., Okamoto, K., Perlman, P. S., & Butow, R. A. (1998). Functions of the high mobility group protein, abf2p, in mitochondrial dna segregation, recombination and copy number in *Saccharomyces cerevisiae*. *Genetics*, *148*(4), 1763–1776. <https://doi.org/10.1093/genetics/148.4.1763>
- Zelenaya-Troitskaya, O., Perlman, P. S., & Butow, R. A. (1995). An enzyme in yeast mitochondria that catalyzes a step in branched-chain amino acid biosynthesis also functions in mitochondrial dna stability. *The EMBO Journal*, *14*(13), 3268–3276. <https://doi.org/10.1002/j.1460-2075.1995.tb07330.x>
- Zeng, R., Smith, E., & Barrientos, A. (2018). Yeast mitoribosome large subunit assembly proceeds by hierarchical incorporation of protein clusters and modules on the inner membrane. *Cell metabolism*, *27*(3), 645–656.e7. <https://doi.org/10.1016/j.cmet.2018.01.012>
- Zhou, Z. H., Liao, W., Cheng, R. H., Lawson, J. E., McCarthy, D. B., Reed, L. J., & Stoops, J. K. (2001). Direct evidence for the size and conformational variability of the pyruvate dehydrogenase complex revealed by three-dimensional electron microscopy. the "breathing" core and its functional relationship to protein dynamics. *The Journal of biological chemistry*, *276*(24), 21704–21713. <https://doi.org/10.1074/jbc.M101765200>
- Zhou, Z. H., McCarthy, D. B., O'Connor, C. M., Reed, L. J., & Stoops, J. K. (2001). The remarkable structural and functional organization of the eukaryotic pyruvate dehydrogenase complexes. *Proceedings of the National Academy of Sciences*, *98*(26), 14802–14807. <https://doi.org/10.1073/pnas.011597698>
- Zimmermann, L., Stephens, A., Nam, S.-Z., Rau, D., Kübler, J., Lozajic, M., Gabler, F., Söding, J., Lupas, A. N., & Alva, V. (2018). A completely reimplemented mpi bioinformatics toolkit with a new hhpred server at its core. *Journal of molecular biology*, *430*(15), 2237–2243. <https://doi.org/10.1016/j.jmb.2017.12.007>

